

Nuclear magic numbers: new features far from stability

O. Sorlin¹, M.-G. Porquet²

¹Grand Accélérateur National d'Ions Lourds (GANIL),

CEA/DSM - CNRS/IN2P3, B.P. 55027, F-14076 Caen Cedex 5, France

²Centre de Spectrométrie Nucléaire et de Spectrométrie de Masse (CSNSM),

CNRS/IN2P3 - Université Paris-Sud, Bât 104-108, F-91405 Orsay, France

May 19, 2008

Abstract

The main purpose of the present manuscript is to review the structural evolution along the isotonic and isotopic chains around the "traditional" magic numbers 8, 20, 28, 50, 82 and 126. The exotic regions of the chart of nuclides have been explored during the three last decades. Then the postulate of permanent magic numbers was definitely abandoned and the reason for these structural mutations has been in turn searched for. General trends in the evolution of shell closures are discussed using complementary experimental information, such as the binding energies of the orbits bounding the shell gaps, the trends of the first collective states of the even-even semi-magic nuclei, and the behavior of certain single-nucleon states. Each section is devoted to a particular magic number. It describes the underlying physics of the shell evolution which is not yet fully understood and indicates future experimental and theoretical challenges. The nuclear mean field embodies various facets of the Nucleon-Nucleon interaction, among which the spin-orbit and tensor terms play decisive roles in the shell evolutions. The present review intends to provide experimental constraints to be used for the refinement of theoretical models aiming at a good description of the existing atomic nuclei and at more accurate predictions of hitherto unreachable systems.

Contents

1	Introduction	3
2	Effective interactions between nucleons	4
2.1	<i>Properties of two-body forces in nuclear matter</i>	6
2.1.1	<i>Features of the nucleon-nucleon forces</i>	6
2.1.2	<i>Some theoretical approaches used to solve the nuclear many-body problem</i>	7
2.2	<i>Two-Body Matrix Elements and determination of monopole interaction</i>	10
2.2.1	<i>TBME from multiplet of states in odd-odd nuclei and monopole interaction</i>	11
2.2.2	<i>Monopole interaction from double difference of binding energies</i>	13
2.3	<i>Properties of the monopole interaction</i>	15
2.3.1	<i>Effects of the monopole interaction</i>	15
2.3.2	<i>Strength of the monopole interaction</i>	18

2.4	<i>Decomposition of the monopole interaction into central, spin-orbit and tensor parts</i>	19
2.4.1	<i>Formal description of the various components of the NN interaction</i>	20
2.4.2	<i>Selected examples of decomposition of Two Body Matrix Elements</i>	20
2.4.3	<i>Qualitative effects of some parts of the interaction</i>	22
2.5	<i>Summary and Outlooks</i>	23
3	The magic number 8	24
3.1	<i>Evolution of the $N = 8$ shell closure</i>	24
3.1.1	<i>Binding energies and the $N = 8$ shell gap</i>	24
3.1.2	<i>Trends of $E(2^+)$ and $B(E2)$ values in the $N = 8$ isotones</i>	26
3.1.3	<i>Trends of $E(1_1^-)$ state in the $N = 8$ isotones</i>	26
3.1.4	<i>Conclusion</i>	27
3.2	<i>Evolution of the $Z = 8$ shell closures</i>	27
3.2.1	<i>Binding energies and the $Z = 8$ shell gap</i>	27
3.2.2	<i>Trends of $E(2^+)$ and $B(E2)$ values in the Oxygen isotopes</i>	30
3.2.3	<i>Comparison between the C and O isotopic chains and the $N = 14, 16$ subshell closures</i>	30
3.2.4	<i>Conclusion</i>	32
4	The magic number 20	32
4.1	<i>Evolution of the $N = 20$ shell closure</i>	32
4.1.1	<i>Binding energies</i>	33
4.1.2	<i>Trends of $E(2^+)$ and $B(E2)$ values and the onset of collectivity</i>	34
4.1.3	<i>Evolution of neutron SPE's</i>	35
4.1.4	<i>Static properties and β-decay</i>	37
4.1.5	<i>Search for intruder fp states by transfer and knock-out reactions</i>	38
4.1.6	<i>The appearance of a new magic number at $N = 16$</i>	40
4.1.7	<i>Conclusion</i>	41
4.2	<i>Evolution of the $Z = 20$ shell closure</i>	42
4.2.1	<i>Binding energies</i>	42
4.2.2	<i>Trends of $E(2^+)$ and $B(E2)$ values</i>	43
4.2.3	<i>Proton orbits below the $Z = 20$ gap: Levels of ${}_{19}\text{K}$ isotopes</i>	44
4.2.4	<i>Conclusion</i>	48
5	The magic number 28	49
5.1	<i>Evolution of the $N = 28$ shell closure</i>	49
5.1.1	<i>Binding energies</i>	50
5.1.2	<i>Trends of 2^+, 4^+, 0_2^+ energies and $B(E2)$ values</i>	51
5.1.3	<i>Evolution of the proton SPE</i>	53
5.1.4	<i>Evolution of the neutron SPE for $Z < 20$</i>	54
5.1.5	<i>Evolution of the neutron SPE for $Z > 20$</i>	56
5.1.6	<i>Conclusion</i>	57
5.2	<i>Evolution of the $Z = 28$ shell closure</i>	58
5.2.1	<i>Evolution of the binding energies</i>	58
5.2.2	<i>Trends of 2^+ energies and $B(E2)$ values</i>	59
5.2.3	<i>Proton orbits above the $Z = 28$ gap: Levels of the ${}_{29}\text{Cu}$ isotopes</i>	61
5.2.4	<i>Conclusion</i>	64
6	The magic number 50	65
6.1	<i>Evolution of the $N = 50$ shell closure</i>	65
6.1.1	<i>Evolution of the binding energies</i>	66
6.1.2	<i>Trends of 2^+ and $B(E2)$ values</i>	67
6.1.3	<i>Evolution of the $N = 50$ gap viewed from p-h states</i>	67
6.1.4	<i>Neutron orbits above the $N = 50$ gap: Levels of $N = 51$ isotones</i>	69
6.1.5	<i>Conclusion</i>	73
6.2	<i>Evolution of the $Z = 50$ shell closure</i>	73
6.2.1	<i>Binding energies</i>	74
6.2.2	<i>Trends of first collective excitations of Sn isotopes</i>	75

6.2.3	<i>Proton orbits above the $Z = 50$ gap: Levels of ${}_{51}\text{Sb}$ isotopes</i>	77
6.2.4	<i>Conclusion</i>	82
7	The magic number 82	82
7.1	<i>Evolution of the $N = 82$ shell closure</i>	83
7.1.1	<i>Evolution of the binding energies</i>	83
7.1.2	<i>Trends of the first collective excitations of the $N = 82$ isotones</i>	85
7.1.3	<i>Neutron orbits above the $N = 82$ gap: Levels of the $N = 83$ isotones</i>	85
7.1.4	<i>Reverse behaviors of the $\nu h_{11/2}$ and $\nu h_{9/2}$ orbits for $Z > 64$</i>	87
7.1.5	<i>Study of the $N = 82$ shell closure below $Z = 50$, Astrophysical implications</i>	88
7.1.6	<i>Conclusion</i>	91
7.2	<i>Evolution of the $Z = 82$ shell closure</i>	92
7.2.1	<i>Evolution of the binding energies</i>	92
7.2.2	<i>Trends in $E(2^+)$ and $B(E2)$</i>	93
7.2.3	<i>Conclusion</i>	93
8	The magic number $N=126$	94
9	The super-heavy elements: What is the next proton shell closure?	95
10	Conclusions and Outlooks	96
11	Annex: Binding energy of the last nucleon in nuclei close to the semi-magic nuclei	101

1 Introduction

As early as 1934, W. Elsasser noticed the existence of "special numbers" of neutrons and protons which confer to the corresponding nuclei a particularly stable configuration [1]. In analogy with atomic electrons, he correlated these numbers with closed shells in a model of non-interacting nucleons occupying energy levels generated by a potential well. This hypothesis was not further pursued at that time both because of the apparent paradox that strong inter-nucleon forces would average out in such a simple way, and the paucity of experimental data in favor of a single-particle description.

More than a decade later, the study of shell structure regained interest through the review of M. Goeppert-Mayer which, including a large number of precise experimental data [2], pointed out to the existence of closed shells at numbers 8, 20, 50, 82 and 126. Unfortunately only the first two, 8 and 20, could be explained from solutions of simple potential wells. Rather *ad-hoc* rearrangements of the level ordering were required to find the higher closed shell numbers. This strongly casted doubt on this view of the nucleus in which independent particles were moving in an average field.

Success was finally achieved in 1949 by Mayer, Haxel, Suess and Jensen who independently showed that the inclusion of a spin-orbit potential could give rise to the observed gaps between the shells [3, 4]. Simultaneously all these special numbers - renamed "magic numbers" - as well as a vast amount of nuclear properties on nuclei reachable at that time, e.g. spins, magnetic moments, isomeric states, and β -decay systematics could then be explained. This discovery opened the path to great progress in the understanding of nuclear structure and these magic numbers were the cornerstones for future theoretical developments in nuclear physics. The permanence of these nuclear magic numbers remained a dogma for several decades.

With the technical possibility of exploring nuclei with relatively large N/Z ratios, the persistence of these magic shells for nuclei far from stability was first examined for $N = 20$. Experimental results on mass, nuclear radius and spectroscopy obtained in the three last decades have shown

that the $N = 20$ gap in energy was quite fragile in nuclei far from stability [5, 6, 7, 8]. These combined results provided the first pieces of evidence that magic numbers were not immutable, and triggered a large number of experimental and theoretical work devoted to study the fate of the magic numbers far from the valley of stability.

Since then, many radioactive ion beam facilities have emerged worldwide and it is widely believed that magic numbers may evolve when extreme proton-to-neutron ratios are explored. The detailed location and magnitude of shell gaps in the neighborhood of the valley of stability have served to develop satisfactory mean-field models. However, these models diverge quickly far from stability, implying that some unknown degrees of freedom are required to describe the low-energy properties of the atomic nuclei.

The main purpose of the present manuscript is to review the major structural features along the isotonic and isotopic chains around the *spherical* magic numbers 8, 20, 28, 50, 82, and 126. Attempts to prove the existence of new magic numbers will also be commented on. A compilation of experimental results is presented on the following properties : (i) evolution of the binding energies of the two orbits bounding the spherical shell gaps, (ii) trends of first collective states of even-even semi-magic nuclei, (iii) characterization of single-nucleon states. Each section is devoted to one magic number, which potentially provides suitable constraints on the spin-orbit and tensor terms contained in the effective interactions used to describe the nuclei. The present compilation intends to lead to a better understanding of the action of nuclear forces in the nucleus and to provide experimental constraints to refine theoretical treatments. Henceforth better predictive power could be achieved throughout the whole nuclear chart, and in particular for the most neutron-rich isotopes which cannot be studied experimentally. In parallel, some of the major remaining experimental challenges arising while exploring the evolution of shell closures will be emphasized.

Foreword

All the experimental information on the excited states discussed in this review can be found in the ENSDF database [9], the references of the original work are not systematically given. The literature has been covered till March 2008. The adopted values of the reduced electric quadrupole transition probabilities $B(E2)$ are those tabulated in Ref. [11], but when a new value has been obtained recently, we refer explicitly to the last measurement. The experimental values of the atomic masses used to compute the nucleon separation energies come from the last atomic mass evaluation [10], except for a few cases explicitly reported in the text. The use of binding energy of the last nucleon as a single-particle energy is discussed in Sect. 11, which also contains the limitations of such a method.

2 Effective interactions between nucleons

Many nuclear structure models exist to describe the properties of the nucleus. One can ask why is there so many models rather than a unique one ? Reasons are both practical and phenomenological. From the practical point of view, the most fundamental approach, which would treat the nucleus as N interacting fermions by means of short-range forces, is often untractable. On the phenomenological side, the nucleus explores different degrees of freedom, ranging from the spherical magic, the deformed (axial, triaxial, pear-like) or cluster shapes, the one or two nucleon haloes, to the particle-unbound systems. It is an extremely changeable system, which is also making the field of nuclear structure so diverse and fascinating. But it is tempting and often wise to use models which are suitable to describe one or few of these observed phenomena.

As the present review is addressing the evolution of spherical shell closures, it implies that we shall focus on nuclei which are sitting at or in the vicinity of shell closures. Their presence is rooted in the approximation of the single-particle (SP) motion of nucleons in a mean-field potential and by the non-uniform distribution of single SP levels. But what makes shell closures to change? Several reasons can be invoked. First, while nucleons occupy various orbits, the interactions between them are changed according to the radial distribution, angular momentum and spin orientation of their orbits. The nuclear mean field and the SP level distribution are modified accordingly. In this spirit, the present review aims at identifying which properties of the nuclear forces can account for observed changes of shell closures. If done properly, better extrapolations to unknown regions of the chart of the nuclides can be proposed. Second, correlations of pairing or quadrupole type can weaken the robustness of spherical shell gaps. These many-body correlations drive the nucleus to deform, acting on top of SP energy changes. Third, for weakly bound nuclei, interactions between bound states, resonances and scattering states [12] can modify the spectroscopic properties of nuclei located close to drip-lines. Their effects could jeopardize extrapolations of nuclear properties far from stability (such as for the study of halo nuclei or for the astrophysical r-process), if neglected. Accents will be however put on the two first changes for which experimental data exist, i.e. the force-driven change of SP energies will constitute the body of the present manuscript and the mechanism to develop correlations will be outlined when encountered.

Three kinds of models could address the evolution of shell closures from nucleon-nucleon interactions (see for instance Fig. 1 of Ref. [13]). The most fundamental approach, the so-called *ab-initio* calculations, use *realistic* nucleon-nucleon (NN) forces derived from the results of the free nucleon-nucleon scatterings (such as Argonne v_{18} [14], CD-Bonn [15] and the recent soft interaction V_{lowk} [16]). As these calculations are very computationally demanding, they have kept pace with recent technological progresses. Despite this, the actual precision in describing nuclei with such two-body forces is still not fully satisfactory, pointing out to the need of three-body forces [17]. Also technical problems of convergence remain for nuclei with $A > 20$ (see for instance [18, 19]). Therefore, even if very promising, other approaches should be used at present in order to describe the evolution of shell structure over a wide range of atomic masses.

An alternative manner is to use a large-scale shell-model approach (for recent reviews, see Refs. [20, 21, 22]). Starting from a core nucleus with experimental SP energies, *effective* two-body interactions are used to describe the properties of nuclei in a given valence space. Note that in this model the NN interactions are effective, being different from the bare (or free) ones. This owes to the fact that, as the core is never completely inert, it contains some of the interactions. In addition the nucleons cannot scatter freely to states of the core which are already occupied by nucleons. These effective two-body forces are often derived from G-matrix calculations using realistic microscopic forces, with some empirical readjustments to experimental data (see for instance Fig. 7 of Ref. [20]). They can also be derived from experimental multiplet of states and/or from the evolution of binding energies. The two-body matrix elements (TBME) contain all the ingredients, such as the monopole and multipole energies, which affect the SP energies and the development of correlations, respectively. The monopoles can also be broken into central, spin-orbit and tensor forces, as for the bare NN forces. Doing so one can eventually derive from which of these terms the evolution of SP energy comes from. Even though a systematic comparison between the properties of the realistic and effective forces has not been done, it is seen in Ref. [23] that *some* of the monopole interactions obtained from V_{lowk} and the phenomenological ones used in the fp shell exhibit comparable strength and properties¹.

¹A notable exception arises for the neutron-neutron $V_{\ell j \ell j}$ matrix elements which, in the V_{lowk} approach, are

To model the evolution of nuclear structure in the whole chart of nuclides, the self-consistent mean-field calculations are more often employed. They use effective energy density functionals, the parameters of which are adjusted phenomenologically to reproduce many average nuclear properties like the total energy per nucleon, the size of the nuclei, the nuclear incompressibility... The most common non-relativistic ones are the Skyrme and the Gogny interactions. For recent reviews on non-relativistic and relativistic models, see Refs. [25, 26, 27, 28]). Despite the overall good description of the nuclear properties, two 'problems' remain. As many parametrizations are existing, this method is not yet universal. There is need to agree on parameters to be constrained to chosen experimental data. In addition, the link between *ab initio* calculations using realistic and effective nucleon-nucleon interactions is not yet reached. Therefore the sets of parameters of the effective forces, determined from the properties of known nuclei, will probably not be predictive anymore when applied to regions in which new components of the forces are involved. This explains the large divergence of predictions for unknown atomic masses using various forces. A last remark concern the tensor force. Even if it is intrinsically present in realistic interactions it was, until recently [29, 30, 31, 32, 33], not considered in the effective forces due to the complexity to implement it and the lack of experimental data to constrain it.

This section will introduce first the basic properties of the nuclear force that are required to understand the following parts which review all magic numbers from 8 to 126. Two major theoretical approaches to solve the nuclear many body problem, the mean field and the shell model, will be subsequently presented. The two-body matrix elements are the cornerstones of the shell model approach, which will be extensively used in this review. They govern the evolution of shells through their monopole part, whereas the onset of deformation is driven by the quadrupole correlations. Thus means to derive the monopole matrix elements from the experimental multiplet of states will be shown, followed by a description on how they modify the SP energies. Finally these monopoles are broken into central, spin-orbit and tensor terms. Their effects on the nuclear structure are presented in a qualitative manner for some examples.

2.1 *Properties of two-body forces in nuclear matter*

2.1.1 *Features of the nucleon-nucleon forces*

A brief summary of the most important features of the nucleon-nucleon interaction in nuclear matter are presented below. More details can be found in many textbooks, such as Refs. [34, 35, 36].

- The nuclear interaction is of short range, of the order of 1 fm. As the size of the nucleus scales with $R = r_0 A^{\frac{1}{3}}$, with $r_0 \simeq 1.1\text{-}1.3$ fm, it follows a saturation of the following nuclear properties : the binding energy per nucleon for nuclei with $A > 10$ is almost constant and barely exceeds 8 MeV, the nuclear density remains roughly constant at 0.16 (nucleon) fm^{-3} .
- The nearly identical spectra for mirror nuclei suggest that the nuclear force is 'charge symmetric' (i.e. the proton-proton and neutron-neutron interactions are equal).
- The spectra of nuclei forming isobar triplets indicate that the nuclear force is 'charge independent': It is the same for any pair of nucleons, irrespective of their charges ($\pi\pi$, $\nu\nu$, and $\pi\nu$), provided that they are in the same configuration.

much too small as compared to effective forces. This feature calls for the need of three-body forces, which has already been shown [24] when using realistic interactions such as the Kuo-Brown ones.

- Because of the Pauli principle, two like nucleons in the same orbit cannot have identical quantum numbers, so two-neutron or two-proton configurations only exist in the $S = 0$ total spin state, as a $S = 1$ state would imply that both nucleons have the same spin projection. Hence the 'charge independence' means that the nuclear force is the same for any pair of nucleons in the $S = 0$ total spin state. On the other hand, proton-neutron configurations can have $S = 1$. Moreover the nuclear force binds this $S = 1$ state to form the ground state of the deuteron, whereas the three other configurations with $S = 0$, $\pi\pi$, $\nu\nu$, and $\pi\nu$, are unbound. This feature implies that the nuclear interaction is 'spin dependent'.
- Other properties of the deuteron give important clues on the nuclear interaction. The values of the angular momentum and of the magnetic moment of its bound state indicate that, to a first approximation, the intrinsic spins of the two nucleons are parallel, without contribution from relative orbital angular momentum (i.e. $L = 0$, $S = 1$). However the non-zero quadrupole moment of the deuteron indicates that its ground state configuration should contain an $L = 2$, $S = 1$ admixture which amounts to about 5%. The fact that $L = 0$ is not a good quantum number for the deuteron implies that the nuclear interaction cannot be a pure *central* force, which depends only on the distance r between the nucleons, but also contains a *tensor* part, which depends on the relative orientation of the distance \vec{r} between the nucleons and their intrinsic spins.
- The nuclear interaction has a *spin-orbit* component. A decisive step in the development of the nuclear shell model was the recognition that the assumption of a relatively strong spin-orbit interaction in the nucleonic motion leads to a naturel explanation of the major shell closures at 28, 50, 82, and 126 [3, 4]. This component provokes a large splitting in energy between any two levels having the same orbital momentum ℓ with aligned or anti-aligned intrinsic spins. The 'aligned' configuration, $j \uparrow = (\ell + \frac{1}{2})$, is energetically favored, whereas the anti-aligned one, $j \downarrow = (\ell - \frac{1}{2})$, is at a higher energy. Later, the occurrence of polarization phenomena measured in the nucleon-nucleus scattering process has been a direct proof for the existence of the spin-orbit interaction, ascertaining both its sign and order of magnitude².

A general formulation of *two-body effective NN interactions* in terms of 'central' and 'non-central' (spin-orbit and tensor) forces is given in Sect. 2.4.1.

2.1.2 Some theoretical approaches used to solve the nuclear many-body problem

Soon after the discovery of the main spectroscopic properties, it was realized that a one-body mean-field potential, representing the average interaction of all the nucleons, can be used to model the atomic nucleus. One of the first proposed potential was that of an harmonic oscillator, complemented by a spin-orbit potential and an ℓ^2 term which correct the relatively steep behavior of the harmonic oscillator at the surface [37]. Nowadays self-consistent mean-field potentials provide a better description of the stable and far-off stability (or exotic) nuclei. The basic concept of transforming the many-body problem into a one-body one is briefly depicted below.

Taking only two-body forces into account, the Hamiltonian for A nucleons in interaction is a

²Part of the splitting in energy between spin-orbit partners originates in other terms of the bare $N - N$ interaction, this will be discussed in following sections

sum over the kinetic-energy terms $T(k)$ and the two-body nucleon-nucleon interaction $V(k, \ell)$,

$$H = \sum_{k=1}^A T(k) + \sum_{1=k<\ell}^A V(k, \ell) \quad (1)$$

An exact solution of such a many-body problem can rarely be obtained, except for the lightest masses [17]. Therefore the first step towards an approximate solution is to introduce a single-particle potential $U(k)$ by writing the Hamiltonian as :

$$H = \sum_{k=1}^A [T(k) + U(k)] + \left[\sum_{1=k<\ell}^A V(k, \ell) - \sum_{k=1}^A U(k) \right] = H^{(0)} + H^{(1)} \quad (2)$$

where $H^{(0)}$ describes an ensemble of independent particles moving in an effective average potential $U(k)$ and $H^{(1)}$ corresponds to the residual interactions. The very notion of a mean field is fulfilled when $H^{(1)}$ is small.

The mean field approach

Practically, calculations using a *realistic* two-body force for $V(k, \ell)$ in Eq. 2 are untractable. This was attributed to the hard-core part of the NN interaction [35]. Therefore the Hartree-Fock (HF) theory starts with a parameterized *effective* two-particle interaction $V(k, \ell)$ to derive the corresponding mean-field potential which can at best reproduce selected properties of the atomic nucleus. Results obtained with some effective forces widely used today, the Gogny and the Skyrme interactions, have been recently reviewed in Refs. [25, 26]. Similar Relativistic Mean Field (RMF) models are based on forces originating from the exchange of effective mesons between the nucleons [27, 28].

Although mean-field theories start from effective interactions which are not directly connected to 'bare' NN interactions, they are very helpful to understand some phenomenological aspects of the nuclear structure. In the following we consider the SO part of the interaction. Starting from a Skyrme interaction, it can be shown that the two-body SO interaction leads to one-body SO potentials for neutrons and protons, $V_{ls}^n(r)$ and $V_{ls}^p(r)$, respectively, which scale with the derivative of the neutron $\rho_n(r)$ and proton $\rho_p(r)$ densities as [38]:

$$V_{ls}^n(r) \propto \frac{1}{r} \frac{\delta}{\delta r} [2\rho_n(r) + \rho_p(r)] \vec{\ell} \cdot \vec{s}, \quad (3)$$

$$V_{ls}^p(r) \propto \frac{1}{r} \frac{\delta}{\delta r} [\rho_n(r) + 2\rho_p(r)] \vec{\ell} \cdot \vec{s}, \quad (4)$$

These definitions contain a weighting factor in front of the proton or neutron densities which is twice as large when applied to like particles. In particular, it follows that any change of neutron density influences more the neutron SO splitting than the proton density does. For some parametrisations of Skyrme interaction as well as for relativistic mean field descriptions, equal weightings between like and unlike particles are used. This in particular relates to the iso-vector part of the SO interaction, the intensity of which is very small in the RMF approaches. Experimental data are required to justify the choice of these weight factors. Anyhow, the SO interaction provokes a large splitting in energy between any two levels having the same orbital momentum ℓ with aligned or anti-aligned intrinsic spins, as shown in the upper part of Fig. 1. As the SO interaction scales with the derivative of the nucleon densities, it is believed to be peaked at the surface where this derivative is maximum. It naturally follows that, with the advent of new

radioactive ion beams facilities, searches for possible reductions of the SO interaction have been oriented to very neutron-rich atomic nuclei where the surface is more diffuse and the derivative of the nuclear density is weaker [39]. So far these attempts were not conclusive enough, as the effect is substantial only for large N/Z nuclei.

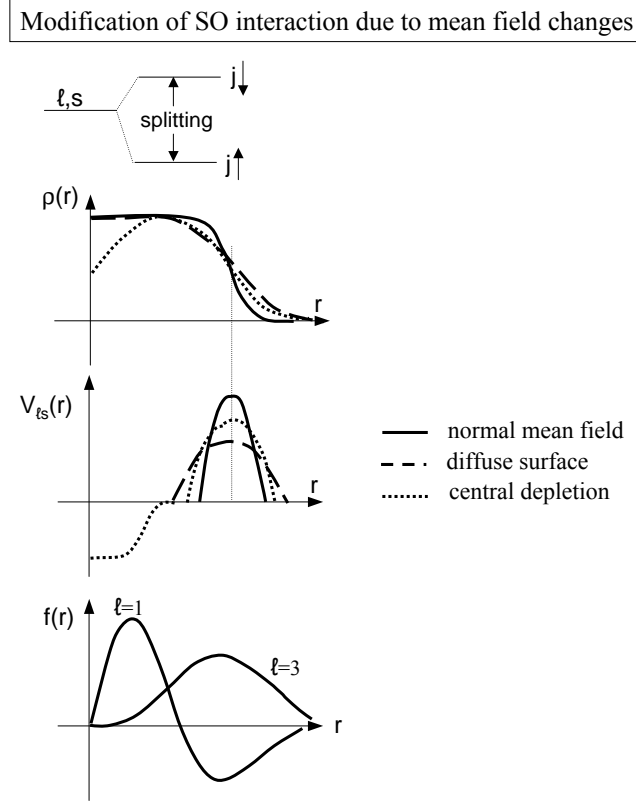


Figure 1: Schematic illustration showing the effect of a modification of the nucleon density $\rho(r)$ on the SO potential $V_{\ell s}(r)$. The graph on the first row shows various density distributions for nuclei exhibiting a standard value (full line), a diffuse surface (dashed line), and a central density depletion (dotted line). On the second row, the corresponding $V_{\ell s}(r)$ profiles are shown. The last row shows examples of $\ell = 1$ and $\ell = 3$ radial wave functions in order to judge how they could be influenced by surface or central density changes.

It should be noted that a depletion of the density at the center of the nucleus should also induce a reduction of the SO splitting for the nucleons in vicinity. The derivative of the density in the interior of the nucleus is of the opposite sign to the one obtained at the surface. It follows a global reduction of the SO interaction for nucleons located in the center. As the centrifugal barrier prevents nucleons of high orbital momentum ℓ to reside there, such a reduction of the SO splitting would be seen for the lowest ℓ -values, i.e. mainly for $\ell=1$ (p states). The reduction of the $\nu p_{1/2} - \nu p_{3/2}$ SO splitting as $s_{1/2}$ protons are removed from the interior of the nucleus is taken as an illustrative example of this phenomenon in Sect. 5.1.5.

Pictorial descriptions of the aforementioned mean-field effects which modify the strength of the SO interaction are given in Fig. 1. Such changes appear in a self-consistent manner in the mean-field description, as soon as the densities are modified. As will be discussed in Sect. 2.4,

additional modifications of the *SOsplitting* are also expected from the tensor interaction³. This points to the fact that, if a reduced *SOsplitting* is found, this does not necessarily imply a change of the SO one-body potential in the terms depicted here.

The Shell-model approach

In the interacting shell-model (SM) approaches (see for instance [20, 21, 22]), the spherical mean field produced by the closed core -the $H^{(0)}$ part- is a standard phenomenological single-particle potential given by an harmonic oscillator. Configuration mixings between all valence nucleons outside the core -interacting through the $H^{(1)}$ part- are taken into account for describing nuclei in a given model space. For the large-scale SM calculations, the effective interactions can be derived from the free NN interaction (various ways can be found in [40]), i.e. the so-called *realistic interactions*. They can also be obtained in a more phenomenological manner, combining results from the free NN interaction and from fits on selected experimental data [20, 21, 22].

The numerical values of some two-body matrix elements (TBME) of the *effective NN forces* can be directly determined from the experimental data, as described in the following section. The sets of TBME can be subsequently decomposed into multipole expansion, monopole, dipole, quadrupole, ... (the formula are given in Ref. [41]). The monopole part implicitly contains central, spin-orbit and tensor terms, the intensity of which are discussed in Sect. 2.4.

2.2 Two-Body Matrix Elements and determination of monopole interaction

The Hamiltonian of a nucleus formed by an inert core and two orbiting nucleons in the valence shells can be split into two parts, $H = H_{core} + H_{12}$. Using the same notations as those of Eq. 2,

$$H_{core} = \sum_{k=3}^A [T(k) + U(k)] + \left[\sum_{3=k<\ell}^A V(k, \ell) - \sum_{k=3}^A U(k) \right], \quad (5)$$

$$H_{12} = \sum_{k=1}^2 [T(k) + U(k)] + \left[\sum_{k=1}^2 \sum_{\ell=3}^A V(k, \ell) + V(1, 2) - \sum_{k=1}^2 U(k) \right], \quad (6)$$

H_{core} refers to the interactions between the core particles (labeled by $k = 3, \dots, A$). H_{12} describes the contribution from the two additional particles. It can be written in the following way, $H_{12} = H_{12}^{(0)} + H_{12}^{(1)}$ where $H_{12}^{(0)} = [T(1) + U(1)] + [T(2) + U(2)]$ comprises the single-particle kinetic and potential energies felt by particles 1 and 2 while $H_{12}^{(1)}$ denoted the residual interaction,

$$H_{12}^{(1)} = \left[\sum_{\ell=3}^A V(1, \ell) - U(1) \right] + \left[\sum_{\ell=3}^A V(2, \ell) - U(2) \right] + V(1, 2). \quad (7)$$

These equations hold for any average field $U(k)$. By choosing $U(k) = \sum_{\ell=3}^A V(k, \ell)$, it follows that

$$H_{12}^{(1)} = V(1, 2). \quad (8)$$

since only the two-particle term $V(1, 2)$ remains in Eq. 7. In other words, information on the properties of the NN interaction, $V(k, \ell)$, can in principle be obtained by analyzing the contribution of the two particles to the total energy of nuclei composed by an *inert core plus 2 nucleons*. The same arguments can be applied to other nuclei, provided that their corresponding cores are inert enough to isolate the contribution of the two valence particles. In the following section typical examples showing how to extract these TBME are given.

³Several attempts have been recently made to include tensor terms in mean-field approaches [29, 30, 31, 32, 33]

2.2.1 TBME from multiplet of states in odd-odd nuclei and monopole interaction

As an example for determining $\pi - \nu$ matrix elements, we consider the $(Z + 1, N + 1)$ odd-odd nucleus formed by the (Z, N) core and two extra nucleons located in the j_π and j_ν orbits respectively ⁴. An empirical eigenvalue of the truncated Hamiltonian, $H_{core} + H_{12}^{(0)}$, (i.e. without residual interaction) is given by $M_{free}c^2$, with

$$M_{free}(Z + 1, N + 1) = M(Z, N) + M_\pi + M_\nu \quad (9)$$

The contributions of the two extra nucleons, M_π and M_ν , are added free of any interaction to the measured mass $M(Z, N)$ of the even-even core. The M_π and M_ν terms are determined from the odd-A neighboring nuclei as,

$$M_\pi = M(Z + 1, N) - M(Z, N), \quad M_\nu = M(Z, N + 1) - M(Z, N). \quad (10)$$

The empirical value $M_{free}(Z + 1, N + 1)$ differs from the measured mass of the odd-odd nucleus $M_{exp}(Z + 1, N + 1)$ because of the residual interaction provided by $H_{12}^{(1)}$ (or $V(1,2)$, see Eq. 8) between the two added particles.

The left part of Fig. 2 illustrates how the TBME arising from the $\pi d_{3/2} - \nu f_{7/2}$ interaction in the case of $^{38}_{17}\text{Cl}_{21}$ are extracted. Starting from the binding energy of the closed-shell core, $^{36}_{16}\text{S}_{20}$, one adds successively contributions of the odd $\pi d_{3/2}$ and $\nu f_{7/2}$ particles, the binding energies of which are derived from the ^{37}Cl and ^{37}S nuclei, respectively. When applying this method we obtain a value denoted $^{38}\text{Cl}(\text{free})$. It is less bound by 1804 keV than the measured ground state, $^{38}\text{Cl}(\text{exp})$. The experimental ^{38}Cl spectrum contain several states, with spin values ranging from $J = |j_\pi - j_\nu| = 2$ (the ground state) to $J = j_\pi + j_\nu = 5$, originating from the $\pi d_{3/2} - \nu f_{7/2}$ configuration. Hence the $\pi - \nu$ residual interaction lifts the degeneracy in energy of the multiplet of J states, in addition to provide a *global* gain of binding energy.

The values of the TBME, $E_J(j_\pi, j_\nu)$, for ^{38}Cl are reported as a function of J in the left part of Fig. 3. In this case of two particles (pp interaction⁵), the interaction is attractive and the TBME values are negative. The largest amounts to -1804 keV for 2^- state, whereas the smallest is -493 keV for the 4^- one. The dashed line drawn in this figure shows the mean energy of the two-particle interaction, $V_{j_\pi j_\nu}^{pn}$, averaged over the relative orientations, J , of the orbits. In this procedure, each E_J is weighted by its $(2J + 1)$ degeneracy, that is the number of magnetic sub-states:

$$V_{j_\pi j_\nu}^{pn} = \frac{\sum (2J + 1) \times E_J(j_\pi, j_\nu)}{\sum (2J + 1)}. \quad (11)$$

This mean energy corresponds to a certain proton-neutron interaction, the so-called *monopole* term. It does not depend on the J value anymore, and can be written as $V_{d_{3/2}f_{7/2}}^{pn}$ in the present case.

The monopole term corresponds to the mean energy brought to the nucleus by the addition of two interacting nucleons, irrespective of the relative orientation of their orbits. It contains the fundamental properties of the NN interactions which influence the evolution of shells closures [42], as described in Sect. 2.3. Noteworthy is the fact that for the two extreme values of J , corresponding to states in which the two nucleon orbits are coplanar (here, $J = 5$ when j_π and j_ν have the same

⁴Another example using a $(Z - 1, N + 1)$ odd-odd nucleus will be given later. This procedure can be generalized to any system comprising a core \pm one neutron \pm one proton.

⁵To avoid possible confusion of particle-particle interaction with proton-proton interaction, we use the following notations, p stands for particle and π for proton.

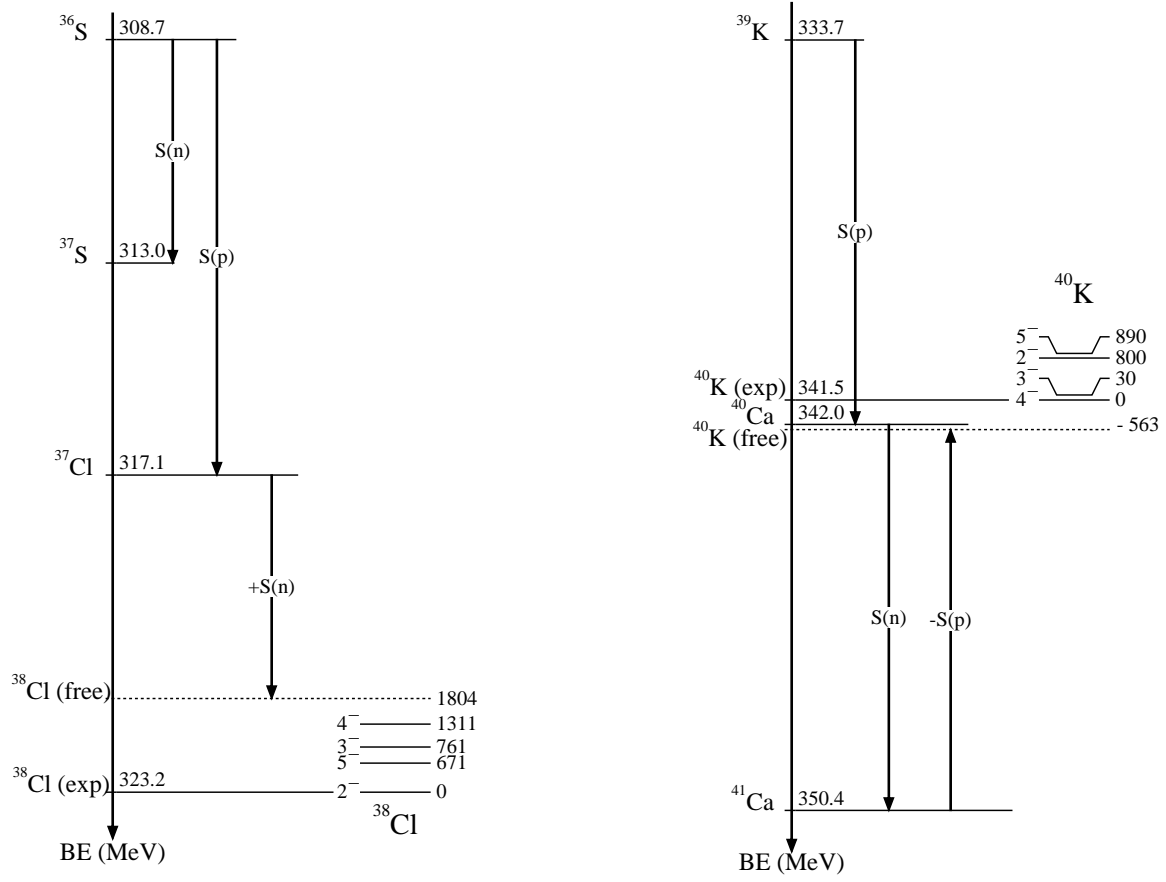


Figure 2: Pictorial illustration of the empirical $\pi - \nu$ interaction energies in two cases, the $(\pi d_{3/2})^{+1}(\nu f_{7/2})^{+1}$ configuration in $^{38}_{17}\text{Cl}_{21}$ starting from the $^{36}_{16}\text{S}_{20}$ closed-shell core (left) and the $(\pi d_{3/2})^{-1}(\nu f_{7/2})^{+1}$ configuration in $^{40}_{19}\text{K}_{21}$ from the $^{40}_{20}\text{Ca}_{20}$ closed-shell core (right).

direction and $J = 2$ when j_π and j_ν have opposite directions), the gain in energy exceeds that of the sole monopole. Conversely, when nucleons are orbiting orthogonal to each other, their TBME is the weakest. This J -dependent part of the two-body matrix elements is contained in the multipole components (dipole, quadrupole, ...). The method of decomposition is given in Ref. [41]. It is important to note that the quadrupole term usually has, after the monopole, the highest amplitude and it is responsible for the parabolic behavior of $E_J(j_\pi, j_\nu)$ as a function of J .

A similar procedure can be applied to determine the same monopole interaction from a $(Z - 1, N + 1)$ odd-odd nucleus formed by a (Z, N) core, one proton hole in the j_π orbit and one neutron particle in the j_ν orbit. The right part of Fig. 2 shows the case of $^{40}_{19}\text{K}_{21}$. Starting from the binding energy of the closed-shell core $^{40}_{20}\text{Ca}_{20}$, adding the contribution of the $\nu f_{7/2}$ particle neutron from ^{41}Ca and subtracting the one of the $\pi d_{3/2}^{-1}$ hole proton from ^{39}K , we obtain the value denoted $^{40}\text{K}(\text{free})$. Owing to the $\pi - \nu$ interaction, the ^{40}K states are found to be less bound by a quantity varying from 563 keV for the 4^- state to 1443 keV ($=563 + 890$) for the 5^- state. Here, the residual interaction between one particle and one hole (ph) is mainly repulsive. The values of the two-body matrix elements, $E_J(j_\pi, j_\nu)$, are positive for the ph configuration (as shown in Fig. 3).

In summary, the TBME of the $\pi d_{3/2} - \nu f_{7/2}$ interaction were determined from the pp and ph configurations in the $^{38}_{17}\text{Cl}_{21}$ and $^{40}_{19}\text{K}_{21}$ nuclei. It is interesting to compare the values derived in

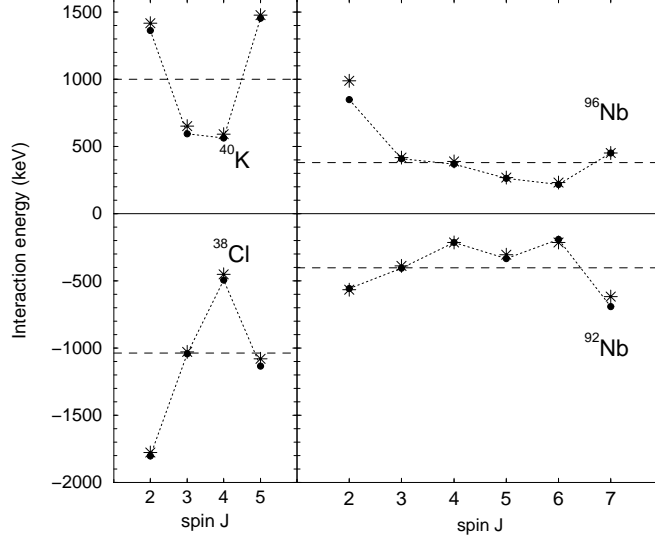


Figure 3: Empirical interaction energy in two configurations as a function of angular momentum: $\pi d_{3/2}\nu f_{7/2}$ extracted from the level schemes of $^{38}_{17}\text{Cl}_{21}$ (pp excitation) and $^{40}_{19}\text{K}_{21}$ (ph excitation), $\pi g_{9/2}\nu d_{5/2}$ from $^{92}_{41}\text{Nb}_{51}$ (pp) and $^{96}_{41}\text{Nb}_{55}$ (ph). The results of the Pandya transformation of the four experimental sets (filled circles) are drawn with stars. The dashed lines indicate the values of the monopole contribution to the interaction energies of each configuration.

both cases. Using the so-called Pandya transformation [41, 36] the pp matrix elements can be converted into ph ones, and vice-versa. The result of these transformations are indicated by stars in Fig. 3, whereas the experimental points are shown as the filled circles. The very good agreement between the TBME extracted from the pp or ph configurations ascertains the reliability of the procedure, i.e. both ^{36}S and ^{40}Ca can be considered as good cores.

The same procedure has been applied to the $\pi g_{9/2} - \nu d_{5/2}$ interaction, using experimental results of $^{92}_{41}\text{Nb}_{51}$ (pp configuration) and $^{96}_{41}\text{Nb}_{55}$ (ph configuration). Similar agreement is obtained using the Pandya transformation. The only exception is for the 2^+ state of ^{96}Nb whose energy would be expected 150 keV higher than that measured. This state is likely to be mixed to nearby 2^+ state of another configurations, leading to a decrease of its excitation energy.

2.2.2 Monopole interaction from double difference of binding energies

The method depicted in the previous paragraph is extremely powerful to determine both the monopole and the other multipole terms. However it requires that all the J values of $E_J(j_\pi, j_\nu)$ are experimentally known, which is seldom the case. An alternative way to determine the monopole term is to use differences in binding energies between neighboring nuclei.

Let us consider an inert core of closed shells, the (Z, N) nucleus, and its three neighbors, the $(Z + 1, N)$, $(Z, N + 2)$, and $(Z + 1, N + 2)$ nuclei. The difference in the binding energies of the $(Z + 1, N)$ nucleus and the core is due to the interaction of the added proton with the core. In the same manner, the difference in the binding energies of the $(Z, N + 2)$ nucleus and the core is due to the interaction of the two added neutrons with the core. Lastly, the difference in the binding energies of the $(Z + 1, N + 2)$ nucleus and the core is due to three terms, the interactions of the

extra proton with the core, of the two extra neutrons with the core, and of the extra proton with the two extra neutrons. Therefore the interaction of the extra proton and two neutrons, V^{1p-2n} , is given by the differences,

$$V^{1p-2n} = [BE(Z+1, N+2) - BE(Z, N)] - [BE(Z+1, N) - BE(Z, N)] - [BE(Z, N+2) - BE(Z, N)] \quad (12)$$

$$= [BE(Z+1, N+2) - BE(Z, N+2)] - [BE(Z+1, N) - BE(Z, N)] \quad (13)$$

Assuming that the proton and the two neutrons occupy the j_π and j_ν single-particle orbits, respectively, we obtain formally

$$V^{1p-2n} = 2 V_{j_\pi j_\nu}^{pn}, \quad (14)$$

where $V_{j_\pi j_\nu}^{pn}$ is the same as in Eq. 11. Indeed all the nuclei involved in Eq. 12 have an even number of neutrons. Therefore the single proton interacts with paired neutrons without any privileged axis, meaning that the V^{1p-2n} value is implicitly averaged on all the possible orientations.

This method is applied in the case of the odd- Z $_{41}\text{Nb}$ isotopes for $N = 50-56$. The experimental binding energies of the last proton, located in the $\pi g_{9/2}$ orbit, display an almost constant decrease as a function of the number of neutrons filling the $\nu d_{5/2}$ orbit (see the left part of Fig. 4). The values of the proton-neutron interaction extracted from the slopes of these binding energies, which amount to ~ -400 keV, are given in the middle part of Fig. 4. As previously mentioned, the multiplet of the $\pi g_{9/2} \nu d_{5/2}$ states observed in the odd-odd ^{92}Nb provided a monopole value as well, and is given in the right part of Fig. 4. The two methods compare reasonably well.

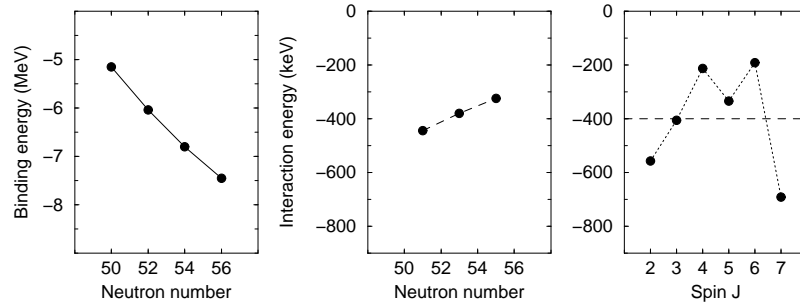


Figure 4: **Left** : Experimental binding energies of the $\pi g_{9/2}$ orbit in the odd- A $_{41}\text{Nb}$ isotopes as a function of neutron number. **Middle** : Mean proton-neutron interaction extracted from the slopes of the proton binding energies. **Right** : Monopole interaction $V_{g_{9/2}d_{5/2}}^{pn}$ (dashed line) from the multiplet of states in ^{92}Nb (see caption of Fig. 3 for details).

This example illustrates the fact that the monopole term $V_{g_{9/2}d_{5/2}}^{pn}$ can be obtained from the shift of the 'experimental' single-proton energy, provided that it displays a quasi-linear behavior for the whole interval of the $\nu d_{5/2}$ filling, from $N = 50$ to $N = 56$. Deviations to the linear trend are seen by the slight variation of the monopole values drawn in the middle part of Fig. 4. It is seen from this example that the evolution of single-particle levels and subsequently of shell gaps are, to a first order, governed by monopole interactions. This feature is discussed in more details in the next sections.

2.3 Properties of the monopole interaction

2.3.1 Effects of the monopole interaction

Case of unlike nucleons

The forthcoming discussion illustrates the effects of monopole proton-neutron interactions to modify two neutron binding energies, ϵ_{n1} and ϵ_{n2} , due to the addition of protons in two successive shells. In this example, the value of the monopole $V_{j_{p1}j_{n2}}^{pn}$ is chosen to be significantly more attractive than the three others, $V_{j_{p1}j_{n1}}^{pn} \simeq V_{j_{p2}j_{n1}}^{pn} \simeq V_{j_{p2}j_{n2}}^{pn}$.

Within the Shell-Model approach, the monopole interaction induces a shift of the effective *spherical* single-particle energy (ESPE), ϵ_{ni} , of the neutron orbits ni, j_{ni}, ℓ_{ni} by the mean field generated by protons added to an inert core Z_{core} . Starting from the energy ϵ_{n1} of a potentially occupied state j_{n1} , the variation of ESPE is linear with the monopole proton-neutron interaction $V_{j_{p1}j_{n1}}^{pn}$ when x protons occupy the j_{p1} orbit ($0 < x < 2j_{p1} + 1$) :

$$\Delta\epsilon_{n1} = x V_{j_{p1}j_{n1}}^{pn} \quad (15)$$

The same relation applies to the variation of ϵ_{n1} during the filling of the j_{p2} orbit, as well as the variation of ϵ_{n2} as protons are added in the j_{p1} and j_{p2} orbits (see the schematic view in Fig. 5). From the trends of ESPE, the variation of the neutron gap between Z_{core} and Z_{p1} can be expressed as the difference of the involved monopoles:

$$\Delta(GAP) = (2j_{p1} + 1) (V_{j_{p1}j_{n2}}^{pn} - V_{j_{p1}j_{n1}}^{pn}) \quad (16)$$

As exemplified in Fig. 5, the neutron gap is weakened between Z_{core} and Z_{p1} and remains constant

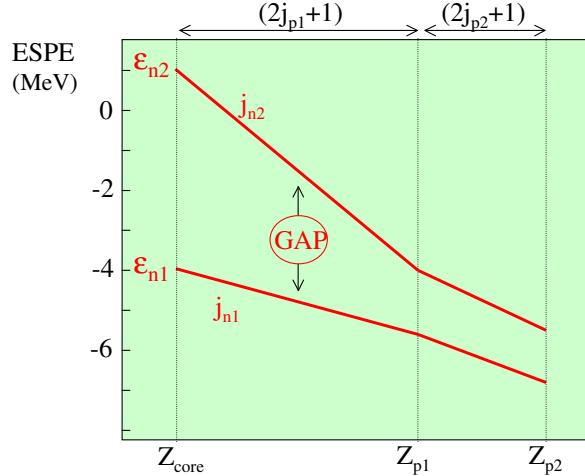


Figure 5: Evolution of effective spherical single-particle energy (ESPE) of two neutron states $n1$ and $n2$ due to the addition of protons in the j_{p1} and j_{p2} shells. Starting from energies ϵ_{n1} and ϵ_{n2} of the core nucleus Z_{core} , the monopole interactions involved while filling the j_{p1} orbit give rise to a steep increase of binding energy of ϵ_{n2} and a large reduction of the neutron gap 'GAP'.

later. These features arise from the fact that the monopole $V_{j_{p1}j_{n2}}^{pn}$ has been chosen to be significantly more attractive than the three others. The presence of one dominating monopole term

compared to many others with a small intensity, is widespread throughout the chart of nuclides. It arises in particular in the $N = 20$ isotones, where $V_{d_{3/2}d_{5/2}}^{pn}$ is significantly larger than any other monopole in the sd valence space (this is discussed in Sect. 4.1.3).

When the 'experimental' binding energies (BE) display a linear behavior for a wide interval, the corresponding monopole matrix elements can be derived from the slopes of the experimental BE as shown in Fig. 4. The analysis of the binding energies of the last proton (neutron) in semi-magic nuclei will be largely used in this paper to pin down the role of the residual interactions, particularly those dealing with certain specific proton-neutron configurations only available in exotic nuclei. However we should bear in mind the following points:

- Any observed curvature in the experimental BE trend indicates that either the core nucleus cannot be considered as inert anymore or/and that mixing between added nucleons is present. In particular when several orbits are close in energy, they are filled together because of the pairing correlations between them. Then the evolution of ESPE arises from an averaged monopole interactions of the degenerate orbits, weighted by their occupation number.
- This representation in term of ESPE provides an oversimplified view of the global evolution of nuclear shells due to NN interactions. In the relativistic and non-relativistic mean-field (MF) approaches a progressive re-arrangement of the mean field potential occurs. Therefore direct comparison between ESPE derived from the shell model approach and the trends on binding energy obtained with MF calculations cannot be made in a straightforward way.

Case of like nucleons

Before closing this section we need to add a few remarks on the strength of monopoles between *like* nucleons, and on how they modify the shell gaps. The major difference with the interaction between *unlike* nucleons is a consequence of the Pauli principle and the antisymmetrisation of the two-nucleon wave function, which requires the space-spin part of the wave function to be antisymmetric.

When the two *like* nucleons occupy the same orbit j , the only allowed J states are those with even values, $J = 0, 2, 4, \dots (2j - 1)$. Conversely the wave functions with odd values of J ($1, 3, 5, \dots 2j$), which are allowed for two *unlike* nucleons, have a symmetric space-spin part. As an example, the case of two nucleons in the $g_{9/2}$ orbit is shown in the left part of Fig. 6. Their interaction energies as a function of J have been extracted from $^{90}_{41}\text{Nb}_{49}$, $^{92}_{42}\text{Mo}$ and $^{88}_{40}\text{Zr}_{48}$, using the relations given in Sect. 2.2.1. The interaction energies obtained for the even J values are very similar irrespective of the nucleons concerned, $\pi\pi$, $\nu\nu$ or $\pi\nu$. In particular a very favored configuration corresponds to the pairing situation $J_{min} = 0$: Here, nucleons move in opposite directions in coplanar orbits. Another very favored configuration corresponds to $J_{max} = 9$, such a total J value can be only obtained when the two nucleons have exactly the same quantum numbers (classically, they move in the same direction in coplanar orbits). As mentioned above, such a situation is only allowed for *unlike* nucleons.

As shown in the left part of Fig. 6, there is a large difference in the interaction energies for the high- J values, the odd ones displaying a larger attraction. This is also a consequence of the Pauli principle. To attain a high- J value, the two j momenta have to be close in direction, this implies nearly coplanar orbits in which the two nucleons orbit in the same direction. The condition of an antisymmetric space-spin wave function for *even* J can be viewed classically as a rotation out of phase, so the two nucleons always remain at large distance and have a very weak interaction [43].

The major consequence of the Pauli principle in this context is that the monopole interaction between *like* particles is about two times weaker than those between *unlike* particles, as shown in

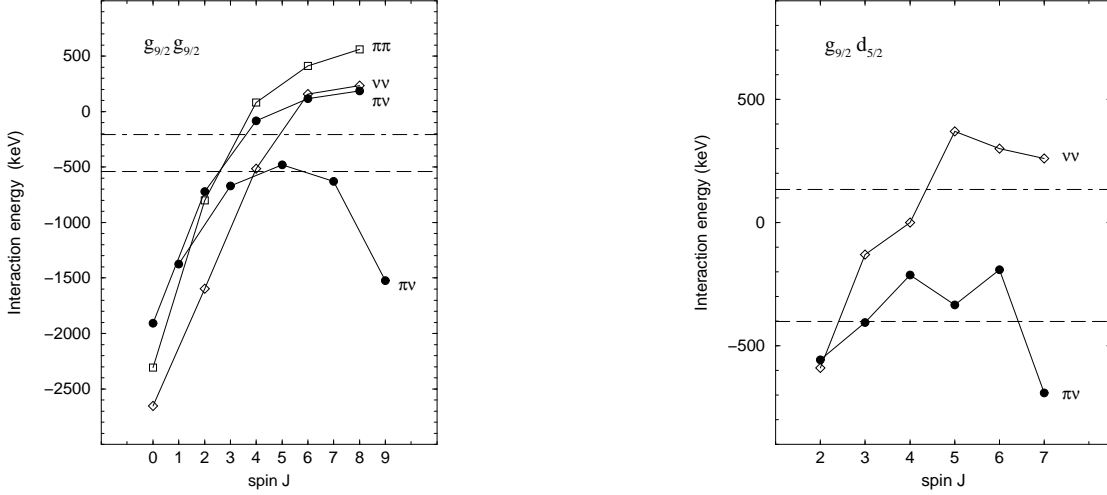


Figure 6: Empirical interaction energy between two nucleons in the same orbit (left) and in two different orbits (right). For the $g_{9/2}^2$ case, results for the three configurations are presented, $\pi\pi$ from $^{92}_{42}\text{Mo}$, $\nu\nu$ from $^{88}_{48}\text{Zr}$ and $\pi\nu$ from $^{90}_{41}\text{Nb}$. For the $g_{9/2}d_{5/2}$ case, the $\pi\nu$ results come from $^{92}_{41}\text{Nb}$ and the $\nu\nu$ ones from $^{90}_{50}\text{Zr}$. The dashed line indicate the monopole energy obtained for the *unlike* nucleons and the dashed-dotted line, the one for *like* nucleons.

the case of two interacting nucleons in $g_{9/2}$ orbit (dashed and the dashed-dotted lines in the left part of Fig. 6).

The right part of Fig. 6 displays another case, the interaction energies between two particles occupying two different orbits, $g_{9/2}$ and $d_{5/2}$. The interaction energies for $\pi\nu$ configuration come from $^{92}_{41}\text{Nb}$ and those for the $\nu\nu$ configuration from excited states of $^{90}_{50}\text{Zr}$ [44]. Whereas the interaction between the two *unlike* particles is attractive for all spin values, resulting in a monopole value of -400 keV (see the dashed line in the right part of Fig. 6), the other one is mainly repulsive with a positive monopole value of 130 keV (see the dashed-dotted line).

Even if weaker in strength, the monopole terms between *like nucleons* may play an important role to modify the shell gaps. To give a first example, the gap between the $\nu f_{7/2}$ and $\nu p_{3/2}$ orbits strongly increases from $N = 20$ to $N = 28$, i.e. during the filling of the $\nu f_{7/2}$ shell. The single-particle states of $^{41,49}\text{Ca}$ have been thoroughly studied using (\vec{d}, p) reactions [45, 46], with the observation of the whole strength of the fp shells. The obtained results are shown in the left part of Fig. 7. The behaviors of the four single-particle states during the filling of the $\nu f_{7/2}$ shell are those expected from the effect of the monopole interactions, which are attractive between two *like* nucleons in the same orbit and repulsive for two *like* nucleons in different orbits, as mentioned above. Using the experimental binding energies displayed in the left part of Fig. 7, one obtains $V_{f_{7/2}f_{7/2}}^{nn} \sim -230$ keV, $V_{f_{7/2}p_{3/2}}^{nn} \sim +160$ keV, $V_{f_{7/2}p_{1/2}}^{nn} \sim +170$ keV, and $V_{f_{7/2}f_{5/2}}^{nn} \sim +20$ keV, values close to the ones extracted from the effective TBME used in the fp valence space. As a consequence, the $N = 28$ gap increases by ~ 3 MeV, making ^{48}Ca a doubly-magic nucleus. It also leads to a large change in the SO splitting of the νf orbits from $N = 20$ to $N = 28$.

The appearance of the $N = 14$ gap between the $\nu d_{5/2}$ and $\nu s_{1/2}$ orbits in $^{22}\text{O}_{14}$ has a similar origin. While they are very close in energy at $N = 8$ (see the right part of Fig. 7), the addition of six neutrons in the $\nu d_{5/2}$ orbit leads to a new shell gap of about 4.4 MeV (this will be discussed

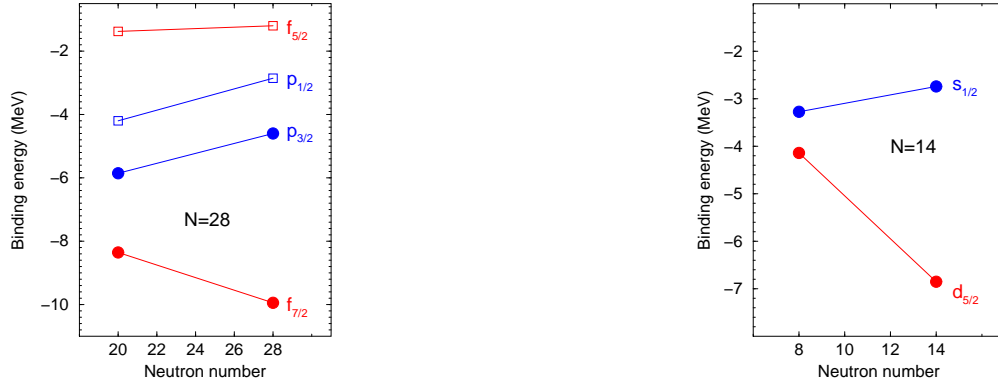


Figure 7: **Left:** Experimental binding energies of the neutron fp orbits in Ca isotopes, at the beginning and at the end of the $\nu f_{7/2}$ shell filling. The straight lines display the evolution expected from the effect of the monopole interactions (as depicted in Fig. 5). **Right:** Experimental binding energies of the $\nu d_{5/2}$ and $\nu s_{1/2}$ orbits in O isotopes, at the beginning and at the end of the $\nu d_{5/2}$ filling.

in Sects. 3.2.2 and 3.2.3). Using the experimental binding energies displayed in the right part of Fig. 7, one obtains $V_{d_{5/2}d_{5/2}}^{nn} \sim -540$ keV and $V_{d_{5/2}s_{1/2}}^{nn} \sim +90$ keV.

Finally it is important to note that SM calculations using two-body *realistic* interactions derived from the free NN force fail to reproduce some shell closures. As was already mentioned for the *ab-initio* calculations (see Sect. 2.1.1), the three-body forces have to be taken into account. Thus many of the previously observed discrepancies are now solved [24, 22].

2.3.2 Strength of the monopole interaction

Many TBME values were determined throughout the periodic table thirty years ago from the experimental data available at that time [47]. Using the latest experimental results in odd-odd exotic nuclei, and the AME2003 atomic mass evaluation [10], we propose new monopole values of various *proton-neutron* configurations [48]. These are displayed as a function of mass number in Fig. 8. The most obvious feature is that the monopole energy of the two-body proton-neutron interaction strongly decreases with the mass number, from ~ -1 MeV for $A = 30$ to ~ -300 keV for $A = 210$. Therefore the effects of the monopole interactions to modify shell gaps, if any, are expected to be more sudden in the light-mass nuclei.

In many Shell-Model calculations, the TBME values are assumed to scale with $A^{-1/3}$ (the two dashed-dotted lines in Fig. 8). Such a behavior is relevant when the mass range is not too large, which is the case in all the SM calculations which apply to restricted valence spaces. When examining a wider mass range, an $A^{-2/3}$ trend for the $V_{j_1j_2}^{pn}$ is more appropriate, as shown by the dashed line in Fig. 8. This latter scaling factor indicates that the strength of residual interactions varies inversely to the surface of the nucleus, consistent with the fact that the valence nucleons are mainly located at the nuclear surface.

In addition to this global trend, the empirical monopoles displayed in Fig. 8 clearly exhibit large spreading in strength for a given mass number. As seen around masses $A \simeq 30, 90$ and 200 , it amounts to about $\pm 30\%$ of the mean value. This could be accounted for by multiple properties of the specific proton and neutron configurations involved in the monopoles. This is borne out by the properties of the monopole interaction, which explore some specific parts of the NN interactions,

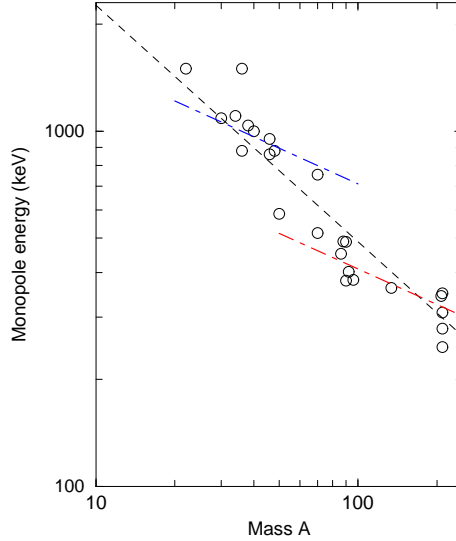


Figure 8: Absolute values of the proton-neutron monopole energies calculated from many multiplets identified in odd-odd nuclei, as a function of the mass number [48]. The dashed line is a fit performed within the total mass range, $V_{j_1 j_2}^{pn} \propto A^{-2/3}$, the two other ones (dashed-dotted lines) being $\propto A^{-1/3}$.

discussed in the following section.

The case of weakly bound systems or more generally of extreme isospin values is also to be discussed both for the like- and unlike-nucleon cases. While comparing V^{pp} and V^{nn} derived for weakly bound systems involving similar orbits, the Coulomb field should lead to a significant breaking of the charge independence of the NN interaction, giving rise to $V^{pp} \neq V^{nn}$. Generally speaking, the interaction with states in the continuum may change the value of the derived monopoles for weakly bound systems as they potentially contain interaction with unbound states of similar configurations. The monopole interaction V^{nn} extracted in weakly-bound neutron-rich nuclei should drop more steeply than the $A^{-2/3}$ factor. This is ascribed to the fact that the radius of the nucleus no longer scales with $A^{1/3}$, as a wide neutron cloud develops as the neutron binding energy decreases. Finally at extreme isospin values, protons and neutrons have considerably different binding energies, which reduces the overlap of their wave functions. This effect could lead to weaker V^{pn} monopole matrix elements.

2.4 Decomposition of the monopole interaction into central, spin-orbit and tensor parts

For most of the descriptions of the nucleus (except for the *ab-initio* calculations), two-body *phenomenological effective forces* are introduced (i) in MF approaches to describe the interaction of two nucleons in the presence of other nucleons, (ii) in the SM to describe the interaction of two nucleons added to a core nucleus from TBME. In both cases, the absolute values of the two-body effective interactions significantly differ from the 'bare' NN values. However reminiscent properties of the NN forces -such as those of the central, spin-orbit and tensor terms- prevail in the atomic nucleus, as witnessed by significant modifications of shell structure.

The present section first reviews the main general components of an effective NN force. Some

TBME derived from the study of atomic nuclei are split into these components, triggering comments on their respective amplitudes and their spin-dependence. Finally some examples on how nuclear shell gaps and SO splitting are affected are discussed qualitatively.

2.4.1 Formal description of the various components of the NN interaction

The more general potentials between two nucleons depend on three vector coordinates of the radius, spin and isospin as follows :

$$V(1, 2) = V(\vec{r}_1, \vec{\sigma}_1, \vec{\tau}_1; \vec{r}_2, \vec{\sigma}_2, \vec{\tau}_2). \quad (17)$$

Following the general prescription derived in Sect. 2.1.1, the nucleon-nucleon interaction can be expanded in two main parts which are 'central' and 'non-central'. The various components are written as a function of the coordinate combinations, provided that they fulfill the standard required symmetries.

Using the spin-isospin representation, the *central* interaction is decomposed in four terms,

$$V_c(1, 2) = V_0(r) + V_\sigma(r) \vec{\sigma}_1 \cdot \vec{\sigma}_2 + V_\tau(r) \vec{\tau}_1 \cdot \vec{\tau}_2 + V_{\sigma\tau}(r) \vec{\sigma}_1 \cdot \vec{\sigma}_2 \vec{\tau}_1 \cdot \vec{\tau}_2 \quad (18)$$

where $r = |\vec{r}_1 - \vec{r}_2|$ is the distance between the two nucleons.

The *non-central* interaction contains two terms,

(i) the two-body *spin-orbit* interaction given by

$$V_{LS}(1, 2) = \left(V_{LS}^{is}(r) + V_{LS}^{iv}(r) \vec{\tau}_1 \cdot \vec{\tau}_2 \right) \vec{L} \cdot \vec{S}, \quad (19)$$

where \vec{L} is the relative orbital momentum between the two interacting nucleons, \vec{S} is their total intrinsic spin, $\vec{S} = \frac{1}{2}(\vec{\sigma}_1 + \vec{\sigma}_2)$, and the superscript *is* and *iv* hold for iso-scalar and iso-vector part of the potential.

(ii) the *tensor* part defined by

$$V_T(1, 2) = \left(V_T^{is}(r) + V_T^{iv}(r) \vec{\tau}_1 \cdot \vec{\tau}_2 \right) S_{12}(r), \quad (20)$$

where

$$S_{12}(r) = \frac{3}{r^2} (\vec{\sigma}_1 \cdot \vec{r})(\vec{\sigma}_2 \cdot \vec{r}) - \vec{\sigma}_1 \cdot \vec{\sigma}_2 \quad (21)$$

An example of a realistic NN interaction comprising such components is the Argonne V18 interaction [14]. The eight functions of r , i.e. $V_0(r)$, $V_\sigma(r)$, $V_\tau(r)$, $V_{\sigma\tau}(r)$, $V_{LS}^{is,iv}(r)$ and $V_T^{is,iv}(r)$, are chosen according to the specific problem which is handled. Various radial functions can be used, such as $\delta(r)$ for contact interaction (zero range) or Gauss forms for finite-range interactions. All of them depend on a certain number of parameters which are adjusted to reproduce selected experimental data.

2.4.2 Selected examples of decomposition of Two Body Matrix Elements

The present part aims at a decomposition of the monopole interaction into the various components mentioned above, i.e. the *central*, *spin-orbit* and *tensor* parts in order to assess their possible effect on the shell evolution.

For this purpose a transformation from the *jj*-coupled representation, which holds for a direct comparison to experimental data where $J = |\vec{j}_\pi + \vec{j}_\nu|$, to the *LS*-coupled scheme has to be achieved.

In order to perform this decomposition, it is necessary to have a *whole set* of TBME available, i.e. all the J states of the *four* multiplet states dealing with the spin-orbit pairs ($j_\pi = \ell_\pi \pm \frac{1}{2}$ and $j_\nu = \ell_\nu \pm \frac{1}{2}$) have to be known⁶. This is by far not an easy task as it often requires the spectroscopy of very exotic nuclei. This is especially true for determining TBME in which a deeply bound proton ($j_\pi \uparrow$) interacts with a weakly bound neutron ($j_\nu \downarrow$).

Such decompositions have been achieved in constructing semi-empirical effective interactions in the $1s0d$ shell [49] and more recently, in the $0p$ [50] or $0p - 1s0d$ shells [51], and in the $sd - fp$ shells [52]. Typical results obtained from these sets⁷ are gathered in Table 1. They corroborate the general features of the proton-neutron interaction given in Sects. 2.1.1 and 2.4.1.

Table 1: Decomposition of monopole interactions (in MeV) into central, spin-orbit and tensor parts for some configurations involving spin-orbit partners.

		Total	Central			Spin-Orbit	Tensor
			tot	$S = 0$	$S = 1$		
case A Table IV of [50]	$\pi 0p_{3/2}\nu 0p_{1/2}$	-3.59	-3.47	(-0.10	-3.37)	+0.14	-0.26
	$\pi 0p_{1/2}\nu 0p_{1/2}$	-3.21	-4.30	(-0.33	-3.97)	+0.57	+0.53
	variation	+0.38	-0.83			+0.43	+0.79
B Ref. [51]	$\pi 0p_{3/2}\nu 1s_{1/2}$	-1.59	-1.52	(-0.03	-1.49)	-0.07	0.0
	$\pi 0p_{1/2}\nu 1s_{1/2}$	-1.38	-1.52	(-0.03	-1.49)	+0.14	0.0
	variation	+0.21	0.0			+0.21	
C Ref. [51]	$\pi 0d_{3/2}\nu 0d_{5/2}$	-1.88	-1.79	(-0.20	-1.59)	+0.01	-0.19
	$\pi 0d_{3/2}\nu 0d_{3/2}$	-1.68	-2.03	(-0.18	-1.85)	+0.07	+0.29
	variation	+0.20	-0.24			+0.06	+0.48
D Ref. [52]	$\pi 0d_{3/2}\nu 0f_{7/2}$	-1.27	-1.27	(-0.23	-1.04)	+0.22	-0.22
	$\pi 0d_{3/2}\nu 0f_{5/2}$	-0.99	-1.23	(-0.08	-1.15)	-0.05	+0.29
	variation	+0.28	+0.04			-0.27	+0.51
E Ref. [52]	$\pi 0d_{3/2}\nu 1p_{3/2}$	-0.93	-1.03	(-0.13	-0.90)	+0.16	-0.06
	$\pi 0d_{3/2}\nu 1p_{1/2}$	-0.91	-1.00	(-0.06	-0.94)	-0.03	+0.12
	variation	+0.02	+0.03			-0.19	+0.18

- Whatever the orbits, the strongest term of the monopoles comes from the *central* part , particularly the one corresponding to $S = 1$, the term responsible for the bound state of the deuteron. Moreover for configurations dealing with the same ℓ_π and ℓ_ν values (such as cases A and C), the central term is more attractive for $j_\pi = j_\nu$ than for $j_\pi = j_\nu \pm 1$.

⁶All the relations used to obtain the three components (central, spin-orbit and tensor terms) of the TBME can be found in Ref. [49].

⁷It has to be noted that some terms of these decompositions may be modified in the future if better experimental determinations of TBME arise from experimental data far from the valley of stability. Therefore this discussion may to some extent be not fully quantitative.

- Compared to the central part, the absolute values of the *spin-orbit* term are weaker. Nevertheless the differential value between spin-orbit partners is sometimes larger than the one obtained from the central part, e.g. cases B and E.
- *Tensor terms* are present both when identical as well as different ℓ_π and ℓ_ν values are involved. They amount to about 20% of the total monopole force in case D. In case B no tensor effect is present as no preferred spin-orientation could arise when a $s_{1/2}$ nucleon is involved.

The tensor term is repulsive (positive energies in the table) when the intrinsic spins are both aligned or both anti-aligned with the orbital momenta, and attractive (negative energies) otherwise. In particular, this counteracts the effect of the central part when $\ell_\pi = \ell_\nu$. For instance, while the central term of $V_{d_{3/2}d_{3/2}}$ is more attractive than the one of $V_{d_{3/2}d_{5/2}}$, its total monopole becomes less attractive because of the tensor term.

Within two $\pi\nu$ configurations dealing with spin-orbit partners -such as those presented in the table- the following identity (see Ref. [53])

$$(2j_\uparrow + 1) V_T(j', j_\uparrow) + (2j_\downarrow + 1) V_T(j', j_\downarrow) = 0 \quad (22)$$

can be derived from angular momenta algebra by summing all spin and orbital magnetic substates for a given ℓ . This sum rule is fulfilled, e.g. applied to the $d_{3/2} - p_{3/2}$ versus $d_{3/2} - p_{1/2}$ monopoles, it writes as $-0.06 \times 4 + 0.12 \times 2 = 0$.

2.4.3 Qualitative effects of some parts of the interaction

As shown in the previous section, the values of the monopole interaction strongly depend on the $\pi\nu$ configurations. Particularly those involving spin-orbit partners display large differences, which may modify the shell structure and the gap values. Some typical examples are given now.

The first example, dealing with nucleons having the *same* orbital momentum ℓ , is given in the left part of Fig. 9. The strongly attractive $\pi d_{5/2} - \nu d_{3/2}$ force generates large $Z = 14$ and $N = 20$ gaps in $^{34}\text{Si}_{20}$, which consequently behaves as a doubly magic nucleus. As soon as protons are removed from the $\pi d_{5/2}$ orbit, the $\nu d_{3/2}$ becomes much less bound (and actually particle unbound in the neutron-rich O isotopes). This closes the $N = 20$ shell gap to the benefit of a new growing $N = 16$ one, formed between the neutron $s_{1/2}$ and $d_{3/2}$ shells. This re-arrangement of shell gaps explains also why $^{24}\text{O}_{16}$ has the properties of a doubly magic nucleus (with $Z = 8$ and $N = 16$ shell gaps), and why $^{28}\text{O}_{16}$ is unbound with respect to neutron emission (see the discussions and references included in Sect. 4.1.3). As this interaction acts differentially on spin-orbit partners, a reduction of the proton $d_{5/2} - d_{3/2}$ SO splitting is expected while removing neutrons from the $d_{3/2}$ orbit, i.e. from $^{34}\text{Si}_{20}$ to $^{30}\text{Si}_{16}$.

This particular effect acting in a $\pi\nu$ configuration with $\Delta\ell = 0$ was ascribed in Ref. [54] to the the fourth term of the central potential derived in Eq. 18, $V_{\sigma\tau}(r) \vec{\sigma}_1 \cdot \vec{\sigma}_2 \vec{\tau}_1 \cdot \vec{\tau}_2$. However in a later publication [55], the same authors have claimed that such a term is not strong enough, so this interaction between spin-flip proton-neutron partners has to come from the tensor term of the NN interaction (see Eq. 20). As derived in the decomposition of the monopole interaction in the previous section (see Table 1), the tensor interaction is attractive when the intrinsic spins of the neutron and the proton are anti-parallel and repulsive when they are parallel and is strong enough to counteract the difference in the central parts when the two nucleons have the same orbital momentum ℓ .

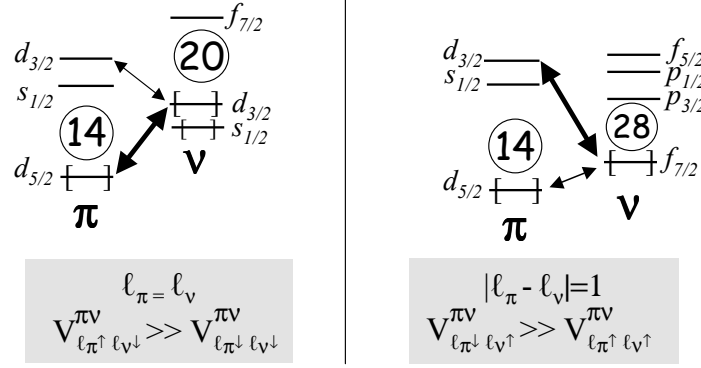


Figure 9: Variation of the $\pi d_{5/2} - \pi d_{3/2}$ SO splitting induced by the properties of the NN interaction. Left: Case of $\pi d - \nu d$ from a $\Delta\ell = 0$ tensor term. Right: Case of $\pi d - \nu f$ from a $\Delta\ell = 1$ tensor term.

The second example, dealing with nucleons having $\Delta\ell = 1$, is given in the right part of Fig. 9. The $V_{d_{3/2}f_{7/2}}^{pn}$ monopole contains an attractive tensor term (see Table 1), which acts in favor of a large $N = 28$ shell gap in ^{48}Ca where the $\pi d_{3/2}$ orbit is filled completely. The removal of all $d_{3/2}$ protons provokes a reduction of the neutron $f_{7/2} - f_{5/2}$ SO splitting, and a reduction of the $N = 28$ gap. Important is to note however that the reduction of the $N = 28$ gap does not come solely from this effect (see Sect. 5.1 for details).

In a more general manner, the proton-neutron tensor force felt by a given nucleon orbiting in j' globally cancels when the two orbits j_\uparrow and j_\downarrow are filled, as given by the tensor sum rule of Eq. 22. When only the j_\uparrow orbits are filled for both protons and neutrons, the tensor forces that prevail in the nucleus are maximized. Applied to the case of $^{42}_{14}\text{Si}_{28}$ (see the discussion and references in Sect. 5.1.2), the last occupied proton and neutron shells are $\pi d_{5/2}$ ($\ell = 2, j_\uparrow$) and $\nu f_{f/2}$ ($\ell = 3, j_\uparrow$) (shown in the right part of Fig. 9). The proton-induced tensor force $V_{\pi d_{5/2} \nu f_{f/2}, \downarrow}$ reduces the neutron $f_{7/2} - f_{5/2}$ SO splitting as compared to the situation in which both the $d_{5/2}$ and $d_{3/2}$ orbits are filled, as in ^{48}Ca . In a symmetric manner, the neutron-induced tensor $V_{\pi d_{f/2}, \downarrow \nu f_{7/2}}$ force weakens the proton $d_{5/2} - d_{3/2}$ SO splitting as compared to ^{34}Si , in which no neutron occupies the $\nu f_{f/2}$ orbit. Added together, these mutual proton and neutron induced tensor forces give rise to significant reductions of *both* proton and neutron SO splittings and hereby of the $Z = 14$ and $N = 28$ shell gaps which were generated by the SO force. In the case of ^{42}Si , in which only the proton and neutron j_\uparrow configurations are filled, the tensor force acts against the SO force.

To summarize this part, the tensor interactions which strongly act in $\pi\nu$ configurations either with $\Delta\ell = 0$ or with $\Delta\ell = 1$, can significantly modify the SO *splittings*, and hereby the shell gap for magic numbers originating from the SO interaction.

2.5 Summary and Outlooks

The present section has provided an introduction to the properties and effects of the effective nuclear forces in atomic nuclei. Though they differ in definitions, effective forces are widely used in various theoretical approaches such as mean field calculations (Skyrme, Gogny and RMF forces) and shell models (through Two-Body Matrix Elements). This use is due to the fact that the solving of the N-body problem, from the 'bare' NN forces, is untractable already for medium mass nuclei.

Even though the effective forces differ with the 'bare' ones (at least in strength), they do contain some reminiscent properties of the bare interaction, such as the existence of SO and tensor forces. These forces are expected to play key roles in the evolution of nuclear structure.

In the SM approach these forces are implicitly contained into the Two Body Matrix Elements (TBME) of the interaction, among which the so called monopole term - the average value of TBME over all directions - is one of the fundamental pillars. Indeed, the evolution of the spherical shell structure is guided by the changes of this monopole term, illustrated through the variations of Effective Single Particle Energies (ESPE). The TBME used in the SM approach were decomposed into various components, e.g. central, SO and tensor forces. Quantitative and qualitative effects of these terms have been discussed. By gathering all these pieces of information, one notices that new nuclear degrees of freedom - such as those provided by the action of the tensor and change in the nuclear density - are expected to modify the apparent SO splitting and hence the nuclear magic shells. If some of these features were already invoked more than thirty years ago (see Ref. [56]), renewed interest is growing nowadays from the experimental possibility to explore these new facets of the in-medium NN interaction. Being aware of the possible importance of these effects to model the atomic nucleus, new parameters are being implemented into the effective forces, such as that of the tensor forces.

One fundamental question will therefore pervade the whole document: to what extent will the properties of the NN interaction be seen in the nucleus or will they be diluted among other degrees of freedom such as configuration mixings? After having reviewed the properties of all major-shell closures, this will be addressed in the conclusions.

3 The magic number 8

The magic number 8 naturally comes from any phenomenological mean-field description of the nucleus. There are so large distances in energy between the first eigenvalues of the Hamiltonian with a central potential, whatever its radial form (square well, harmonic oscillator, Woods-saxon, ...) that the $0p$ states are well separated from the $1s0d$ ones. The $N, Z = 8$ shell gaps are thus formed between occupied states having negative parity and valence ones having positive parity. In this section, we limit our discussion to the evolution of the $N, Z = 8$ shell closures in terms of single-particle energies, trying to derive which components of the NN force have predominant roles. This description can be applied up to a certain limit, as the very concept of mean field is often in trouble for light nuclei close to the drip-lines. It intends to pave the way for other theoretical approaches taking into account correlations inherent to cluster [57, 58, 59] or halo systems [60, 61, 62].

This section is divided in two parts. The first one reviews the evolution of the $N = 8$ shell closure whereas the second describes the evolution of shell structure along the $Z = 8$ isotopic chain. The neighboring isotopic chains of F ($Z = 9$) and C ($Z = 6$) will be discussed as well.

3.1 Evolution of the $N = 8$ shell closure

3.1.1 Binding energies and the $N = 8$ shell gap

The neutron $N = 8$ shell gap is formed between the occupied $p_{1/2}$ and the valence $d_{5/2}$ and $s_{1/2}$ orbits. The binding energies of the corresponding states $1/2^-$, $5/2^+$ and $1/2^+$ are shown in the left part of Fig. 10. Taking the binding energy values at $Z = 6$, it is found that the size of $N = 8$ shell gap amounts to about 6 MeV. The $1/2^-$ state at $Z = 8$ contains additional binding energy due to

the Wigner term, the ^{16}O nucleus being a self conjugate $N = Z$ nucleus. Taking the prescription of Chasman [63], the Wigner energy to subtract in order to determine the size of the gap is 5 MeV in the case of ^{16}O . Doing so the $N = 8$ gap at $Z = 8$ amounts to 7 MeV. The unbound $3/2^+$ states are reported also in Fig. 10, showing the existence of a sizeable $N = 16$ subshell gap of about 3 MeV. These data points at $Z = 6$ and $Z = 8$ correspond to the first $3/2^+$ states which carry a large -but for ^{15}C not the full- spectroscopic strength observed in the $^{14}\text{C}(\text{d,p})^{15}\text{C}$ and $^{16}\text{O}(\text{d,p})^{17}\text{O}$ stripping reactions, respectively. A crossing between the $5/2^+$ and $1/2^+$ states occurs between

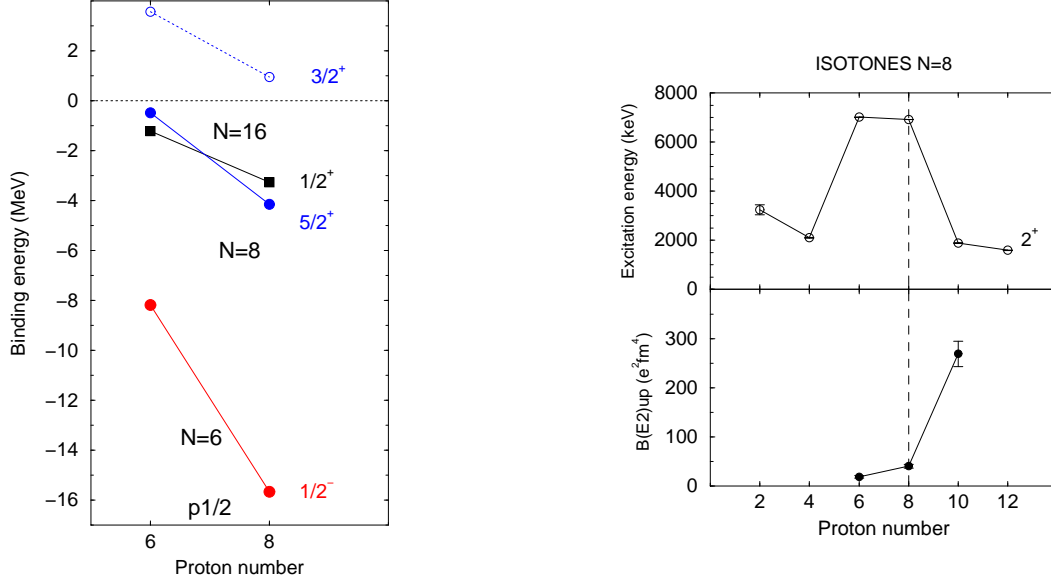


Figure 10: **Left:** Binding energies of the $1/2^-$ ($5/2^+$, $1/2^+$, $3/2^+$) states located below (above) the $N = 8$ magic number (see Sect. 11). The proton $p_{1/2}$ orbit is getting filled between $Z = 6$ and $Z = 8$. **Right:** Experimental $E(2^+)$ and $B(E2; 0^+ \rightarrow 2^+)$ values in the $N = 8$ isotones.

$Z = 6$ and $Z = 8$, while the proton $p_{1/2}$ orbit is getting filled. These states $5/2^+$ and $1/2^+$ arise from the $d_{5/2}$ and $s_{1/2}$ orbits, respectively. As early mentioned by Talmi and Unna [64] "the order of the filling of the neutron shells ($d_{5/2}$ and $s_{1/2}$) may depend on the proton configuration". In the present case the addition of 2 protons in the $p_{1/2}$ shell induces a differential change of the neutrons binding energies of the $d_{5/2}$ and $s_{1/2}$ orbits and provoke their inversion. The $V_{p_{1/2}d_{5/2}}^{pn}$ has larger absolute intensity than the $V_{p_{1/2}s_{1/2}}^{nn}$ one. The former matrix element contains an attractive tensor term, whereas the second contains a repulsive two-body spin-orbit term (see Table 1). Taking the experimental energies of the first $1/2^+$ and $5/2^+$ in $^{15}\text{C}_9$ and $^{17}\text{O}_9$, the monopole energy difference $2(V_{p_{1/2}d_{5/2}}^{pn} - V_{p_{1/2}s_{1/2}}^{pn})$ amounts to approximately -1.6 MeV. This value should be taken with caution as the full spectroscopic strength of these $5/2^+$ and $1/2^+$ states is not found in ^{15}C .

One would also be tempted to comment on the variation of the neutron $d_{5/2} - d_{3/2}$ spin-orbit splitting between $Z = 6$ and $Z = 8$ by taking the energy difference between the $5/2^+$ and $3/2^+$ states. Doing so, one finds a reduction of about 1 MeV, taking the mean energy values of the resonant $3/2^+$ states in ^{15}C and ^{17}O . Taken at face value, this indicates that a differential change of binding energy is occurring between the $d_{5/2}$ and $d_{3/2}$ orbits, as two protons are added to the $p_{1/2}$ orbit. In the present case, the $V_{p_{1/2}d_{5/2}}^{pn}$ monopole would globally be more attractive than the $V_{p_{1/2}d_{3/2}}^{pn}$ one, such as $2(V_{p_{1/2}d_{5/2}}^{pn} - V_{p_{1/2}d_{3/2}}^{pn}) \simeq -1$ MeV. The action of tensor forces could account for

this variation. However, as said earlier, this conclusion should be ascertained by further theoretical calculations to derive the single-particle energies from the experimental states which inevitably contain some amount of correlation.

3.1.2 Trends of $E(2^+)$ and $B(E2)$ values in the $N = 8$ isotones

The top right part of Fig. 10 shows the systematics of the 2^+ energies in the $N = 8$ isotones. From the left to the right hand side of the figure, 2^+ energies of ^{10}He , ^{12}Be , ^{14}C , ^{16}O , ^{18}Ne , and ^{20}Mg [65] are reported. Large 2^+ energies are found for the two doubly magic nuclei ^{14}C and ^{16}O , while they drop by a factor of two to three on each side of the valley of stability. This effect does not necessarily document for a sudden erosion of the $N = 8$ gap. Indeed it arises principally from the fact that 2^+ states can be created by proton excitations, which are hindered in the ^{14}C and ^{16}O nuclei due to the existence of large $Z = 6$ and $Z = 8$ shell gaps (see the next Sections).

The trend of the $B(E2)$ values confirms the statements given in the previous paragraph. The low $B(E2)$ values of ^{14}C and ^{16}O owe to the fact that they are doubly-magic nuclei. The $B(E2)$ of ^{16}O is larger by a factor of 2 as, being a self-conjugate nucleus, its 2_1^+ state contains an almost equal amount of neutron and proton excitations. As protons carry the major fraction of the effective charge, this enhancement of proton excitation accounts for the relatively large $B(E2)$ value for ^{16}O . On the other hand, the 2^+ state of ^{14}C has a dominant wave function built with neutron excitation. At $Z = 10$ the $B(E2)$ value suddenly rises to a large value [66]. This coincides with the filling of the proton sd shells, in which 2^+ excitations can be easily generated. The large value, $B(E2)=18(2)$ W.u., indicates that ^{18}Ne is rather collective.

3.1.3 Trends of $E(1_1^-)$ state in the $N = 8$ isotones

To get a further insight into the evolution of the $N = 8$ shell closure as a function of the proton number, one can look at the evolution of the energy of cross shell excitations. The $N = 8$ shell gap is formed between the $p_{1/2}$ and $s_{1/2}$ (or $d_{5/2}$ in ^{16}O) orbits. Therefore particle-hole excitation across this gap give rise to states having total spin values $J = 0^-, 1^-$. Such states should be found at approximately the energy of the $N = 8$ gap, shifted by the residual energies of the $(\nu p_{1/2})^{-1}(\nu s_{1/2})_{J=0,1}^{+1}$ configurations. Energies of the first 1^- state in three lightest isotones are shown in Fig. 11, as compared to the size of the $\nu p_{1/2} - \nu s_{1/2}$ gap extracted from Fig. 10. The data point on $^{12}_4\text{Be}$ has been obtained by means of the inelastic scattering technique at intermediate energy at the RIKEN facility [67]. In this experiment two targets (Pb and C) were used to ascertain the multipolarity of the transition and the 1^- assignment of the observed state. The strong decrease of $E(1_1^-)$ in ^{12}Be has been ascribed to a drastic narrowing of the $N = 8$ shell gap there. The authors argued that the large measured $B(E1)$ value is consistent⁸ with a quasi-degeneracy between the $p_{1/2}$ and $s_{1/2}$ states, a feature which is also present in ^{11}Be [68]. Additionally knockout reaction of ^{12}Be measured at the NSCL/MSU facility has also shown a strong indication of shell melting in its the ground state [69]. Where a pure $\ell = 1$ wave function would have been expected for an $N = 8$ closed shell, the ground-state wave function contains two-thirds of $\ell = 0, 2$ admixtures.

This sudden reduction of the $N = 8$ shell gap for $Z < 6$ could be interpreted in term of proton-neutron interactions, at least on a semi-quantitative manner. Below $Z = 6$, protons are removed

⁸For weakly bound nuclei exhibiting a well developed neutron halo, the transition between p and s states occurs with a sudden increase of neutron radius. As the $E1$ operator scales with the nuclear radius, it follows that enhanced $B(E1)$ transition is a generic property of halo nuclei.

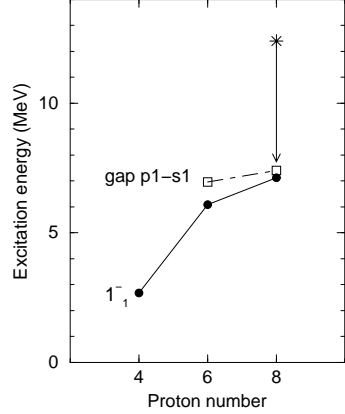


Figure 11: Experimental $E(1_1^-)$ values in the $N = 8$ isotones, $^{12}_4\text{Be}$, $^{14}_6\text{C}$ and $^{16}_8\text{O}$ (filled circles). The values of the $N = 8$ gap are shown with empty squares. The data point for ^{16}O (indicated with a star) contained the Wigner energy, which has been subtracted to give the real size of the gap (see Sect. 3.1.1 for details).

from the $p_{3/2}$ orbit. The reduction of the $\nu p_{1/2} - \nu s_{1/2}$ gap could be ascribed to the monopole matrix element difference ($V_{p_{3/2}p_{1/2}}^{pn} - V_{p_{3/2}s_{1/2}}^{pn}$) per proton removed from the $p_{3/2}$ orbit. This linear extrapolation was early made in Ref. [64] to account for the inversion between the $\nu p_{1/2}$ and $\nu s_{1/2}$ state in ^{11}Be . As the spin-flip proton-neutron matrix element $V_{p_{3/2}p_{1/2}}^{pn}$ is strongly attractive, the $\nu p_{1/2}$ orbit becomes suddenly much less bound while the partner $\pi p_{3/2}$ shell empties. This effect weakens the $N = 8$ gap. Following the trend of the 1^- state (see Fig. 11), the inversion between the $p_{1/2}$ and $s_{1/2}$ states will be found at $N = 8$ in the drip-line ^{10}He nuclei.

This description in term of single particle energy evolution, making use of the 'monopole-driven' reduction of shell gaps, should be taken as qualitative only as states in halo or cluster nuclei are no of longer single particle nature.

3.1.4 Conclusion

The $N = 8$ shell gap is formed between the $p_{1/2}$ and $d_{5/2}$ and the nearby $s_{1/2}$ orbits. In ^{16}O the protons occupying the $p_{3/2}$ and $p_{1/2}$ orbits bind the neutron $p_{1/2}$ as compared to other neutron orbits. While the p protons are progressively removed, the $\nu p_{1/2}$ shell become less bound. Therefore the $N = 8$ shell gap is quickly eroded, provoking finally an inversion between the $p_{1/2}$ and $s_{1/2}$ states. This reduction is inferred from the ground-state components of ^{12}Be , the low energy of its first 1^- state as well as the large value of its reduced transition probability $B(E1)$. Incidentally, the inversion of levels in addition to the presence of a nearby s orbit available, give birth to halo nuclei.

3.2 Evolution of the $Z = 8$ shell closures

3.2.1 Binding energies and the $Z = 8$ shell gap

The proton $Z = 8$ shell gap is formed between the occupied $p_{1/2}$ and the valence $d_{5/2}$ and $s_{1/2}$ orbits. The binding energies of the corresponding states $1/2^-$, $5/2^+$ and $1/2^+$ are shown in the left part of Fig. 12, the proton-unbound states of the ^{12}O and ^{15}F nuclei being also included. The

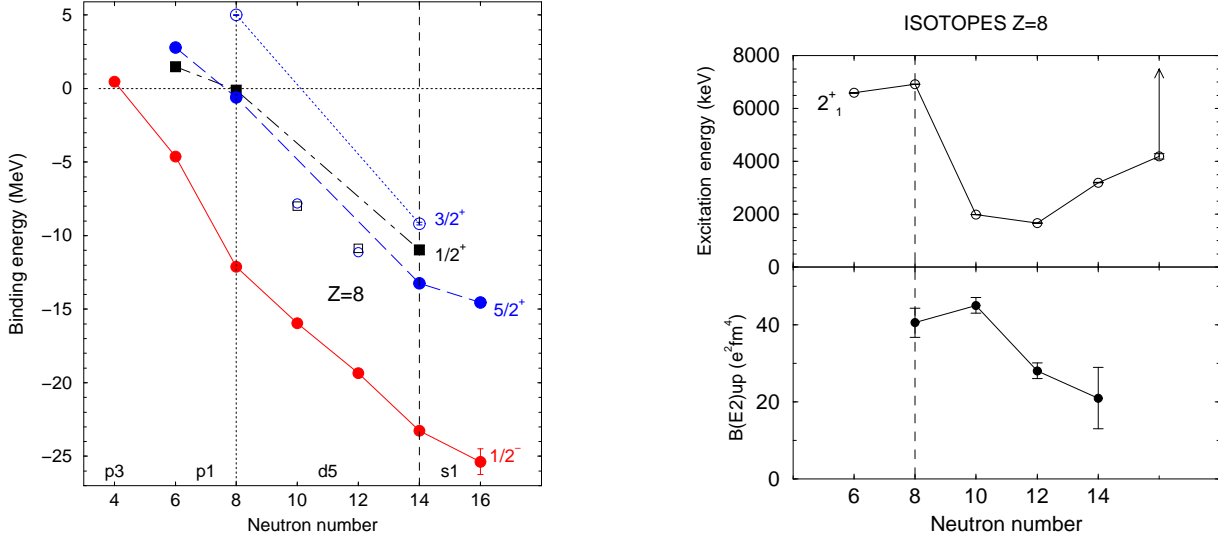


Figure 12: **Left:** Binding energies of the $1/2^-$ ($5/2^+$, $1/2^+$) states located below (above) the $Z = 8$ magic number. The neutron orbitals which are getting filled as a function of increasing Z , $p_{3/2}$, $p_{1/2}$, $d_{5/2}$ and $s_{1/2}$, are indicated above the neutron number axis. **Right:** Experimental $E(2^+)$ and $B(E2; 0^+ \rightarrow 2^+)$ values in the oxygen isotopes. The $E(2^+)$ value of $^{24}\text{O}_{16}$ is greater than the neutron emission threshold (see text).

very last measured mass values of the ^{24}O and ^{23}N neutron-rich nuclei, by B. Jurado et al. [70], have been used for the neutron-rich side of the figure. As regards the $5/2^+$ state, the filled symbols are used for nuclei which are thought to be spherical. Conversely, empty symbols at $N = 10, 12$ correspond to binding energies involving deformed ^9F isotopes. These data points are located aside of the interpolation lines, as they correspond to nuclei containing additional correlation energy due to their deformation. The binding energy values for the ^{16}O nucleus contains the Wigner term as being an $N = Z$ nucleus. Taking all these remarks into account, it is found that the $Z = 8$ shell gap equals to about 10 MeV. This value is large enough to preserve a spherical shape for all ^8O nuclei.

The drip line occurs already at $N = 16$ in the O chain, while one would have expected the doubly magic nucleus $^{28}\text{O}_{20}$ to be bound. By looking at the evolution of the calculated ESPE in Fig. 13, one sees that the $d_{3/2}$ orbit is only bound by about 1 MeV there. The pairing correlations in ^{26}O increase the binding energy of this nucleus, thus making ^{28}O unbound relative to ^{26}O . Interesting is the fact that the addition of one proton makes the F isotopes bound up to $N = 20$ and even beyond (the $^{31}\text{F}_{22}$ isotope has been observed [71]). This feature is discussed in detail in Sect. 4.1 which describes the behavior of the $N = 20$ shell closure. But from Fig. 13, one already understands the mechanism which is responsible from this sudden change of structure between O and F isotopes. The addition of a single proton in the $\pi d_{5/2}$ orbit makes its spin-flip partner $\nu d_{3/2}$ orbit more bound by about the value of the monopole involved, i.e. by $V_{d_{5/2}d_{3/2}}^{pn} \simeq 2$ MeV (see Table 1). This large value is enough to bind all the F isotopes. In addition to this monopole energy, the F isotopes located between the $N = 8$ and $N = 14$ shell closures gain quadrupole energy, as discussed in the previous paragraph. One notes that, as the $Z = 8$ gap is large, a similar gain of quadrupole energy is hindered for the O isotopes.

The slope of the binding energy curves could provide information on the strength of the

monopole proton-neutron interactions at play⁹. In particular, the steepest slopes correspond to the largest monopole terms, as for instance the ones involving the same angular momenta and number of nodes in their proton and neutron wave functions. Ranked by decreasing intensity, one finds $V_{p_{1/2}p_{3/2}}^{pn}$, $V_{p_{1/2}p_{1/2}}^{pn}$ and $V_{d_{5/2}d_{5/2}}^{pn}$. The $V_{p_{1/2}d_{5/2}}^{pn}$ monopole looks important as well, possibly due to the fact that it contains an attractive tensor part. After having passed the $N = 14$ neutron number, smoother slopes for the $5/2^+$, and to a weaker extent for the $1/2^-$ binding energy curves are found. This is due to the fact that the monopoles $V_{d_{5/2}s_{1/2}}^{pn}$ and $V_{p_{1/2}s_{1/2}}^{pn}$ are weaker than the ones involved before $N = 14$. As these latter monopoles link orbits separated by at least one unit of angular momentum, the overlap of valence proton and neutron wave functions is small.

The structure of the $^{23}\text{F}_{14}$ nucleus has been recently studied in order to identify the proton single-particle states lying above the $Z = 8$ gap [72], i.e. $d_{5/2}$, $s_{1/2}$ and $d_{3/2}$ orbits. The situation is expected to be simple as its core, ^{22}O , behaves as a doubly-magic nucleus (as discussed in Sect. 3.2.3). In this experiment, done at the secondary-beam line in the RIKEN Accelerator Research Facility, the identification of the proton single-particle states has been done from the comparison of the population strengths of the excited states in ^{23}F from four direct reactions: the one-proton transfer reaction onto ^{22}O , the α inelastic scattering of ^{23}F , the neutron knock-out from ^{24}F , and the two-nucleon knock-out from ^{25}Ne . Such a comparison is appropriate for identifying single-particle states among the many excited states. The states at 2268 and 4059 keV are good candidates, having large cross-sections in the proton transfer reaction while their populations are weak in the neutron knock-out reaction. They are assigned to be the $\pi s_{1/2}$ and $\pi d_{3/2}$ states respectively, by analysis of the population strengths and the angular distributions of the outgoing ^{23}F nuclei. The authors conclude that the energy gap between the two spin-orbit partners, $\pi d_{5/2} - \pi d_{3/2}$, amounts to 4.06 MeV, since the ground state of ^{23}F is $5/2^+$ [73]. The decrease of the $\pi d_{5/2} - \pi d_{3/2}$ splitting by about 1 MeV, from ~ 5.0 MeV in ^{17}F to 4.06 MeV in ^{23}F (as seen in the left part of fig. 12), occurs simultaneously to the addition of 6 neutrons into the $\nu d_{5/2}$ orbit. Therefore this reduction of the proton d SO splitting was attributed in [74] to the differential action of the proton-neutron tensor forces, viz $\pi d_{5/2} - \nu d_{5/2}$ the versus $\pi d_{5/2} - \nu d_{3/2}$ forces.

Complementary to these works, Signoracci and Brown [75] have compared the same data on ^{23}F and other existing data on ^{19}F to shell model calculations using various versions of the USD interactions (USD [76], USDA and USDB [77]). By taking into account the full single-particle strength, the size of the $\pi d_{5/2} - \pi d_{3/2}$ splitting is increased by about 50% as compared to the value computed from the lowest state energies. The USDB interaction gives remarkable agreement with the energies obtained for the first $3/2^+$ and $5/2^+$ states in ^{23}F . Such an excellent agreement is not found in the case of ^{19}F , which has very fragmented single-particle strengths, as being a rather deformed nucleus. The authors could unfortunately not use experimental data on ^{17}F , which are rather yet incomplete. By comparing calculated and experimental level schemes and spectroscopic factors, the authors of Ref. [75] deduced that the proton d SO splitting is 6.2(4) MeV in ^{23}F and stays almost constant as a function of neutron number, from the proton-drip line, 6.0 MeV in $^{17}\text{F}_8$, to the neutron drip line, 6.9 MeV in $^{29}\text{F}_{20}$, within the present uncertainties inherent to the calculations.

To conclude, it seems that a more detailed study of proton transfer reactions on $^{16,22}\text{O}$ is required to determine more precisely the proton single-particle energies in $^{17,23}\text{F}$. This remark is especially true for the ^{17}F case. This is required to clarify the present situation concerning the evolution of the $\pi d_{5/2} - \pi d_{3/2}$ SO splitting along the F isotopic chain, while the $\nu d_{5/2}$ orbit is

⁹Doing so, we assume that most of the spectroscopic factors are contained in these states, which is reasonable only for spherical nuclei. Additional word of caution concern the use of the $N = 8$ data point, the energy of which is shifted by the Wigner energy term of the $N = Z$, ^{16}O nucleus.

filled. This is undoubtedly a crucial test with respect to the action and strength of tensor forces in atomic nuclei.

3.2.2 Trends of $E(2^+)$ and $B(E2)$ values in the Oxygen isotopes

In addition to the doubly magic $N = Z$ nucleus, ^{16}O , the Oxygen isotopic chain contains three quasi doubly-magic nuclei ^{14}O , ^{22}O and ^{24}O . This owes to the $N = 6$, $N = 14$ and $N = 16$ large neutron subshell gaps between the $\nu p_{3/2} - \nu p_{1/2}$, $\nu d_{5/2} - \nu s_{1/2}$ and $\nu s_{1/2} - \nu d_{3/2}$ orbits, respectively (see fig. 10). The presence of the $N = 6$ subshell closure leads to a large 2^+ energy at 6.5 MeV as well as a 1^- state at 5.17 MeV in $^{14}\text{O}_6$. The latter state corresponds to a cross-shell excitation $\nu p_{3/2}^{-1} \otimes \nu p_{1/2}^{+1}$ configuration. Concerning the neutron-rich isotopes, the 2^+ energy rises up to 3.2 MeV at $^{22}\text{O}_{14}$ [78], and at more than 4.19(10) MeV at $^{24}\text{O}_{16}$. As no γ -ray was observed during the de-excitation of ^{24}O , it was surmised in Ref. [78] that all excited states, including the 2_1^+ one, lie about the neutron emission threshold¹⁰. Hence this value is a lower limit of the 2^+ energy in ^{24}O (drawn with an arrow in the top right part of Fig. 12).

The trend of the $B(E2)$ values corroborates the existence of an $N = 14$ subshell closure (see the bottom right part of Fig. 12). Within the present error bars, the $B(E2)$ value of ^{22}O is the smallest of the isotopic chain [79]. As the $Z = 8$ shell gap is rather large, the configuration of the 2^+ in most of the oxygen isotopes is *mainly* of neutron origin [80]. This statement does not hold for the $N = Z$ nucleus, the 2^+ state of which is made of equally mixed protons and neutrons configurations, as already mentioned in Sect. 3.1.2.

3.2.3 Comparison between the C and O isotopic chains and the $N = 14, 16$ subshell closures

The ^{14}C nucleus has the remarkable properties of a doubly magic nucleus, such as a high 2^+ energy value at 7.012 MeV and a weak $B(E2)$ value of $18.7(2) e^2 fm^4$. These properties arise from the combination of large $Z = 6$ and $N = 8$ shell gaps. As the size of the $Z = 6$ gap is almost equivalent to that of the $Z = 8$ one, a comparison between the ${}_6\text{C}$ and ${}_8\text{O}$ isotopic chains towards the neutron drip line is therefore interesting. The subshell closures at $N = 14$ and $N = 16$ in the oxygen isotopes have been presented in the previous sub-section. By comparing the 2^+ energy trends of the O and C nuclei represented in Fig. 13, one sees a similar behavior up to $N = 12$ and a drastic change at $N = 14$. Instead of a rise at $N = 14$, the 2^+ energy remains constant at $^{20}\text{C}_{14}$. This demonstrates that the $N = 14$ subshell closure no longer exists in the C isotopes, making it effective only in the O chain. What is the reason for this difference of behavior at $N = 14$ between the O and C isotopic chain ?

To answer this question, one should first understand the mechanism leading to the formation of the $N = 14$ gap in oxygen, and second brings reasons for its non-existence in the carbon isotopes. The evolution of Effective Single Particle Energies (ESPE) of the $\nu d_{5/2}$ and $\nu s_{1/2}$ orbits is shown for the O isotopes in the bottom left part of Fig. 13. These values are obtained when using the USDB interaction [77], the matrix elements of which were derived by adjustments to many experimental data in this mass region. From Fig. 13 one sees that the $N = 14$ gap is created by the filling of 6 neutrons in the $d_{5/2}$ shell between $N = 8$ and $N = 14$. As the monopole matrix element $V_{d_{5/2}d_{5/2}}^{nn}$ is globally attractive, the ESPE of the $d_{5/2}$ orbit gains binding energy¹¹. Meanwhile the

¹⁰The value reported in the figure, $S_n=4.19(10)$ MeV, is computed from the new atomic masses of Ref. [70]

¹¹Interesting here to remark is that this mechanism is generic. It creates other magic numbers such as the $N=28$ and $N=50$ ones by the filling of 8 and 10 neutrons in the $f_{7/2}$ and $g_{9/2}$ orbits, respectively (see the end of Sect. 2.3.1).

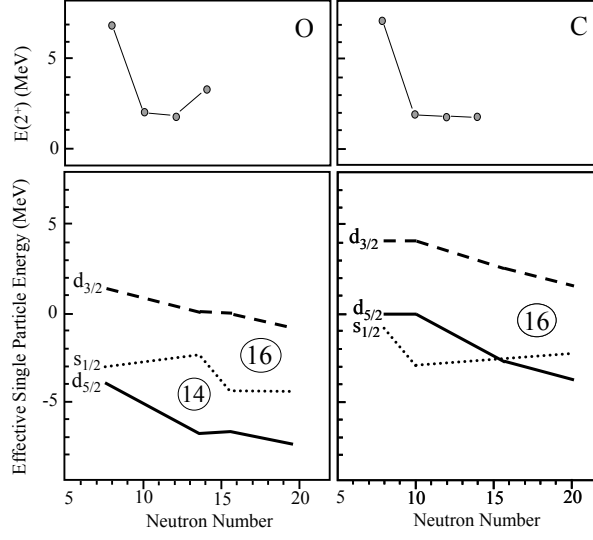


Figure 13: **Top** : 2^+ energies in the O (left) and C (right) isotopic chains. **Bottom** Neutron Effective Single Particle Energies (ESPE) as a function of the neutron number in the O (left) and C (right) isotopic chains. The variation of the ESPE have been derived by using the monopole matrix elements of the USDB interaction [77, 81].

ESPE of the $s_{1/2}$ moves upwards, due to the fact that the $V_{d_{5/2}s_{1/2}}^{nn}$ monopole is slightly repulsive. As the neutrons start to fill the $s_{1/2}$ orbit, the ESPE of the $\nu s_{1/2}$ orbit suddenly drops down to large binding energy by virtue of the large $V_{s_{1/2}s_{1/2}}^{nn}$ matrix element. It is seen that a large $N = 16$ gap is preserved up all along the O isotopic chain. The $^{24}\text{O}_{16}$ behaves as a doubly magic nucleus, as being surrounded by two neutrons gaps, $N = 14$ and $N = 16$. This Figure should however be taken in a qualitative manner as few monopoles involved far off stability, such as $V_{d_{3/2}d_{3/2}}^{nn}$, are not yet strongly constrained by experimental data. The major constraint existing so far is to get the neutron $d_{3/2}$ unbound with respect to 2 neutron emission at $N = 20$ to account for the particle instability of $^{28}\text{O}_{20}$ (this is also shown in the right part of fig. 15 in Sect. 4.1.3, for another set of TBME).

Why is the $N = 14$ gap not existing in the C chain? The difference of structural behavior between the C and O nuclei originates from the inversion of the $1/2^+$ and $5/2^+$ levels between the ^{17}O and ^{15}C isotones (shown in the left part of Fig. 10). Taking this early change into account, the structural evolution in the neutron-rich C isotopes can be straightforwardly deduced using the same V^{nn} terms as those involved in the spectroscopy of the O nuclei ¹². Soon after $^{14}\text{C}_8$, the $\nu s_{1/2}$ orbit is filled first, making the study of ^{15}C of particular interest for the appearance of a one-neutron halo, as the $s_{1/2}$ orbit is weakly bound ($S_n=1.22$ MeV). This has been searched for in one-neutron break-up reactions [84], but the results were not conclusive enough. After ^{16}C the $\nu d_{5/2}$ orbit starts to be filled. Its binding energy increases gradually, to eventually cross the $\nu s_{1/2}$ orbit at $N \sim 15$. This change of ESPE has three noticeable consequences : the $N = 14$ subshell gap is not formed, large admixtures are present between the nearby $\nu d_{5/2}$ and $\nu s_{1/2}$ orbits, and halo nucleus shows up at $N \sim 15$. This latter feature was derived in the one-neutron break-up

¹²This assumption assumes that the neutron-neutron monopoles in the O and C chains could be considered to be similar. As stated in Refs. [82, 83] the monopoles of the C chain are lower by about 20% as compared to those of the O chain. But the global picture described here still holds.

of ^{19}C [85, 86, 84]. Moreover a greatly enhanced $E1$ strength at low excitation energy has been measured in the Coulomb dissociation of ^{19}C , in agreement with the halo structure [87].

It is also seen from Fig. 13 that the $N = 16$ subshell gap is expected to be a large, making $^{22}\text{C}_{16}$ a good candidate for a new doubly-magic nucleus. Even more interestingly, ^{22}C would be a two-neutron halo nucleus, with a large $(\nu s_{1/2})^2$ component, weakly bound to the ^{20}C core.

3.2.4 Conclusion

The $Z = 6$ and $Z = 8$ shell closures have been studied in this chapter. The existence of a large $Z = 8$ shell gap together with large neutron subshell gaps allows the existence of four almost doubly-magic nuclei, $^{14,16,22,24}\text{O}_{6,8,14,16}$. The new magic numbers at $N = 14$ and $N = 16$ come from large gaps in energy at subshell closures. These nuclei serve as good cores to derive the role of nucleon-nucleon interactions at play in this mass region and explain the spectroscopy of neighboring nuclei. In particular, the strongly attractive spin-flip $\pi d_{5/2} - \nu d_{3/2}$ interaction explains why the neutron drip line extends up to $N = 20$ and beyond in the ${}_9\text{F}$ isotopes, whereas it is located at $N = 16$ in O . Another example is the role of the $\nu d_{5/2} - \nu d_{5/2}$ interaction to create the $N = 14$ gap. In the C isotopic chain, this subshell gap no longer exists. This was ascribed to other specific proton-neutron interactions, involving the $\pi p_{1/2}$ orbit, and leading to the swapping of the $\nu s_{1/2}$ and $\nu d_{5/2}$ shells between ^{17}O and ^{15}C . Note that in these light nuclei, the values of the monopole interactions are rather large (~ 2 MeV for many of them). Therefore sudden changes in nuclear structure quickly occur while adding or removing few nucleons. In addition to local magic numbers, haloes or cluster shapes are omnipresent in this mass region when approaching the proton or neutron drip-lines.

4 The magic number 20

The magic number 20 arises naturally when using a harmonic oscillator potential well to simulate the mean field interactions in fermionic systems. The shell gaps $N, Z = 20$ are formed between the $d_{3/2}$ and $f_{7/2}$ orbits originating from the $N = 2$ and $N = 3$ major oscillator shells, respectively. These orbits have opposite parities, which is essential to explain the behavior of this magic number against collective nucleonic excitations. The following sections treat the evolution of the $N = 20$ and $Z = 20$ shell closures at the two extremes of the valley of stability. Historically, the first indication of a reduction of a shell closure among those identified nowadays in the nuclear chart was obtained for the magic number $N = 20$. Contrary to what has been and is still often taught in the textbooks, the magic numbers can evolve far from the valley of stability due for instance to specific proton-neutron interactions. This discovery has triggered the physics of "exotic nuclei", a term which was inspired by the discoverers of exotic lands during their journey all around the world.

4.1 Evolution of the $N = 20$ shell closure

The first indications of a vanishing of a shell closure in the chart of nuclides were revealed around the neutron magic number $N = 20$. It was found that $^{31}_{11}\text{Na}$ and $^{32}_{12}\text{Mg}$ exhibit anomalies in their binding energies [5], mean-square radii [6] and nuclear spectra [7, 8]. The extra binding energy of these nuclei, with respect to their neighbors, was attributed to their deformation which was quickly associated with particle-hole excitations across the $N = 20$ shell gap [88, 89, 90]. The spherical $N = 20$ gap is thus not large enough to prevent excitations and correlations to develop

to the fp shells in the $_{12}\text{Mg}$ isotopic chain. As these orbits lie outside the normal model space description of the sd shells, they are often referred to as *intruder states*. For some nuclei, the intruder and normal configurations are inverted in energy. They belong to the so-called "Island of Inversion" [90]. Soon after this finding many experimental and theoretical efforts have been devoted to determine the boundaries of this Island, and to understand the underlying physics driving this sudden change between pure sd and full $sdfp$ configurations. The gain of binding energy through deformation was invoked to explain why the drip line extends further in the F and Ne than in the O isotopic chain. Experiments performed at GANIL [91, 92, 93], RIKEN [71, 94] and NSCL [95] facilities have shown that ^{26}O and ^{28}O are unbound against particle decay, whereas the heaviest F and Ne isotopes contain 6 and 8 more neutrons, respectively. It is fascinating to understand how a single proton added to the ^{24}O nucleus can bind 6 additional neutrons to form the ^{31}F nucleus. Also why the drip line is so close to stability in the O chain ? These were burning questions raised among nuclear physicists that lasted the end of the previous century and the beginning of the present one. It was surmised that the onset of deformation at $N = 20$ originates from the reduction of the $N = 20$ spherical shell gap, although there was no direct experimental proof of this assumption. Additionally, while the $d_{3/2}$ single particle moves closer in energy to the fp orbits to reduce the $N = 20$ shell gap, a new shell gap at $N = 16$ should be formed below, between the $s_{1/2}$ and the $d_{3/2}$ orbits. Also there was no proof for the emergence of this new $N = 16$ shell gap.

Thanks to the recent advent of radioactive ion-beam facilities worldwide, the evolution of the $N = 20$ shell closure and the appearance of a new magic number at $N = 16$ far from the valley of stability are now well established and much better understood. In the following sections we will use different experimental information to investigate the evolution of the $N = 20$, starting with the systematics of the binding energies, followed by trends in 2^+ energies and reduced transition probabilities $B(E2; 0^+ \rightarrow 2^+)$, beta-decay studies and transfer reactions. Finally the underlying physics parameters which reduce the size of the $N = 20$ gap and increase that of the $N = 16$ ones will be discussed.

4.1.1 Binding energies

The binding energies of the last neutron in the $N = 21$ and 20 isotones are drawn in the left part of Fig. 14. The energy difference between the two binding-energy curves - or the size of the $N = 20$ shell gap - amounts to about 5 MeV. This curve displays a maximum at $Z = 20$, due to the extra binding energy of ^{40}Ca which is self-conjugate (see Sect. 11). The $N = 20$ shell gap remains large and almost constant until 6 protons are removed from the $d_{3/2}$ and $s_{1/2}$ shells. Below $Z = 14$, the size of the $N = 20$ *spherical* gap can no longer be obtained due to the onset of deformation that is occurring there. The corresponding data points for $Z = 12$ are also shown in Fig. 14. As compared to a spherical case, they contain additional binding energy due to quadrupole correlations. Interestingly the $Z = 8$ proton shell closure should in turn lead $^{28}\text{O}_{20}$ nucleus to be bound and spherical in shape. As we know that it is unbound by a certain amount, the slope of the neutron binding energy curve of the $3/2^+$ state below $Z = 14$ (as protons are removed from the $d_{5/2}$ orbit) should be steeper than above $Z = 14$ (as protons occupy the $d_{3/2}$ and $s_{1/2}$ orbits). This means that the strength of the proton-neutron interactions is changing at $Z = 14$, while entering the island of inversion.

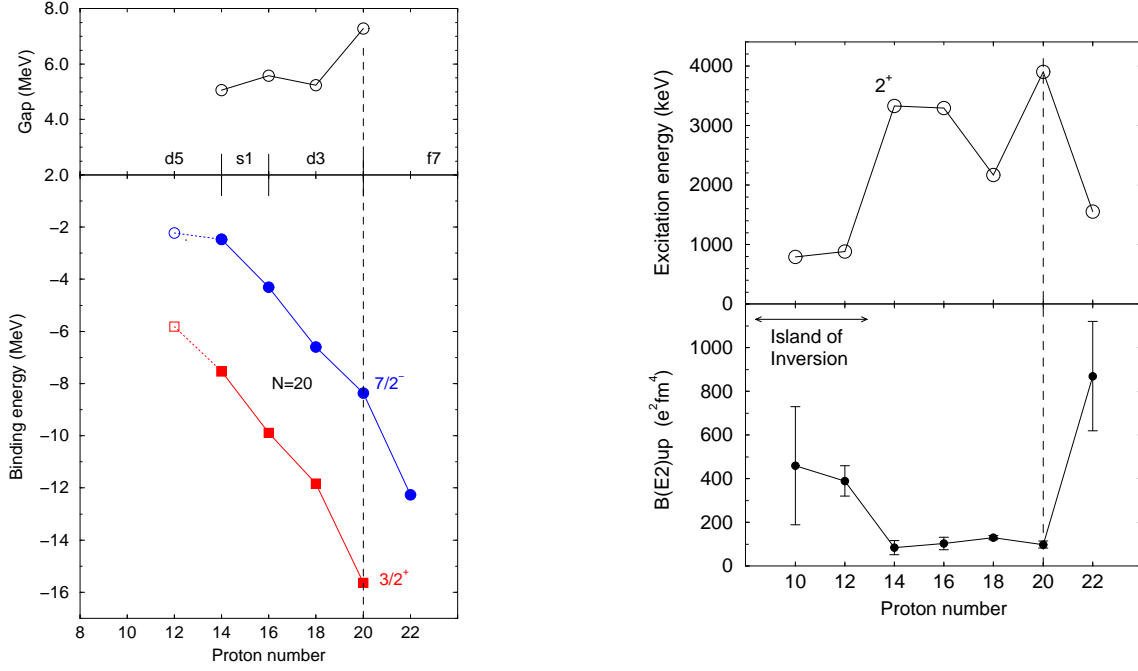


Figure 14: **Left:** Binding energies of the states $3/2^+$ ($7/2^-$) located below (above) the $N = 20$ magic number and difference of the binding energies of these two states surrounding the gap at $N = 20$ (see Sect. 11). The proton orbitals which are getting filled as a function of increasing Z are given in the middle of the figure. **Right:** Experimental $E(2^+)$ and $B(E2; 0^+ \rightarrow 2^+)$ values in the $N = 20$ isotones.

4.1.2 Trends of $E(2^+)$ and $B(E2)$ values and the onset of collectivity

The disappearance of the $N = 20$ spherical shell closure far from the valley of stability is now a well established phenomenon. It is however interesting to remember that the $N = 20$ shell closure remains quite strong from $^{40}_{20}\text{Ca}$ to $^{34}_{14}\text{Si}$ after the removal of 6 protons, successively from the $d_{3/2}$ and $s_{1/2}$ orbitals. There are a plethora of experimental data which strengthen this statement, in particular derived from atomic masses, 2^+ excitation energies, and reduced transition probabilities $B(E2; 0^+ \rightarrow 2^+)$. From atomic masses, it is found that the size of the $N = 20$ shell gap remains almost constant and large, as shown in the left part of Fig. 14. The 2^+ energies amount to about 4 MeV for ^{40}Ca and 3.5 MeV for the ^{36}S and ^{34}Si isotones, (see the right part of Fig. 14). In ^{40}Ca , a minimum of $2p - 2h$ excitations is required to create a $J = 2$ positive-parity state across the gap formed by orbits of different parities (sd (fp) orbits have positive (negative) parities). As a consequence the $B(E2; 0^+ \rightarrow 2^+)$ value (drawn in the right part of Fig. 14) is low as quadrupole excitations to the fp shells can proceed only via small matrix elements provided by the overlap of the sd and fp wave functions. While decreasing the number of protons from $^{40}_{20}\text{Ca}_{20}$, the vacant proton holes created within the sd shells should *a priori* increase the possibility to generate $p - h$ excitations to reach a maximum value of the $B(E2)$ at the mid proton sd shell. As the full sd shell contains a total of 12 protons, we would have expected a maximum collectivity for 6 protons in the sd shells, i.e. for the $^{34}_{14}\text{Si}_{20}$ isotope. Experimental $B(E2)$ values [11, 96] clearly deviate from this simple argument, which assumed that the sd states were quasi-degenerate in energy. It is the presence of significant sub-shell closures at $Z = 14$ (~ 4.3 MeV) and $Z = 16$ (~ 2.5 MeV) and

the persistence of a large $N = 20$ shell gap that keeps the $B(E2)$ at small values and the 2^+ state at high energy in the ^{36}S and ^{34}Si nuclei [97].

For isotopes below $Z = 14$ the picture changes suddenly. The 2^+ energy drops down to 885 keV [8] in $^{32}_{12}\text{Mg}_{20}$, whereas the $B(E2)$ value increases by a factor of about 4. The value reported in the right part of Fig. 14 is obtained from the weighted averaged results of the measurements obtained by Coulomb excitation at intermediate energy at RIKEN [98, 99] and NSCL [100, 101]. The energy of the first 2^+ state in ^{30}Ne has been tentatively determined to be 791(26)keV from proton inelastic scattering measurement [102] at RIKEN. A liquid hydrogen target was bombarded by a radioactive beam of $^{30}_{10}\text{Ne}_{20}$ at intermediate energy with a mean intensity of 0.2 ions per second. γ -rays emitted in flight were detected by an array of Na(Tl) scintillator detectors placed around the target. As mentioned by the authors, the identification of the scattered particles based on the energy loss and total energy method was difficult. Despite this problem, a $B(E2)$ value of $460(270)e^2fm^4$ has been derived for $^{30}_{10}\text{Ne}$. This value is, within error bars, similar to that of $^{32}_{12}\text{Mg}$. The sudden increase of the $B(E2)$ values at $Z = 12$ indicate that neutrons are occupying not only the sd but also the fp shells. Otherwise the $B(E2)$ values would have been much lower [98].

The large values of $B(E2)$ in the Mg chain can arise only if the valence neutrons include the fp orbits. Within the $N_p N_n$ scheme, the $B(E2)$ values are expressed as a function of the product of the number of valence protons N_p and neutrons N_n [43]. If the $N = 20$ shell gap is large, the twelve neutrons above the ^{16}O core are blocked inside the sd shells. Thus $N_n \simeq 0$ and hence the value of $B(E2)$ value is small. Conversely, if the $N = 20$ shell gap vanishes, neutrons can move in a wider space which extends to the fp shells, leading to $N_n=12$. Shell model calculations restricted to the sd shells cannot account for the sudden increase of $B(E2)$ from ^{34}Si to ^{32}Mg (see the right part of Fig. 14). It is sufficient to invoke $2p - 2h$ neutron excitation from the sd to the fp shells to increase the $B(E2)$ value. For the nuclei which reside in the Island of Inversion, the ground states are dominated by $2p - 2h$ configurations. There, the loss of energy due to the promotion of 2 neutrons across the $N = 20$ shell gap ($2E_{gap}$) is largely compensated by the gain of correlation energy obtained from $2p - 2h$ excitations [103]. As described by Heyde et al. [104] this correlation energy comprises proton-neutron and neutron-neutron monopole and quadrupole terms, the sum of which is larger than $2E_{gap}$ in ^{32}Mg . Naturally the dominance of $2p - 2h$ over the normal sd configuration will also be favored if the single-particle energy difference between the $d_{3/2}$ to the fp orbits, E_{gap} , is lowered. Between $Z = 20$ and $Z = 14$, no such reduction is found as shown in Fig. 14. But at $Z = 12$, the nucleus suddenly becomes deformed. This sudden change of structure triggers several questions that the following section intends to address. Why does the removal of six protons leave the nuclei in a spherical shape, whereas the removal of two additional ones leads to prompt deformation? In other words, what is the major deformation-driving mechanism below $Z = 14$ and what makes it so efficient? Fundamental reasons are taken from properties of the nucleon-nucleon interactions which are at play in these nuclei.

4.1.3 Evolution of neutron SPE's

The $N = 20$ shell gap is formed between the $\nu d_{3/2}$ and the $\nu f_{7/2}$ (or $\nu p_{3/2}$) orbit. To simplify the discussion we do not consider the $\nu p_{3/2}$ orbit, to which similar arguments could be applied. From $^{40}_{20}\text{Ca}_{20}$ to $^{36}_{16}\text{S}_{20}$, 4 protons are removed from the $d_{3/2}$ orbit. Therefore the size of the $N = 20$ gap scales with the difference of monopole interactions (see Sect. 2.3.1), $4 \times (V_{d_{3/2}f_{7/2}}^{pn} - V_{d_{3/2}d_{3/2}}^{pn})$. The fact that the $N = 20$ gap remains constant comes from the fact that the two monopole interactions, $V_{d_{3/2}f_{7/2}}^{pn}$ and $V_{d_{3/2}d_{3/2}}^{pn}$, are almost similar in strength. They are determined to be $\simeq -1$ MeV from several experimental binding energy curves and energies of multiplets in several

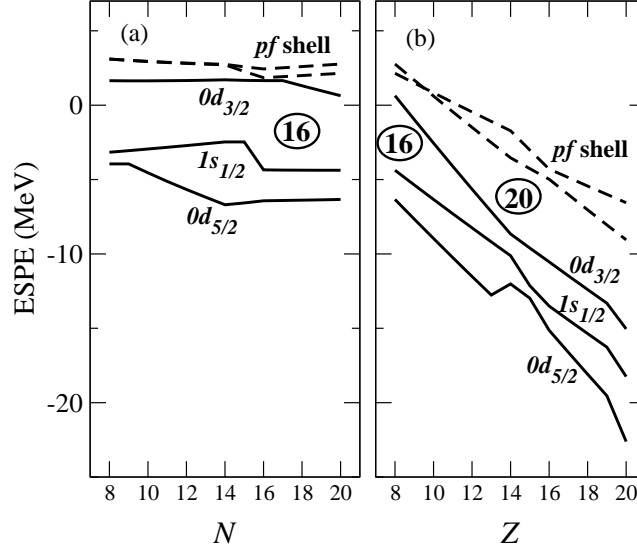


Figure 15: Effective Single Particle Energies (ESPE) of neutrons in the ${}_8\text{O}$ isotopic chain (left) and in the $N = 20$ isotones with $8 < Z < 20$ (right). These figures have been adapted from Fig. 5 of Ref. [105] and Fig. 1 of Ref. [106].

odd-odd nuclei [48].

As soon as protons are removed from the $d_{5/2}$ orbit, the size of the $N = 20$ gap is changing by virtue of another difference of monopole interactions, i.e. $(V_{d_{5/2}f_{7/2}}^{pn} - V_{d_{5/2}d_{3/2}}^{pn})$. As mentioned by Otsuka et al. [54, 55] and shown in Fig. 15, the $V_{d_{5/2}d_{3/2}}^{pn}$ value is expected to be large, due to the spin-isospin dependence of the nuclear interaction. This interaction is maximized for the exchange of nucleons and spin orientations, and when protons and neutrons have the same orbital momentum. Conversely the overlap of protons and neutrons wave functions in the $V_{d_{5/2}f_{7/2}}^{pn}$ matrix element is weaker as their angular momenta are different ($\ell_p = 2$, $\ell_n = 3$). As the spins of the protons in $d_{5/2}$ and the neutrons in $f_{7/2}$ are both aligned with respect to their angular momenta, the $V_{d_{5/2}f_{7/2}}^{pn}$ interaction contains repulsive tensor forces. These two effects make the $V_{d_{5/2}f_{7/2}}^{pn}$ monopole smaller in absolute value than the $V_{d_{5/2}d_{3/2}}^{pn}$ one, giving rise to a large reduction of the $N = 20$ shell gap. The monopole values used in Ref. [105] and Fig. 15 have several origins: the USD interaction for the sd -shell part has been fitted so as to reproduce the structure of stable nuclei, the fp -shell part (Kuo-Brown) has been obtained from the renormalized G matrix, whereas the cross-shell part is based on the Millener-Kurath interaction. Several monopole interactions had to be subsequently modified in order to reproduce the location of the drip-line in the O isotopic chain. Moreover the variation of the ESPE shown in Fig. 15 is based on some estimated monopole values, the intensity of which could be updated if new physics ingredients are added in the future.

The present predictions on the evolution of ESPE lead to several consequences that should be ascertained experimentally. First, as the $N = 20$ shell gap decreases, $2p - 2h$ excitations are increased and the ground state wave-function of nuclei in the island of inversion should contain admixtures of sd and fp states. Second, the 'intruder' fp states should be present at the proximity of the ground state for lighter, less deformed, nuclei. Third, the reduction of $N = 20$ is associated to the emergence of a new shell gap at $N = 16$. The search for this new shell gap, which is predicted to be large for the heaviest O isotopes (see left part of Fig. 15) has been carried out by

several means these last years. These three topics are addressed in the next sections.

4.1.4 Static properties and β -decay

Static properties of the nuclei, such as the g -factors and quadrupole moments [107], and β -decay schemes have been extensively used to map the island of inversion. Looking at the Mg isotopic chain [108, 110, 112], these combined approaches are bringing a wealth of information on the spin-parities of the ground states and their mixed configurations involving normal and intruder orbits.

Starting at $^{29}\text{Mg}_{17}$, the measured g -factor and quadrupole moments are in good agreement with the ones calculated with the USD interaction [108] which applies to a valence space limited to the sd orbits. This nucleus is therefore sitting outside the Island of Inversion. The low-energy level scheme and the Gamow-Teller distribution of ^{31}Mg have defined $N = 19$ as the neutron number at which the transition takes place [109]. The spin, parity and magnetic moment of its ground state have been determined by Neyens et al. [110] by combining hyperfine-structure and β -NMR measurements with an optically polarized ion beam at ISOLDE (CERN). A $J = 1/2^+$ configuration of the ground state, with $\mu_{exp} = -0.88355\mu_N$ can be accounted for by an almost pure $2p - 2h$ configuration. Shell model calculations using the SDPF-NR interaction reproduce perfectly the ground state as well as the high level density below 500 keV [111]. Hence the global physics picture is well understood.

The β -decay pattern of these nuclei is also very sensitive to the configurations of the mother and daughter nuclei. In the neutron-rich Mg isotopes, the β^- decay occurs mainly through the $\nu d_{3/2} \rightarrow \pi d_{5/2}$ Gamow-Teller transition. If the filling of the neutron is restricted to the sd orbits, the $\nu d_{3/2}$ orbit contains two neutrons in $^{30}\text{Mg}_{18}$ and four neutrons in $^{32}\text{Mg}_{20}$. The β -decay transitions of the $J^\pi = 0^+$ ground state of these even-even nuclei feed mainly $J^\pi = 1^+$ states in the daughter odd-odd nuclei via allowed Gamow-Teller transition with $\Delta\ell = 0, \Delta J = 1$. In the $^{30}\text{Mg} \rightarrow ^{30}\text{Al}$ decay, the feeding to the first 1^+ state at 688 keV exhausts almost all the β -decay strength, according to Ref. [113]. This shows that only neutrons from the sd shell contribute to this decay pattern. On the other hand, the β -decay of ^{32}Mg proceeds to the 1^+ ground state of ^{32}Al with a β -feeding I_β of about 55%. Another large part goes to high lying levels at 2.7 and 3.2 MeV, with I_β of about 25 and 10%, respectively. The remaining 5% goes to neutron-unbound states giving rise to β -delayed neutron emission. The β feeding writes as a function of the β strength S_β and the Q_β value as follows:

$$I_\beta(E^*) = \frac{S_\beta(E^*) \times (Q_{\beta\alpha} - E^*)^5}{\sum_{E^*} S_\beta(E^*) \times (Q_{\beta\alpha} - E^*)^5} \quad (23)$$

the $(Q_{\beta\alpha} - E^*)^5$ factor, originating from the phase space in the β -decay, strongly favors the decay to low excited states, such as the ground state with $E^* = 0$. In the case of the ^{32}Mg decay, the $Q_{\beta\alpha}$ value amounts to about 10 MeV. When assuming a given value of S_β , a ratio of $(10/7)^5 \simeq 6$ is found between the ground state and a level at 3 MeV. Taking this phase space factor into account, it is found that the observed strength to excited states is indeed four times larger than that to the ground state. Had the neutrons been restricted to the sd shells, the β -decay pattern would have been similar to that in the ^{30}Mg nucleus, i.e. almost all focused to low energy states. When assuming that the ^{32}Mg ground state has a fairly large $2p - 2h$ component, part of the $d_{3/2}$ neutrons have moved to the fp orbits¹³. Thus the β -decay pattern is shared in two parts, the one which arises from the remaining $d_{3/2}$ neutrons occurs to the ground state, the other which

¹³ Single-neutron knock-out experiments on $^{30,32}\text{Mg}_{18,20}$ projectiles have been performed, revealing significant

originates from neutrons in the fp orbits is found at higher energy. This qualitative description is of course over simplified as the complete mixing of configurations of the mother and daughter nuclei have to be taken into account.

Finally the discovery of an allowed β -decay from $^{33}_{11}\text{Na}_{22}$ to the ground state of $^{33}_{12}\text{Mg}_{21}$, with $\log(ft)=5.27(26)$, also provides direct evidence of the inversion of the $7/2^-$ and $3/2^+$ states [115]. With this inversion, the $\nu d_{3/2} \rightarrow \pi d_{5/2}$ decay becomes possible between the ground-state levels. Otherwise the allowed β -strength would have been found at higher excitation energy.

4.1.5 Search for intruder fp states by transfer and knock-out reactions

As depicted in the previous paragraph, the *ground-state* composition of a given nucleus could be partly probed from its β -decay pattern. Stripping (d, p) or one-nucleon knock-out reactions are known to be ideal tools to determine the single-particle energy and the spectroscopic factors (SF) or occupancies of the valence and occupied orbits, respectively. These complementary methods have been used to search for the presence of intruder states, with the aim of determining which fraction of the nucleons are promoted from the sd to the fp shells.

The reduction of the $N = 20$ shell gap should be accompanied with the appearance of negative-parity states (arising from the fp orbits) at low excitation energy. In the two $N = 17$ isotones, $^{31}_{14}\text{Si}$ and $^{29}_{12}\text{Mg}$, the energy of the first negative-parity state drops by more than 2 MeV with respect to the $3/2^+$ ground state as shown in the left part of Fig. 16. This feature is likely to be due to the reduction of the $N = 20$ shell gap or/and to the appearance of deformation below $Z = 14$. In this later case, the wave functions of these states carry a small fraction of the total single-particle strength originating from the spherical orbits. Experimental (d, p) results obtained so far in these two nuclei do not really permit to determine the evolution of the $N = 20$ shell closure as the spectroscopic factors of the states are either unknown (in $^{29}_{12}\text{Mg}$) or incertain (in $^{31}_{14}\text{Si}$). This task is not an easy one as the core nuclei ^{30}Si and ^{28}Mg do not exhibit strong closed-shell configurations. Therefore, the neutron single-particle states mix with excited states of the cores. A proper unfolding of these correlations should be undertaken before attributing this sudden change of excitation energy to a change of proton-neutron monopole matrix elements below $Z = 14$.

As compared to the $^{29}_{12}\text{Mg}_{17}$ case, the situation is expected to be a little simpler in the $^{27}_{10}\text{Ne}_{17}$ nucleus as its ^{26}Ne core has a weaker $B(E2)$ value and a 2^+ state at higher energy as compared to ^{28}Mg . The ground-state configuration is due to a single neutron in the $d_{3/2}$ shell. Shell model calculations within the sd shell predict a single bound excited state in ^{27}Ne , $J = 1/2^+$, at about 800 keV. Its configuration corresponds to a hole into the neutron $s_{1/2}$ orbit, a pair of neutron being coupled to $J = 0^+$ in the $d_{3/2}$ shell. The presence of intruder states in the $N = 17$ isotones would reveal the reduction of the $N = 20$ shell gap between the $\nu d_{3/2}$ and $\nu f_{7/2}$ or $\nu p_{3/2}$ orbits. By including the possibility of excitations into the fp shells, and estimations of the relevant monopoles matrix elements, two intruder states are predicted below 1 MeV using the SDPF-M effective interaction [105].

The $^{26}_{10}\text{Ne}(d, p)$ reaction has been used in inverse kinematics by Obertelli et al. [116] to determine the states in $^{27}_{10}\text{Ne}_{17}$ from the observation of their γ -decay into segmented Ge detectors. Two states were fed at 765 keV and 885 keV. The (d, p) cross section for the state at 765 keV leads to a SF value, $C^2S(d, p) = 0.6 \pm 0.2$. This is consistent with the value obtained with the SDPF-M

direct population of negative-parity intruder states of $^{29,31}\text{Mg}$ [114]. The total observed spectroscopic strength to these states are 0.60(12) and 1.78(38) respectively, indicating a large increase of the $2p - 2h$ component from $N = 18$ to $N = 20$.

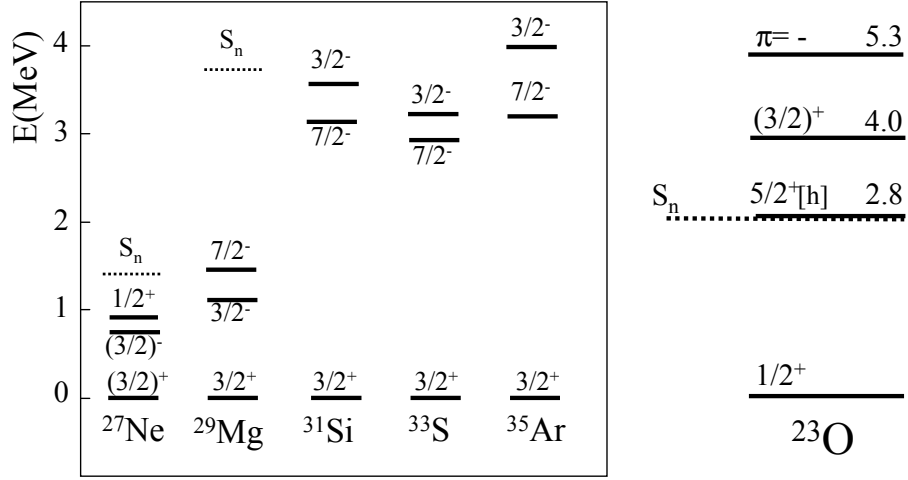


Figure 16: **Left** : Experimental energies of the excited states in the $N = 17$ isotones, showing the decrease of the intruder states $3/2^-$ and $7/2^-$ with respect to the ground state (adapted from the results of [116, 117]). **Right**: Experimental energies in $^{23}\text{O}_{15}$ taken from Refs. [118, 119], [h] corresponds to a hole state.

interaction for a negative parity state which could be $3/2^-$ or $7/2^-$. A weaker spectroscopic factor, $C^2S(d, p) = 0.3 \pm 0.1$ is found for the state at 885 keV for which a spin assignment of $1/2^+$ was suggested on the basis of its excitation energy and spectroscopic factor values. One expects a rather small SF for the $s_{1/2}$ level, which is in principle fully occupied when pair scattering to the $d_{3/2}$ state is not taken into account. As protons were stopped into the thick target used to induce the (d, p) reaction, their angular distribution could not be used to ascertain the spin assignments of the observed states.

Complementary information on ^{27}Ne was obtained from the work of Terry et al. [117]. The one-neutron knock-out reaction $-1n$ from a ^{28}Ne beam was used to study excited states in ^{27}Ne . As compared to the (d, p) technique which aimed at probing neutron valence states, the one-neutron knock-out occurs from occupied levels. To see any component arising from an intruder state would mean that the ground state wave function of ^{28}Ne already contains some amount of intruder configuration. A segmented Ge array surrounded the production target for the detection of γ -rays in coincidence with the ^{27}Ne nuclei in the focal plane of a spectrograph. The level scheme was found to be similar to the one proposed in Ref. [116]. In addition, a *prompt* γ transition between the $1/2^+$ and the intruder state has been observed. This discards a spin assignment of $7/2^-$ for the intruder state, which would have no decay to the $1/2^+$ due to their large spin difference. Moreover momentum distributions of the knock-out residues were used to determine the spin values and spectroscopic factors of the two excited states. It was found that the intruder state has an orbital angular momentum value, $\ell \leq 1$. Combining these pieces of information, it was inferred that the state at 765 keV is likely to have a $J = 3/2^-$ (from the $p_{3/2}$ orbit) and not a $7/2^-$ (from the $f_{7/2}$ orbit) configuration. Its spectroscopic factor $C^2S(-1n)$ of 0.32(4), means that the intruder $p_{3/2}$ shell is partly occupied in ^{28}Ne . This roughly agrees with the one predicted (0.24) by the shell model calculations using the SDPF-M interaction.

The presence of intruder state was also investigated in the $^{23}\text{O}_{15}$ nucleus by Elekes et al. [118] using the $^{22}\text{O}(d, p)^{23}\text{O}$ reaction with a 30 mg/cm² thick CD₂ target. Protons were detected in

the backward direction by 156 CsI(Tl) scintillators, while an array of 80 NaI(Tl) crystals was used to detect de-excited γ -rays produced during the stripping reaction. A neutron wall was used additionally to detect neutrons emitted after the feeding of neutron-unbound states in ^{23}O . Their energy was deduced from their time of flight. The excitation spectrum of ^{23}O (see the right part of Fig. 16) was reconstructed from the momentum of the neutron and the total energy of the ^{22}O nucleus measured in a telescope of Si detectors. Two states were discovered above the neutron separation energy of 2.74 MeV. The one at 4.0 MeV (unbound by about 1.3 MeV) was assigned to a $3/2^+$ configuration, while a negative parity was surmised for the state at 5.3 MeV. The energy difference between these two unbound levels is as small as ~ 1.3 MeV. It is related to the considerable shrink of the $N = 20$ shell gap, the energy of which is compatible with that obtained from the Monte Carlo Shell Model calculations based on the SDPF-M interaction [120].

4.1.6 *The appearance of a new magic number at $N = 16$*

As was discussed in the previous paragraph, experimental evidences for the reduction of $N = 20$ and the proximity of intruder states have been found. The emergence of a new shell gap at $N = 16$ for $Z < 14$ should naturally result from the reduction of the $N = 20$ gap. Apart from the fascinating discovery of a new doubly-magic nucleus, such as ^{24}O , this feature would ensure that the global evolution of nuclear structure is understood in this mass region.

The existence the $N = 16$ shell closure was first inferred from the systematics of the two neutron separation energies S_{2n} by Ozawa et al. [121]. There, a break in the S_{2n} values at $N = 16$ was observed for nuclei having a large isospin number $T_Z = 7/2$. In the same paper, sudden increase of interaction cross sections (σ_I) were observed in the F, O and N isotopes at $N \simeq 15$. The σ_I values for the ^{23}O and ^{25}F isotopes could be reproduced with a dominance of the $s_{1/2}$ shell for the valence orbit. This was corroborated by Sauvan et al. [122] who measured relatively narrow longitudinal momentum distributions from the one-neutron removal reaction. Confirmation was obtained by Cortina-Gil et al. [123] for ^{23}O using the exclusive one-neutron knock-out reaction in coincidence with de-exciting γ -rays of the core nucleus ^{22}O . A large occupancy of the $s_{1/2}$ orbit has been deduced from these works, which suggests that the $s_{1/2}$ orbit is well separated from the $d_{5/2}$ and $d_{3/2}$ orbits by the $N = 14$ and $N = 16$ gaps, respectively. Had one of these gap been weakened, the pairing interaction would have provided a large mixing between the s and d wave functions for the ground state of ^{23}O . The size of the $N = 14$ shell gap has been first determined from the spectroscopy of the ^{22}O nucleus, which was studied by Stanoiu et al. [124] by means of the in-beam γ -ray spectroscopy in the fragmentation of stable and radioactive beams. The energy of the first 2^+ and 3^+ states have been found to be 3.2 MeV and 4.58 MeV, respectively. These excited states have a $1p - 1h$ configuration with one particle in the $s_{1/2}$ orbit coupled to one hole in the $d_{5/2}$ orbit, the energy of the two states (2^+ and 3^+) being splitted by the residual $1p - 1h$ interaction. A $(2J+1)$ weighted average value of 4.0 MeV is obtained from their measured excitation energies, meaning that the distance in energy between the two neutron orbits, $\nu d_{5/2}$ and $\nu s_{1/2}$, is likely 4.0 MeV in ^{22}O . This value was predicted by the USD interaction [20], and has been recently confirmed by the work of Schiller et al. [119], from the observation of a resonance in neutron-fragment coincidences. This corresponds to the decay of the first excited state of ^{23}O at 2.8 MeV, assigned as the $5/2^+$ hole state, into the ground state of ^{22}O (see the right part of Fig. 16).

The in-beam technique could in principle be used to determine the energy of excited states in the ^{23}O and ^{24}O nuclei to evaluate the size of the $N = 16$ shell gap. The non observation of any γ -ray [124] from these nuclei has suggested that all the excited states lie above the neutron

decay threshold, which amounts to 3.7 MeV in ^{24}O . Based on the arguments derived above from the study of the ^{22}O nucleus, a lower limit could be set on the size of the $N = 16$ gap to be $\simeq 3.7$ MeV. As already reported in the previous section (see the right part of Fig. 16), an unbound state at 4.0 MeV above the $1/2^+$ ground state has been populated in ^{23}O by means of the $^{22}\text{O}(d, p)$ reaction [118]. This resonance was assigned to the $d_{3/2}$ level on the basis of the proton angular distribution and spectroscopic factor value. The size of the $N = 16$ gap therefore amounts to about 4 MeV, in accordance with the shell model calculations of Refs. [105, 20].

4.1.7 Conclusion

Since the discovery of the major shell closures and the shell gaps between them, about 40 years of nuclear physics have sustained the postulate of protons and neutrons shell closures which survived all through the nuclear chart. The $N = 20$ shell closure is the first in which a weakened gap has been invoked to explain the anomalies in atomic masses, charge radii, and spectroscopy around the ^{32}Mg nucleus. At that time already, the underlying mechanisms which produced this disappearance of closed were proposed by the shell model and mean field approaches through particle-hole excitation and the restoration of broken symmetries, respectively.

These pioneering works have undoubtedly triggered a new era in the study of nuclear structure, that of the study of the so-called "exotic nuclei". Thanks to the development of suitable radioactive ion beams worldwide, further studies of these nuclei became available. Now the properties of this shell closure as well as the reasons for its reduction are rather well understood and are summarized below.

- The $N=20$ magic number is formed between two shells of the harmonic oscillator well having opposite parities. Therefore $1p - 1h$ excitations cannot form positive parity states, such as 2^+ excitations. Therefore, quadrupole collectivity develops only with a minimum of $2p-2h$ excitations across $N = 20$. As the size of the $N = 20$ remains as large as 5 MeV between the $_{20}\text{Ca}$ and $_{14}\text{Si}$ isotopic chains such excitations are limited to high-lying states such as the superdeformed bands in ^{40}Ca [125].

- The $2p-2h$ excitations may be favored over the $0p-0h$ configuration as soon as the size of the $N = 20$ shell gap is reduced. This phenomenon occurs suddenly between the Si and Mg isotopic chain by the action of the proton-neutron interaction $\pi d_{5/2}-\nu d_{3/2}$ which weakens the $N = 20$ gap by about 1.2 MeV by the removal of 2 protons, from an initial value of about 5 MeV.

- As the $V_{d_{5/2}d_{3/2}}^{pn}$ matrix element has by far the highest value among the other monopoles which intervene in this region of the chart of nuclides, it rules the evolution of the nuclear structure as soon as it is involved. Its large intensity comes from the intrinsic properties of the nucleon-nucleon interaction.

- When removing further protons to reach the $_{8}\text{O}$ chain, the $N = 20$ gap plummets. Intruder states originating from excitations across the $N = 20$ gap to the fp shells have been discovered only about 1 MeV above the last occupied $d_{3/2}$ shell.

- A remarkable consequence of the disappearance of the $N = 20$ shell closure is the emergence of a new magic number at $N = 16$, formed in $^{24}_{8}\text{O}_{16}$ between the occupied $s_{1/2}$ and the unbound valence $d_{3/2}$ orbit. This gap amounts to about 4 MeV and the $d_{3/2}$ orbit is unbound by about 1.5 MeV. The neutron-neutron interactions due to the filling of this orbit do not suffice to bind the $^{26,28}_{18,20}\text{O}$ nuclei.

Last but not least, the present study can undeniably serve to explain similar sudden disappearance of the harmonic oscillator shell closures, $N = 8$ and $N = 40$, while removing two protons from $^{14}_6\text{C}_8$ to $^{12}_4\text{Be}_8$ and from $^{68}_{28}\text{Ni}_{40}$ to $^{66}_{26}\text{Fe}_{40}$ nuclei, respectively. For these two cases also, the role

of the proton-neutron spin-isospin interactions (such as $\pi p_{3/2}-\nu p_{1/2}$ and $\pi f_{7/2}-\nu f_{5/2}$, respectively) are essential to create other islands of inversion at $N = 8$ [67, 69, 126] and $N = 40$ [127, 128].

4.2 Evolution of the $Z = 20$ shell closure

The ${}_{20}\text{Ca}$ isotopic chain spans over about 22 hitherto discovered isotopes, among which four ones behave as doubly-magic nuclei. This is ascribed to the presence of the well-known $N = 20$ and $N = 28$ major-shell closures and of the newly-observed $N = 16$ and $N = 32$ sub-shell closures. As the Ca core is hardly polarized by adding neutrons, the neutron single-particle energies in the Ca and neighboring isotopes serve as references to constraint effective nuclear interactions used for the shell model or mean field calculations. Also, the evolution of the $d_{3/2}$, $s_{1/2}$ and $d_{5/2}$ proton single-particle energies in the ${}_{19}\text{K}$ isotopic chain with the filling of the neutron $f_{7/2}$ orbit brings a wealth of information on the tensor forces acting between the πd and νf orbits. These ingredients will in turn become essential to understand the evolution of other magic numbers, such as the $N = 28$ ones.

4.2.1 Binding energies

The left part of Fig. 17 shows the evolution of the binding energies of the proton orbits (bottom) together with that of the $Z = 20$ shell gap (top), for a neutron number N ranging from $N = 18$

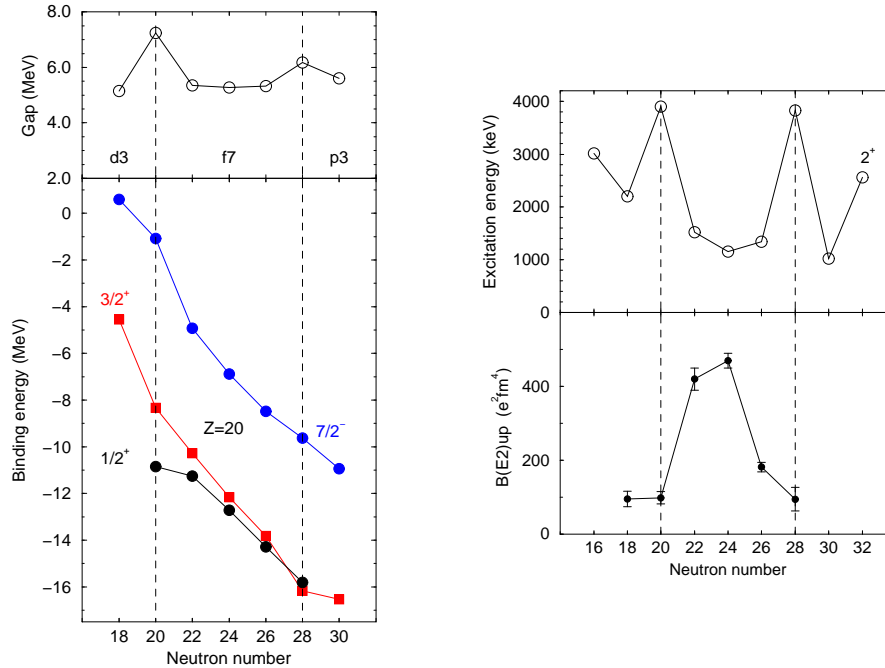


Figure 17: **Left:** Binding energies of the states located just above and just below the $Z = 20$ magic number and difference of the binding energies of the two states surrounding the gap at $Z = 20$ (see Sect. 11). The neutron orbitals which are getting filled as a function of increasing N are given in the middle of the figure. **Right:** Experimental $E(2_1^+)$ and $B(E2; 0^+ \rightarrow 2_1^+)$ values in the ${}_{20}\text{Ca}$ isotopic chain.

to $N = 30$. While the ground-state spin value of the ${}_{21}\text{Sc}$ isotopes is $7/2^-$ for the whole interval,

the one of the ^{19}K isotopes changes at $N = 28$, and is tentatively established at $N = 30$. Apart from the large singularity that shows up at the $N = 20$ neutron magic number, the size of the $Z = 20$ gap is constant, $\simeq 5.3$ MeV between $N = 22$ to $N = 26$, i.e. as the $\nu f_{7/2}$ is being filled. It seems to be slightly larger at $N = 30$ than at $N = 22 - 26$. However the present knowledge on the binding energies of the neutron-rich K-Ca-Sc isotopes is not enough to ascertain this hypothesis. On the proton-rich side, such an estimation of the gap cannot be obtained below $N = 18$ as the ^{39}Sc nucleus is already located beyond the proton drip line. As the size of the $Z = 20$ gap remains large and almost constant along the whole Ca isotopic chain, core excitations of the Ca isotopes should remain relatively weak at low excitation energy. This isotopic chain is therefore an ideal test bench for exploring the spherical neutron shell and sub-shell closures at $N = 16$, $N = 20$, $N = 28$, $N = 32$ and possibly $N = 34$ as their existence would be decoupled from the proton core excitations. This assertion of a weak core excitation is corroborated by the behaviors of the 2_1^+ energies and the $B(E2; 0^+ \rightarrow 2^+)$ values in the Ca isotopic chain, discussed in the following section.

4.2.2 Trends of $E(2^+)$ and $B(E2)$ values

The systematics of the 2^+ and $B(E2)$ values from ^{40}Ca to ^{48}Ca (see the right part of Fig. 17) is often used in textbooks to model multi-particle configurations of valence nucleons in one particular orbit, in the present case the $\nu f_{7/2}$ one. In this framework, the 2_1^+ energies are maximum at the beginning and end of the shell and almost constant in between. The $B(E2)$ values follow a bell-shape curve with minima at the two extremes of the shell.

A strong sub-shell closure is found at $N = 16$, through the observation of a large 2^+ energy, $E(2^+) = 3.015(16)$ MeV, in ^{36}Ca (see Fig. 17). This state was populated by the one neutron knock-out reaction from a ^{37}Ca beam at the GSI facility [129]. Similar result has been obtained at GANIL using the same experimental technique [130]. This 2^+ state decayed in-flight by γ -ray emission, even though the 2^+ state is located about 400 keV above the proton emission threshold. This feature is *a priori* surprising as particle decay is usually much faster than γ -decay. The Coulomb barrier partly delays the particle emission. However the main hindrance factor against proton decay is due to the weak overlap of the wave functions of the 2^+ state and the ground state of the $^{35}\text{K}_{16}$ nucleus. The former is of almost pure neutron origin due to excitations across the $N = 16$ sub-shell, whereas the second has a proton hole configuration with respect to ^{36}Ca .

An $N = 32$ sub-shell closure has been evidenced in the ^{52}Ca nucleus through the observation of the first 2^+ state at 2.52 MeV. This state was populated through the β -decay of ^{52}K at the CERN/ISOLDE facility [131]. This $N = 32$ sub-shell is formed between the neutron $p_{3/2}$ and $p_{1/2}$ orbits, the $f_{5/2}$ orbit being located upwards in energy. The $N = 32$ gap is present in the Ca isotopic chain in which the proton $f_{7/2}$ orbit is empty. As protons are added into this orbit, the strong $\pi f_{7/2} - \nu f_{5/2}$ interaction acts to progressively move the neutron $f_{5/2}$ orbit between the neutron $p_{3/2}$ and $p_{1/2}$ orbits, destroying the $N = 32$ shell gap. Therefore the increase of 2^+ energy at $N = 32$ is gradually smoothened in the ^{22}Ti [132] and ^{24}Cr chains [133], to eventually vanish in the ^{26}Fe and ^{28}Ni chains. Compared to neighboring isotopes, the $B(E2)$ values at $N = 32$ are slightly reduced in the Ti [134] and Cr [135] isotopic chain. This feature matches with the existence of a subshell closure at $N = 32$, which induces a local reduction of the collectivity.

A fairly large $N = 34$ sub-shell gap has been predicted by Honma et al. between the $\nu f_{5/2}$ and $\nu p_{1/2}$ orbits using the effective GXPF1 interaction [136]. So far the energy of the 2_1^+ state has not been determined in the ^{54}Ca isotope. However no significant enhancement of the $N = 34$ gap was found from the study of the excited states in the neutron-rich $^{50-52}\text{Ca}$ nuclei [137], which

correspond to $f_{5/2} \otimes p_{1/2}$ excitations. In addition the 2^+ energy in $^{56}_{22}\text{Ti}_{34}$ has been determined to be 1129 keV from the β -decay of ^{56}Sc , which is smaller than that of the $N = 32$ nucleus $^{56}_{22}\text{Ti}_{32}$ which amounts to 1495 keV [132].

4.2.3 Proton orbits below the $Z = 20$ gap: Levels of ^{19}K isotopes

The evolution of the energy of the three single-proton orbits $d_{3/2}$, $s_{1/2}$, and $d_{5/2}$ (located below the $Z = 20$ gap) during the filling of the $\nu f_{7/2}$ sub-shell, is essential to derive information on the various components of the proton-neutron interactions within the πsd - $\nu f_{7/2}$ configurations. In particular, the strength of tensor forces between the $\pi d_{3/2}$ and $\pi d_{5/2}$ orbits and the $\nu f_{7/2}$ one could be determined. So far several publications [53, 138, 139, 140] are using various intensities of this force. Therefore all the relevant experimental data are summarized in the following.

The $\pi d_{3/2}$ and $\pi s_{1/2}$ orbits

From $N = 18$ to $N = 26$, the ground state of the ^{19}K isotopes has a $3/2^+$ spin value, which originates from the $\pi d_{3/2}$ orbit. The spin value of the first excited state is $1/2^+$. Its energy follows that of the 2^+ excitation of the Ca core from $N = 18$ to $N = 24$, as shown in the left part of Fig. 18. This feature means that, up to $N = 24$, the $1/2_1^+$ state possibly arises from the coupling

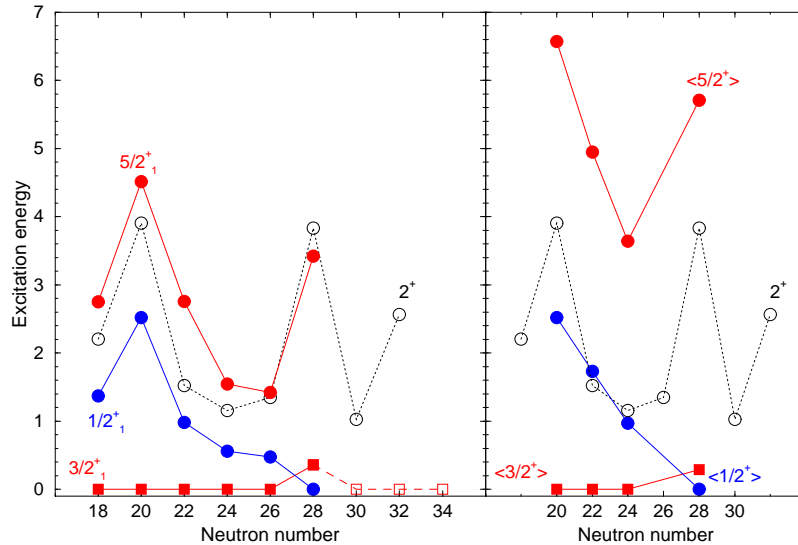


Figure 18: **Left:** Energy of the $3/2_1^+$, $1/2_1^+$, and $5/2_1^+$ states of the ^{19}K isotopes as a function of the neutron number. **Right:** Average energy of all the $3/2^+$, $1/2^+$, and $5/2^+$ states populated in the $^{20}\text{Ca}(d,^3\text{He})$ pick-up reactions [141, 142, 143] (see Tables 2 and 3). The energy of the first 2^+ excitation of the Ca core is also drawn (empty circles, dotted line).

between the $3/2^+$ state and the 2^+ excitation of the core, and to a weaker extent from the $\pi s_{1/2}$ single-particle state. For $N > 24$, the excitation energy of the $1/2_1^+$ state decreases so rapidly that it becomes the ground state of $^{47}\text{K}_{28}$. This indicates, without ambiguity, that the energy spacing between the two sub-shells, $\pi d_{3/2}$ and $\pi s_{1/2}$, which defines the $Z = 16$ sub-shell closure, is strongly decreasing during the filling of the $\nu f_{7/2}$ orbital.

A more quantitative description of this shell evolution can be obtained from the study of the $(d,^3\text{He})$ pick-up reactions on stable Ca targets, which provide the energies and spectroscopic fac-

tors of the $3/2^+$ and $1/2^+$ proton-hole states in the odd-A $_{19}\text{K}$ isotopes. In the work of Doll et al. [141], four targets ($^{40,42,44,48}\text{Ca}$) have been used. For each $_{19}\text{K}$ isotope, only one state of orbital momentum $\ell = 2$ has been assigned to the $\pi d_{3/2}$ sub-shell : the ground state for $^{39,41,43}\text{K}_{20,22,24}$ and the first excited state for $^{47}\text{K}_{28}$. States of higher energy with orbital momentum $\ell = 2$ have been assigned to the $\pi d_{5/2}$ sub-shell, as reported below. Later, Bank et al. [142] have used a polarized beam of deuterons to distinguish between levels in which the intrinsic spin is aligned ($j=\ell+1/2$) or anti-aligned ($j=\ell-1/2$) with the orbital momentum ℓ . From this study, a second $\ell = 2$ state at 3.88 MeV has been assigned to the $\pi d_{3/2}$ orbit in ^{47}K . Concerning the $\pi s_{1/2}$ orbit, its strength is split into 2 or 3 states, the first one having the largest spectroscopic factor. The left part of Table 2 gives the experimental results of $^{39,41,43}\text{K}$ from Ref. [141] and ^{47}K from Ref. [142]. The

Table 2: The $3/2^+$ and $1/2^+$ states observed in the $^{40,42,44,48}\text{Ca}(d,^3\text{He})$ pick-up reactions [141, 142] and summary of the properties of the $\pi d_{3/2}$ and $\pi s_{1/2}$ orbits in the K isotopes

	E(MeV)	l	sub-shell	$(2J+1)C^2S$	$\pi d_{3/2}$		$\pi s_{1/2}$	
					E_{aver}	$(2J+1)\Sigma C^2S$	E_{aver}	$(2J+1)\Sigma C^2S$
^{39}K [141]	0	2	d3/2	3.70	0	3.70	2.52	1.65
	2.52	0	s1/2	1.65				
^{41}K [141]	0	2	d3/2	3.43	0	3.43	1.73	1.58
	0.98	0	s1/2	0.77				
	1.57	0	s1/2	0.17				
	2.67	0	s1/2	0.64				
^{43}K [141]	0	2	d3/2	3.15	0	3.15	0.97	1.47
	0.56	0	s1/2	1.15				
	2.45	0	s1/2	0.32				
^{47}K [142]	0	0	s1/2	1.55	0.87	4.86	0.58	1.83
	0.36	2	d3/2	4.16				
	3.80	0	s1/2	0.28				
	3.88	2	d3/2	0.70				

single-particle energies (SPE) of the two shells, $\pi d_{3/2}$ and $\pi s_{1/2}$, are obtained by averaging the energies of the states $3/2^+$ and $1/2^+$, respectively, weighted by their spectroscopic factors (see the right parts of Table 2 and Fig. 18). Recently, another experiment has been performed on ^{47}K by means of the $^{48}\text{Ca}(e, e'p)$ reaction [143]. The spectroscopic factors of the populated states have been determined using the spin values assigned from the $(\vec{d}, ^3\text{He})$ reaction. Their values are systematically smaller than those obtained with the $(\vec{d}, ^3\text{He})$ reaction, i.e. $(2J+1)\Sigma C^2S(\pi d_{3/2})=2.6$ and $(2J+1)\Sigma C^2S(\pi s_{1/2})=1.2$ [143], as compared to 4.86 and 1.83 [142], respectively. Error bars of about 20-30% should be applied to the SF values. The apparent discrepancy between SF obtained in $(e, e'p)$ and $(d, ^3\text{He})$ experiments has been investigated in Ref. [143]. It disappears if the latter ones are reanalyzed with a nonlocal finite-range DWBA analysis with a bound state wave function that is obtained from $(e, e'p)$ experiments. However, as the averaging procedure only involves the relative SF, the two sets of SPE are close, i.e. $E_{aver}(\pi d_{3/2}) = 0.81$ MeV and $E_{aver}(\pi s_{1/2}) = 0.52$ MeV [143], as compared to 0.87 and 0.58 MeV [142], respectively. In both cases, the energy difference between the $s_{1/2}$ and $d_{3/2}$ at $N = 28$ is negative, and amounts to about -0.29 MeV. This indicates that the $\pi d_{3/2}$ and $\pi s_{1/2}$ shells cross at $N = 28$. Their spacing decreases from 2.52 MeV at $N = 20$ to -0.29 MeV at $N = 28$, by a total amount 2.81 MeV. As the $f_{7/2}$ orbit contains

up to eight neutrons, the reduction of the $d_{3/2} - s_{1/2}$ spacing amounts to $2.81/8 \simeq 350$ keV per neutron. This variation can be formally written in terms of the energy difference between the two proton-neutron monopole interactions involved in the reduction of the proton $d_{3/2} - s_{1/2}$ spacing,

$$V_{d_{3/2}f_{7/2}}^{pn} - V_{s_{1/2}f_{7/2}}^{pn} \simeq -350 \text{ keV}. \quad (24)$$

Beyond $N > 28$ the physical picture changes as another orbit, $\nu p_{3/2}$, starts to be filled. Therefore there is no reason to believe that the $\pi s_{1/2}$ - $\pi d_{3/2}$ spacing would follow the same trend. The spin of the ground state of ^{49}K has been assigned tentatively to $3/2^+$ from its β -decay pattern [144]. Indeed three $I^\pi = 5/2^+$ neutron-unbound states of ^{49}Ca are strongly fed at 6.55, 6.69 and 7.06 MeV with $\log(ft)$ values of 4.5, 4.5 and 4.6, respectively. These intensities correspond to Gamow-Teller transitions between states with $\Delta J=0, \pm 1$, which holds true only if the g.s. of ^{49}K is $3/2^+$. The ground state spin values of $^{51,53}\text{K}$ have been assigned as $3/2^+$ state from their β -decay studies [145]. Corresponding states are drawn in the left part of Fig 18 using empty symbols and dashed line. Firm assignments for the g.s. spin values of $^{49,51,53}\text{K}$ and the location of $1/2^+$ excited state are important to obtain the monopole matrix elements involved there. For $N > 28$, the spacing of the proton orbits $s_{1/2} - d_{3/2}$ scales with the difference of the monopole matrix elements, $V_{d_{3/2}p_{3/2}}^{pn} - V_{s_{1/2}p_{3/2}}^{pn}$.

The $\pi d_{5/2}$ orbit

The exact location of the $\pi d_{5/2}$ orbit is hard to determine as it is deeply bound. Consequently its strength is fragmented into several deeply bound states which carry small spectroscopic factor each [141, 142]. Table 3 summarizes the number of $5/2^+$ states, their range of excitation energy, the sum of the spectroscopic factors (the $(2J+1)C^2S$ sum rule should amount to 6 in the $d_{5/2}$ orbit) as well as the weighted averaged mean energies. The sum of the spectroscopic factors barely exceeds 65% at $N = 20$ and $N = 28$.

Along the whole K isotopic chain, the energy of the $5/2_1^+$ state follows exactly that of the 2^+ energy of the core nucleus as shown in the left part of Fig. 18. Same is almost true for the average energy of the $5/2^+$ states, shown in the right part of the same figure. This feature shed little doubt on the validity of the location and evolution of the $d_{5/2}$ single particle energy. Moreover, we can refer to the introduction of Ref. [141], from which these data have been extracted : " ... we shall show that the data are very suggestive of a strong influence of collective modes, not only on the widths but on the energies of quasi-holes too", and to the conclusion "The quasi-hole energy should not be confused with a centroid separation energy whose determination would require a knowledge of the full $1d_{5/2}$ hole strength."

Table 3: States populated in the pick-up ^4Ca ($d, ^3\text{He}$) $A-1\text{K}$ reactions with orbital angular momentum $\ell = 2$ and assigned to the $\pi d_{5/2}$ orbit [141, 142].

	number of states	E_{\min} - E_{\max} (MeV)	$(2J+1)\Sigma C^2S$	E_{aver} (MeV)
^{39}K [141]	13	5.27 - 8.90	4.8	6.57
^{41}K [141]	9	3.19 - 6.63	3.8	4.95
^{43}K [141]	12	1.54 - 5.90	3.1	3.64
^{47}K [142]	10	3.32 - 8.02	3.9	5.71

With some words of caution, we could make use of the results on the two semi-magic isotopes, ^{39}K and ^{47}K to derive the variation between the $\pi d_{3/2}$ and $\pi d_{5/2}$ SPE. The $d_{3/2} - d_{5/2}$ spacing

decreases from 6.57 MeV to 4.84 MeV, the latter value resulting from the difference of the SPE between the $\pi d_{5/2}$ energy of 5.71 MeV (reported in Table 3) and that of the $\pi d_{3/2}$ state at 0.87 MeV (reported in Table 2), giving a variation of about 1.7 MeV. This is possibly an *upper bound*, as the fraction of the identified $\pi d_{5/2}$ hole strength is lower at $N = 28$ than at $N = 20$. It is anyhow much weaker than the value of 2.7 MeV used in Ref. [138]. As the $\nu f_{7/2}$ orbit contains up to 8 neutrons, the variation of the $\pi d_{3/2} - \pi d_{5/2}$ splitting amounts to $1.7/8 \simeq 0.210$ MeV per neutron. This could be written formally as a function of the relevant monopoles:

$$V_{d_{3/2}f_{7/2}}^{pn} - V_{d_{5/2}f_{7/2}}^{pn} \simeq -210 \text{ keV} \quad (25)$$

A proper unfolding of the correlations should be performed to better determine the evolution of the $d_{5/2}$ single-particle energy between $N = 20$ and $N = 28$. This requires to consider proton core-excitations which may not be taken into account so far.

Theoretical predictions on the evolution of the three orbits

As said in the introduction of this section, the evolution of the relative energies of the $\pi d_{3/2}$, $\pi s_{1/2}$, and $\pi d_{5/2}$ shells during the filling of the $\nu f_{7/2}$ orbit, can provide robust information on the various components of the proton-neutron interaction.

As a starting point, we can compare the experimental data of the ^{19}K isotopic chain to the results of HFB self-consistent calculations we have obtained using the D1S Gogny force [146]. There, nuclear interactions are given by the sum of central and spin-orbit terms, without tensor interaction. The description of an odd-A nucleus is done using the blocking method, imposing that the odd particle is located in one particular orbit chosen by its value of angular momentum and parity. The calculated binding energy of the nucleus is then analyzed as a function of the occupied orbital, that gives the ground state and the excited states. The results of the calculations on the odd-A K isotopes are drawn in the right part of Fig. 19. The excitation energy of the $1/2^+$ state decreases during the filling of the $\nu f_{7/2}$ sub-shell and then increases for $N > 28$. This is in qualitative agreement with the experimental results, shown for convenience in the left part of Fig. 19. Nevertheless, the theoretical slope is less steep than the experimental one: Between $N = 20$ and $N = 28$, the calculated variation of $[E(1/2^+) - E(3/2^+)]$ amounts to 1.2 MeV, to be compared to the value of 2.8 MeV derived from experimental data (see Table 2). By adding a tensor term to the D1S Gogny force, the reduction of the $1/2^+ - 3/2^+$ splitting would be larger, coming closer to the experimental values. No variation of the $\pi d_{3/2} - \pi d_{5/2}$ splitting is predicted during the filling of the neutron $f_{7/2}$ orbit. There again, a tensor term would reduce this splitting either.

Shell model calculations have been using constantly improved effective interactions to describe the structure of the nuclei involving the $\pi(sd)$ and $\nu(fp)$ orbits. The $sd - pf$ interaction was originally developed by Retamosa et al. [147]. The proton-neutron matrix elements involving the proton in the $d_{3/2}$, $s_{1/2}$, and $d_{5/2}$ orbits with the neutron in the $f_{7/2}$ one were constrained by the systematics of the proton SPE in the K isotopic chain. Later, the energy differences between the $3/2^-$ excited and $7/2^-$ ground states in the $^{37}_{16}\text{S}_{21}$ and $^{35}_{14}\text{Si}_{21}$ nuclei were used to refine the matrix elements involving the $\pi s_{1/2}$ and the $\nu f_{7/2}$ and $\nu p_{3/2}$ matrix elements. The energy of the $3/2^-$ state in $^{35}_{14}\text{Si}$ was obtained from the β -decay of ^{35}Al [148]. Further refinements have been done to account for spectroscopic information of nuclei lying in the $sd - fp$ shells [140, 149]. Several recent publications have discussed about a tensor component of the nucleon-nucleon interaction (see for instance Refs. [53, 138, 139, 140]). In the three former works the tensor term of the $V_{d_{3/2}f_{7/2}}^{pn}$ monopole interaction, $\tilde{V}_{d_{3/2}f_{7/2}}^{pn}$, amounts to about - 200 keV. In the latter, it is shown than even a weaker value of the tensor interaction suffice to reduce the $Z = 14$ subshell gap and

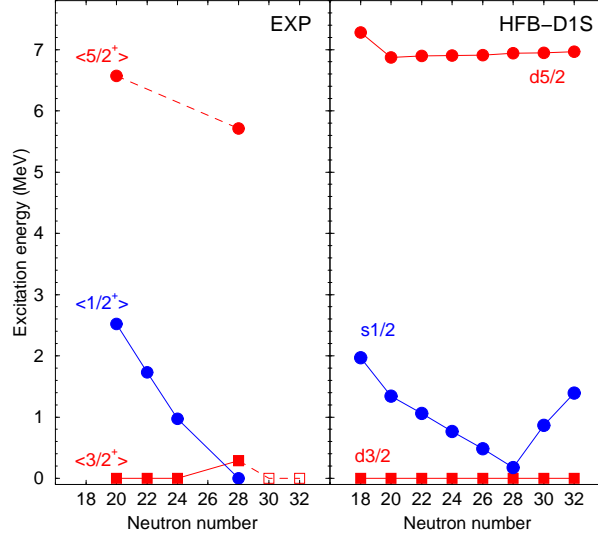


Figure 19: **Left:** Average energy of all the $3/2^+$, $1/2^+$, and $5/2^+$ states populated in the $^{20}\text{Ca}(d,^3\text{He})$ pick-up reactions (see the right part of Fig. 18). **Right:** Evolution of the energies of the $3/2^+$, $1/2^+$, and $5/2^+$ spherical states of the odd-A K isotopes from $N = 18$ to $N = 32$ predicted in the HFB self-consistent calculations using the D1S effective force of Gogny and the method of blocking.

account for the enhanced collectivity of the $^{42}\text{Si}_{28}$ nucleus. This peculiar case will be discussed in the Sect. 5.1.2.

4.2.4 Conclusion

The $Z = 20$ isotopic chain is an ideal test bench for nuclear models, and to derive effective interactions, would they be neutron-neutron or proton-neutron ones. The reason is that the gap remains large enough to avoid coupling between single particle states and collective excitations at low energy. Thus shell and subshell closures have been studied in the Ca isotopic chain, such as the $N = 16$, $N = 20$, $N = 28$ and $N = 32$ ones.

To induce quadrupole collectivity, a minimum of $2p - 2h$ is required, as the $Z = 20$ gap is bound by states having opposite parities. Hence the $B(E2; 0^+ \rightarrow 2_1^+)$ values remain relatively weak. Deformed and superdeformed bands have been found at high excitation energy [125], showing that the multiparticle-multihole picture is extremely efficient to generate quadrupole collectivity [150].

The energies of the proton-single particle states below the $Z = 20$ gap have been determined in the ^{19}K isotopic chain through transfer reactions between $N = 20$ to $N = 28$. A collapse of the $Z = 16$ gap, formed between the proton $d_{3/2}$ and $s_{1/2}$ orbits, is found. Experimental data also seem to show a reduction of the proton $d_{3/2} - d_{5/2}$ splitting, which can be accounted for by the $\pi d - \nu f_{7/2}$ tensor forces. This compression of the proton d orbits echoes that of the f orbits around the $N = 28$ shell closure, which will be addressed in a following section.

5 The magic number 28

The magic number 28, revealed for instance in the doubly-magic nucleus $^{48}_{20}\text{Ca}_{28}$, originates from the spin-orbit coupling in atomic nuclei. Guided by the existence of such a term in atomic physics, M. Goeppert Mayer [3] and O. Haxel et al. [4] independently postulated in 1949 the existence of a strong spin-orbit (SO) force in the nuclear potential to reproduce the so-called ‘magic numbers’ above 20. The SO interaction is attractive for nucleons having their angular momentum aligned with respect to their spin (denoted as ℓ_{\uparrow}) and repulsive in case of anti-alignment (ℓ_{\downarrow}). Its strength was constrained to reproduce the size of the shell gaps of the various magic numbers formed by this interaction (28, 50, 82 and 126). As for the number 28, the effect of such a SO interaction was to lower the $f_{7/2}$ orbit into the middle of the gap between the sd and fp oscillator shells, resulting in the magic number between the $f_{7/2}$ and $p_{3/2}$ orbits. Nevertheless, the history is not complete since, as discussed in the end of Sect. 2.3.1 and shown in Fig. 7, we know now that a large part of the $N = 28$ gap observed at ^{48}Ca comes from the attractive monopole interaction, $V_{f_{7/2}f_{7/2}}^{nn}$.

The sequence of the orbits around 28 exhibits 2 pairs of spin-orbit partners $f_{7/2}$, $p_{3/2}$, $p_{1/2}$ and $f_{5/2}$, ranked as a function of decreasing binding energies. It therefore follows from this ordering of levels that the existence or vanishing of this shell closure is possibly linked to the evolution of the SO force.

Within the mean-field approaches, the SO interaction is maximum at the surface and vanishes in the interior of the nucleus where the potential varies slowly for most of the nuclei. Therefore a wide consensus still holds on the fact that reductions of the SO interaction, and henceforth of shell gaps, would occur for neutron-rich nuclei with increased surface diffuseness (see for instance Ref. [39, 151]). More recently, a reduction of SO was suggested when the matter density is strongly depleted in the center of the nucleus [152].

Beyond the classical mean-field approaches, it was argued that the proton-neutron tensor interaction modifies the energies of the ℓ_{\uparrow} and ℓ_{\downarrow} components when specific proton and neutron orbits are filled [53]. This effect could modify for instance the $\nu f_{5/2}$ - $\nu f_{7/2}$ splitting as protons are added or removed into the $\pi d_{3/2}$ orbit or the $\pi f_{5/2}$ - $\pi f_{7/2}$ splitting as neutrons are added to the $\nu g_{9/2}$ orbit.

5.1 Evolution of the $N = 28$ shell closure

The study of the evolution of $N = 28$ magic shell far from stability is an ideal tool for probing the nuclear forces at play such as the spin-orbit and tensor terms for nuclei with a reduced binding energies or/and with a depletion of the density in their interior. A lot of experimental studies aimed at determining whether the $N = 28$ shell closure is eroded in very neutron-rich nuclei through complementary methods, which are direct or indirect ones. The very first indirect hints of the vanishing of the $N = 28$ gap were obtained by β -decay [153], mass measurements [154] and Coulomb-excitation [155] experiments. This subsequently triggered other theoretical works, in turn followed by new experiments. The present understanding of the physics behind the $N = 28$ shell closure results from a subtle interplay between theory and experiments.

The following sections will start with the systematics of binding energies and be followed by the evolution of quadrupole properties of the $N = 28$ isotones. A deeper understanding of the nuclear forces involved around the $N = 28$ magic shell will be obtained by determining the evolution of proton and neutron single particle energies. These pieces of information will be used to describe the physics towards the lightest even- Z $N = 28$ nuclei, such as $^{42}_{14}\text{Si}$.

5.1.1 Binding energies

The binding energies of the last neutron in the $N = 28$ and $N = 29$ isotones are drawn in the left part of Fig. 20. These data are restricted to nuclei which are likely to be spherical. They are taken

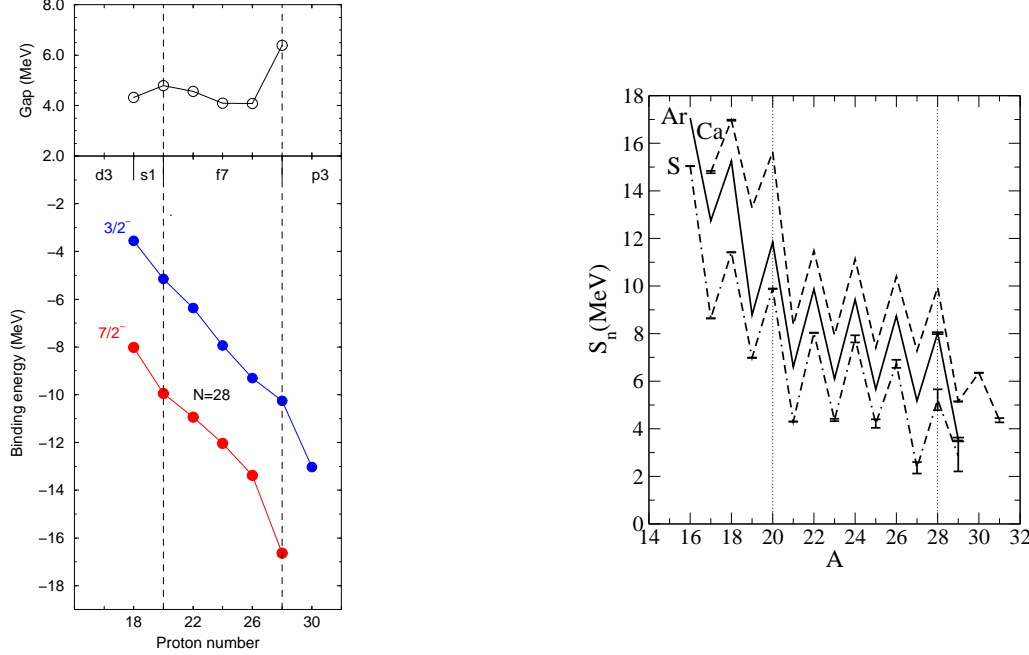


Figure 20: **Left:** Binding energies of the states located just above and just below the $N = 28$ magic number and difference of the binding energies of the two states surrounding the gaps at $N = 28$ (see Sect. 11). The proton orbitals which are getting filled as a function of increasing Z are given in the middle of the figure. **Right:** Neutron separation energies S_n as a function of the atomic mass for the ${}_{20}\text{Ca}$, ${}_{18}\text{Ar}$ and ${}_{16}\text{S}$ isotopic chains.

from the AME2003 atomic mass table [10], to which the result for the ${}^{47}_{18}\text{Ar}$ isotope [139] has been added. The distance in energy between the two binding-energy curves is shown in the top part of Fig. 20 as a function of the proton number. With the exception of the maximum at $Z = 28$ (see Sect. 11), the $N = 28$ gap amounts to about 4.5 MeV. It is found that the $N = 28$ gap has decreased by 330(80) keV between $Z = 20$ and $Z = 18$. This point is essential to understand the evolution of the nuclear structure below $Z = 20$. This will be discussed more extensively later on.

Below $Z = 18$ the separation energies of the last neutron in ${}^{44,45}_{16}\text{S}$, recently measured [70], have not been included in Fig. 20 as the ${}^{44}\text{S}$ ground state is likely to be deformed. This can be viewed in the right part of Fig. 20 which displays the evolution of one-neutron separation energy $S_n(A, Z)$ as a function of the neutron number N . In the Ca isotopic chain, the decrease of the S_n values is abrupt after $N = 28$ due to the presence of the $N = 28$ shell gap between the $f_{7/2}$ and $p_{3/2}$ orbitals. This drop of the S_n values after having passed $N = 28$ is not observed anymore in the ${}_{16}\text{S}$ isotopic chain. This means that a significant mixing between these f and p orbits have reduced the magnitude of the gap, which is a typical feature of a deformed nucleus. The mass-excess of the nucleus ${}^{42}_{14}\text{Si}$ has been determined in Ref. [70]. As compared to a liquid drop model, an excess of binding energy is found. This gain of binding energy could be due the presence of sub-shell gap or large deformation. The mass-excess for ${}^{43}_{14}\text{Si}$ should be determined to judge between these two assumptions.

The evolution of the $N = 28$ shell gap has been yet viewed from mass excesses or binding energies. Other complementary data are required to ascertain the breaking of the spherical $N = 28$ gap, and to see whether this effect is restricted to $^{44}_{16}\text{S}$ or extends down to the $^{42}_{14}\text{Si}$ nucleus. This is addressed in the following section.

5.1.2 Trends of 2^+ , 4^+ , 0_2^+ energies and $B(E2)$ values

The determination of the 2^+ , 4^+ , 0_2^+ energies and reduced transition probabilities $B(E2)$ provide complementary pieces of evidence of significant structural changes in atomic nuclei, as the onset of deformation. Magic (spherical) nuclei are commonly characterized by high $E(2_1^+)$ and weak $B(E2; 0_1^+ \rightarrow 2_1^+)$ values. At the mid-shell occupancy the 2_1^+ energy drops and the $B(E2)$ value increases. Fig. 21 shows the evolution of the energies of the 2_1^+ states and of their reduced transition probabilities $B(E2)$ as a function of the neutron number in the $^{20}_{20}\text{Ca}$, $^{16}_{16}\text{S}$ and $^{14}_{14}\text{Si}$ isotopes. At $N = 20$ the 2^+ energies are high for the three isotones, $^{40}_{20}\text{Ca}$, $^{36}_{16}\text{S}$ and $^{34}_{14}\text{Si}$, and their $B(E2)$ values are small and similar. This picture is consistent with a strong shell closure $N = 20$ which persists between $Z = 20$ to $Z = 14$ as already reported in the Sect. 4.1.3. As shown in Fig. 21, the correlated increase of the 2^+ energies, and reduction of $B(E2)$ does not hold at $N = 28$. There the 2^+ energies of the $N = 28$ isotones, $^{44}_{16}\text{S}$ and $^{42}_{14}\text{Si}$, are much weaker than at $N = 20$. For $^{44}_{16}\text{S}$, its $E(2^+)$ and $B(E2)$ values suggest a configuration which is intermediate between a spherical and deformed nucleus. In $^{42}_{14}\text{Si}$, only the 2^+ energy has been measured. As it is one of the smallest among nuclei in this mass region, this nucleus is likely to be very deformed. Further details about the experimental studies in the S and Si isotopic chains and of the theoretical interpretations are given in the two following paragraphs.

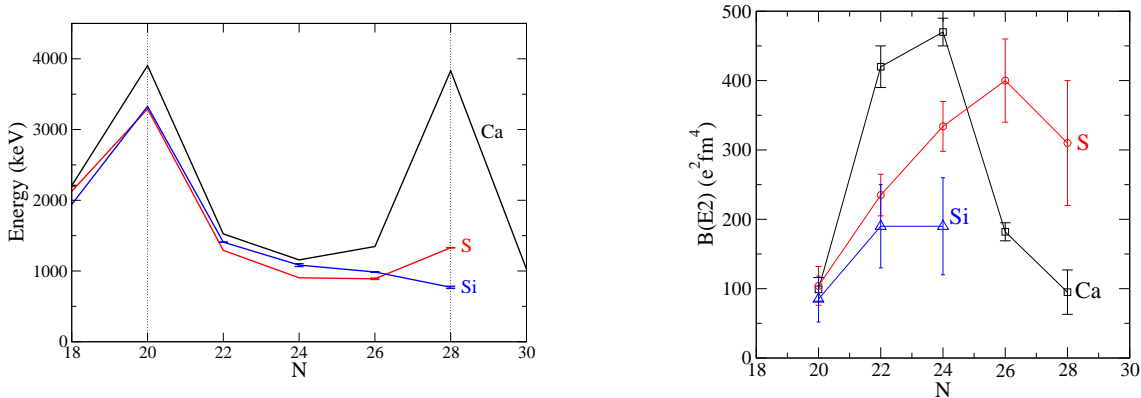


Figure 21: Experimental $E(2_1^+)$ energies (left) and $B(E2; 0_1^+ \rightarrow 2_1^+)$ values (right) in the $^{14}_{14}\text{Si}$, $^{16}_{16}\text{S}$ and $^{20}_{20}\text{Ca}$ isotopic chains as a function of the neutron number N . Data are taken from the compilation of Ref. [11], except for $^{38}_{14}\text{Si}$ [156], $^{40}_{14}\text{Si}$ [83], $^{42}_{14}\text{Si}$ [140], and $^{40}_{16}\text{S}$ [157]

To understand the evolution of the nuclear structure in the neutron-rich S isotopes, the first 2^+ state in the neutron-rich $^{40,42}_{16}\text{S}$ isotopes has been studied by means of Coulomb excitation at intermediate energy [158]. As shown in the right part of Fig. 21, the $B(E2)$ value of the $^{42}_{16}\text{S}_{26}$ nucleus remains large, contrary to the $^{46}_{20}\text{Ca}_{26}$ isotone. Complementary pieces of information on the energy of higher excited states of the S isotopes have been obtained through in-beam γ -ray spectroscopy using the fragmentation reaction of a ^{48}Ca beam [159]. The level schemes were

extended to the 2_2^+ and 4^+ states, the assignments of which were obtained by γ -ray angular distributions with respect to the direction of each produced fragment. From the energy ratio of excited states, such as $E_{4_1^+}/E_{2_1^+} \sim 3.0$ in ^{42}S , and the comparison to HFB predictions using the Gogny D1S interaction [159, 160], it has been deduced that ^{42}S is a γ -soft deformed nucleus. This confirmed the earlier assumption of a deformed nucleus inferred from its $B(E2)$ value [158].

In $^{44}\text{S}_{28}$ the 2_1^+ energy and the $B(E2)$ value were found to be intermediate between a deformed and a spherical nucleus [155]. This situation is suggestive of a possible shape mixing between these two configurations, an assumption which can be confirmed by the search for a low lying 0_2^+ state. Such a state was found to be isomer with a lifetime of $2.3 \pm 0.5 \mu\text{s}$ at an energy of 1362.5(1) keV [161]. Combining the conversion-electron and γ -ray spectroscopy it was found that the 0_2^+ state decays both directly to the ground state via internal conversion, and to the 2_1^+ state at 1329 keV. This experiment has been repeated to obtain more statistics and be able to determine the ratio between the two reduced transition probabilities, $B(E2; 0_1^+ \rightarrow 2_1^+)$ and $B(E2; 0_2^+ \rightarrow 2_1^+)$. The analysis is in progress [162]. Similar and large $B(E2)$ values would reveal that the 0_1^+ and 0_2^+ levels have mixed wave functions. A large reduced strength E0 would in turn point to the existence of a spherical and strongly deformed configurations which co-exist before mixing (see for instance [163]).

Excited states in two neutron-rich $_{14}\text{Si}$ isotopes have been recently discovered at the NSCL [83] and GANIL laboratories [140]. These two experiments used nucleon removal reaction from secondary beams centered around ^{42}P and ^{44}S at intermediate energy to produce the ^{40}Si and ^{42}Si nuclei and study the γ -rays from their de-excitation in flight. The detection of the γ -rays was achieved by arrays of detectors which surrounded the production target in which reaction occurred. In the case of Ref. [83] a segmented array of Ge detectors was used, leading to a photo-peak γ -ray efficiency of about 3% at 1 MeV. An array composed of 70 BaF_2 detectors was used in Ref. [140] in order to obtain a higher photo-peak efficiency of about 30% at 1 MeV and 20% at 2 MeV. Campbell et al. [83] have determined the energy of the 2^+ state in $^{40}_{14}\text{Si}_{26}$ at 986(5) keV. While the 2^+ energies increase in Ca isotopes from $N = 24$ to reach a maximum around 4 MeV at $N = 28$, the 2^+ energies in the Si isotopes start to deviate from those of the Ca isotopes at $N = 26$ (see the left part of Fig. 21) which points to a reduced $N=28$ shell gap [83]. However, as 2^+ neutron excitations occurring before the complete filling of the $\nu f_{7/2}$ shell are mainly generated inside the shell, they are not that sensitive to the size of the $N = 28$ gap. Conversely, in $^{42}_{14}\text{Si}_{28}$ the neutron $f_{7/2}$ shell is *a priori* filled completely, and the 2^+ state comes mainly from particle-hole excitations across the $N = 28$ gap. Bastin et al. [140] have established a 2^+ state at 770(19) keV for the $N = 28$ nucleus ^{42}Si . The dramatic decrease of the 2_1^+ energy in ^{42}Si is a proof of the disappearance of the spherical $N = 28$ shell closure at $Z = 14$. This extremely low energy of 770 keV -actually one of the smallest among nuclei having a similar atomic mass - cannot be obtained solely from neutron excitations. Proton core excitations should play an important role, which could in principle be evidenced by measuring the $B(E2)$ values in the Si isotopic chain while reaching $N = 28$.

The $B(E2)$ values in the $_{14}\text{Si}$ isotopic chain [96] seem to rise after $N = 20$, but not as much as in the $_{16}\text{S}$ ones. Whether the $B(E2)$ values remain small, steadily increase up to $N = 28$ or follow a parabola is presently not discernable with the presently large experimental error bars. A reduced $Z = 14$ shell gap would dramatically increase the $B(E2)$ values, as protons are carrying most of the effective charge in the nucleus. A decrease of the $N = 28$ gap solely would barely change the $B(E2)$ values.

To summarize this part, experimental data on the study of excited states in the $_{16}\text{S}$ and $_{14}\text{Si}$ isotopic chains reveal a noticeable change of structure between the $N = 20$ and the $N = 28$

isotones. At $N = 20$ the ^{36}S and ^{34}Si nuclei have all characteristics of doubly-magic nuclei, whereas at $N = 28$ a rapid onset of deformation is occurring. As we shall see in the following, this drastic change originates from a combined reductions of the proton $Z = 14, 16$ and neutron $N = 28$ shell gaps.

5.1.3 Evolution of the proton SPE

The change of structural behavior between the $N = 20$ and $N = 28$ isotones can be partly ascribed to the evolution of the proton Single Particle Energies [164]. The $(d, ^3\text{He})$ reactions from stable $_{20}\text{Ca}$ target have revealed that the energy spacing between the two orbits $\pi d_{3/2}$ and $\pi s_{1/2}$ in $_{19}\text{K}$, which defines the $Z = 16$ sub-shell closure, has completely vanished at $N = 28$. This was already reported in Sect. 4.2.3. The filling of eight neutrons in the $\nu f_{7/2}$ orbital induces more binding of the $\pi d_{3/2}$ orbits compared to the $\pi s_{1/2}$ one, since $|V_{d_{3/2}f_{7/2}}^{pn}| > |V_{s_{1/2}f_{7/2}}^{pn}|$. Taking into account the monopole matrix elements solely, the evolution of $(E(1/2^+) - E(3/2^+))$ between $N = 20$ and $N = 28$ would be linear:

$$[E(1/2^+) - E(3/2^+)]_{20+x} = [E(1/2^+) - E(3/2^+)]_{20} + x(V_{d_{3/2}f_{7/2}}^{pn} - V_{s_{1/2}f_{7/2}}^{pn}), \quad (26)$$

As compared to this linear decrease due to the monopole interactions, shown in the left part of Fig. 22, the experimental evolution between the first $3/2_1^+$ and $1/2_1^+$ states, $(E(1/2_1^+) - E(3/2_1^+))$, is steeper as soon as neutrons are added into the $f_{7/2}$ orbit (compare the left and right parts of Fig. 22). This feature is due to the pairing and quadrupole correlations which already engage at $N = 22$, as soon as the single-particle states $\pi s_{1/2}$ and $\pi d_{3/2}$ come close enough to each others.

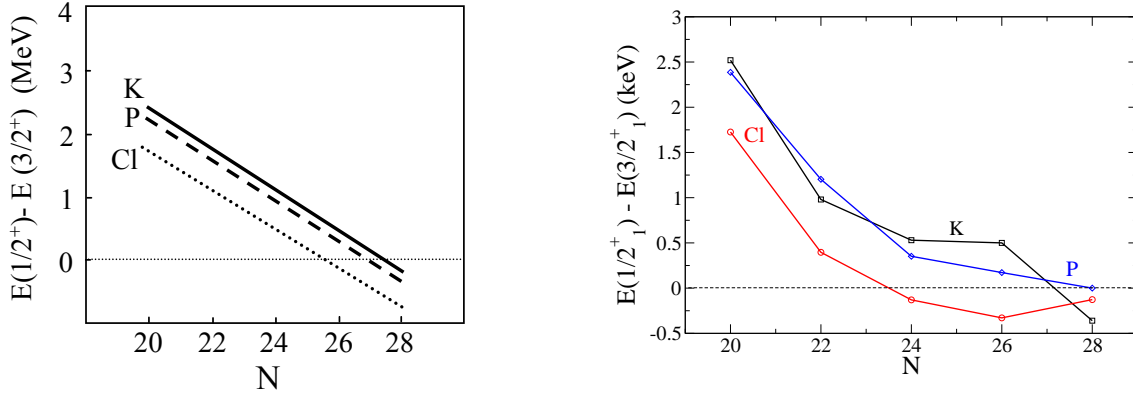


Figure 22: **Left:** Calculated energy difference $E(1/2^+) - E(3/2^+)$ as a function of the neutron number N when using Eq. 26 for the $_{19}\text{K}$, $_{17}\text{Cl}$, and $_{15}\text{P}$ isotopic chains and the monopole matrix elements of Eq. 24. As the ground state spin value in the P isotopic chain is $1/2^+$, the sign of $E(1/2^+) - E(3/2^+)$ has been reversed there to put all data on the same viewgraph. **Right:** Experimental energy difference $E(1/2_1^+) - E(3/2_1^+)$ in the $_{19}\text{K}$, $_{17}\text{Cl}$, and $_{15}\text{P}$ isotopic chains as a function of the neutron number N (see text for references).

One can apply the monopole matrix elements derived in the $_{19}\text{K}$ chain to the $_{17}\text{Cl}$ and $_{15}\text{P}$ ones, starting from the experimental values at $N = 20$. As shown in the left part of Fig. 22 the crossing between the proton $3/2^+$ and $1/2^+$ states is also expected around $N = 28$ in the P, and earlier in

the Cl chain. As for the K isotopes, the evolution of the experimental $3/2_1^+$ and $1/2_1^+$ states shown in the right part of Fig. 22 in the Cl and P isotopic chains is distorted by pairing and quadrupole correlations to account for the mixing between the nearby states [156, 165, 166, 138, 167, 140]. In particular the steep decrease of $[E(1/2_1^+) - E(3/2_1^+)]$ in the Cl chain is mainly caused by the pairing interaction which favors the coupling of proton pairs in the $d_{3/2}$ shell. This leaves a hole in the $s_{1/2}$ orbit, which gives rise to a $1/2^+$ spin value. Apart from this distortion, the reduction of the $Z = 16$ gap in the Cl and P chains is qualitatively accounted for by the monopole part of the nuclear interaction solely. Shell model calculations using the interaction developed in Ref. [148] show excellent agreement with the experimental energy difference between the $1/2^+$ and $3/2^+$ states in the $_{19}\text{K}$, $_{17}\text{Cl}$ and $_{15}\text{P}$ chains [165, 138].

At $N = 28$ the $_{17}\text{Cl}$ and $_{15}\text{P}$ isotones have almost degenerate proton $d_{3/2}$ ($\ell = 2$) and $s_{1/2}$ ($\ell = 0$) orbits, which are separated by $\Delta\ell=2$. This feature is essential to develop quadrupole correlations - and henceforth collectivity- between the s and d nearby states in the $^{43,45}_{17}\text{Cl}$ nuclei [165]. It also accounts for increased quadrupole excitations in the neutron-rich $_{16}\text{S}$ isotopes which lie in between the $_{15}\text{P}$ and $_{17}\text{Cl}$ chains.

The development of collectivity should *a priori* be significantly hindered in the $_{14}\text{Si}$ isotopic chain where proton excitations should arise across the large $Z = 14$ gap, from the deeply bound $d_{5/2}$ to the $d_{3/2}$ and $s_{1/2}$ orbits. However this possibility is essential to account for an increased collectivity in the neutron-rich $^{42}_{14}\text{Si}_{28}$ nucleus derived from its low 2^+ energy. If the $d_{5/2}$ orbit did not come closer to the $d_{3/2}$ and $s_{1/2}$ ones, the ^{42}Si nucleus would remain spherical. The energy difference between these orbits is by far not easy to determine as the $d_{5/2}$ orbit is deeply bound. It was estimated in Sect. 4.2.3 by looking at the variation of the $d_{5/2}$ single particle energy between $N = 20$ and $N = 28$ in the $_{19}\text{K}$ isotopic chain. However its single particle energy strength is spread over many states, the spectroscopic factor sum of which does not exceed 60%. From the estimation given in Sect. 4.2.3 and in Ref. [140], the complete filling of the neutron $f_{7/2}$ shell induces the collapse of the $\pi s_{1/2} - \pi d_{3/2}$ spacing, a reduction of the $\pi d_{3/2} - \pi d_{5/2}$ splitting by about 1.7 MeV and of the $\pi d_{5/2} - \pi s_{1/2}$ splitting by about 400 keV from an initial value of about 6 MeV. These reductions are large enough to provide a low energy of the 2^+ state in ^{42}Si [140]. As mentioned in Sect. 4.2.3, larger reductions of the $\pi d_{3/2} - \pi d_{5/2}$ splitting were predicted in Refs. [53, 138].

To summarize this part, the development of collectivity in the neutron-rich $N = 28$ isotones is partly due to the reduction of the spacing between the protons $d_{5/2}$, $s_{1/2}$ and $d_{3/2}$ as the neutron $f_{7/2}$ orbit is filled. As these orbits are separated by 2 units of angular momentum, quadrupole (E2) collectivity is naturally favored. Added to this, a reduction of the $N = 28$ shell gap would reinforce this tendency to deform.

5.1.4 Evolution of the neutron SPE for $Z < 20$

On the basis of experimental data on atomic masses, on energies of excited states and reduced transition probabilities, it was inferred that the $N = 28$ shell closure is eroded as protons are removed from the doubly magic $^{48}_{20}\text{Ca}$. To ascertain this assumption, and to derive the reasons for such an erosion, the $N = 28$ shell closure has been investigated via the $^{46}_{18}\text{Ar}(d, p)^{47}\text{Ar}$ transfer reaction in inverse kinematics [139]. This information will be used to investigate the change of the $N = 28$ gap from $_{20}\text{Ca}$ to $_{18}\text{Ar}$. A radioactive beam of ^{46}Ar interacted with a thin CD_2 target at 10.2(1) A· MeV. The energy and angle of the reaction protons were measured in eight highly segmented double-sided Si detectors. From the Q value of the transfer reaction, the $N = 28$ gap was found to be of 4.47(9) MeV in ^{46}Ar , which is 330(90) keV smaller than in ^{48}Ca . Transfer to excited states were used to determine the energies and spectroscopic factors of the neutron $p_{3/2}$,

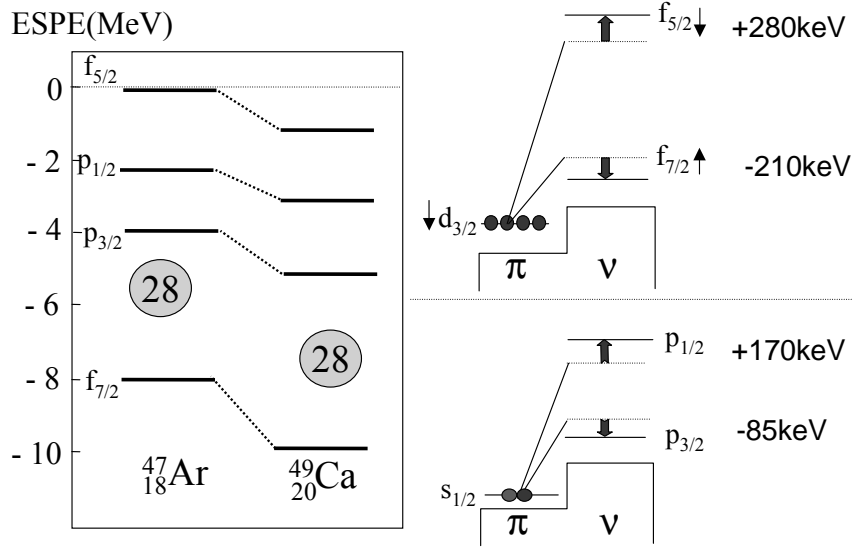


Figure 23: **Left** : Neutron single particle energies (SPE) of the fp orbitals for the $^{47}_{18}\text{Ar}_{29}$ and $^{49}_{20}\text{Ca}_{29}$ nuclei. **Right** : Schematic view of the proton-neutron interactions involved to change the f (top) and p (bottom) SO splittings (derived from Refs. [139, 149]).

$p_{1/2}$ and $f_{5/2}$ states in ^{47}Ar . The fact that only part (about 3/4) of the strength for these states has been observed indicates that some correlation take place in ^{46}Ar , after the removal of only 2 protons from the doubly magic ^{48}Ca nucleus. In particular it was found in Ref. [139] that a fraction (about 1/4) of neutron already occupies the $p_{3/2}$ orbit through $1p-1h$ excitation across the $N = 28$ gap, from the $f_{7/2}$ orbit. Monopole terms of the $sdpf$ [148] interaction calculations were adjusted to match existing experimental data in this mass region [149]. By applying this constraint, the full particle strength of the $\nu f_{7/2}$, $\nu p_{3/2}$ and $\nu p_{1/2}$ and $\nu f_{5/2}$ orbits has been determined in ^{47}Ar . The resulting Single Particle Energies (SPE) are compared to those of the $^{49}_{20}\text{Ca}$ isotone [168, 169] in Fig. 23. It is found that the orbits in which the angular momentum is aligned (ℓ_{\uparrow}) with the intrinsic spin, such as $f_{7/2}$ and $p_{3/2}$, become relatively much less bound than the $f_{5/2}$ and $p_{1/2}$ orbits where the angular momentum and intrinsic spin are anti-aligned (ℓ_{\downarrow}). Bearing in mind that the $d_{3/2}$ and $s_{1/2}$ orbitals are quasi-degenerate at $N = 28$, (see Sect. 5.1.3), the removal of 2 protons between ^{48}Ca and ^{46}Ar is equiprobable from these orbits. Therefore modifications of neutron SPE arise from proton-neutron interactions involving these two orbits [139]. As regards the f states, the experimental trend was mainly ascribed to the fact that the monopoles contain attractive and repulsive tensor terms (see Sect. 2.4) which amount to $\tilde{V}_{d_{3/2} f_{7/2}}^{pn} = -210$ keV and $\tilde{V}_{d_{3/2} f_{5/2}}^{pn} = +280$ keV, respectively. The change of the p SO splitting was principally assigned to the removal of a certain fraction of $s_{1/2}$ protons which deplete the central density of the nucleus. The corresponding spin-dependent part of the monopole terms was extracted to be of +170 keV and -85 keV for $\tilde{V}_{s_{1/2} p_{1/2}}^{pn}$ and $\tilde{V}_{s_{1/2} p_{3/2}}^{pn}$, respectively. These spin-dependent parts of the monopoles amount to about 20% of the central part to which they add. The reduction of the $N = 28$ shell gap arises from a subtle combination of several monopoles involved while 2 protons are taken equiprobably out of the $d_{3/2}$ and $s_{1/2}$ orbits [139].

The variation of the single particle energies in term of monopole interactions can be pursued towards the $^{43}_{14}\text{Si}$ nucleus in which, as compared to $^{49}_{20}\text{Ca}$, 4 protons have been removed from the

$d_{3/2}$ and 2 from the $s_{1/2}$ orbits. Using the monopole matrix elements derived in the interaction, a global shrink between the fp orbits is foreseen, such as reductions of the (i) $N = 28$ gap by $330 \times 3 \simeq 1000$ keV, (ii) f SO splitting by $4(0.28 + 0.21) \simeq 2000$ keV and (iii) p SO splitting by $2(0.17 + 0.085) \simeq 500$ keV. This global shrink of SPE is expected to reinforce particle-hole excitations across $N = 28$, which are of quadrupole nature. The existence of $1p - 1h$ excitations in ^{47}Ar , the discovery of an E0 isomer in $^{44}\text{S}_{28}$ and the weak 2^+ energy in $^{42}\text{Si}_{28}$ (see Sect. 5.1.2) weight in favor of a progressive increase of quadrupole collectivity below $Z = 20$.

5.1.5 Evolution of the neutron SPE for $Z > 20$

Above $Z = 20$ the proton $f_{7/2}$ orbit is getting filled. As compared to the previous section, the physics involved to account for the variation of the neutron $f_{7/2}$, $p_{3/2}$, $p_{1/2}$ and $f_{5/2}$ SPE is different. The spin-isospin interaction between the neutron $f_{5/2}$ and the proton $f_{7/2}$ orbits is expected to play a major role, as it did between the proton and neutrons of the $d_{5/2}$ and $d_{3/2}$ shells in the $N = 20$ region (see Sect. 4.1.3). The strongly attractive part of the $\pi f_{7/2} - \nu f_{5/2}$ interaction is expected to lower the neutron $f_{5/2}$ orbit significantly between $Z = 20$ and $Z = 28$. In the $^{49}\text{Ca}_{29}$ nucleus, it lies about 2 MeV above the $p_{1/2}$ and 4 MeV above the $p_{3/2}$ ground state. The single particle energies in $^{57}\text{Ni}_{28}$ were determined at the ATLAS accelerator at Argonne National Laboratory using the $d(^{56}\text{Ni}, p)^{57}\text{Ni}$ reaction at 250 MeV [170]. It was found that the major part of the $f_{5/2}$ single particle energy is located at 768 keV excitation energy, below that of the $p_{1/2}$ ones located at 1.13 MeV. Though, the authors admitted that large uncertainties on the spectroscopic factors (up to 50%) are possible.

The variation of the binding energies of the $f_{7/2}$ and $f_{5/2}$ orbits as a function of the proton number are shown in Fig. 24. From the mean slopes of the two curves, the monopole matrix

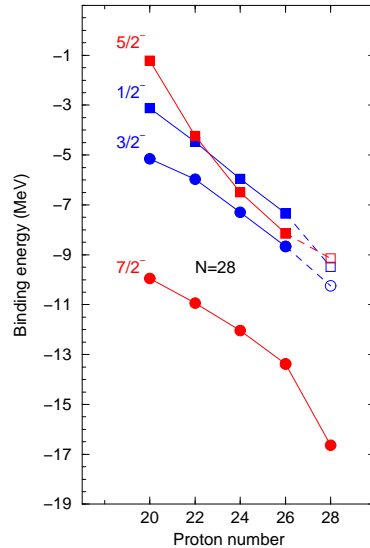


Figure 24: Evolution of the binding energies of the states bounding the $N = 28$ shell closure. The $7/2^-$ states are the ground states of the $N = 27$ isotones. The $3/2^-$, $1/2^-$ and $5/2^-$ energies are the average of all the states populated in (d, p) pick-up reactions on the stable $N = 28$ isotones [171]. The results on ^{57}Ni are drawn with empty symbols as the spectroscopic factors of its three first states are not known.

elements $V_{f_{7/2}f_{7/2}}^{pn}$ and $V_{f_{7/2}f_{5/2}}^{pn}$ can be tentatively determined to be $\simeq -0.6$ MeV and -1.0 MeV,

respectively. Their large difference could be related to the spin-isospin term of the interaction.

The variation of the single- particle states $p_{3/2}$ and $p_{1/2}$ is also shown in the same figure. The energy spacing between these two spin-orbit members does not vary very much with the addition of eight protons in the $f_{7/2}$ orbit. There, no tensor force is changing this SO splitting as the protons and neutrons orbits are separated by 2 units of orbital angular momentum. Noteworthy is the fact that this is clearly at variance with the abrupt change of the p SO splitting with the addition or removal of protons in the proton $s_{1/2}$ orbit discussed in the previous section. In such a case a significant part of the protons and neutrons wave functions were localized in the same regions of the nucleus.

5.1.6 Conclusion

The spectroscopy of the neutron-rich $N = 28$ isotones has been investigated by various complementary methods, such as the Coulomb excitation, in-beam γ -ray spectroscopy, delayed-electron spectroscopy and the neutron stripping (d, p) reaction. By gathering all pieces of information, a coherent description of the evolution of the $N = 28$ shell gap can be proposed for $Z < 20$ and $Z > 20$.

For $Z < 20$ the shell model description of the $N = 20$ and $N = 28$ isotones south of Ca isotopes is significantly different. The $N = 20$ shell gap persists with up to the removal of 4 and 6 protons to the quasi-doubly magic $^{36}_{16}\text{S}_{20}$ and $^{34}_{14}\text{Si}_{20}$ nuclei, respectively. For these nuclei the existence of significant proton sub-shell closures at $Z = 16$ and $Z = 14$ is a warrant of their rigidity against quadrupole excitations. Conversely at $N = 28$, the studies of the proton [141, 142, 164] and neutron single particle energies [168, 169, 139] have revealed significant differences. The combined compression of the energy of the proton and neutron orbits, plus the favored quadrupole excitations across $N = 28$, produce a rich variety of behaviors and shapes in the even $N = 28$ isotones; spherical ^{48}Ca ; oblate non-collective ^{46}Ar ; coexistence in ^{44}S , and two rotors, oblate ^{42}Si and prolate ^{40}Mg [172]. This variety of shapes is also supported by mean-field calculations, relativistic or non-relativistic [173, 174, 175, 160, 176]. Subtle changes in the potential energy surfaces arise from the choice of the mean field effective interactions, in particular for the ^{44}S nucleus. However the global trend to quadrupole deformation is found as it arises from the fact that the occupied and valence proton *and* neutron orbits have $\Delta l = 2$.

The reduction of the f and p SO splittings is tentatively ascribed to new effects that have been put forward these last few years both from theoretical and experimental point of views. In intensity these reductions of SO splittings are much larger than the ones expected by an increased diffuseness of the nuclear matter far from the valley of stability. They are opening up a new vista on the various components giving rise to changes of the SO splittings in hitherto unknown parts of the chart of nuclides. Noteworthy is the fact that similar physics processes (tensor force and $E2$ symmetry) are expected to be at play in other doubly-magic nuclei formed by the SO interaction, such as $^{78}_{50}\text{Ni}_{28}$ and $^{100}_{50}\text{Sn}_{50}$. Whether these nuclei would be spherical or deformed depends strongly on the size of the proton and neutron gaps (depending of the strength of tensor forces, for instance) and on the quadrupole collectivity that is at play.

Above $Z = 20$, the $N = 28$ shell gap is slightly decreasing from a value of about 4.5 MeV at $Z = 20$ to 4 MeV at $Z = 26$. The evolution of the neutron single-particle orbits $f_{7/2}$, $p_{3/2}$, $p_{1/2}$ and $f_{5/2}$ have been determined from gathering information on (d, p) reactions in the $N = 28$ isotones. Even if only partial information exist, it was found that a strong interaction between the protons $\pi f_{7/2}$ and neutrons $\nu f_{5/2}$, which can be due to a spin-isospin term, induces a reduction of the splitting $\nu f_{7/2} - \nu f_{5/2}$ orbits. In ^{28}Ni , the neutron $f_{5/2}$ has drop down to such an extent

that it lies between the $p_{3/2}$ and $p_{1/2}$ orbits. This leads to the disappearance of the $N = 32$ shell closure between Ca and Ni, a topic which has been discussed in Sect.4.2.1. Meanwhile the neutron $p_{3/2} - p_{1/2}$ SO splitting seems to be constant.

5.2 Evolution of the $Z = 28$ shell closure

The $_{28}\text{Ni}$ isotopic chain comprises 30 isotopes discovered so far. At the two extremes of the proton- and neutron-rich sides, the two doubly magic $_{28}^{48}\text{Ni}_{20}$ [177] and $_{28}^{78}\text{Ni}_{50}$ [178, 179] have remarkable interest. The former is a prime candidate for the two-proton radioactivity, whereas the second is an important waiting-point in the path of the rapid-neutron capture process. So far a few nuclei of $_{28}^{78}\text{Ni}_{50}$ have been produced worldwide. Therefore its structure could not have been studied yet. It therefore remains a wonderful challenge for the future.

From the neutron-deficient to neutron-rich nuclei, the ordering of the neutrons shells is as follows: the $\nu f_{7/2}$ shell between $_{28}^{48}\text{Ni}_{20}$ and $_{28}^{56}\text{Ni}_{28}$, the remaining fp shells up to $_{28}^{68}\text{Ni}_{40}$, and the $\nu g_{9/2}$ orbit up to $_{28}^{78}\text{Ni}_{50}$. The $Z = 28$ shell gap is formed between the occupied $\pi f_{7/2}$ and the valence $\pi p_{3/2}$ (or possibly $f_{5/2}$) orbits. The successive filling of the neutron orbits could polarize the proton core by specific proton-neutron interactions. Such effects can be revealed by the studies of the binding energies of the proton orbits, would they belong to the ground or excited configurations, and by the evolution of the $E(2^+)$ and $B(E2)$ values along the Ni isotopic chain. The relative evolution of the $\pi f_{7/2}$ and $\pi f_{5/2}$ spin-orbit partners will be examined to determine whether tensor forces act to reduce the $Z = 28$ shell closure as the neutron $\nu g_{9/2}$ orbit is filled towards ^{78}Ni .

5.2.1 Evolution of the binding energies

The experimental evolution of the $Z = 28$ shell gap, formed between the $f_{7/2}$ and $p_{3/2}$ orbits is drawn in the left part of Fig. 25, for $N = 28$ to $N = 44$. It has been obtained from the variation of the binding energies of the proton $7/2^-$ and $3/2^-$ states, reported in the same figure. Values of atomic masses come from the AME2003 table [10], to which new results for $^{70,72}\text{Ni}$ and ^{73}Cu nuclei [180] have been added. Singularities in the gap evolution are present for $N = 28$ (^{56}Ni), a self-conjugated doubly-magic nucleus (see Sect. 11), and to a weaker extent for $N = 40$ (^{68}Ni). In average the $Z = 28$ gap amounts to about 5 MeV. This is large enough to maintain the spherical shape of all Ni isotopes, even those located at mid-distance between $N = 28$ and $N = 40$.

Between $N = 28$ and $N = 40$ the variation of the proton binding energies can be attributed to the filling of the neutron $p_{3/2}$, $f_{5/2}$ and $p_{1/2}$ orbits. As these orbits lie close in energy, the filling of the neutrons fp orbits as a function of N is averaged between these three shells. Therefore the increase of the binding energy of the $7/2^-$ state -arising from the $\pi f_{7/2}$ orbital- between $N = 28$ and $N = 40$ is mainly due to the strongly attractive interaction between $f_{7/2}$ protons and $f_{5/2}$ neutrons which have the same orbital momentum $\ell=3$ and opposite spin orientations. Other proton-neutron interactions between the $\pi f_{7/2}$ and νp orbits have weaker intensity.

Above $N \simeq 40$, a weaker gain of the $\pi f_{7/2}$ binding energy is found as the $\nu g_{9/2}$ orbital gets filled (see the left part of Fig. 25). This statement is valid with up to about 2 σ confidence level, an uncertainty which could be reduced by measuring the atomic masses of the $_{27}\text{Co}_{N>40}$ isotopes with a better accuracy. If pursued up to $N = 50$, this change of binding energy slopes induces a decrease of the $Z = 28$ gap -formed between the $f_{7/2}$ and $p_{3/2}$ orbits- from $\simeq 6$ MeV in $^{68}\text{Ni}_{40}$ to $\simeq 3.5$ MeV in the doubly-magic $^{78}\text{Ni}_{50}$ nucleus. In such a case, increased proton excitations across the $Z = 28$ gap -or core polarization- would be expected.

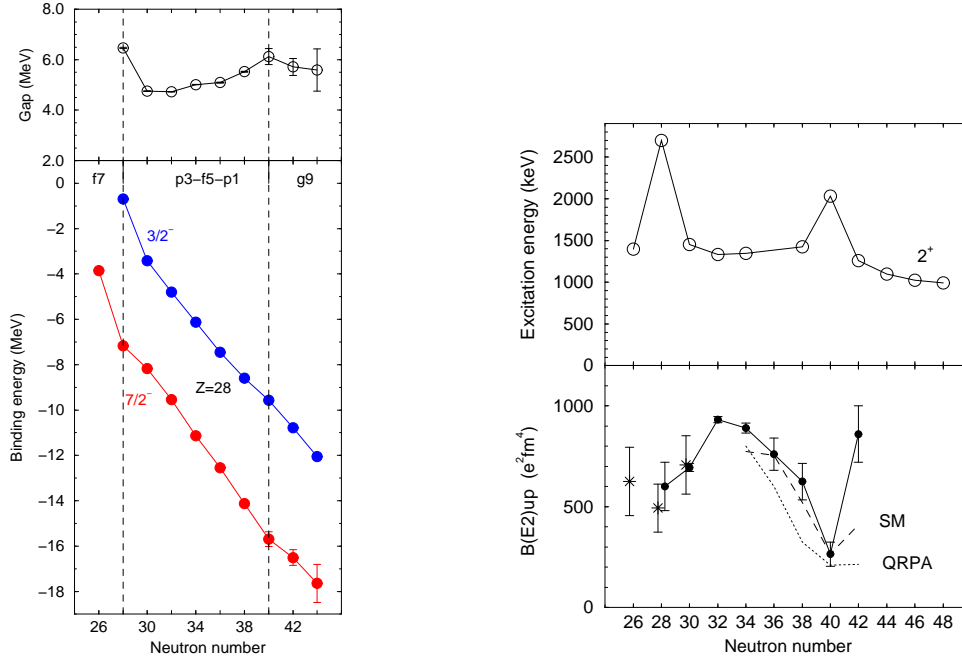


Figure 25: **Left:** Binding energies of the states located just above and just below the $Z = 28$ magic number and difference of the binding energies of the two states surrounding the gap at $Z = 28$ (see Sect. 11). The neutron orbitals which are getting filled as a function of increasing N are given in the middle of the figure. **Right:** Experimental $E(2^+)$ and $B(E2; 0^+ \rightarrow 2^+)$ values in the ${}_{28}\text{Ni}$ isotopic chain. Values (drawn with filled circles) are taken from Ref. [11] for ${}^{56-68}\text{Ni}$ and from Ref. [190] for ${}^{70}\text{Ni}$. The three additional data points (stars) for ${}^{54,56,58}\text{Ni}$ are from Ref. [191]. The $B(E2)$ values calculated with the shell model of Ref. [185] are drawn with dashed line, those with the QRPA model of Ref. [187] with dotted line.

5.2.2 Trends of 2^+ energies and $B(E2)$ values

Between the $N = 28$ and 50 shell closures the Ni isotopes have been subject of extensive experimental and theoretical studies, as can be found in Refs. [181, 182, 183, 184, 185, 186, 187, 188, 189, 190]. The experimental results on the 2_1^+ energies and $B(E2; 0^+ \rightarrow 2^+)$ values are drawn in the right part of Fig. 25. The 2_1^+ energies are maximum at the $N = 28$ and $N = 40$ (sub)shell closures and slightly decrease up to the last known value of ${}^{76}\text{Ni}$. The curve formed by the $B(E2)$ values varies in the opposite way, reaching a maximum at or near mid-occupation by neutrons of the fp shell ($N = 34$) and subsequently decreasing until $N = 40$. Between $N_1 = 28$ and $N_2 = 40$, the $B(E2)$ curve follows the generalized seniority scheme within the fp shells. Within this approach [192, 43] which exploits the property of nucleons paired to $J=0^+$ in nearby orbits, the $B(E2)$ values of ${}^{56-68}\text{Ni}$ follow a parabola along the shell filling,

$$B(E2; 0^+ \rightarrow 2_1^+) = c(\pi fp, \nu fp) F(1 - F) \quad (27)$$

where $c(\pi fp, \nu fp)$ is representative of the strength of the proton-neutron interaction in the fp shells, and F is the fractional filling of the neutron shell which varies between 0 at the beginning and 1 at the end of the shell. For a nucleus containing N neutrons between $N_1 = 28$ and $N_2 = 40$, F expresses as $F = (N - N_1)/(N_2 - N_1)$. As neutrons are chargeless particles, they cannot contribute

directly to the increase of $B(E2)$ but by inducing core-polarization. Therefore the height of the parabola can be used to derive the strength of neutron-induced proton-core excitations. The proton core polarization occurs through quadrupole excitations via $(\pi f_{7/2})^{-1}(\pi p_{3/2})^{+1}$ configurations [181, 185].

Deviation to the parabola of Eq. 27 exist at the two extremes, ^{56}Ni and ^{68}Ni for which the $B(E2)$ values are slightly higher than expected with this simple model. For $^{56}\text{Ni}_{28}$ this is due to the extended possibilities for creating 2^+ excitations across $N, Z = 28$ in the fp shell for protons and neutrons [193, 194] and a consequence of a strong proton-neutron interaction characterizing the $N = Z$ nuclei [195, 196]. At $N = 40$, the $B(E2)$ value reaches a minimum in the Ni chain. The low $B(E2)$ of $^{68}\text{Ni}_{40}$, 3.2(7) $W.u.$, is commonly assumed to be the signature for a doubly-magic nucleus. This value is comparable to that of doubly magic nuclei, ^{16}O (3.3(3) $W.u.$), ^{40}Ca (2.3(4) $W.u.$) and ^{48}Ca (1.6(5) $W.u.$). Such a minimum has been ascribed to the existence of an $N = 40$ sub-shell gap and to the lack of E2 excitations between the fp and the $g_{9/2}$ orbitals of different parity value [183, 185, 187]. Without some amount of neutron pair-scattering between the fp and g shells (or a superfluid effect [185]) the $B(E2)$ value would have even be weaker.

Beyond $N = 40$ the $B(E2)$ value rises steeply for $^{70}\text{Ni}_{42}$, even though error bars are rather large. This suggests an increased collectivity in the heavy Ni isotopes induced by the interaction of protons in the fp and neutrons in the $g_{9/2}$ shell with a strength $c(\pi fp, \nu g)$ (cf. Eq. 27 with $N_1 = 40$ and $N_2 = 50$). This enhanced collectivity goes in concert with a gradual reduction of 2_1^+ excitation energies from $^{70}\text{Ni}_{42}$ to $^{76}\text{Ni}_{48}$ [189] which cannot be understood solely from pure neutron excitations within the $g_{9/2}$ shell. These features can attributed to a reduction of the $Z = 28$ gap, as surmised already from the proton binding energy curves of the left part of Fig. 25. As a matter of comparison the steep rise of the $B(E2)$ between $^{68}\text{Ni}_{40}$ and $^{70}\text{Ni}_{42}$ could be compared to the more modest variations between $^{56}\text{Ni}_{28}$ [193, 194] and $^{54}\text{Ni}_{26}$ or $^{58}\text{Ni}_{30}$ [191].

A better insight on the polarization strength in the 2_1^+ state of ^{70}Ni can be obtained from the evolution of the $B(E2; J \rightarrow J - 2)$ values along the 8^+ , 6^+ , 4^+ , 2^+ components of the $(\nu g_{9/2})^2$ multiplet. The 8_1^+ state is expected to be almost only of neutron origin, as a 8^+ spin value cannot be built solely with protons in the fp orbitals. The $B(E2; 8_1^+ \rightarrow 6_1^+)$ value would therefore correspond to a reference value for the weakest core polarization. Recently E2 transition strengths were measured for all the first states in ^{70}Ni [197, 198, 78, 190], and a new empirical $T=1$ effective interaction was derived in the pure neutron $p, f_{5/2}, g_{9/2}$ model space [199]. In this approach, the experimental $B(E2; 8^+ \rightarrow 6^+) = 19(4)$, $B(E2; 6^+ \rightarrow 4^+) = 43(1)$, and $B(E2; 2^+ \rightarrow 0^+) = 172(28)e^2\text{fm}^4$ values are calculated as 17, 45 and 92 $e^2\text{fm}^4$ using an effective neutron charge $e_\nu = 1.2e$. The good agreement for the high-spin states breaks down for the $2_1^+ \rightarrow 0^+$ transition, which points to an enhanced proton-core polarization at low excitation energy. This conclusion is at variance with the QRPA [187] and shell model results [185, 200] (see the right part of Fig. 25) which predict that the $B(E2; 0^+ \rightarrow 2_1^+)$ strength in ^{70}Ni predominantly corresponds to neutron excitations, decoupled from the proton core. For the shell model calculations of Refs. [185, 200], the valence space that was used may not be large enough to account for the observed enhanced collectivity.

This strong polarization in the Ni isotopes beyond $N = 40$ is likely to be due to the *attractive* $\pi f_{5/2} - \nu g_{9/2}$ monopole interaction [201, 21, 202, 199], assigned to the tensor force of the in-medium nucleon-nucleon interaction [53]. This force is also predicted to act through the *repulsive* $\pi f_{7/2} - \nu g_{9/2}$ interaction, hereby explaining the weaker slope of the $\pi f_{7/2}$ binding energy observed for $N > 40$ in the left part of Fig. 25. On the whole, the tensor term $\pi f - \nu g_{9/2}$ would reduce both the $Z = 28$ gap and the $\pi f_{7/2} - \pi f_{5/2}$ splitting. This will be discussed in the following section.

5.2.3 Proton orbits above the $Z = 28$ gap: Levels of the ${}_{29}\text{Cu}$ isotopes

The variation of the binding energy of the proton orbits located *above* the $Z = 28$ gap, i.e. $p_{3/2}$, $p_{1/2}$ and $f_{5/2}$, can be inferred from experimental studies along the ${}_{29}\text{Cu}$ isotopic chain. They are depicted below as a function of increasing neutron number. During the filling of the neutron fp and g shells the energies of these valence proton shells display large changes, as the $\pi f_{7/2}$ one evoked in Sect. 5.2.1.

The ground-state configuration of the ${}^{57-73}\text{Cu}_{28-44}$ isotopes arises from the $\pi p_{3/2}$ orbital. Two excited states, $1/2^-$ and $5/2^-$, are located at excitation energies well below that of the 2^+ state of the even-even Ni core. Their evolution as a function of the neutron number is shown in Fig. 26.

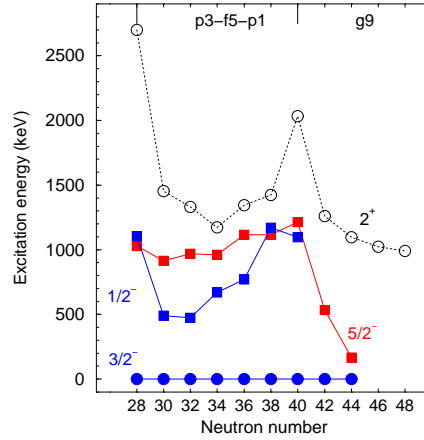


Figure 26: Evolution of the first states of the ${}_{29}\text{Cu}$ isotopes as a function of the neutron number. The energy of the 2^+ excitation of the Ni core is also drawn. The neutron orbitals which are getting filled as a function of increasing N are given on top of the figure.

The energy of the first 2^+ of the ${}^{56}\text{Ni}$ core is above 2.5 MeV. Therefore, the low-lying excited states measured in ${}^{57}\text{Cu}_{28}$ likely correspond to the single-proton orbits $\pi p_{1/2}$ and $\pi f_{5/2}$ rather than states originating from the coupling $\pi p_{3/2} \otimes 2^+$. States in ${}^{57}\text{Cu}$ have been populated by the proton-capture reaction in inverse kinematics, $p({}^{58}\text{Ni}, {}^{57}\text{Cu} \gamma)2n$ [203]. Photons of 1028(4), 1106(4) and 2398(10) keV have been measured in coincidence with the ${}^{57}\text{Cu}$ nuclei detected in a recoil spectrometer. Using analogies with its mirror nucleus, ${}^{57}\text{Ni}$, these γ -rays have been attributed to the direct decay of three excited states (of spin $(5/2^-)$, $(1/2^-)$ and $(5/2^-)$ respectively) to the ground state [203]. Only the two first excited states, at 1028 and 1106 keV, are reported in Fig. 26. New measurements on ${}^{57}\text{Cu}$ would be welcome in order to confirm the energies and the spin values of its excited states. Furthermore the determination of the spectroscopic factors (SF) is essential to characterize the orbitals $\pi p_{3/2}$, $\pi p_{1/2}$ and $\pi f_{5/2}$ for $N = 28$.

The ${}^{59-65}\text{Cu}_{30-36}$ isotopes have been studied using the $({}^3\text{He}, d)$ stripping reactions on stable Ni targets. Although a lot of states with spin values $3/2^-$, $1/2^-$ and $5/2^-$ have been identified, the sum of their individual SF is systematically lower than the maximum value expected for each orbital, meaning that the single-particle energies lie at higher energy. Nevertheless it is important to note that the three states drawn in Fig. 26 have the highest SF values, approximately 50 % of the sum rule. Even though the $1/2^-$ and $5/2^-$ states have to be considered as a mixing of two components (the individual configuration, $\pi p_{1/2}$ or $\pi f_{5/2}$, and the coupling $\pi p_{3/2} \otimes 2^+$) their *relative* evolution with respect to the $3/2^-$ ground state will be used, in the following, to figure

out changes in the single-particle energies of the $p_{3/2}$, $f_{5/2}$ and $p_{1/2}$ orbits. Between $N = 28$ and $N = 40$, we can tentatively ascribe these changes to the various proton-neutron interactions while neutrons occupy successively the $p_{3/2}$, $f_{5/2}$ and $p_{1/2}$ orbits.

The increase of the $1/2_1^-$ energy with respect to the ground state observed for $32 \leq N \leq 38$, i.e. during the filling of $\nu f_{5/2}$, is an interesting feature to start with. It may be connected to a progressive increase of the energy spacing between the two orbits, $\pi p_{1/2}$ and $\pi p_{3/2}$, since the 2^+ energy of the Ni core does not vary very much in this range of neutron number (see Fig. 26). The $\pi p_{3/2} - \pi p_{1/2}$ splitting has increased by 695(20) keV with the addition of 6 neutrons (see Fig. 26), i.e. 116 keV per neutron. Such an increase is related to the monopole difference $V_{p_{1/2}f_{5/2}}^{pn} - V_{p_{3/2}f_{5/2}}^{pn}$ which contain a difference of tensor terms of opposite signs, attractive $\tilde{V}_{p_{3/2}f_{5/2}}^{pn}$ and repulsive $\tilde{V}_{p_{1/2}f_{5/2}}^{pn}$. As the proton and neutron orbits involved in these matrix elements are separated by two units of orbital momentum ($\ell=1$ for the p orbits and $\ell=3$ for the f ones), the tensor components could be relatively weak.

The spacing between the $5/2_1^-$ and $3/2_1^-$ states evolves smoothly from $N = 28$ to $N = 40$. This is suggestive of a subtle balance between the two components of the $5/2_1^-$ state in the one hand, and between the relative evolution of the ESPE's due to the proton-neutron monopoles involved there (the tensor term is repulsive in $V_{p_{3/2}p_{3/2}}^{pn}$ and $V_{f_{5/2}f_{5/2}}^{pn}$, and attractive in $V_{p_{3/2}f_{5/2}}^{pn}$) in the other hand. The coupled component of the $5/2_1^-$ state is expected to be reduced at $N = 40$. Indeed its SF obtained from the $^{70}\text{Zn}(d, ^3\text{He})$ and (t, α) pick-up reactions have very large values [204, 205]. Nevertheless as the peaks of interest are broader than the others, the authors have assumed that two levels in ^{69}Cu are approximately equally populated, the spacing of the two unresolved states being less than 15 keV, each of them displaying a lower SF value.

Above $N = 40$, i.e. as the neutron $g_{9/2}$ orbit gets filled, the situation changes dramatically. As shown in Fig. 26, a strong decrease in energy of the $5/2_1^-$ state is observed in the $^{71,73}\text{Cu}_{42,44}$ nuclei from the β -decay study of $^{71,73}\text{Ni}$ [206, 201]. Collective properties of the low-lying levels in the odd-A $^{67-73}\text{Cu}$ have been recently investigated by Coulomb excitation with radioactive beams at REX-ISOLDE [207], where the values of transition probabilities $B(E2; 5/2_1^- \rightarrow 3/2_{gs}^-)$ have been measured. A significant reduction of $B(E2)$ is observed at $N = 40$. It points to a transition from a rather collective $5/2_1^-$ state in ^{67}Ni to a single-particle-like structure in $^{69-73}\text{Ni}$.

Assuming that the $5/2_1^-$ state has a pure proton single-particle configuration for $N = 40 - 44$, the binding energy of the $\pi f_{5/2}$ level can be computed and drawn together with the $\pi p_{3/2}$ and $\pi f_{7/2}$ levels (see left part of Fig. 27). The strong decrease of the $\pi f_{5/2} - \pi p_{3/2}$ energy spacing arises in concert with the reduction of the $\pi f_{7/2} - \pi p_{3/2}$ energy spacing. This leads to a reduction of the $\pi f_{5/2} - \pi f_{7/2}$ spin-orbit splitting, which could be due to the action of tensor forces between the protons f and the neutrons in the $g_{9/2}$ orbit.

As seen in the right part of Fig. 27, the residual interactions V^{pn} involving the $\pi f_{7/2}$ orbit, derived simply from the evolution of its binding energy (as described in Sect. 2.2.2), have decreased from ~ 750 keV within the neutron fp shells to ~ 400 keV as soon as the neutron g orbit is filled, i.e. above $N = 40$. There, the mean intensity of the residual interaction for the $5/2^-$ state -which we assume to be of single-particle origin only- is larger ($\sim 900\text{keV}$). However, it is worthwhile to remind that these statements are not firm enough as the uncertainties on the atomic masses of the Co isotopes around $N = 40$ are relatively large and the spectroscopic factors of the $5/2_1^-$ states in the heavy Cu isotopes are unknown.

The strong decrease of the energy difference between the $5/2_1^-$ and $3/2_1^-$ states (assumed to contain a significant part of the $\pi f_{5/2}$ and $\pi p_{3/2}$ strengths) comes when the $\nu g_{9/2}$ orbit is filled in the Cu isotopes. This situation is in many aspect similar to the one arising between the $3/2_1^+$ and

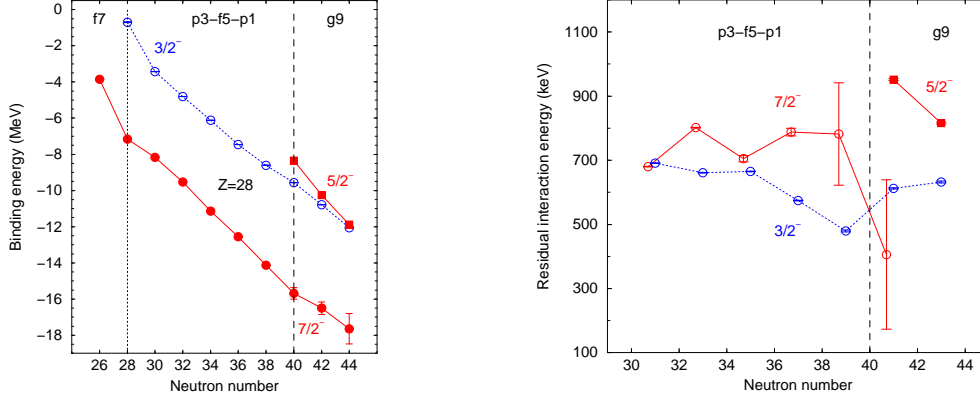


Figure 27: **Left:** Evolution the binding energies of the $7/2^-$ and $5/2^-$ states compared to those of the $3/2^-$ states, on either side of the $Z = 28$ gap (see text). **Right:** Neutron-proton residual interactions extracted from the slopes of the binding energies of the proton states. The neutron orbitals which are getting filled as a function of increasing N are given on top of the figures.

$1/2_1^+$ states (from the $\pi d_{3/2}$ and $\pi s_{1/2}$ orbits) when the $\nu f_{7/2}$ orbit is filled in the P isotopes (see Fig. 22 in Sect. 5.1.3). There, it is seen that the slope of the energy difference $E(1/2_1^+ - 3/2_1^+)$ (right part of the Figure) is much steeper than that of the monopole energy difference $E(1/2^+ - 3/2^+)$ (left hand side of the same Figure) when the neutron $f_{7/2}$ orbit starts to be filled after $N = 20$. The slope becomes much smoother later on. Deviation of the $E(1/2_1^+ - 3/2_1^+)$ energy difference to the monopole trend $E(1/2^+ - 3/2^+)$ can be assigned to correlations which are maximum at mid-shell. These correlations arise from the coupling between the single proton in the P nucleus and the 2^+ excitations created by the neutrons in the Si chain. A similar situation is expected in the Cu isotopic chain, in which $E(5/2_1^- - 3/2_1^-)$ should vary steeply at the beginning of the filling of the $g_{9/2}$ orbit and more smoothly when neutrons are added to fill the shell to completion. Using this comparison, it can be derived that a similar tensor force is at play in the two cases. However the strength of the force is hitherto hard to quantify in the Cu isotopic chain.

Theoretical results

The neutron-rich Cu isotopes have been studied between $N = 28$ and $N = 50$ within the framework of the shell-model approaches in Refs [202, 201, 200]. Their results are summarized below.

The shell-model calculations of Smirnova et al. [202] use an effective interaction based on the G matrix [208, 209]. The experimental energies of the first $3/2^-$, $5/2^-$ and $1/2^-$ states in the Cu isotopic chain are correctly reproduced by the model. The major discrepancy occurs at $N = 40$, where the calculated energy of the $5/2_1^-$ state is overestimated by about 600 keV. Beyond $N = 40$, the $5/2_1^-$ state decreases with the same slope as observed experimentally. This excess in energy is maintained for N beyond 40 : the calculated energy of the $5/2_1^-$ in $^{73}\text{Cu}_{44}$, $\simeq 750$ keV, is larger than the measured value of 166 keV. Hence the crossing between the $5/2_1^-$ and $3/2^-$ states is predicted at $N = 50$ as compared to $N = 45$ extrapolated from the experimental data. Concerning the SF values, the ground state $3/2^-$ of the odd-A Cu isotopes is found to be almost pure along the whole isotopic chain, exhausting 70 % - 100 % of the single-proton $\pi p_{3/2}$ state. On the other hand, the structure of the $5/2_1^-$ state changes a lot as a function of the neutron number. While it is rather pure single particle for $N = 28$ or $N = 50$, its spectroscopic factor drops down

to $\simeq 0$ for $N = 38$. This suggests that at mid-distance between $N = 28$ and $N = 50$ this state is very sensitive to correlations beyond the monopole interactions. Experimental SF of the $5/2_1^-$ state in the Cu chain determined up to $A = 65$, are significantly larger than the calculated ones. As mentioned by the authors of Ref. [202] this discrepancy points to a deficiency in the realistic interaction of hitherto unknown origin. The $1/2_1^-$ state has a calculated SF value of about 40% between $A = 59$ and $A = 77$. Experimental values are available up to $A = 65$. They are in accordance with these calculations.

The excited levels of odd-A $^{69-79}\text{Cu}_{40-50}$ nuclei have been also compared to results of realistic shell-model calculations [201] using another residual interaction (the so-called S3V set, from Ref. [210]). In this work, the ESPE's have been adjusted in order to reproduce the spectroscopy of the Ni and Cu isotopes around $N = 40$. Therefore the S3V set applies to nuclei with $N \geq 40$ only. As in Ref. [202] the distance in energy between the $\pi p_{3/2}$ and $\pi f_{5/2}$ subshells decreases rapidly during the filling of the $\nu g_{9/2}$ orbital. This was attributed to the strong attractive monopole interaction $V_{f_{5/2}g_{9/2}}^{pn}$. It is worth pointing out that the S3V interaction slightly overestimates the 2_1^+ energies of the neutron-rich $^{70-76}\text{Ni}$ isotopes, as shown in Fig. 4 of Ref. [189].

The realistic interaction of Lisetskiy et al. [199] has been derived from a fit to existing experimental data for the Ni isotopes from $A = 57$ to $A = 76$ and the $N = 50$ isotones from ^{79}Cu to ^{100}Sn , for neutrons and protons respectively. In particular, its strength has been adjusted to produce the crossing of the $3/2_1^-$ and $5/2_1^-$ states of Cu isotopes at $N \simeq 45$ [200], as expected from the experimental results. This interaction reproduces successfully the evolution of the 2^+ energies in the Ni isotopic chain up to $N = 48$ [189]. This agreement indicates that the proton-neutron monopole matrix elements involving the $g_{9/2}$ orbit would be well determined. However the calculated E2 transition strength¹⁴ of ^{70}Ni , $B(E2; 2_1^+ \rightarrow 0^+) = 64e^2fm^4$ [199] is smaller than the measured one [190], $B(E2)\uparrow=860(140)e^2fm^4$, giving $B(E2)\downarrow=172(28)e^2fm^4$. The model space that has been used is not wide enough to account explicitly for the full excitations to develop, in particular those across the $Z = 28$ shell gap.

5.2.4 Conclusion

The Ni isotopic chain offers a variety of doubly-magic nuclei:

- the $^{48}_{28}\text{Ni}_{20}$, lying at the edge of particle stability, which is the mirror of $^{48}_{20}\text{Ca}_{28}$,
- the $N = Z$ nucleus $^{56}_{28}\text{Ni}_{28}$,
- the "superfluid" $^{68}_{28}\text{Ni}_{40}$ in which the neutron Harmonic Oscillator shell number provides a very specific role with respect to parity conservation,
- the $^{78}_{28}\text{Ni}_{50}$ nucleus which is composed of two magic numbers $Z = 28$ and $N = 50$, both originating from the spin-orbit interaction.

The structural evolution of the Ni isotopes is related to that of the $Z = 28$ shell gap, the size of which varies according to proton-neutrons interactions. The $Z = 29$ Cu isotopic chain provides a mean to determine the strength of the various effective interactions involved between protons and neutrons in the f, p, g shells and their decomposition in term of central, spin-orbit, tensor components.

The evolution of the $Z = 28$ shell closure, formed between the proton $f_{7/2}$ and $p_{3/2}$ orbits, has been discussed using the experimental and theoretical results of the Co, Ni and Cu isotopic chains. The $Z = 28$ gap slightly increases between $N = 30$ to $N = 40$ (from about 4.8 to 5.5 MeV) reaching a partial maximum at ^{68}Ni and a minimum of quadrupole collectivity there. Adding neutrons above $N = 40$ seems to provoke the decrease of the $Z = 28$ gap (see the left

¹⁴using an effective neutron charge $e_\nu = 1.0e$

part of Fig. 25), as the $\pi f_{7/2}$ orbit gets less bound as compared to the $\pi p_{3/2}$ one. This picture could account for the increase of cross-shell core excitations required to explain the $B(E2)$ values of ^{70}Ni [190], as well as the neutron-rich Zn isotopes (this is discussed in a next section, see Sect. 6.1.2). In parallel, following the trend of Fig. 26 one would expect that the ground state of the heavy Cu isotopes become $5/2^-$ instead of $3/2^-$. Would these states have a rather pure single particle configuration, the $\pi f_{5/2}$ single-particle orbit decreases to eventually cross the $\pi p_{3/2}$ orbit at a neutron number $N \simeq 45$. Then the $Z = 28$ would become bound by the $\pi f_{7/2}$ and $\pi f_{5/2}$ orbits.

As the increase of binding energy of the $\pi f_{5/2}$ orbit occurs simultaneously to the decrease of binding energy for the $\pi f_{7/2}$ ones, the filling of the $\nu g_{9/2}$ orbital induces a reduction of the $\pi f_{7/2} - \pi f_{5/2}$ SO splitting. This is qualitatively interpreted by the action of tensor forces which are attractive (repulsive) between neutrons in the $g_{9/2}$ and protons in the $f_{5/2}$ ($f_{7/2}$) orbits (see Ref. [53] and Sect. 2.4). From these combined actions, the $Z = 28$ gap in ^{78}Ni could decrease down to 2.5 MeV only, a value which is small enough to permit excitations across $Z = 28$. We remind that the present assumptions concerning the evolutions of the $\pi f_{5/2}$ and $\pi f_{7/2}$ orbits hold *mainly* on two facts, (i) the evolution of the $5/2_1^-$ state in the $_{29}\text{Cu}$ isotopes, and (ii) the determination of atomic masses for the $_{27}\text{Co}$ isotopes. For the first point the role of correlations should be quantified by further experimental and theoretical works, whereas for the second more precise atomic masses are required.

Noteworthy is the fact that the role of tensor forces that is surmised here holds for several other regions of the chart of nuclides, discussed in the next sections.

6 The magic number 50

Various experimental facts indicating the particular stability of shells of 50 neutrons or 50 protons have been listed sixty years ago [2]. For instance the large number of stable $N = 50$ isotones (6) and $Z = 50$ isotopes (10) has been stressed. At that time, the magic number 28 was not put forward as the experimental results were not conclusive enough. So the magic number 50 was the first which did not have a natural description in terms of a square well potential. This has been considered for a while as an indication of the breakdown of the shell model for heavy nuclei, until a strong spin-orbit coupling was assumed [3, 4]. The magic number 50 originates from the spin-orbit part of the nuclear interaction which lowers the energy of the $g_{9/2}$ orbit from the $N = 4$ major shell so that it is located close to the orbits from the $N = 3$ major shell. Its partner, the $g_{7/2}$ orbit, lies on the upper edge of the gap, immediately above or below the $d_{5/2}$ orbit.

6.1 Evolution of the $N = 50$ shell closure

Experimental information, even scarce, is available along the $N = 50$ isotonic chain from $^{78}_{28}\text{Ni}$ to $^{100}_{50}\text{Sn}$. These two *a priori* doubly-magic nuclei attract physicists attention, the former is very neutron rich ($N/Z \simeq 1.8$) while the latter, located at the proton drip-line, is self-conjugate. Both of them have been synthesized and identified in-flight using the projectile fragmentation method. However, as only a few nuclei of each have been produced worldwide their excitation modes remain unknown and rely on the extrapolations of the properties measured in their neighbors.

Possible evolution of the size of the $N = 50$ shell gap between $Z = 28$ to $Z = 50$ depends on proton-neutron interactions between the πfp and $\pi g_{9/2}$ shells and the neutron orbits which form the $N = 50$ gap, i.e. $\nu g_{9/2}$ below and $\nu d_{5/2}$ or $\nu g_{7/2}$ above. As diverse interactions are

involved, among which some contain a tensor part, it is expected that the $N = 50$ gap will vary along the isotone chain. The following sections intend to probe these evolutions through various experimental methods: evolution of atomic masses, trends of collective states, spectroscopy of high spin-states and transfer reactions.

6.1.1 Evolution of the binding energies

The binding energies of the last neutron in the $N = 51, 50$ isotones are drawn in the left part of Fig. 28. Their values are taken from the atomic mass table [10], to which the result for ^{83}Ge has been added [216]. Whereas the curve corresponding to the $5/2^+$ states shows a quasi-linear

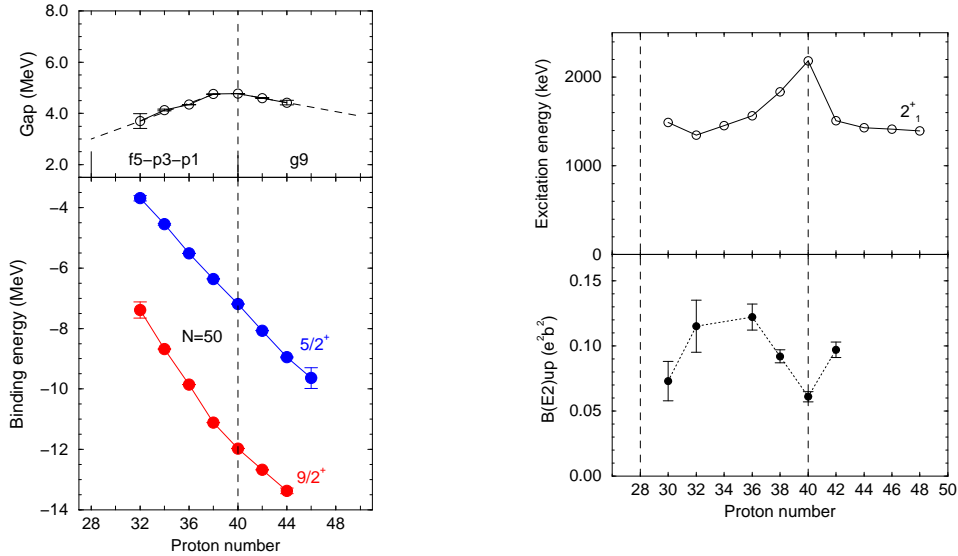


Figure 28: **Left:** Binding energies of the states $9/2^+$ ($5/2^+$) located below (above) the $N = 50$ magic number and difference of the binding energies of these two states surrounding the gap at $N = 50$ (see Sect. 11). The proton orbitals which are getting filled as a function of increasing Z are given in the middle of the figure. **Right:** Experimental $E(2^+)$ and $B(E2; 0^+ \rightarrow 2^+)$ values in the $N = 50$ isotones.

behavior from $Z = 32$ to $Z = 46$, the one corresponding to the $9/2^+$ states displays a steeper slope for $32 \leq Z \leq 38$ than for $Z \geq 40$. This change can be related to the different interactions which come into play with the progressive filling of the proton $f_{5/2}$, $p_{3/2}$, and $p_{1/2}$ orbits for $Z \leq 40$, and $g_{9/2}$ for $Z \geq 40$.

As shown in the left part of Fig. 28 the size of the $N = 50$ gap can be extrapolated to be 3.0(5) MeV for ^{78}Ni . This extrapolation holds on the fact that similar proton-neutron interactions are at play between $Z = 38$ and $Z = 28$ as protons are equiprobably removed from the $f_{5/2}$ and $p_{3/2}$ orbits which are very close in energy. A similar extrapolation of the $N = 50$ gap can be also undertaken from ^{94}Ru to ^{100}Sn between which the $\pi g_{9/2}$ orbit is progressively filled. The size of the $N = 50$ gap would amount to 3.9(4) MeV for $^{100}\text{Sn}^{15}$.

The constancy of the slope of the binding energy for the $5/2^+$ states reveals that all the proton-neutron interactions involving the $\nu d_{5/2}$ orbit have similar intensity, whatever the proton

¹⁵This value does not contain the singularity coming from the Wigner energy (see Sect. 11), such as those discussed in previous sections for ^{40}Ca or ^{56}Ni .

orbits that are considered. On the other hand, the binding energy curve of the $9/2^+$ states has an inflexion point at $Z = 40$, meaning that the filling of the $\pi g_{9/2}$ shell binds the $\nu g_{9/2}$ orbit less than the πfp shells do. In other words, the matrix element $V_{g_{9/2}g_{9/2}}^{pn}$ is weaker than any $V_{(f,p)g_{9/2}}^{pn}$ ones involving the proton fp shells. Among the latter, the $V_{f_{5/2}g_{9/2}}^{pn}$ matrix element contains an attractive component from the tensor interaction, which may enhance its strength with respect to other monopoles¹⁶. On the contrary the $V_{g_{9/2}g_{9/2}}^{pn}$ interaction (acting for $Z > 40$) contains a repulsive term arising from the tensor part of the nucleon-nucleon interaction.

6.1.2 Trends of 2^+ and $B(E2)$ values

As the $N = 50$ shell gap is large, the 2_1^+ state in the $N = 50$ isotonic chain is expected to be mainly built on *proton* excitations within the fp g shells. The experimental 2_1^+ excitation energies and the $B(E2; 0^+ \rightarrow 2_1^+)$ values shown in the right part of Fig. 28 clearly point to the persistence of the $N = 50$ shell closure both towards the heaviest and lightest isotones measured yet. As far as the $B(E2)$ measurement is concerned, the route to $^{100}_{50}\text{Sn}$ is longer than to $^{78}_{28}\text{Ni}$. This is due to the recent works achieved at the HRIBF (Oak Ridge) for $^{82}_{32}\text{Ge}$ [211] and the Rex-Isolde facility for $^{80}_{30}\text{Zn}$ [212]. The $B(E2)\uparrow$ value of $^{82}_{32}\text{Ge}$ has been determined using the Coulomb excitation of the radioactive beam produced from the proton-induced fission of uranium, separated on-line and post-accelerated to 220 MeV. The value of $0.115(20) e^2 b^2$ is close to the one of $^{86}_{36}\text{Kr}$. This situation is expected in the framework of the generalized seniority scheme described in Sect. 5.2.2, where the $B(E2)$ value is maximized at mid-shell (here at $Z = 34$) and decays at each side symmetrically (see Eq. 27). The Coulomb excitation of the $^{80}_{30}\text{Zn}$ nucleus was achieved at the Rex-Isolde facility. The mass-separated radioactive Zn were accumulated, cooled and bunched into a Penning trap. They were subsequently brought to a high charge, separated in A/q and post accelerated by the Rex linear accelerator to about 2.8 A.MeV. A $B(E2)\uparrow$ value of $0.073(15) e^2 b^2$ has been extracted for $^{80}_{30}\text{Zn}$ which, as shown in Fig. 28, is sensibly weaker than that of ^{82}Ge . Shell model calculations reproduce rather well the experimental $B(E2)$ results in the $N = 50$ isotones as well as in the Zn isotopes with two sets of interactions. However, they require large proton e_π effective charge. This indicates a rather strong $Z = 28$ core polarization [212].

6.1.3 Evolution of the $N = 50$ gap viewed from $p-h$ states

The size of a gap is related to the energy of the states arising from the $1p - 1h$ excitations across it. As the $N = 50$ shell gap is formed between the $g_{9/2}$ and $d_{5/2}$ orbits, the corresponding $1p - 1h$ states have a $(\nu g_{9/2})^{-1}(\nu d_{5/2})^{+1}$ configuration. This gives rise to a multiplet of six states with spin values J ranging from 2 to 7. In $^{90}_{40}\text{Zr}$, all the members of this multiplet have been selectively populated using the neutron pick-up reaction, $^{91}\text{Zr}_{51}(^3\text{He}, \alpha)^{90}\text{Zr}_{50}$ by requiring a transferred angular momentum $\ell=4$. Their energies, reported in the left part of Fig. 29 as a function of J , follow a parabola of positive curvature. The energies of the two states having the extreme spin values, $J = 2^+$ and $J = 7^+$, are less lowered by the $p - h$ residual interaction, as expected by the coupling rules reminded in Sect. 2.2.1. These states have also been identified in $^{88}_{38}\text{Sr}$ using the neutron stripping reaction $^{87}\text{Sr}_{49}(d, p)$ in which a transferred angular momentum $\ell=2$ was identified. Such a complete identification of all the members of the $1p - 1h$ multiplet could not be obtained when unstable species are involved.

¹⁶ A similar matrix element is involved to account for the structural evolution of the neutron-rich Cu isotopes (Sect. 5.2.3). There the binding of the $\pi f_{5/2}$ orbit increases with the filling of the $\nu g_{9/2}$ one.

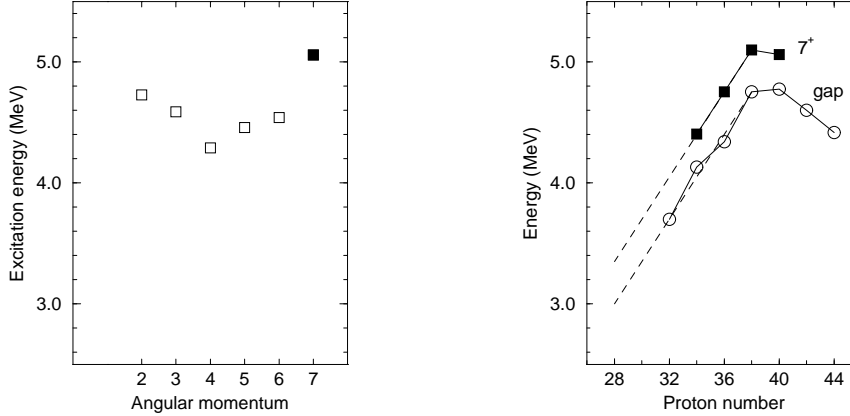


Figure 29: **Left:** Excitation energies of the six states of the $(\nu g_{9/2})^{-1}(\nu d_{5/2})^{+1}$ configuration measured in ^{90}Zr , as a function of their spin J . **Right:** Comparison of the energy of the 7^+ state from the $(\nu g_{9/2})^{-1}(\nu d_{5/2})^{+1}$ configuration in the even-even $N = 50$ isotones (filled squares) and of the gap $N = 50$ (empty circles, see the left part of Fig. 28).

The route to access these states for neutron-rich unstable species $A \sim 80 - 130$ is to use either fusion-fission reactions or spontaneous fission of actinides. In these experiments the high sensitivity of large arrays of Compton-suppressed Ge detectors is needed to detect the large number of photons emitted by the $\simeq 150$ different nuclides produced simultaneously. The assignment of γ -rays to a particular fragment requires an exceptional selectivity. This is achieved by selecting, among the high-fold data, those which contain several γ -rays originating from a well identified fission partner.

Using the gamma-ray spectroscopy method from fusion-fission reaction, the 7^+ yrast states of $^{86}_{36}\text{Kr}$ and $^{84}_{34}\text{Se}$ have been recently identified, which enlarges the knowledge of the evolution of the $(\nu g_{9/2})^{-1}(\nu d_{5/2})^{+1}$ configuration in the light $N = 50$ isotones [213]. As seen in the right part of Fig. 29, the energy of the 7^+ state follows remarkably that of the gap, which confirms its decrease towards $Z = 28$. The energy of the 7^+ state is shifted by about +350 keV with respect to the gap value. This difference comes from the repulsive particle-hole interaction $(\nu g_{9/2})^{-1}(\nu d_{5/2})^{+1}$ (see Sect. 2.2.1).

More recently, medium-spin states in $^{82}_{32}\text{Ge}$ have been studied from spontaneous fission of ^{248}Cm [214]. Two new excited levels with spins and parities $(5, 6^+)$ have been proposed at 2930 and 3228 keV. At least one of them can be attributed to the $(\nu g_{9/2})^{-1}(\nu d_{5/2})^{+1}$ configuration. Its low energy, as compared to the heavier isotones, supports the decrease of the $N = 50$ shell gap.

Following the correlation between the $N = 50$ gap and the energy of the 7^+ state, one should find an hitherto unknown 7^+ state at ~ 4.0 MeV in $^{82}_{32}\text{Ge}$, ~ 3.7 MeV in $^{80}_{30}\text{Zn}$, and ~ 3.4 MeV in $^{78}_{28}\text{Ni}$. As said earlier, this extrapolation relies on the fact that the same $\pi p_{3/2}$ and $\pi f_{5/2}$ orbits are involved between $Z = 38$ and $Z = 28$ and that they are closely packed in energy. In such a case the pairing correlations smooth their occupancies, leading to a regular decrease of the gap and of the $J = 7^+$ energy as protons are removed.

Access to the neutron-deficient nuclei has been obtained by the use of the fusion-evaporation technique. A 12^+ isomeric state has been identified in the $^{98}_{48}\text{Cd}$ isotope through the γ transition at 4.207 MeV to the 8^+ component of the multiplet arising from $(\pi g_{9/2})^{-2}$ configuration [215]. The composition of this isomer is expected to be pure $(\pi g_{9/2})^{-2}(\nu g_{9/2})^{-1}(\nu d_{5/2})^{+1}$, which involves

the neutron cross-shell excitation. Besides the repulsive interaction, $(\nu g_{9/2})^{-1}(\nu d_{5/2})^{+1}$ (such as that of the neutron-rich isotones, as said previously) the 4.207 MeV energy also contains proton-neutron interactions, $(\pi g_{9/2})^{-1}(\nu d_{5/2})^{+1}$ (repulsive terms) and $(\pi g_{9/2})^{-1}(\nu g_{9/2})^{-1}$ (the 0^+ term is strongly attractive), which have to be determined beforehand in order to get the $N = 50$ neutron gap at $Z = 48$.

6.1.4 Neutron orbits above the $N = 50$ gap: Levels of $N = 51$ isotones

As shown in Fig. 28, the $\nu d_{5/2}$ shell is located just above the $N = 50$ shell gap. The evolution in energy of the two next shells, $\nu s_{1/2}$ and $\nu g_{7/2}$, as a function of increasing proton number can be derived from the study of the $N = 51$ isotones. This provides pertinent information on the residual proton-neutron interactions at work, as discussed now.

Experimental results

Experimental results on the $N = 51$ isotones cover a broad range of masses, from $^{83}_{32}\text{Ge}$ to $^{101}_{50}\text{Sn}$. For stable nuclei detailed spectroscopic information exist, whereas for neutron-rich or neutron-deficient nuclei the information is more sparse. However several results have been recently published on the ^{83}Ge [216, 217], ^{85}Se [218, 219], and ^{87}Kr [220] nuclei. These add to the low-spin level scheme of ^{85}Se that was obtained about 15 years ago from the β -decay of mass-separated ^{85}As nuclei [221]. As for the neutron-deficient part, first data on states of $^{101}_{50}\text{Sn}$ have been newly obtained [222, 223]. All these results will be discussed in the following with the aim of looking at the evolution of the neutron orbits as a function of the valence protons.

The ground-state spin value of all $N = 51$ isotones between $Z = 36$ and $Z = 44$ has been firmly established to be $5/2^+$, whereas for the others this $5/2^+$ assignment is compatible with the spectroscopic properties known so far. Thus for all the proton numbers considered here, the $\nu d_{5/2}$ sub-shell can be considered as the first valence orbit above the $N = 50$ gap. The coupling of the $\nu d_{5/2}$ orbit to the first 2^+ excitation of the proton core provides a multiplet of states with spin values between $1/2^+$ and $9/2^+$. Therefore the $1/2^+$ and $7/2^+$ states originating from the $\nu s_{1/2}$ and $\nu g_{7/2}$ orbits can be mixed to those obtained with the coupling to the core excitation. The five states of the multiplet have been firmly identified in $^{89}_{38}\text{Sr}$. Their centroid energy is similar to that of the 2^+ state in $^{88}_{38}\text{Sr}$ [217].

The energies of the first excited states measured in the $N = 51$ isotones are displayed in the left part of Fig. 30, relative to that of the $5/2^+$ ground state. First of all, the $9/2^+$ state is likely to have a rather pure coupled configuration, $\nu d_{5/2} \otimes 2^+$, as the $g_{9/2}$ orbit is too deeply bound (by about 3.5 MeV) to give a fraction of single-particle state at low energy. Such a configuration for the $9/2^+$ state is confirmed by the fact that its energy follows closely that of the 2^+ state. On the other hand, the energies of the $1/2^+$ and $7/2^+$ states depart significantly from that of the 2^+ core at $Z < 38$ and $Z > 44$, respectively. This means that, for these proton numbers, their composition is likely to be mostly of single-particle origin, with a weaker amount of mixing with the coupled configurations.

The (d, p) transfer reactions on the stable $N = 50$ targets help to unfold the composition of both contributions, as the neutron stripping to single-particle states is strongly enhanced as compared to collective states. Several $7/2^+$ and $1/2^+$ states have been populated in $^{87}_{36}\text{Kr}$, $^{89}_{38}\text{Sr}$, $^{91}_{40}\text{Zr}$, and $^{93}_{42}\text{Mo}$, their angular momenta being assigned to $\ell = 4$ or $\ell = 0$, respectively. The $7/2^+$ and $1/2^+$ states have the largest spectroscopic factors. It is therefore likely that the $7/2^+$ and $1/2^+$ states displayed in the left part of Fig. 30 correspond mainly to $\nu d_{5/2} \otimes 2^+$ configurations. The same holds true for the $9/2^+$ state which has not been populated in the stripping reactions.

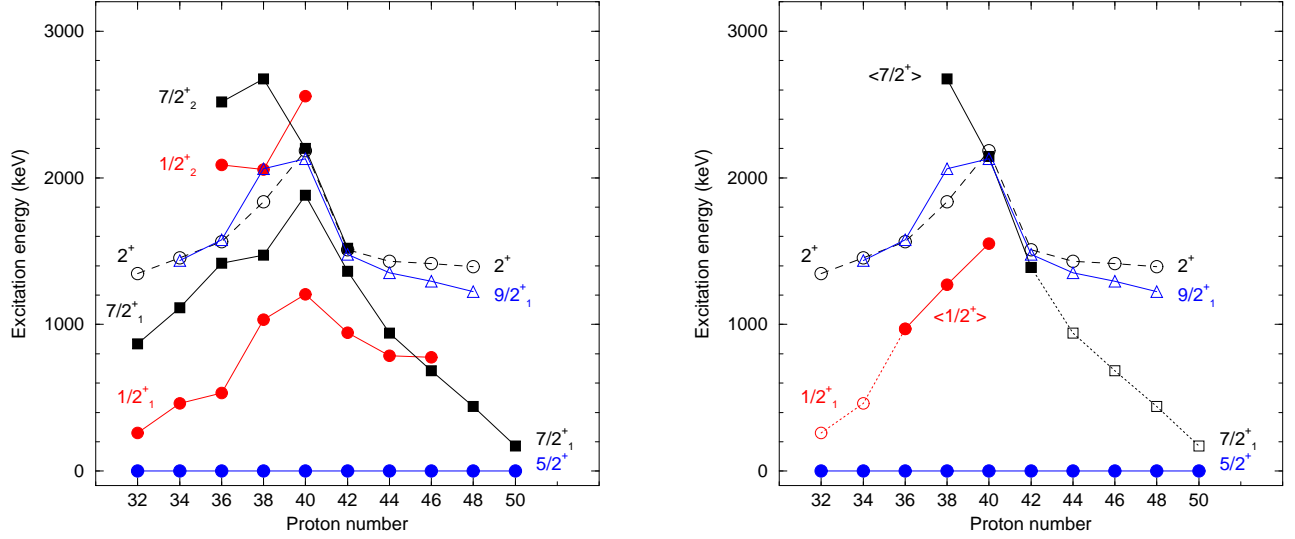


Figure 30: **Left:** First excited states observed in the $N = 51$ isotones. The evolution of the 2^+ energy of the corresponding core is also drawn. **Right:** Possible evolution of the $\nu s_{1/2}$ and $\nu g_{7/2}$ single-particle energies obtained from (i) the average energy (filled symbols) of all the $1/2^+$ and $7/2^+$ states populated in the (d, p) stripping reactions on the stable targets, ^{86}Kr , ^{88}Sr , ^{90}Zr , and ^{92}Mo , (ii) the energy of the $1/2_1^+$ state (empty circles) of the lightest isotones, (iii) the energy of the $7/2_1^+$ state (empty squares) of the heaviest isotones.

This confirms the assumption made in the previous paragraph.

Stripping (d, p) reactions in inverse kinematics have been recently performed with the radioactive ^{82}Ge and ^{84}Se nuclei [216, 218]. The two radioactive beams were produced from the proton-induced fission of uranium, separated on-line, and post-accelerated to 330 MeV and 378 MeV respectively. With such low-energy beams, only the single-neutron states at low-energy could be identified in $^{83}\text{Ge}_{51}$ and $^{85}\text{Se}_{51}$ through the detection of the protons in a highly-segmented silicon detector array. Angular distributions of protons associated to the population of their ground and first-excited states have been obtained. They are consistent with $\ell = 2$ and $\ell = 0$ transferred momenta giving rise to $5/2^+$ and $1/2^+$ spin assignments, respectively. Spectroscopic factors account for only half of the single-particle strengths. The remaining part is likely to be present at higher excitation energy. A similar result had been already obtained in ^{87}Kr , which displays around half of the single-particle strengths, both for the $\nu d_{5/2}$ and the $\nu s_{1/2}$ orbits.

The β decay of ^{101}Sn has been newly studied at the GSI on-line mass separator, this very neutron-deficient isotope being produced by using the $^{50}\text{Cr}(^{58}\text{Ni}, \alpha 3n)$ fusion-evaporation reaction [222]. By comparing the experimental energy spectrum of β -delayed protons to a theoretical prediction, the $5/2^+$ spin and parity assignments for the ^{101}Sn ground state have been confirmed. Moreover the $^{46}\text{Ti}(^{58}\text{Ni}, 3n)$ reaction was used to determine the first excited state of ^{101}Sn at the Argonne facility [223]. Prompt γ -rays emitted by ^{101}Sn have been identified through correlations with β -delayed protons following its decay, using the recoil-decay tagging (RDT) method. The γ -rays were detected in a large array of Ge detectors surrounding the target, whereas the products of the reaction were separated from the unreacted beam and dispersed according to their M/Q ratio in the fragment mass analyzer. A new γ -ray line with an energy of 171.7(6) keV has been assigned to ^{101}Sn and interpreted as the transition between the single-neutron $g_{7/2}$ and $d_{5/2}$

orbitals.

The right part of Fig. 30 displays the average energy (filled symbols) of all the $1/2^+$ and $7/2^+$ states, weighted by their SF values. These states were populated in the (d,p) stripping reactions on the stable targets (using the same method as in Sect. 4.2.3). Added to these points the empty symbols display the energy of the $1/2_1^+$ and $7/2_1^+$ states identified in the lightest and heaviest $N = 51$ isotones, respectively. The obvious outcomes of this figure are (i) a reduction of the energy between the $\nu d_{5/2}$ and $\nu g_{7/2}$ orbits when Z increases, (ii) a similar decrease of the energy spacing between the $\nu d_{5/2}$ and $\nu s_{1/2}$ orbits for low Z values. Nevertheless the excitation energy of the $1/2_1^+$ ($7/2_1^+$) state measured in the lightest (heaviest) isotones is not an absolute determination of the single particle energy spacing because their wave functions may contain an unknown fraction of mixing to the $\nu d_{5/2} \otimes 2^+$ configuration.

The item (i) can be ascribed to the attractive term of the interaction between the $\pi g_{9/2}$ protons and the $\nu g_{7/2}$ neutrons, from the tensor term. It is very strong in this particular configuration in which protons and neutrons orbits with identical angular momentum and opposite spin are involved, i.e. πg_{\uparrow} and νg_{\downarrow} . Likewise the interaction between the $\pi g_{9/2}$ protons and the $\nu g_{9/2}$ neutrons, $V_{g_{\uparrow}g_{\downarrow}}^{pn}$, displays a repulsive part, as already mentioned in Sect. 6.1.1. These opposite behaviors between the aligned $\nu g_{9/2}$ and anti-aligned $\nu g_{7/2}$ orbits during the filling of the $\pi g_{9/2}$ orbit can be seen in the left part of Fig. 31. The monopole interactions V^{pn} involving the $\nu g_{9/2}$ and

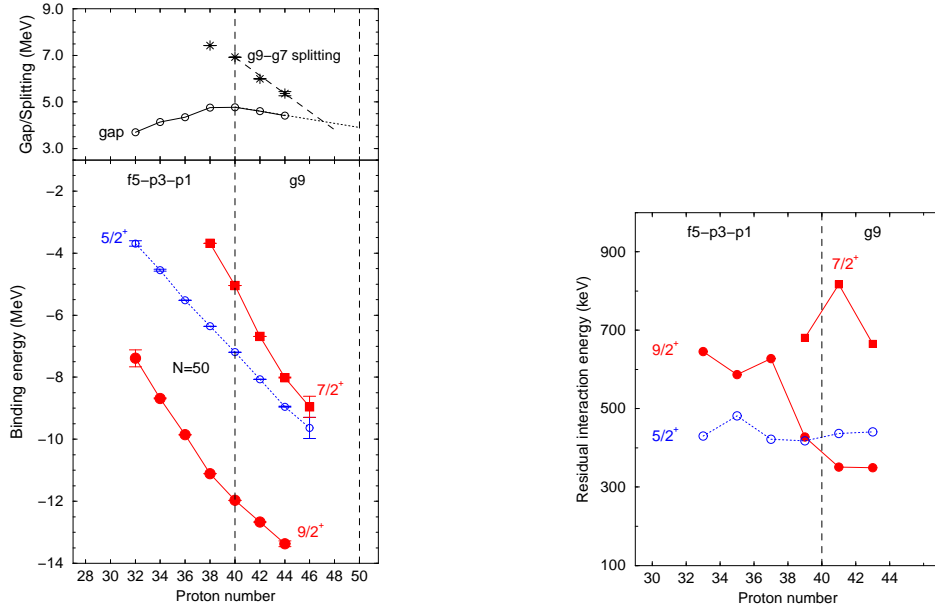


Figure 31: **Left:** Evolution of the binding energies of the $9/2^+$ and $7/2^+$ states compared to those of the $5/2^+$ states. The $9/2^+$ and $5/2^+$ states are the ground states of the $N = 49$ and $N = 51$ isotones respectively, the $7/2^+$ states being those drawn in the right part of Fig. 30. Energy splitting between the $9/2^+$ and $7/2^+$ states (stars) and the $N = 50$ gap (empty circles). **Right:** Evolution of the proton-neutron residual interactions extracted from the slopes of the binding energies of the neutron states shown in the left part. The proton orbitals which are getting filled as a function of increasing Z are given in the top of the figures.

$\nu g_{7/2}$ orbits can be tentatively derived from the evolution of their binding energies as a function

of the proton number (see Sect. 2.2.2). They are compared to the ones involving the $\nu d_{5/2}$ orbit in the right part of Fig. 31. From the constancy of the slope for the $\nu d_{5/2}$ orbit before and after $Z = 40$, one derives that the monopoles involving this orbit have similar values of about 440 keV. For the $\nu g_{9/2}$ and $\nu g_{7/2}$ orbits the monopole matrix elements $V_{g_{9/2}g_{9/2}}^{pn} \sim 350$ keV and $V_{g_{9/2}g_{7/2}}^{pn} \sim 750$ keV can be extracted. The energy difference between the two values is about 400 keV, which could be ascribed to the tensor terms for these $\ell = 4$ orbits.

An extrapolation of the energy splitting between the $9/2^+$ and $7/2^+$ states can be made towards $Z = 50$ to give a value of 3.0(3) MeV for $Z = 50$ as shown in Fig. 31. This value is smaller than 3.9(5) MeV, obtained from the extrapolated size of the $\nu g_{9/2}$ - $\nu d_{5/2}$ gap. This suggests that the $\nu g_{7/2}$ orbit could cross or come close to the $\nu d_{5/2}$ one around the $^{100}_{50}\text{Sn}$ nucleus. Experimentally, the $7/2^+$ state remains about 170 keV above the $5/2^+$ state at least up to $Z = 50$, as seen in Fig. 30 and surmised in Ref. [223]. However both the size of the shell gap and the SO splitting are reduced.

Theoretical results

Shell-model calculations reproduce the decrease of the $7/2_1^+$ energy of all the heavy isotones, except for the $^{99}_{48}\text{Cd}$ isotope [40] in which the energy of the $\nu g_{7/2}$ orbit has to be increased arbitrarily by 0.26 MeV in order to obtain a good description of its high-spin states [224]. The same values of single-particle energies and matrix elements have been then used to calculate the low-lying levels in $^{101}_{50}\text{Sn}$, unknown at that time. Its ground state has been predicted to be $5/2^+$, with the $7/2^+$ state lying ~ 100 keV above. This is in good agreement with the value of 172 keV energy newly measured in $^{101}_{50}\text{Sn}$ [223].

We have carried out self-consistent calculations using the D1S Gogny force and imposing the spherical symmetry, to obtain the first excited states of the $N = 51$ isotones. The blocking method was used, imposing that the odd neutron is successively located in one particular orbit, $d_{5/2}$, $s_{1/2}$, and $g_{7/2}$. The overall change of excitation energy as a function of the proton number is *partly* accounted for as shown by comparing the left and right parts of Fig. 32. The energy of the first

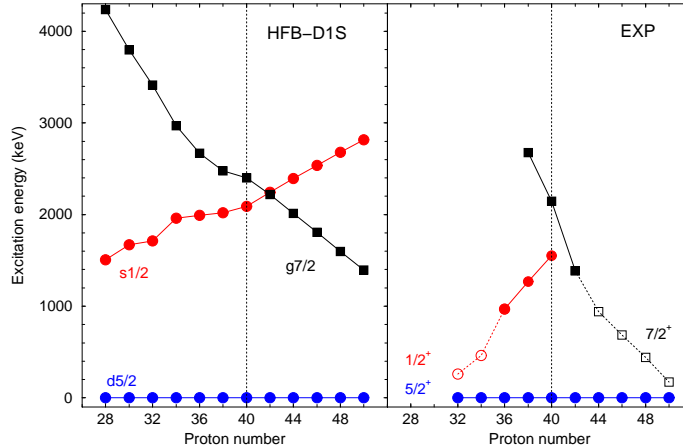


Figure 32: **Left** Evolution of the $\nu s_{1/2}$ and $\nu g_{7/2}$ excitation energies in the $N = 51$ isotones predicted within the self-consistent approach using the D1S effective force of Gogny and the blocking method (see text). **Right** Possible evolution of the $1/2^+$ and $7/2^+$ excitation energies obtained from experimental results (cf. the right part of Fig. 30)

excited state in the lightest isotones ($I^\pi=1/2^+$), as well as in the heaviest ones ($I^\pi=7/2^+$) are

found at around 1.5 MeV. This is significantly larger than the experimental values of 280(20) keV for $^{83}_{32}\text{Ge}$ and 172 keV for $^{101}_{50}\text{Sn}$. Moreover the experimental slope of excitation energy and the reduction of the $\pi g_{9/2} - g_{7/2}$ SO splitting are not reproduced by these calculations. This leaves room for additional effects of the nuclear interaction, such as tensor, to be added to the Gogny interaction. Nevertheless one has to bear in mind that these experimental energies do not directly correspond to those of the single-particle states $\nu s_{1/2}$ and $\nu g_{7/2}$. Indeed the $1/2^+$ and $7/2^+$ states may comprise a certain mixing with $\nu d_{5/2} \otimes 2^+$ configuration. Therefore experimental pieces of information has to be extended on the $N = 51$ isotones to derive the *true* single-particle energies at the two extremes of the valley of stability. With this in hand, better comparisons between experiment and theory could be made.

6.1.5 Conclusion

The $N = 50$ shell gap is formed between the $g_{9/2}$ and the $d_{5/2}$ or $g_{7/2}$ orbits. The evolution of this gap has been studied over a wide range of masses thanks to the recent experimental data obtained very far from stability. The largest gap is found in nuclei close to the stability valley at $Z = 40$. On both side of this valley, towards $^{78}_{28}\text{Ni}$ and $^{100}_{50}\text{Sn}$, the gap decreases. These features have been attributed to the specific proton-neutron interaction involved below and above $Z = 40$.

Between $Z = 28$ and $Z = 38$ the attractive tensor part of the $\pi f_{5/2}\nu g_{9/2}$ interaction could explain the steep increase of the $\nu g_{9/2}$ binding energy as compared to the $\nu d_{5/2}$ one during the filling of the $\pi f_{5/2}$ orbit.

Above $Z = 40$ the repulsive tensor component of the $\pi g_{9/2} - \nu g_{9/2}$ interaction reduces the size of the $N = 50$ shell gap. Simultaneously the strongly attractive component of the $\pi g_{9/2} - \nu g_{7/2}$ interaction provokes a reduction of the νg SO splitting and the quasi-degeneracy of the $d_{5/2}$ and $g_{7/2}$ orbits at $Z = 50$. Altogether, significant reductions of the $N = 50$ shell evolution are found with hints of increasing core excitations. Nevertheless, the present experimental results indicate that all the $N = 50$ isotones keep on behaving as spherical nuclei. Whether this assertion would hold or not for $^{100}_{50}\text{Sn}$ and $^{78}_{28}\text{Ni}$ cannot be given today, as some experimental information is still missing. The study of the two far edges of the $N = 50$ isotone chain offers a wonderful challenge for the future. Thanks to the new worldwide facilities soon available, they are close at hand.

6.2 Evolution of the $Z = 50$ shell closure

The $Z = 50$ shell gap is formed between the proton $g_{9/2}$ and $d_{5/2}$ or $g_{7/2}$ orbits. The $^{50}_{50}\text{Sn}$ isotopic series contains the two doubly-magic nuclei $^{100}_{50}\text{Sn}_{50}$ and $^{132}_{50}\text{Sn}_{82}$. The synthesis of the self-conjugated $^{100}_{50}\text{Sn}$ isotope, located at the proton drip line, is a very difficult task because of the very low cross sections. Thus no experimental data on its excited states has been obtained up to now. On the other hand, the $^{132}_{50}\text{Sn}$ can be produced with a higher rate in the asymmetric fission of actinides. Therefore properties of this neutron-rich nucleus and its close neighbors are better documented.

As for other shell gaps, possible variation of the proton single-particle energies could be caused by proton-neutron interactions. As the five neutron orbits involved between $N = 50$ and $N = 82$ are very close in energy, the pairing correlation dilutes their respective occupancies and smoothen possible changes of binding energies due to specific proton-neutron interactions over several components.

The present section intend first to address the evolution of the proton single-particle energies and collectivity around the Sn isotopic chain. Afterwards the following paragraphs present

experimental data on the $_{51}\text{Sb}$ isotopes obtained by transfer reactions, followed by theoretical interpretations. As experimental results disagree with respect to the single-particle or mixed configuration of the proton states, the possibility to extract the strength of the SO or tensor interactions directly from experimental data is uncertain. This also sheds doubt on the possibility to implement the tensor interaction there, as many mean-field calculations tried without success.

6.2.1 Binding energies

The evolution of the experimental binding energies of the proton orbits located below and above the $Z = 50$ shell closure is shown in the left part of Fig. 33. The slope of the binding energy of the $9/2^+$ state changes at the $N = 64$ subshell closure : it is steeper when neutrons are filling the first shells, $d_{5/2}$ and $g_{7/2}$, than when filling the next $s_{1/2}$, $h_{11/2}$, and $d_{3/2}$ ones. This shell ordering is reported in Fig. 33. It has been established from the ground-state spin values of the odd-A Sn isotopes. As mentioned earlier pairing correlations induce a simultaneous filling of the neutron orbits located either below or above the $N = 64$ subshell. Their action is evidenced by the quasi-regular variation of the binding energy curves before and after $N = 64$. Without pairing correlations, a sequence of various slopes of binding energies would have been found, corresponding to the progressive filling of individual orbits.

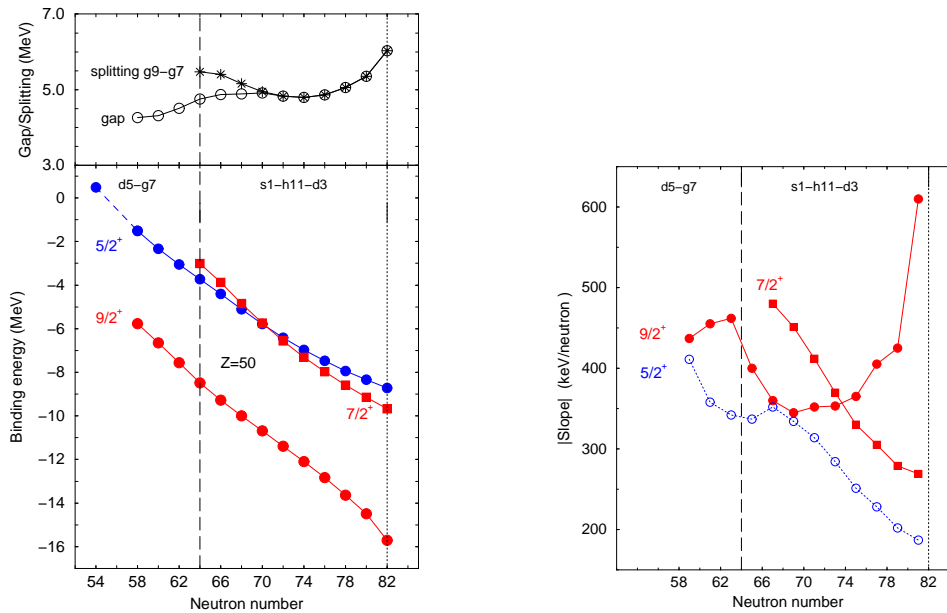


Figure 33: **Left:** Binding energies of the states located just above and just below the $Z = 50$ magic number and differences of the binding energies of the two states surrounding the gap at $Z = 50$ (empty circles) and of the binding energies of the two $\ell = 4$ spin-orbit partners (stars) (see Sect. 11). The proton drip line has been delineated at $^{105}\text{Sb}_{54}$ (being a proton emitter, its proton binding energy is positive). The neutron orbitals which are getting filled as a function of increasing N are given in the middle of the figure (see text). **Right:** Absolute values of the slopes of the experimental binding energies of the $9/2^+$, $5/2^+$ and $7/2^+$ proton states bounding the $Z = 50$ shell closure, as a function of neutron number.

Above the $Z = 50$ gap, the angular momentum of the *ground state* of the odd-A $_{51}\text{Sb}$ isotopes changes from $I^\pi = 5/2^+$ to $I^\pi = 7/2^+$ between ^{121}Sb and ^{123}Sb , the two stable isotopes of antimony.

Consequently the $Z = 50$ gap becomes progressively formed between the $9/2^+$ and $7/2^+$ states, which likely arise from the proton $g_{9/2}$ and $g_{7/2}$ orbits, respectively. If the $9/2^+$ and $7/2^+$ levels are pure single-particle states, their energy spacing will reflect the change of the spin-orbit splitting for the $\ell = 4$ orbits. The left part of Fig. 33 shows both the evolution of the $9/2^+ - 7/2^+$ splitting and that of the $Z = 50$ gap. The latter evolves from 4.3 MeV ($N = 58$) to 6 MeV ($N = 82$). Below $N = 64$, the gap is reduced as the slope of the $\pi g_{9/2}$ binding energy is steeper than that of the $\pi d_{5/2}$ one (see the right part of Fig. 33). This likely arises from the fact that the $V_{d_{5/2}g_{7/2}}^{pn}$ matrix element is weaker than $V_{g_{9/2}g_{7/2}}^{pn}$ one, as in the former, neither the orbital momenta nor the number of nodes of the proton and neutron wave functions are equal, contrary to the latter.

As done in the previous sections, we have calculated the slopes of the experimental binding energies of the states bounding the gap (see the right part of Fig. 33). The results are very different from the other cases, particularly above $N = 64$ where the values changes continuously up to a factor $\simeq 2$. This hints for the presence of correlations beyond the pure monopole-induced variations. The relation (15) (see Sect. 2.3.1) can no longer apply in this case, the effects of the different monopole interactions involved there are obscured by changes of the cores.

6.2.2 Trends of first collective excitations of Sn isotopes

As the $Z = 50$ gap is almost constant and large over a wide mass range, proton excitations across it require large excitation energy. Consequently, apart from ^{132}Sn , the first excited 2^+ levels of Sn at $\simeq 1.2$ MeV (see Fig. 34) are likely almost pure neutron states. The small rise and fall of the state around $N = 64$ witnesses the presence of a weak subshell closure. Apart from this effect the almost constancy of the 2^+ energies at each side of the $N = 64$ subshell closure confirms that pairing correlations acts to dilute shell occupancies and generate 2^+ states of similar configurations.

On the other hand, the drastic increase of the 2^+ state for the $^{132}_{50}\text{Sn}_{82}$ nucleus arises from the fact that both neutron and proton excitations across the $Z = 50$ and $N = 82$ shell gaps require large energies. Important is to note also that the 2^+ state may not be of pure neutron origin anymore, but can contain proton excitations as well.

Experimental $B(E2)^\uparrow$ values shown in the left part of Fig. 34 are taken from Ref. [11] for the stable Sn isotopes, whereas the filled data points for unstable nuclei are obtained from Coulomb excitation using radioactive ion beams [225, 226, 227, 228, 229]. For $N > 64$ the $B(E2)$ value follows the parabolic trend of the generalized seniority scheme described in Sect. 5.2.2, with the sole exception for the $N = 82$ nucleus. There, as said earlier, the wave function of the first 2^+ state contains more proton excitations, which enhances the $B(E2)$ in a significant manner.

On the proton-rich side ($N < 64$), the $B(E2)$ values exhibit a very different pattern. Those drawn with filled symbols remain almost constant, indicating an increase of collectivity towards $^{100}_{50}\text{Sn}_{50}$. This behavior goes in concert with the slight decrease of the shell gap observed for $N < 64$ and shown in the top left part of Fig. 34. At first consideration this corroborates an increase of collectivity due to easier proton core excitations. However, the $B(E2; 2_1^+ \rightarrow 0^+)$ value of ^{112}Sn has been remeasured recently by using the Doppler-shift attenuation method [228]. The new strength (drawn with empty symbol) is significantly weaker than the one previously adopted. As the former $B(E2)$ value in ^{112}Sn was used as normalization to derive the $B(E2)$ value in ^{108}Sn [226], the value of ^{108}Sn should be downscaled accordingly. With these new values for $^{108,112}\text{Sn}$ shown with empty symbols, the $B(E2)$ values in the Sn isotopes display a more symmetric pattern at each side of $N = 64$ mid-shell. Further experimental work has to be made to reduce uncertainties and agree on mean $B(E2)$ values.

On the theoretical point of view, the behaviour of the $B(E2)$ values along the isotopic chain

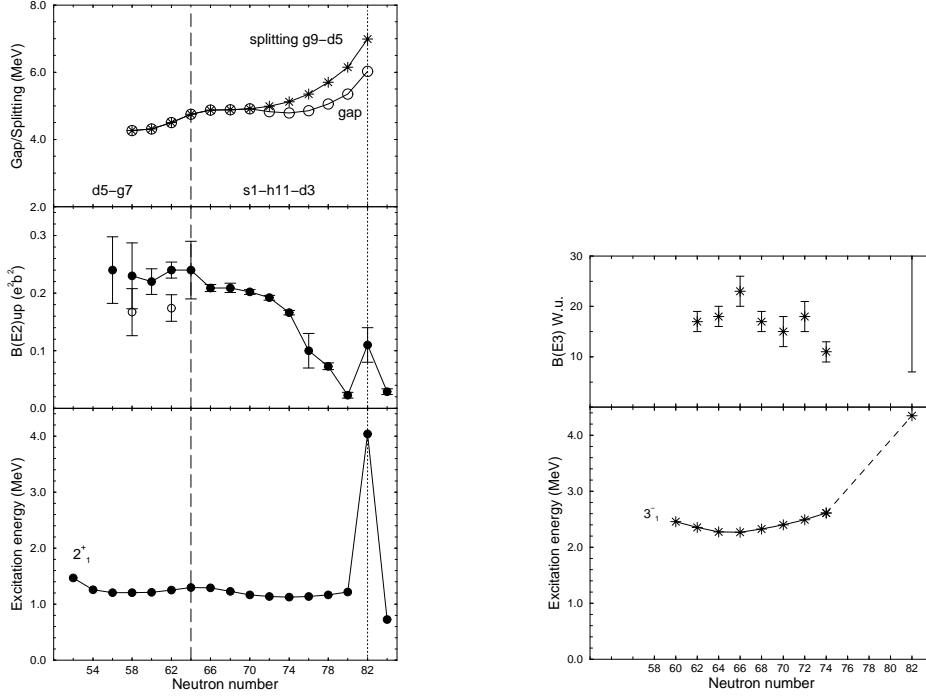


Figure 34: **Left** Experimental 2_1^+ energies (bottom) and $B(E2; 0^+ \rightarrow 2_1^+)$ values (middle) in the Sn isotopic chain. Differences of the binding energies of the two states surrounding the gap at $Z = 50$ and of the binding energies of the $\Delta\ell = 2$ orbits (top). The neutron orbitals which are getting filled as a function of increasing N are given in the middle of the figure (see text). **Right** Experimental 3_1^- energies (bottom) and $B(E3; 3_1^- \rightarrow 0^+)$ values (top) in the Sn isotopic chain.

of Sn has been analyzed up to ^{130}Sn in the framework of large-scale shell model calculations[226]. Calculations well reproduce experimental data on the neutron-rich side, whereas they agree or are significantly underestimated below $N = 64$ when comparing to the empty or filled symbols in Fig. 34, respectively. As said earlier, the experimental situation has to be clarified below $N = 64$. On the shell model point of view, the evolution of the $Z = 50$ is an essential ingredient to consider to determine $B(E2)$ values. In the work of Ref. [226] this gap is increased below $N = 64$ (towards ^{100}Sn), whereas the experimental trend shown in the top part of Fig. 34 rather indicates a decrease.

The local increase of $B(E2)$ at ^{132}Sn was predicted in Ref. [230] using the quasiparticle random phase approximation (QRPA) method. The wave function of the 2_1^+ states of tin isotopes is dominated by neutron excitations. However, at $^{132}_{50}\text{Sn}_{82}$, *both* proton and neutron low-energy excitations are hindered due to the presence of shell gaps. Therefore the energy of the 2_1^+ state suddenly increases and its wave function have mixed components, *both* from neutron and proton, the latter leading to the local increase of the $B(E2)$ value. After having passed the $N = 82$ shell closure, the neutron excitations take over again, a small $B(E2)$ value being measured in the $^{134}_{50}\text{Sn}_{84}$ nucleus [229].

A 3_1^- state is observed around 2.5 MeV excitation energy throughout the Sn isotopic chain, as shown in the right part of Fig. 34. The large $B(E3)$ values values of $\simeq 10 - 20 W.u.$ indicate that these states are collective. Their configuration can be written in terms of neutron excitations involving the negative parity intruder $h_{11/2}$ orbit and the positive-parity ones $d_{5/2}$ and $g_{7/2}$.

In summary, the proximity of several neutron orbits with $\Delta\ell = 2$ and $\Delta\ell = 3$ give rise to E2 and E3 collective excitations in Sn isotopes. As these modes occur at relatively low excitation energy the single-proton states above the $Z = 50$ shell closure could easily couple to them. Therefore they should be considered carefully when determining the proton SPE in the $_{51}\text{Sb}$ isotopes.

6.2.3 Proton orbits above the $Z = 50$ gap: Levels of $_{51}\text{Sb}$ isotopes

The present chapter deals with the evolution of the proton orbit above the $Z = 50$ shell gap as a function of increasing neutron number. By virtue of the closed $Z = 50$ core, the low-energy states of the even-N $_{51}\text{Sb}$ isotopes could be interpreted in terms of single-proton states and their coupling to the 2_1^+ and 3_1^- excitations of the Sn cores. In the following, we discuss on the identification of the single-proton states located above the $Z = 50$ gap. The evolution of the proton $d_{5/2}$, $g_{7/2}$ and $h_{11/2}$ orbits with respect to proton-neutron interactions is discussed as well.

Evolution of the $\pi d_{5/2}$ and $\pi g_{7/2}$ orbits

The evolution of the first excited states with $5/2^+ \leq I^\pi \leq 11/2^+$ as well as the 2^+ excitation of the core nuclei are shown in the left part of Fig. 35 for an increasing neutron number. The spin value of the ground state of the odd-A Sb isotopes changes from $I^\pi = 5/2^+$ to $I^\pi = 7/2^+$, between the two stable isotopes of antimony, $^{121}\text{Sb}_{70}$ and $^{123}\text{Sb}_{72}$. Taken at face value this indicates a crossing of the $\pi d_{5/2}$ and $\pi g_{7/2}$ orbits, if these states will be of single-particle origin.

The coupling of the 2^+ core excitation to these single-proton states $d_{5/2}$ and $g_{7/2}$ also gives rise to $7/2^+$ and $5/2^+$ states. Therefore one needs to examine which levels originate from (i) a core coupling, (ii) a mixing between these two configurations or (iii) a single-particle state.

The most straightforward assignment for case (i) could be obtained for the $9/2^+$ and $11/2^+$ states which have the maximum spin values reached by the $2^+ \otimes d_{5/2}$ and $2^+ \otimes g_{7/2}$ couplings, respectively. As suspected the $9/2^+$ and $11/2^+$ states nicely follow the energy of the 2^+ excitation of the Sn core [231, 232] in the light and heavy Sb isotopes, respectively (see left part of Fig. 35).

The behavior of the two $7/2^+$ states between $N = 62$ and $N = 70$ is a good illustration for case (ii). Where a crossing of the $7/2_1^+$ and $7/2_2^+$ levels would have been expected at about 1 MeV, as indicated by the dashed and dotted lines in the left part of Fig. 35, they repel each others. The shift in energy from the crossing point is similar for both state, $\Delta E = \pm 0.18$ MeV, in agreement with a two-state mixing process [232]. In the lightest isotopes the $7/2_1^+$ state is a member of the multiplet from the $\pi d_{5/2} \otimes 2^+$ configuration, while in $^{111-115}\text{Sb}_{60-64}$, it has a mixed wave function $\pi g_{7/2}$ and $\pi d_{5/2} \otimes 2^+$.

Above $N = 66$ the $7/2_1^+$ energy decreases quasi-linearly with respect to the $5/2^+$ one, whereas the $7/2_2^+$ energy follows that of the 2^+ of the Sn cores (therefore it corresponds mainly to a $\pi d_{5/2} \otimes 2^+$ configuration). These features indicate that the amplitude of mixing is reduced above $N = 66$. The $7/2_1^+$ state becomes rather a single-particle state from the $g_{7/2}$ orbit (case (iii)). This is confirmed by the $^4\text{Sn}(^3\text{He}, d)$ transfer reactions, in which the $7/2_1^+$ state feeding amounts to about 75% of the $\pi g_{7/2}$ strength. As already presented in Sect. 6.2.1, the binding energy curves of the $7/2_1^+$ and $5/2_1^+$ states are not linear when increasing the neutron number (see Fig. 33), which witnesses that some correlations beyond the monopole trend are still present. As their curvatures are similar, the origin of correlations is similar as well.

Above the neutron magic number $N = 82$, the energy of the first $5/2^+$ excited state drops suddenly from 963 keV in ^{133}Sb to 282 keV in ^{135}Sb [233, 234, 235], as shown in the left part of Fig. 35. This reverse behavior between the $5/2^+$ and $7/2^+$ states triggered new studies. In particular, using the fast time-delayed $\gamma\gamma$ coincidence technique, the half-life of the first excited state of ^{135}Sb

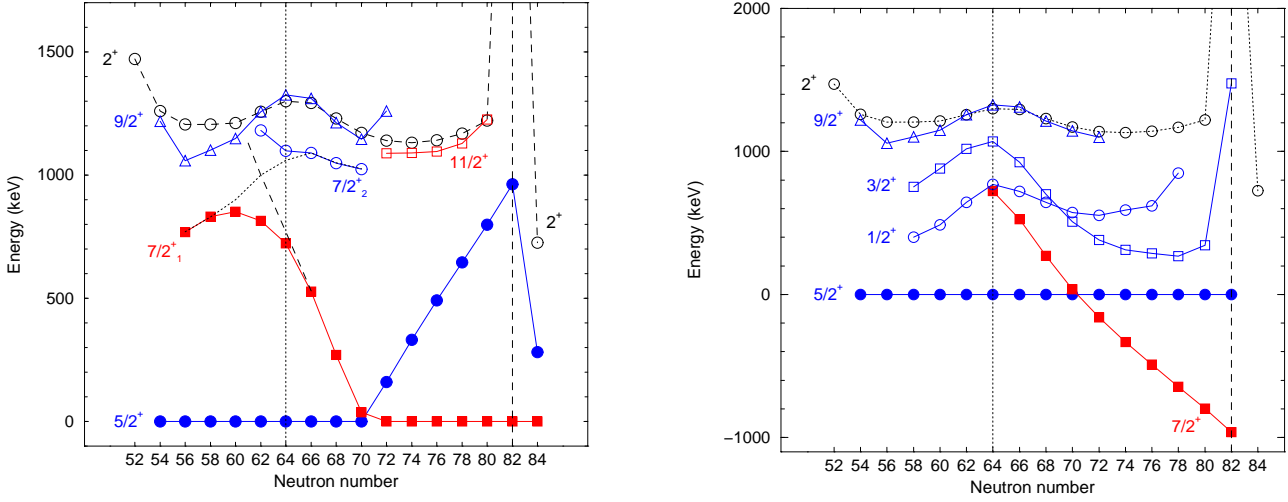


Figure 35: **Left:** Evolution of the first excited states with $5/2^+ \leq I^\pi \leq 11/2^+$ in the odd- A $_{51}\text{Sb}$ isotopes as a function of the neutron number. **Right:** Evolution of the excitation energy of the $1/2^+$, $3/2^+$, $7/2^+$ and $9/2^+$ states relative to the $5/2^+$ state in $^{105-133}\text{Sb}_{54-82}$. The energy of the 2^+ state of the Sn cores is also drawn (the 2^+ energy of ^{132}Sn is not shown, being well above the maximum scale).

at 282 keV has been measured to be $T_{1/2} = 6.0(7)$ ns [236]. Assuming a pure M1 transition, this lifetime implies a $B(M1)$ of $2.9 \cdot 10^{-4} \mu_N^2$, i.e. $1.6 \cdot 10^{-4}$ Wu. This extremely small value was interpreted [236] to be due to a transition between the two single-proton states, $\pi d_{5/2} \rightarrow \pi g_{7/2}$. Such an M1 decay is hindered because of the difference of angular momentum ($2\hbar$) between the d and g orbits.

The sudden change between the energy of the $7/2^+$ and $5/2^+$ states above $N = 82$ has been recently studied in the framework of the Shell-Model approach [237]. Quantitatively, the two-body matrix elements involving the $\pi g_{7/2} - \nu f_{7/2}$ and $\pi d_{5/2} - \nu f_{7/2}$ configurations have been derived from the CD-Bonn nucleon-nucleon potential. The resulting energy of the $5/2^+$ state of ^{135}Sb matches well the experimental value. Moreover these new matrix elements give rise to good results in the odd-odd $^{134}\text{Sb}_{83}$ nucleus [238] and in the even-even neighbors of ^{132}Sn .

The trends of the $5/2^+ - 7/2^+$ relative energy before and after $N = 82$ can be *qualitatively* interpreted in terms of proton-neutron residual interaction and the overlap of the radial wave functions. To a first order, it scales with the number of nodes of the wave functions involved. The nodeless proton $\pi g_{7/2}$ and neutron $h_{11/2}$ and $g_{7/2}$ wave functions have large overlap. At the opposite the $\pi d_{5/2}$ wave function has one node, making its overlap with the neutron $h_{11/2}$ and $g_{7/2}$ orbits weaker. Consequently, the absolute value of $V_{d_{5/2}h_{11/2}}^{pn}$ is weaker than this of $V_{g_{7/2}h_{11/2}}^{pn}$, leading to the steep decrease of the $7/2^+$ state and the crossing with the $5/2^+$ ones. Above $N = 82$ the situation does change. As the first neutron orbit which comes into play $f_{7/2}$ has one node, the arguments with respect to the $\pi g_{7/2}$ and $\pi d_{5/2}$ orbits are reversed and the $5/2^+ - 7/2^+$ spacing is brutally reduced.

The crossing of the $\pi d_{5/2}$ and $\pi g_{7/2}$ sub-shells at $N = 70$ is well reproduced by the self-consistent calculations using the D1S Gogny force [239]. Since the detailed spectroscopic study of all these antimony nuclei (see the discussion in Ref. [232]) indicates that the $5/2^+$ and $7/2^+$

states are associated to a spherical shape, all the calculations have been performed imposing the spherical symmetry.

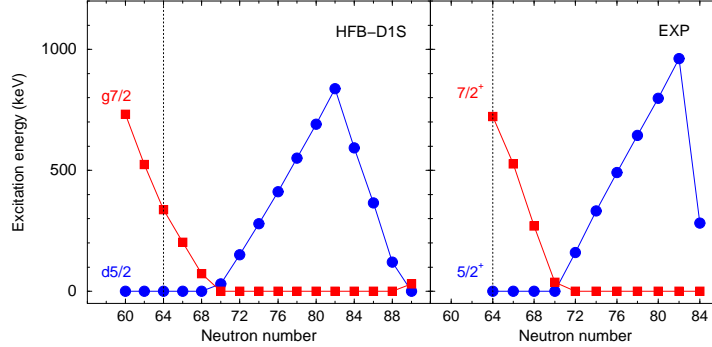


Figure 36: **Left:** Evolution of the energies of the $\pi d_{5/2}$ and $\pi g_{7/2}$ states of the odd-A Sb isotopes from $N = 60$ to 90 , predicted in the HFB self-consistent calculations using the D1S effective force of Gogny and the method of blocking, the spherical symmetry being imposed (results published in ref. [239] for $N \leq 82$). **Right:** Evolution of the experimental energies of the $5/2_1^+$ and $7/2_1^+$ states of the odd-A Sb isotopes (part of Fig. 35).

The comparison between the theoretical results drawn in the left part of Fig. 36 and the experimental ones shown in the right part indicates that (i) the crossing of the $5/2^+$ and $7/2^+$ states is found at the right neutron number, (ii) the decrease of the $5/2^+$ state is found beyond the $N = 82$ shell closure. Therefore most of the underlying physics is taken into account by the self-consistency of such a calculation, i.e. the continuous change of the cores evidenced by the non-linear variations of the binding energies (see Fig. 33). However, as for the results obtained in the $N = 51$ isotones (see Fig. 32), there is room for additional effects of the nuclear interaction, as the predicted variations are not as large as the observed ones.

The $\pi s_{1/2}$ and $\pi d_{3/2}$ orbits

The $\pi s_{1/2}$ and $\pi d_{3/2}$ orbits are located above the $Z = 50$ gap. They should lead to $1/2^+$ and $3/2^+$ single-particle states in the Sb isotopes. However their exact location is not trivial, as the $\pi d_{5/2} \otimes 2^+$ coupling also gives rise to $1/2^+$ and $3/2^+$ states. From several stripping or pick-up reactions, numerous states with $I^\pi = 1/2^+$ and $3/2^+$ (populated with $\ell = 0$ and 2 respectively) have been identified in $^{113-129}\text{Sb}_{62-78}$. As their spectroscopic factors are weak their wave functions are likely mixed. By looking at the right part of Fig. 35, it is seen that the $1/2_1^+$ and $3/2_1^+$ states follow the trend of the 2^+ of the Sn core, but in a different manner before and after $N = 64$. This can be ascribed to a change of the configuration of the 2^+ of the Sn core. Even though its *energy* does not vary significantly, its *composition* changes as a function of the neutron number. Below $N = 64$ the $\nu d_{5/2}$ and $\nu g_{7/2}$ orbits are strongly involved to form a 2^+ . Above $N = 64$ it is the turn of the $\nu h_{11/2}$ orbit. Therefore the behaviors of the $1/2_1^+$ and $3/2_1^+$ states of Sb isotopes are driven by *different combinations* of residual proton-neutron interactions.

The $\pi h_{11/2}$ orbit

The $h_{11/2}$ orbit, with an angular momentum $\ell = 5$, arises from the Harmonic Oscillator shell $N = 5$. The strength of the spin-orbit interaction is large enough to lower this $j = \ell + 1/2$ state into the preceeding $N = 4$ major shell in which the $g_{7/2}$ orbit ($\ell=4$ and $j = \ell - 1/2$) is located. Any

variation of the SO interaction for the $\ell=5$ or/and $\ell=4$ orbits would be magnified when looking at the energy difference between the states assigned to these proton $h_{11/2}$ and $g_{7/2}$ orbits, as shown in the left part of Fig. 37. This method was proposed recently in Ref. [240] to derive the variation of the SO interaction as a function of the neutron number, using experimental results obtained in the Sb isotopic chain. The discovery of the $11/2^-$ states in the $^{113-125}\text{Sb}_{62-74}$ isotopes was made

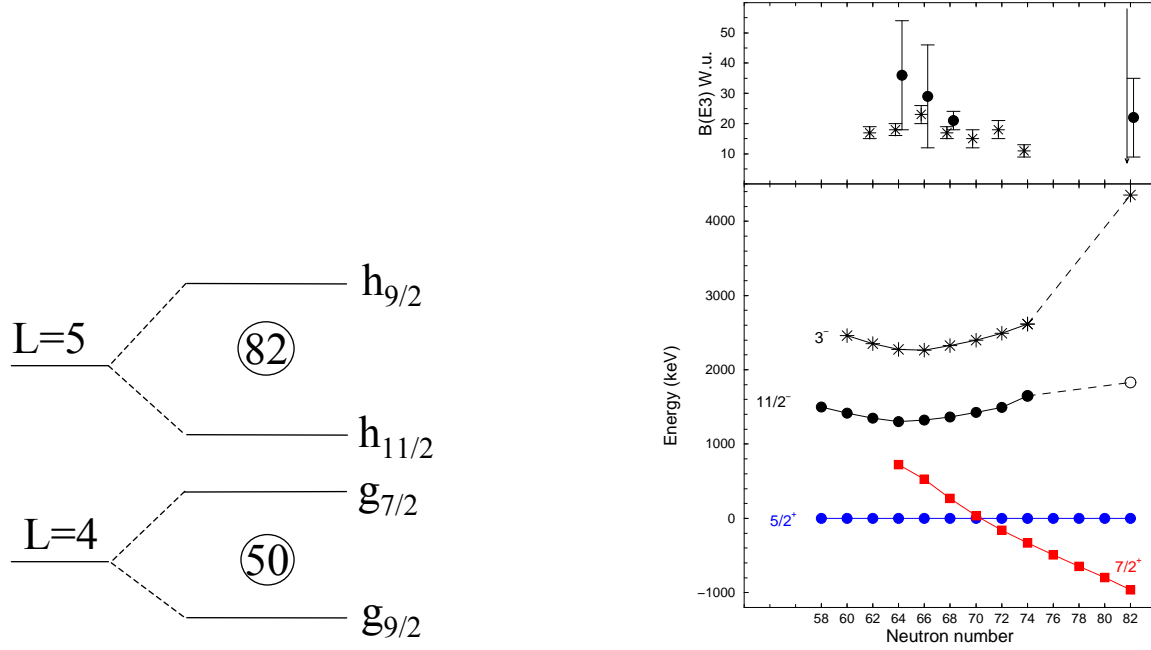


Figure 37: **Left** : Schematic view of the effect of the SO interaction on the proton g and h splittings. Any reduction of this interaction enhances the $g_{7/2} - h_{11/2}$ spacing. **Right, Bottom**: Evolution of the excitation energy of the $11/2^-$ state relative to the $5/2^+$ state in the $^{109-125}\text{Sb}$, and of the 3^- octupole state of the corresponding ^{A-1}Sn cores. **Top**: Probability of reduced transition $B(E3)$, in Weisskopf units, for the $11/2^- \rightarrow 5/2^+$ transition in the odd-A Sb isotopes (circles) and the $3^- \rightarrow 0^+$ transition in the even-even Sn cores (stars).

in the seventies using the one-nucleon transfer ($^3\text{He},d$) reaction on isotopically-enriched even Sn targets [241]. An $\ell = 5$ state, with a spectroscopic factor of about 0.5, was identified around 1.4 MeV above the $5/2^+$ state for all isotopes. Later on, a more complete spectroscopic information has been obtained for $^{117}\text{Sb}_{66}$ using the $^{116}\text{Sn}(^4\text{He},t)$ reaction at 80 MeV [242]. The spectroscopic factors of the first excited states are in agreement with the ones of Ref. [241], 0.64 for the $7/2^+$ state and 0.42 for the $11/2^-$ state. Moreover several states with $\ell = 4, 5$ were identified between 1.5 and 5.0 MeV, pointing to a large fragmentation of both the $\pi g_{7/2}$ and $\pi h_{11/2}$ single-particle strengths. One can therefore conclude from this work that the $11/2^-$ level has not to be assigned to a pure $\pi h_{11/2}$ single-particle state, regardless the complex analysis of the cross sections to extract the spectroscopic factors.

To get a better insight on the single-particle nature of the $11/2^-$ state in the $^{A+1}_{51}\text{Sb}$ isotopes, one can compare the evolution of its energy and lifetime to that of the 3^- state in the $^A_{50}\text{Sn}$ core nuclei. From these comparisons one would appreciate whether the wave function of the $11/2^-$ state contains some amount of $\pi d_{5/2} \otimes 3^-$ coupling. As said before, the 3^- state of the Sn isotopes is

provided by neutron excitations involving mainly the $\nu g_{7/2}$ or $\nu d_{5/2}$ orbits with the $\nu h_{11/2}$ one. As shown in the bottom part of Fig. 37, the excitation energy of the $11/2_1^-$ state above the $5/2_1^+$ state follows exactly that of the 3^- state. The lifetimes of the $11/2_1^-$ states in the $^{113-119}\text{Sb}_{62-68}$ isotopes were determined through their direct decay to the $5/2_1^+$ ground state. From these lifetimes, $B(E3; 11/2_1^- \rightarrow 5/2_1^+)$ transition probabilities are extracted and compared to the $B(E3; 3^- \rightarrow 0^+)$ values of the core nuclei in the top part of Fig. 37. The $B(E3)$ values of the Sb isotopes are close to those measured in the Sn cores. On the basis of the energy evolution of the $11/2_1^-$ with respect to the 3^- state, the $B(E3)$ systematics, the former determination of SF in Ref. [241, 242] and the fragmentation of the $\pi h_{11/2}$ strength measured in ^{117}Sb [242] one can reasonably deduce that the $11/2_1^-$ state is not of pure single-particle origin. It may therefore be hazardous to use the *absolute* evolution of the $11/2_1^-$ state with respect to the $7/2_1^+$ state to derive the variation of the $\pi h_{11/2} - \pi g_{7/2}$ splitting. For instance, shell model calculation has been undertaken in the ^{114}Sn nucleus [30]. It shows that by including proper correlations, the binding energy of the $11/2_1^-$ and $7/2_1^+$ states may change by about 1 MeV and 0.5 MeV, respectively.

The recent results obtained by Schiffer et al. [240] are clearly at variance with the aforementioned conclusions. In this work the spectroscopic factors of the $7/2_1^+$ and $11/2_1^-$ states in $^{113-125}\text{Sb}_{62-74}$ have been determined from a new set of experimental data on the $^A\text{Sn} (^4\text{He}, t)^{A+1}\text{Sb}$ transfer reactions, with A extending from 112 to 124. By using a beam of α particles at 40 MeV, the proton pick-up with angular momenta $\ell = 4, 5$ is kinetically well matched giving rise to relatively large cross sections. Tritons were momentum analyzed in an Enge split-pole magnetic spectrograph. The measured normalized spectroscopic factors of the $7/2_1^+$ and $11/2_1^-$ states were found to be close to 1 for the whole set of nuclei, which was given as the signature of a single-particle character of the $7/2_1^+$ and $11/2_1^-$ states. Their energy spacing varies from 576 keV at $N = 64$ to 1890 keV at $N = 74$ (see the bottom part of Fig. 37). By adding 10 neutrons this amounts to an increase of the energy spacing $\pi g_{7/2} - \pi h_{11/2}$ by about 1.4 MeV, and a reduction of the relative SO splittings involving the $\ell = 4$ and $\ell = 5$ orbits by the same value [240].

Several mean field calculations, relativistic or not [29, 30, 31, 32] tried to reproduce these latter experimental data by adding tensor terms in their interaction. This procedure required a subsequent readjustment of parameters of these effective forces, which were established from other nuclear properties. Whatever the effective force in use, the gap between the two proton orbits $g_{7/2} - h_{11/2}$ is predicted to widen from $N = 64$ to $N = 82$, i.e. during the filling of the $\nu h_{11/2}$ orbit, the tensor term giving both a repulsive effect on the excited $\pi h_{11/2}$ orbit and an attractive one on the low-lying $\pi g_{7/2}$ orbit. Nevertheless the *absolute* distances between the two single-proton energies is very far from the experimental one given in Ref. [240] (see Fig. 37). These discrepancies, on the one hand between old and new experimental data, and on the other hand between new experimental data and theory, should encourage other physicists to delve into this subject. In particular a proper unfolding of correlations should be undertaken throughout the Sb isotopic chain to derive the variation of the single-particle energies. With this in hand, a more precise discussion on the effect of the tensor interaction could be envisaged.

At $N = 82$, the $11/2_1^-$ energy of $^{133}\text{Sb}_{82}$ does not follow the rise in energy of the 3^- state of its Sn core, as shown in Fig. 37. This state could be assigned as a pure $\pi h_{11/2}$ single particle. However, the $B(E3; 11/2_1^- \rightarrow 5/2_1^+)$ value of $22(13) W.u.$ extracted from its lifetime is, within the error bars, too large to correspond to the transition between two single-proton states ($\leq 4 W.u.$ in the neighboring nuclei). It is closer to the collective octupole strength of the $^{132}_{50}\text{Sn}_{82}$ core, $B(E3) > 7 W.u.$. Therefore the configuration of the $11/2_1^-$ state in ^{133}Sb is still likely to be mixed, $\pi h_{11/2}$ single particle and $\pi d_{5/2} \otimes 3^-$ coupling. Transfer reactions using radioactive beams around

^{132}Sn would give us this important information in a near future.

6.2.4 Conclusion

The $Z = 50$ shell closure has been analyzed in a large range, between the two doubly magic nuclei ^{100}Sn at $N = 50$ and ^{132}Sn at $N = 82$. Numerous recent experimental data such as transfer, Coulomb excitation, decay spectroscopy, have been considered to obtain a global understanding of the evolution of this proton shell gap and on the proton orbits located above it. These aimed in particular at determining the resistance of the $Z = 50$ gap against excitations and the role of tensor forces.

To start with, the Sn nuclei exhibit 2^+ and 3^- excitations are about 1.2 and 2.5 MeV, respectively. These states are composed of neutron excitations involving the $d_{5/2}$, $g_{7/2}$ and $h_{11/2}$ orbits. As they are present at relatively low energy, the proton single-particle states can easily couple to these modes. Therefore the variation of the $5/2^+$, $7/2^+$ and $11/2^-$ states observed in the $_{51}\text{Sb}$ isotopes cannot be directly attributed to that of the $\pi d_{5/2}$, $\pi g_{7/2}$ and $\pi h_{11/2}$ single-particle states, respectively.

From the trends derived from the proton binding energies, it can be inferred that the size of the $Z = 50$ remains large above $N = 64$. This accounts well for the doubly magic character of ^{132}Sn . On the other hand this gap is decreasing below $N = 64$ (towards ^{100}Sn), a fact that could favor core excitation and increase collectivity. Experimental $B(E2)$ values, even if not all agreeing, globally point to this collectivity enhancement for the lightest Sn isotopes.

Several tensor interactions were expected to play a role in this isotopic chain. Two of them were discussed in the text. First the $\pi g_{9/2} - \nu g_{7/2}$ interaction was invoked to explain the reduction of the $Z = 50$ gap for the lightest Sn isotopes. Second the crossing of the $5/2^+$ and $7/2^+$ states (likely to originate partly from the $\pi d_{5/2}$ and $\pi g_{7/2}$ orbits) was indebted to the filling of the $\nu h_{11/2}$ shell. However, as the filling of neutron orbits between $N = 50$ and $N = 82$ is diluted by the effect of pairing correlations and spread over several orbits, the effects of specific proton-neutron interactions are considerably smoothened. Therefore a proper unfolding of the various kind correlations involved -pairing, quadrupole and octupole- should be undertaken to draw decisive conclusion about the effect of these interactions.

These isotopic chains contain many potential interests on both sides of the valley of stability that have been recently put forward. Many theoretical models have started exploiting and interpreting experimental results. This will undoubtedly continue in the future with further discoveries to come, as for the study of ^{100}Sn .

7 The magic number 82

This magic number appears after the complete filling of the $N = 4$ major shell and the $h_{11/2}$ intruder orbit. As shown below, the orbits bounding the $N = 82$ neutron and the $Z = 82$ proton gaps are not the same. This occurs partly because the Coulomb field -not negligible anymore - distorts the mean potential felt by the protons, changing the order of the levels accordingly. Also, very different $\pi\nu$ interactions come into play to modify the binding energies of the orbits involved, because of the large differences in the respective nucleon numbers (the $N = 82$ isotones with $Z \simeq 50 - 70$ as compared to the $_{82}\text{Pb}$ isotopes with $N \simeq 104 - 130$).

7.1 Evolution of the $N = 82$ shell closure

This shell closure is formed between the $h_{11/2}$ (or the nearby $s_{1/2}$ and $d_{3/2}$) and the $f_{7/2}$ orbit. The $N = 82$ closure is so strong that seven $N = 82$ isotones with $54 \leq Z \leq 62$ are stable. The $N = 82$ chain contains one known doubly-magic nucleus, $^{132}_{50}\text{Sn}$. For the heavy $N = 82$ isotones, the $Z = 64$ proton gap is large enough to provide a doubly-closed character to $^{146}_{64}\text{Gd}$, its first excited level is a 3^- state, as for the doubly-magic nucleus ^{208}Pb . The lighter $N = 82$ isotones have been much less extensively studied. Potentially another magic nucleus, $^{122}_{40}\text{Zr}$, could be found. It is formed by the combination of the $Z = 40$ shell closure, the effect of which has been evidenced in the $^{90,96}\text{Zr}$ nuclei, and by the $N = 82$ one evidenced for $^{132}_{50}\text{Sn}$. The persistence of the $N = 82$ closure below $Z = 50$ is an open question which is in particular essential for modelling the explosive neutron-capture nucleosynthesis processes.

In the following, experimental results on the neutron binding energies of states surrounding the gap as well as the trends of collective states are presented to shed light on the $N = 82$ shell evolution as a function of the proton number. Afterwards the action of some terms of the NN forces to reduce the $\nu h_{11/2} - \nu h_{9/2}$ SO splitting will be demonstrated and quantified. Finally the motivations for studying the lightest $N = 82$ isotones ($Z < 50$) will be emphasized in the frameworks of the NN interactions and astrophysics.

7.1.1 Evolution of the binding energies

Figure 38 displays the experimental binding energies of states around the $N = 82$ shell closure as a function of proton number, ranging from $Z = 50$ (^{132}Sn) to $Z = 68$ (^{150}Er). They are taken from the atomic mass table [10], to which the very new results for $^{131-133}\text{Sn}$ isotopes [243] have been added.

While the heavy-mass part is close the proton-drip line, there is a wide region to explore in the neutron-rich nuclei below $Z = 50$.

The $N = 81$ isotones exhibit three states below 800 keV excitation energy, with spin values $1/2^+$, $3/2^+$, and $11/2^-$ respectively. As indicated from neutron pick-up reactions using all available stable targets ($Z = 54 - 62$, $N = 82$) these states correspond to neutron holes in the three orbits located below the $N = 82$ gap, namely $\nu s_{1/2}$, $\nu d_{3/2}$ and $\nu h_{11/2}$. Their spectroscopic factors are rather large, greater than 0.7. For $^{131}_{50}\text{Sn}$, the excitation energy of its long-lived isomeric state $11/2^-$ has been determined using the β -decay of $^{131}_{49}\text{In}$. It is proposed to lie 65.1 keV above the $3/2^+$ ground state [246].

The linear variation of the binding energy of the $11/2^-$ state, and henceforth of the $\nu h_{11/2}$ orbit, indicates that the filling of the proton $g_{7/2}$ and $d_{5/2}$ orbits occur simultaneously from $Z = 50$ to $Z = 64$. A successive filling of these two orbits would give rise to a change of slope at $N = 58$. Therefore its actual variation results from the combined effects of two proton-neutron interactions, $\pi g_{7/2} - \nu h_{11/2}$ and $\pi d_{5/2} - \nu h_{11/2}$. The former monopole matrix element should dominate over the latter, as discussed already in Sect. 6.2.3.

The binding energy for the $1/2^+$ and $3/2^+$ states display a more rounded curve as protons are added above $Z = 50$ (see the left part of Fig. 38). There the $1/2^+$ and $3/2^+$ states are likely influenced by correlations beyond the monopole interactions.

On the theoretical point of view, whatever the mean field potentials in use (such as those obtained from several parameterizations of the Skyrme force, BSk1, SLy6, and SkI3, the D1S Gogny force, or the relativistic mean-field forces NL3 and NL-Z2), the $\nu h_{11/2}$ orbit is predicted to lie at about 1 MeV above any other shells as the $\nu d_{3/2}$ and $\nu s_{1/2}$ ones [25]. The ground state of all

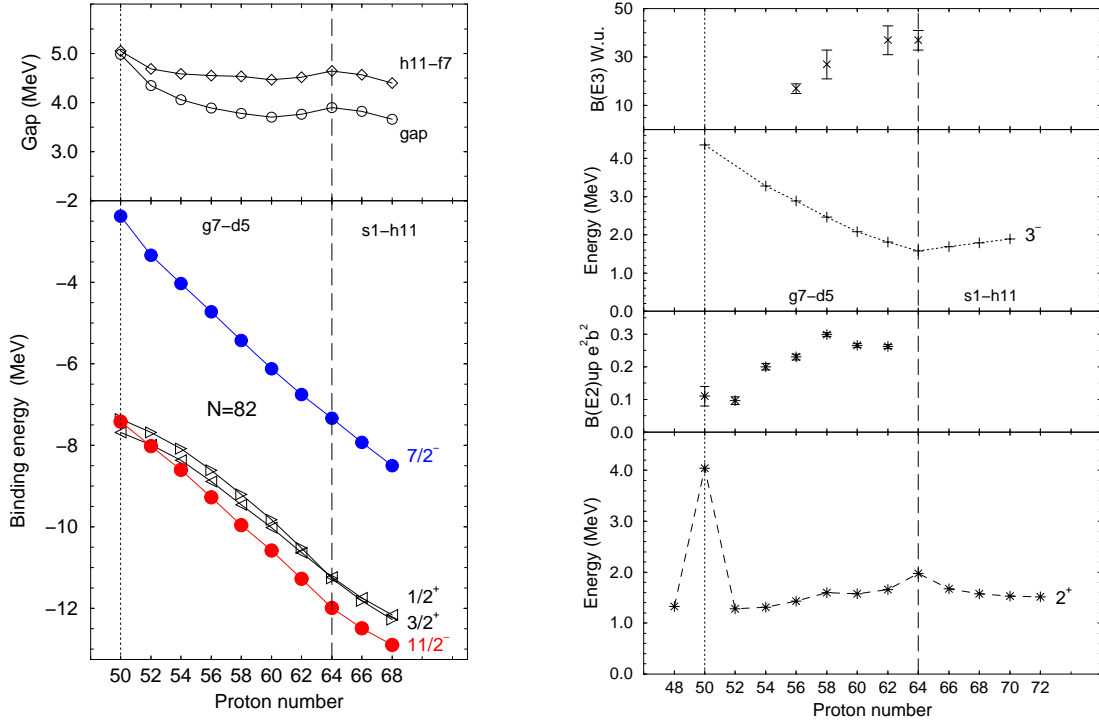


Figure 38: **Left:** Binding energies of the states located below and above the $N = 82$ magic number and differences of the binding energies of the two states surrounding the gap at $N = 82$ (labelled as 'gap') and of the $11/2^-$ and $7/2^-$ states (labelled as 'h11-f7') (see Sect. 11). The proton orbitals which are getting filled as a function of increasing Z are given in the middle of the figure. **Right:** Experimental 2_1^+ energies and $B(E2) \uparrow$ values (bottom), 3_1^- energies and $B(E3)$ values (top) in the $N = 82$ chain. $B(E2)$ values of ^{132}Sn and ^{134}Xe come from Refs. [244, 245] respectively.

the $N = 81$ isotones is therefore predicted to have a $\nu h_{11/2}^{-1}$ hole state configuration, at variance with experimental results.

The $N = 82$ gap, of about 4 MeV for $Z > 54$, increases for lower Z values (see left part of Fig. 38). This happens as the slope of the $3/2^+$ binding energy is reduced. This variation can be attributed to a progressive change of configuration of the $3/2^+$ state, which becomes of more single-particle origin towards $Z = 50$. From this trend, it follows that the $N = 82$ gap is large, in particular for the ^{132}Sn nucleus. Combined with a large $Z = 50$ gap, ^{132}Sn has a well established doubly-magic structure. This statement is confirmed from its collective properties described in the following section.

Below $Z = 50$, the properties of the $N = 82$ gap cannot be extrapolated directly as the change of binding energy of the neutron orbits surrounding the gap will be dictated by the yet unknown residual interactions involving the $\pi g_{9/2}$ orbit. First β - and γ -spectroscopic decay studies of $^{130}_{48}\text{Cd}$ are in favor of an $N = 82$ shell quenching [247]. This assumption was derived from the rather high Q_β value of $^{130}_{48}\text{Cd}$ which compares well with results from mass models including a shell quenching. A direct determination of a possible reduction of the $N = 82$ shell gap when the $\pi g_{9/2}$ orbit is being emptied needs at least accurate atomic masses of $^{129,130,131}_{48}\text{Cd}$ isotopes.

7.1.2 Trends of the first collective excitations of the $N = 82$ isotones

The experimental energies and reduced transition probabilities for the first 2^+ and 3^- states of the $N = 82$ isotones are reported in the right part of Fig. 38. Neutrons excitations at $N = 82$ can hardly produce a low-energy 2^+ state as the spacing between orbits $h_{11/2}$ and $f_{7/2}$ which can generate quadrupole excitations is large (see the curve labelled 'h11-f7' in the left hand side of Fig. 38). Therefore the configuration of the 2_1^+ state in the $N = 82$ isotones is mainly built with protons from the $\pi g_{9/2}$ orbit below $Z = 50$, from the $\pi g_{7/2}$ and $\pi d_{5/2}$ orbits between $Z = 52$ and $Z = 64$, and from the $\pi h_{11/2}$ orbit above $Z = 64$.

The $^{132}_{50}\text{Sn}_{82}$ nucleus exhibits all the characteristics of a doubly-magic nucleus, i.e. a high energy for the first excited states and a weak transition probability $B(E2)$. Apart from this spectacular behavior of $^{132}_{50}\text{Sn}$, the energy of the 2^+ state varies smoothly along the whole $N = 82$ isotonic chain. A small increase is observed at $Z = 64$, which is due to the sub-shell closure between the $\pi g_{7/2}/d_{5/2}$ and $\pi h_{11/2}$ orbits.

Below $Z = 50$, the $\pi g_{9/2}$ orbit is likely to be involved in turn. Two experiments have been carried out at the GSI facility to search for the cascade of γ -rays de-exciting the 8^+ isomeric state expected from the $(\pi g_{9/2})^{-2}$ configuration of $^{130}_{48}\text{Cd}_{82}$, as in $^{98}_{48}\text{Cd}_{50}$. The isomer has been populated both in the fragmentation of a ^{136}Xe beam as well as in projectile fission of ^{238}U [248]. The energy of the $2^+ \rightarrow 0^+$ transition, displayed in the bottom right part of Fig. 38, is found at 1.325 MeV, an energy close to that of the valence mirror nucleus $^{98}_{48}\text{Cd}_{50}$ (1.395 MeV).

The $N = 82$ isotones exhibit a collective 3^- state with large transition probabilities $B(E3) = 20 - 40 W.u.$. When present at low excitation energy, this state originates from $p - h$ excitations between the positive-parity *proton* orbits located below $Z = 64$ ($g_{7/2}$ and $d_{5/2}$) and the negative-parity $h_{11/2}$ orbit above $Z = 64$. At the opposite neutrons can hardly generate a 3^- state across the $N = 82$ shell gap. The $B(E3)$ value is maximum at $^{146}_{64}\text{Gd}$, where the energy of this 3^- state is minimum. This is attributed to the fact that the number of particle and holes to generate the 3^- state is maximized at $Z = 64$, which is approximately at the mid-distance between $Z = 50$ and $Z = 82$.

As the 2^+ and 3^- states of the $N = 82$ nuclei have relatively small excitation energy, the single-neutron particle strengths in the neighboring odd- N will be fragmented due to couplings with these collective states. This feature should be kept in mind in the following paragraphs.

7.1.3 Neutron orbits above the $N = 82$ gap: Levels of the $N = 83$ isotones

The low-energy orbits in the $N = 83$ isotones arise from the $N = 5$ major shell. The first one, $\nu f_{7/2}$, is the ground state of all the $N = 83$ isotones which have been identified so far from $Z = 50$ to $Z = 70$. The coupling of the $\nu f_{7/2}$ single-neutron state to the first 2^+ and 3^- excitations of the core gives rise to two multiplet of states with spin values ranging from $1/2^-$ to $11/2^-$ and $1/2^+$ to $13/2^+$, respectively. Single-neutron states coming from the $\nu p_{3/2}$ and $\nu h_{9/2}$ orbits, as well as from the $\nu i_{13/2}$ intruder one are expected to be present in addition to states provided by couplings to core excitations. Therefore mixing between the single-particle and coupled states are expected and cannot be neglected.

The experimental energies of the first excited states in the $N = 83$ isotones are given in Fig. 39, those with negative (positive) parity being gathered in the left (right) part. The quadrupole (octupole) collective excitations of the core nuclei are also reported in the left (right) part of this figure. Until recently, the $13/2^+$ excited state in the $N = 83$ isotones had not been identified below $^{139}_{56}\text{Ba}$. The neutron transfer reactions, $^9\text{Be}(^{134}\text{Te}, ^8\text{Be})$ and $^{13}\text{C}(^{134}\text{Te}, ^{12}\text{C})$, were studied with ^{134}Te

radioactive beams at energies slightly above the Coulomb barrier in order to determine the energy of the $13/2^+$ level (2109 keV) in $^{135}_{52}\text{Te}$ [229].

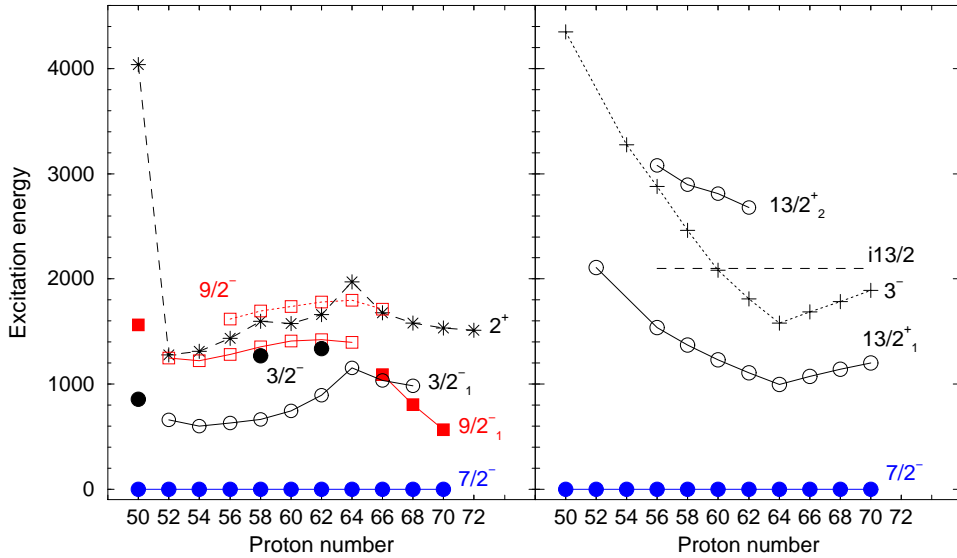


Figure 39: First excited states observed in the $N = 83$ isotones: The full symbols correspond to the states having a large single-particle character, the empty symbols those containing a large collective component (see text). The evolution of the 2^+ and 3^- energies of the corresponding core are also drawn, as well as the $\nu i_{13/2}$ energy assumed in the two-state mixing calculation [250] (see text).

For $Z < 68$, the first excited state of the $N = 83$ isotones has $I^\pi = 3/2^-$ (see the left part of Fig. 39). Its energy follows the 2^+ excitation energy of the core. Moreover its normalized spectroscopic factor, measured by neutron-transfer (d, p) reactions from ${}_{54}\text{Xe}$ to ${}_{62}\text{Sm}$, amounts to $\simeq 0.5$. This confirms that this first state has not a pure single-neutron $\nu p_{3/2}$ configuration. In ${}^{141}_{58}\text{Ce}$ and ${}^{145}_{62}\text{Sm}$ other $3/2^-$ states have been identified at higher excitation energy, which brings the sum of the spectroscopic factors close to one. The energy of the $\nu p_{3/2}$ orbit, reported with a full symbol, was calculated by averaging the energies weighted by the corresponding spectroscopic factors. As the 2^+ state of ${}^{132}\text{Sn}$ is very high, one can speculate that the $3/2^-$ state of ${}^{133}\text{Sn}$ is mainly of single-neutron character. Therefore a full symbol has also been included for this nucleus in Fig. 39. Using these three results, one would speculate that the spacing in energy between the $\nu f_{7/2}$ and $\nu p_{3/2}$ orbits is slowly increasing from $Z = 50$ to $Z = 62$, i.e. during the filling of the $\pi g_{7/2}$ and $\pi d_{5/2}$ orbits. Nevertheless this argument is weak by many aspects. For instance, the assignment of the first excited state of ${}^{133}\text{Sn}$ at 853 keV has to be confirmed, being based from a single experiment with low statistics [249].

One or two states with $I^\pi = 9/2^-$ have been identified, as shown in the left part of Fig. 39. In every isotone but ^{133}Sn and those with $Z \geq 66$, the energy of the $9/2_1^-$ is slightly lower than the 2^+ excitation of the core. In parallel the energy of the $9/2_2^-$ is slightly higher. The presence of two $9/2^-$ states at each side of the 2^+ one points to a mixing of wave functions, $\nu h_{9/2}$ and $\nu f_{7/2} \otimes 2^+$. Furthermore, the spectroscopic factors measured by neutron-transfer (d, p) reactions from ^{54}Xe to ^{62}Sm , confirms that none of these $9/2^-$ states has the single-neutron $\nu h_{9/2}$ configuration. The large mixing of the two components is also proved in $^{147}_{64}\text{Gd}$, as its two $9/2^-$ states are strongly

populated ($\log ft=4.3$ and 4.8) in the favored β -decay of the $^{147}_{65}\text{Tb}$ isomeric state, $\pi h_{11/2} \rightarrow \nu h_{9/2}$. On the other hand, only one Gamow-Teller branch is observed in the heavier masses, meaning that the $9/2^-$ states of $^{149}_{66}\text{Dy}$, $^{151}_{68}\text{Er}$, and $^{153}_{70}\text{Yb}$ progressively become more of single-particle character. Beyond $Z = 66$ the energy of the $9/2^-$ state decreases, whereas the 2^+ excitation remains almost constant. This likely implies a strong decrease of the energy spacing between the two orbits, $\nu f_{7/2}$ and $\nu h_{9/2}$ during the filling of the $\pi h_{11/2}$ orbit. We will come back to this important point in the next section (Sect. 7.1.4) when discussing about the proton-neutron interactions.

As regards the $\nu i_{13/2}$ orbit in the $N = 83$ isotones, the evolution of its energy has been recently discussed in terms of change of the nuclear spin-orbit interaction with increasing neutron excess [240], similarly to the evolution of the $\pi h_{11/2}$ orbit in the $Z = 51$ isotopes (see Sect. 6.2.3). In this work, the first excited state with $I^\pi = 13/2^+$, identified in every $N = 83$ isotone, has been assumed to have the single-neutron $\nu i_{13/2}$ configuration. The location of the $\nu i_{13/2}$ single-particle energy was debated already in Ref. [250], in which configurations of the high-spin states of nuclei close to $^{146}_{64}\text{Gd}_{82}$ were assigned. Noticeable is the fact that the excitation energy of the $13/2^+$ state of the $N = 83$ isotones closely follows that of the 3^- collective state measured in the corresponding $N = 82$ cores, displaying in concert a minimum for $Z = 64$ (as shown in the right part of Fig. 39). By converting the measured half-life of the $13/2^+$ level into $B(E3)$ values, it is found that the $B(E3)$ values are much larger than expected for a $\nu i_{13/2} \rightarrow \nu f_{7/2}$ single-neutron transition. These two sets of energies and lifetimes have been analyzed with a schematic two-state mixing calculation in Ref. [250]. Using a *constant* value of 2.1 MeV (indicated by dashed line in the right part of Fig. 39) for the $\nu i_{13/2}$ single-particle energy from $Z = 56$ to $Z = 70$, the measured energies of the $13/2^+$ and $13/2^-$ states (known for $Z = 56 - 62$), as well as the $B(E3, 13/2^+ \rightarrow 7/2^-)$ values are quite well reproduced [250]. Contrary to what is said in Ref. [240], this result rather indicates no change of the binding energy of the $\nu i_{13/2}$ orbit for increasing Z values, but a fragmentation of the $\nu i_{13/2}$ force occurring from the coupling with the 3^- state. A similar conclusion was obtained in Sect. 6.2.3 with respect to a possible evolution of the $\pi h_{11/2}$ orbit within the $Z = 50 - 82$ major shell.

7.1.4 Reverse behaviors of the $\nu h_{11/2}$ and $\nu h_{9/2}$ orbits for $Z > 64$

The present paragraph intends to show a plausible evolution of the $\nu h_{11/2} - \nu h_{9/2}$ SO splitting as the proton orbit $\pi h_{11/2}$ is progressively filled.

The left-hand side of Fig. 40 displays the binding energies of the $9/2^-$ and the $7/2^-$ states of the $N = 83$ isotones, as well as the binding energies of the $11/2^-$ level of the $N = 81$ isotones. For $Z = 56 - 64$ the energy of the $9/2^-$ has been averaged from the two $9/2^-$ states, weighted by their spectroscopic factors. Beyond $Z = 64$, it was discussed in the previous section that the $9/2^-$ become more of single particle character. The binding energies of these three states display a quasi-linear behavior in the $Z = 50 - 64$ interval, while steeper (smoother) slopes are observed beyond $Z = 64$ for the $9/2^-$ ($11/2^-$) states. These changes of slopes are directly connected to the the new neutron-proton residual interactions that come into play beyond $Z = 64$. Using the method explained in Sect. 2.2.2 the corresponding monopole interactions have been derived from the binding energy slopes and are drawn in the right part of Fig. 40. When the protons are filling the $\pi g_{7/2}$ and $\pi d_{5/2}$ orbits, their residual interactions with $\nu h_{11/2}$, $\nu f_{7/2}$, or $\nu h_{9/2}$ have almost the same values, between -300 and -350 keV. On the other hand, as soon as the $\pi h_{11/2}$ orbit starts to be filled, the $\nu h_{11/2}$ and $\nu h_{9/2}$ orbits exhibit reverse behaviors, the $V_{h_{11/2}h_{9/2}}^{pn}$ matrix element (~ -450 keV) is much more attractive than the $V_{h_{11/2}h_{11/2}}^{pn}$ one (~ -200 keV). This change of effective interaction can be ascribed to the tensor force.

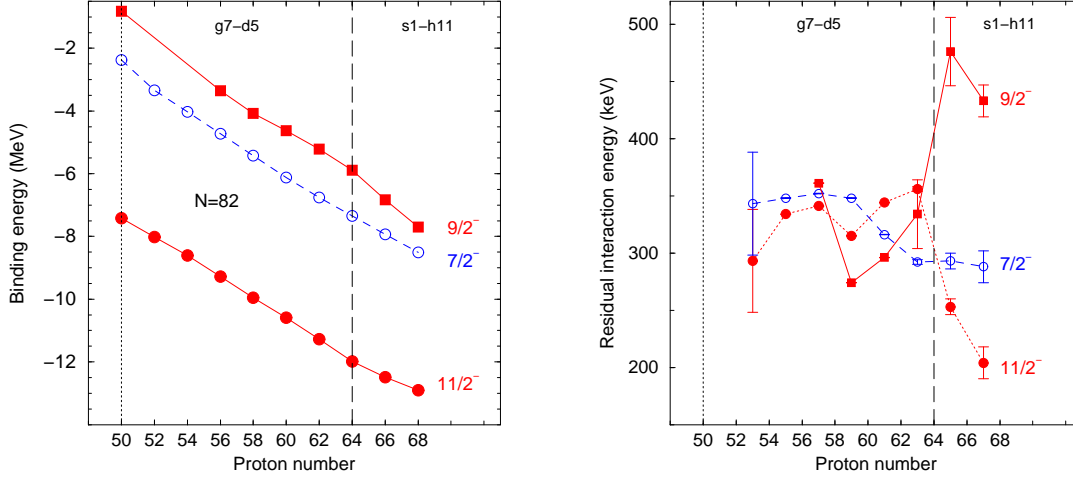


Figure 40: **Left** Evolution of the binding energies of the $11/2^-$ and $9/2^-$ states compared to those of the $7/2^-$ states, around the $N = 82$ gap. **Right** Evolution of the neutron-proton residual interactions (absolute values) extracted from the slopes of the binding energies of the three neutron states. The proton orbitals which are getting filled as a function of increasing Z are given on the top each figure.

7.1.5 Study of the $N = 82$ shell closure below $Z = 50$, Astrophysical implications

As mentioned along the previous chapters of the present work, the properties of NN interactions, such as those of the tensor forces, can significantly alter or reinforce the strength of a shell closure. In addition, the change of the mean field potential of the nucleus, in particular the increased surface diffuseness for large N/Z , weakly bound systems, also modifies the energy of the orbits. Taken together a profound change of the spacing and ordering of levels can occur when moving from stability to the drip line, following for instance a given isotonic chain. The present section shows how these structural changes impact on the development of the rapid-neutron capture nucleosynthesis. We refer the reader for instance to Refs. [251, 252] for recent review papers.

After a brief introduction on the role of this process and the possible astrophysical site where it prevails, the key 'integral' parameters (binding energy, β -decay lifetime and neutron capture cross section) to its development will be listed. Nuclear structure evolution can modify these parameters significantly, changing for instance the location and duration of the r process. Enlighted by the previous chapters on the evolutions of shell closures, expected structural evolutions at $N = 82$ will be commented and put in an astrophysical perspective.

Introduction

Approximately half of the elements beyond Fe are produced via neutron captures on very short time scales in neutron-rich environments. Despite its importance, the exact site(s) where the r -process(es) occurs still remain one of the greatest mystery in science. The most frequently suggested astrophysical environments are high-entropy ejecta from type II supernovae (SN) and neutron-star mergers. The shock-heated He or C outer layer of type II SN could provide a moderate neutron flux (a weak r -process) through $^{13}\text{C}(\alpha, n)$ reactions which could account for several isotopic anomalies found in pre-solar grains. The key for understanding the r -process(es) resides in a close interaction between astronomy, cosmochemistry, astrophysical modeling of explosive scenarios and

nuclear physics.

In very hot and neutron-dense environments, the r-process develops through neutron captures on very short timescales until reaching nuclei with sufficiently small binding energy ($S_n \simeq 2\text{--}3\text{ MeV}$). Typically this occurs at the major shell closures, such as the $N = 82$ one. There, the rate of captures is balanced by that of photodisintegration induced by the ambient photon bath of the exploding star. The process is stalled at these so-called waiting-point nuclei until β -decays occur, depleting the nucleosynthesis to the upper Z isotopic chain where subsequent neutron captures could occur. After successive β -decays and neutron captures at the $N = 82$ closed shell, the process is progressively driven closer to stability where β -decay lifetimes ($T_{1/2}$) become longer (see the zig-zag line along the $N = 82$ shell in the right part of Fig. 41). There, around the Sn isotopic

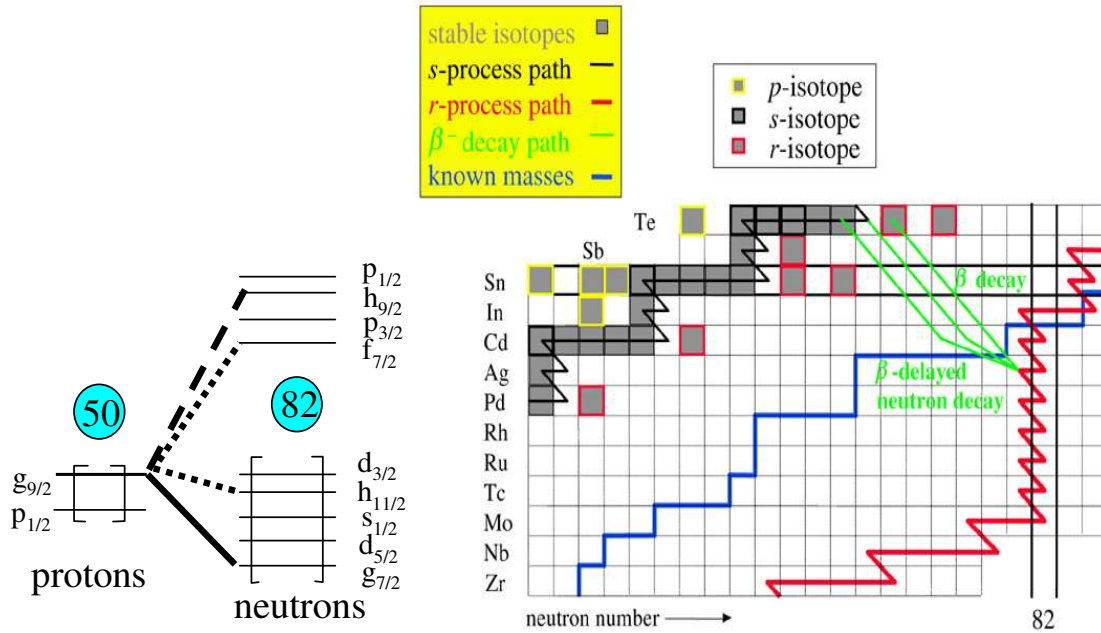


Figure 41: **Left** : Schematic view of the proton-neutron interactions which play a role for the evolution of the $N = 82$ shell gap and for the properties of the $N \simeq 82$ nuclei as proton are removed from the $g_{9/2}$ orbit. Interactions represented with dotted (dashed) lines are expected to contain repulsive (attractive) tensor terms. The interaction between the $\pi g_{9/2}$ and $\nu g_{7/2}$, indicated by a full line, is expected to be the largest among all others involved. **Right**: Schematic representation of the location of the r-process path at the $N = 82$ shell closure (by courtesy of D. Lunney). Present experimental knowledge on the atomic masses is indicated by a thick line. As far as β -decay lifetimes are concerned, measurements extend further from stability, reaching in particular the ^{130}Cd [247] and ^{129}Ag waiting-point nuclei [247, 253].

chain, neutron captures are expected to be shorter than photodisintegration and β -decay rates, driving the r-process nucleosynthesis towards the next shell closure. At the end of the r-process, radioactive progenitors decay back to stability via β or β -delayed neutron emission towards the valley of stability. The accumulation of r-elements which form the r-peaks at masses $A \simeq 80$, $\simeq 130$ and $\simeq 195$ on the abundance curve of the elements is a direct imprint of the existence of waiting point progenitors far from stability. The location, height and shape of the $A = 130$ peak could be traced back from the neutron separation energies (S_n), the half-lives ($T_{1/2}$), the neutron

delayed emission probability (P_n), and the neutron-capture cross section (σ_n) of the nuclei located at the $N = 82$ shell closure. These parameters are imbricated in the structural evolution of the nuclei as depicted in the following paragraph.

Structural evolution

The evolution of the $N = 82$ shell gap south to the doubly magic nucleus $^{132}_{50}\text{Sn}_{82}$ is ruled by the combined effects of the proton-neutron interactions and by the progressive proximity of the continuum states. As from $Z = 50$ to $Z = 40$ solely the proton orbit $g_{9/2}$ orbital is progressively emptied, all the proton-neutron monopole interactions which intervene in the evolution of nuclear structure between $^{132}_{50}\text{Sn}_{82}$ and the close-to-drip-line nucleus $^{122}_{40}\text{Zr}_{82}$, involve the same proton orbit. As shown schematically in the left part of Fig. 41, the differential values of these monopoles could modify the ordering of the neutron orbits, the size of the $N = 82$ gap and subsequently the S_n values as protons are removed. Related to this, the tensor interactions (through the $\pi g_{9/2} - \nu h_{11/2}$ or $\pi g_{9/2} - \nu f_{7/2}$ monopoles) are likely to play important roles.

Likewise, the strength of the tensor term (through the $\pi g_{9/2} - \nu g_{7/2}$ monopole) influences strongly the β -decay lifetimes of the $N = 82$ nuclei. The reason for so is that the β -decay of $N \simeq 82$ nuclei south to $Z = 50$ proceeds mainly through the Gamow-Teller (GT) transition $\nu g_{7/2} \rightarrow \pi g_{9/2}$ transition, as described in Ref. [247]. As protons are progressively removed from the $g_{9/2}$ orbit, the neutron $g_{7/2}$ orbit becomes gradually less deeply bound due to the missing proton-neutron interactions $\pi g_{9/2} - \nu g_{7/2}$. Consequently, the aforementioned GT transition will occur at gradually smaller excitation energy E^* in the daughter nuclei, leading to a drastic shortening of β -decay lifetimes $T_{1/2}$, which scales with $(Q_\beta - E^*)^5$.

Added to the properties of the NN interactions, self-consistent mean-field calculations which encompass the treatment of continuum states show a quenching of the $N = 82$ shell gap when approaching the neutron drip-line [39]. This is primarily caused by the lowering of the low- j orbits relative to those of high- j values. The low- j neutron orbits, such as the $\nu p_{1/2}$ and $\nu p_{3/2}$ ones, may progressively become the valence states immediately above the $N = 82$ gap. Such effects were ascribed to the fact that, close to the drip-line, the low- j neutron orbits of the continuum interact strongly with bound states, whereas the interaction with the high- j ones is much less effective. Qualitatively, the nuclear mean field close to the drip-line could be mimicked by a Nilsson potential without the ℓ^2 term [39]. At exploding star temperatures of typically 10^9 K (or neutron energies of about 100 keV) neutrons can hardly overcome large centrifugal barriers created by high ℓ orbits. Therefore, the presence of low- j or low- ℓ neutron valence orbits at low excitation energy would enhance the neutron capture cross-sections σ_n by several orders of magnitudes, shortening the neutron capture time at the waiting point nuclei accordingly.

Astrophysical consequences of changes in the S_n , $T_{1/2}$ and σ_n values

The influence of the S_n values at the $N = 82$ shell closure to the r-abundance peaks has been emphasized in Refs. [254, 251]. Using masses from "unquenched" models (as FRDM or ETFSI-1), one obtains a local increase of the S_n values around $N = 70$ and a very abrupt drop immediately after $N = 82$. They originate from a predicted strong quadrupole deformation around ^{110}Zr and a strong shell closure at $N = 82$, respectively. As a result, neutron captures are stalled for a while around $A = 110$, $N = 70$ and are subsequently directly driven to the closed shell $N = 82$. This leaves few r-progenitors in between these two regions, leading to a significant trough in the fit of the abundance curve of the elements at $A \simeq 120$ ¹⁷. On the other hand, the "quenched"

¹⁷Noteworthy is the fact that if ^{110}Zr was a doubly magic, a sudden drop of S_n value at $N = 70$ will be found,

mass models (as ETFSI-Q or HFB/SkP) bring back r-progenitors before reaching the $N = 82$ shell closure, thus filling the trough at $A \simeq 120$ in closer agreement with the solar r-abundance curve. The recent determination of the Q_β -value in the β -decay of the ^{130}Cd waiting-point nucleus accredits this weakening [247], which should be confirmed by further investigations. From these arguments, it follows that the determination of the S_n values at the $N = 82$ shell closure is essential. So far theoretical models diverge soon after departing from the last measured nucleus, as discussed for instance in Ref. [255], meaning that the underlying physics which could modify the binding energies of the orbits is poorly known and far from being consensual.

The influence of the β -decay lifetimes of neutron-rich nuclei around $N = 82$ on the abundance curve of the r-elements has been discussed extensively for instance in Ref. [251]. When short-lived nuclei are paving the r-process path, the abundance peaks of the r-elements are barely formed and a total duration of the explosive process of few milliseconds could be long enough to reach the heaviest elements of the chart of nuclides. At the opposite, long-lived nuclei located in the r-process path are the major genitors of stable r-nuclei in the universe (after series of β or β -neutron decays to stability) and are responsible for the existence of significant peaks in the abundance curve of the elements. Therefore accurate half-life predictions or measurements are required along the r-process both to explain the shape of observed peaks but also to constrain the duration of the r-process.

Neutron capture cross-sections are often calculated in the framework of the statistical Hauser-Feshbach model, which assumes the presence of a high density of states above the neutron separation energy with various spin and parity values. The use of this statistical approach is not appropriate to calculate neutron capture cross sections for neutron-rich at closed shell, since the neutron-separation energy is small and the level density low. In such cases, the main contribution is obtained from direct captures on few bound states of low ℓ states, mainly through s or p waves, or/and by resonance capture slightly above the neutron-energy threshold. The fact that the neutron p orbits become the few first valence states is therefore extremely important. This feature is discussed in Ref. [256] for the ^{133}Sn nucleus. As the direct capture cross section proceeds mainly through the same $\nu p_{3/2}$ and $\nu p_{1/2}$ states from $Z = 50$ down to $Z = 40$, the evolution of their energy and spectroscopic factors determines how neutron-capture cross sections will change along the $N = 82$ shell closure. It tells to what extent the r-process will be blocked at this shell closure when the temperature of the exploding system decreases. Since the direct determination of neutron-capture cross sections on very unstable nuclei A is technically not feasible, their determination should be provided by models, constrained by spectroscopic information (such as energy, spin, spectroscopic factors of the bound and unbound levels in the $A+1$ nucleus) obtained by (d, p) transfer reactions. Such pioneering studies have been undertaken for the $N = 28$ shell closure in the neutron-rich ^{48}Ca and ^{46}Ar nuclei where similar p states come into play in the neutron-capture cross sections [257, 258, 259, 260].

To summarize this astrophysical part, experimental and theoretical achievements aiming at a comprehensive understanding of the evolution of the $N = 82$ shell closure will provide significant insight to the understanding of the r-process nucleosynthesis, as these topics are intimately entwined.

7.1.6 Conclusion

On the basis of neutron binding energies, energies and reduced transition probabilities of the 2^+ and 3^- states, it is derived that the $N = 82$ shell gap is large enough to maintain a spherical

leading to the build up of r-process elements at $A \simeq 110$.

configuration for the $N = 82$ isotones. The $^{132}_{50}\text{Sn}$ nucleus behaves as a doubly-magic nucleus. Between $Z = 50$ and $Z = 64$ many different proton-neutron interactions act to modify the neutron binding energies of the $N = 81$ and $N = 83$ nuclei. Owing to the large pairing correlations between neighboring proton orbits such as $g_{7/2}$, $d_{5/2}$, $s_{1/2}$ and $h_{11/2}$, this change of neutron binding energies owes to the action of several interactions that cannot be identified individually. After having passed $Z = 64$ the filling of the proton $h_{11/2}$ orbit induces a reduction of the $\nu h_{11/2} - \nu h_{9/2}$ SO splitting, which can be attributed to the tensor terms of the NN interactions.

The study of the lightest isotones $Z < 50$ is in its infancy as this requires the most powerful facilities which are coming up soon. However hints for weakening of the $N = 82$ shell gap were proposed from β -decay studies. From $Z = 50$ to $Z = 40$, the same proton orbit $g_{9/2}$ is involved. Consequently proton-neutron monopoles involving this orbit play decisive roles to modify the S_n , $T_{1/2}$ and σ_n values, which are all important parameters for the r-process nucleosynthesis. As theoretical calculations give contradictory results at the present time on a possible quenching of the $N = 82$ shell gap, some key measurements are prerequisite to improve extrapolations far from the valley of stability.

7.2 Evolution of the $Z = 82$ shell closure

7.2.1 Evolution of the binding energies

The $Z = 82$ magic number is surrounded by the $\pi s_{1/2}$ (bottom) and the $\pi h_{9/2}$ (top) orbits, giving rise to a $1/2^+$ ground state for the $_{81}\text{Tl}$ isotopes and a $9/2^-$ ground state for the $_{83}\text{Bi}$ isotopes, respectively. The binding energies of the last proton of the $Z = 83$ and $Z = 82$ isotopes are drawn in the left part of Fig. 42. The results on the lightest isotopes are not taken into account, because of the numerous shape coexistences identified at low excitation energy in the nuclei having $N \leq 104$ [261, 262]. In even-even Pb nuclei close to $N = 104$, three different nuclear shapes are predicted to coexist at low excitation energy: a *spherical* ground state associated with the $Z = 82$ shell closure, an *oblate* $2p - 2h$ proton configuration with a moderate deformation ($\beta_2 \simeq -0.15$), and a more strongly deformed *prolate* configuration ($\beta_2 \simeq +0.25$) associated with an excitation of four or even six protons ($4p - 4h$ or $6p - 6h$) from the core. These are the assignments of the three 0^+ states which are the lowest three levels observed in the experimental spectrum of $^{186}\text{Pb}_{104}$ [262].

Apart from the singularities coming from the extra binding energy of the ^{208}Pb doubly-magic nucleus (see Sect. 11), the two curves are very smooth, their slopes remain almost constant along the whole neutron range. This is attributed to the fact that neutron orbits are close in energy, which dilutes effects of specific $\pi\nu$ interactions.

The size of the $Z = 82$ spherical gap, ~ 3 MeV, is not large enough to overcome the development of shape coexistences, as evidenced by the intruder states lying at low excitation energy in the three isotopic chains, $_{81}\text{Tl}$, Pb, and $_{83}\text{Bi}$. Unlike all the ground states of the Tl and Bi isotopes which keep enough single-particle character, the excited states being too mixed with collective excitations cannot be used for determining the evolution of the other proton orbits lying below or above the $Z = 82$ gap.

Speculations were made about a quenching of the $Z = 82$ gap far off the β -stability line, in the neutron-deficient side, in order to explain the variation of the two-proton separation energy gaps, ΔS_{2p} around $Z = 82$ [263]. However the computation of these ΔS_{2p} values involves the atomic masses of neutron-deficient $_{80}\text{Hg}$ and $_{84}\text{Po}$ isotopes which have deformed ground states. Hence the ΔS_{2p} values no longer provide a measurement of the size of the spherical $Z = 82$ gap.

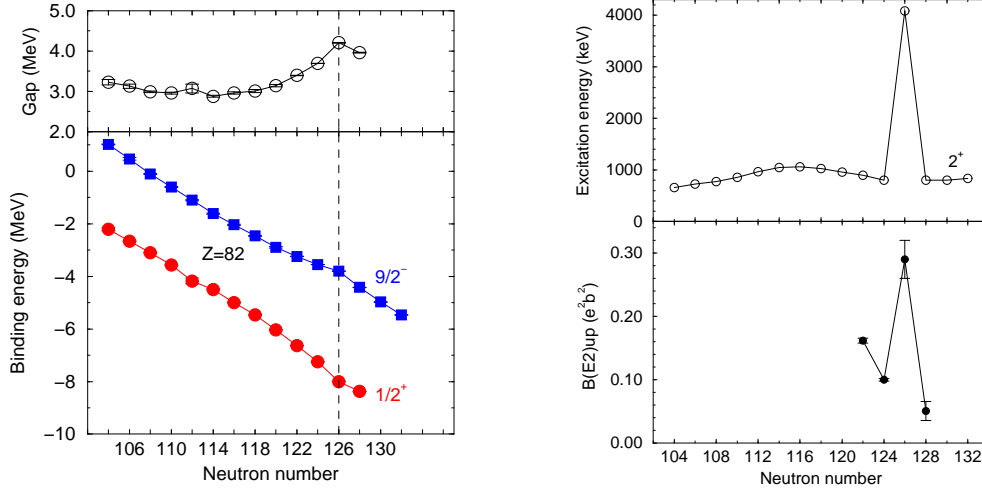


Figure 42: **Left:** Binding energies of the states located just above and just below the $Z = 82$ magic number, for $104 < N < 132$ and difference of the binding energies of the two states surrounding the gap at $Z = 82$ (see Sect. 11). **Right:** Experimental $B(E2; 0^+ \rightarrow 2_1^+)$ values and 2_1^+ energies in the $_{82}\text{Pb}$ isotopes.

Self-consistent mean-field models [264] account well for the observed evolution of ΔS_{2p} , as the ground states of Hg and Po isotopes are predicted to be deformed.

7.2.2 Trends in $E(2^+)$ and $B(E2)$

Except for the doubly-magic nucleus $^{208}_{82}\text{Pb}_{126}$ for which a value as large as 4 MeV is found, the 2^+ energies for $104 \leq N \leq 132$ display a smooth variation with a partial maximum at around $N = 114$ (see right part of Fig. 42). The nearly constancy of the 2^+ energy is due to the closeness of the neutron orbits involved to generate quadrupole excitations. The situation changes dramatically in the doubly-magic nucleus $^{208}_{82}\text{Pb}_{126}$ which also displays a large $B(E2)$ value. This is the same situation as the $^{132}_{50}\text{Sn}_{82}$ one (see Fig. 34), where the 2_1^+ state also acquires some proton excitations leading to a local increase of the $B(E2)$, a quantity which is mainly sensitive to excitation of charged particles.

7.2.3 Conclusion

The $Z = 82$ gap is not strong enough to maintain spherical shapes for the neighboring isotopic series, at variance to all the cases studied in the preceding sections. The density of neutron and proton states increases as a function of the nuclear masses, meaning that the mean distance between the orbits is decreasing, as well as the gap values. Only the doubly-magic nucleus $^{208}_{82}\text{Pb}_{126}$ unambiguously shows a spherical behavior. At mid-major shell ($N \simeq 104$), the $_{82}\text{Pb}$ isotopes are typical examples of different shapes coexisting at very low excitation energy, as quadrupole correlations play a major role. A similar situation could be foreseen in the very neutron-rich isotopes, as soon as the number of neutrons above the $N = 126$ magic number is large enough.

8 The magic number $N=126$

The magic number 126 is due to the spin-orbit coupling which lowers the energy of the $i_{13/2}$ orbit ($N = \ell = 6$, parallel spin) which intrudes into the lower-shell states ($N = 5$). As a result, the magic number 126 is bound by the $g_{9/2}$ orbit (the lower one of the $N = 6$ major shell, that having $\ell = 4$ and a parallel spin) and by the $p_{1/2}$ orbit (the upper one of the $N = 5$ major shell, that having the lowest value of the orbital momentum and an anti-parallel spin).

The binding energies of the last neutron in the $N = 127$ and $N = 126$ isotones are drawn in the left part of Fig. 43. The curves do not show any abrupt change. Starting around 3.5 MeV, the value of the $N = 126$ gap seems to collapse for the largest values of Z (see the top of Fig. 43): It amounts to only 2 MeV for $Z = 92$. Hence we cannot exclude that the ground states of the $N = 126$ isotones with $Z > 92$, which are never been synthesized up to now, are deformed.

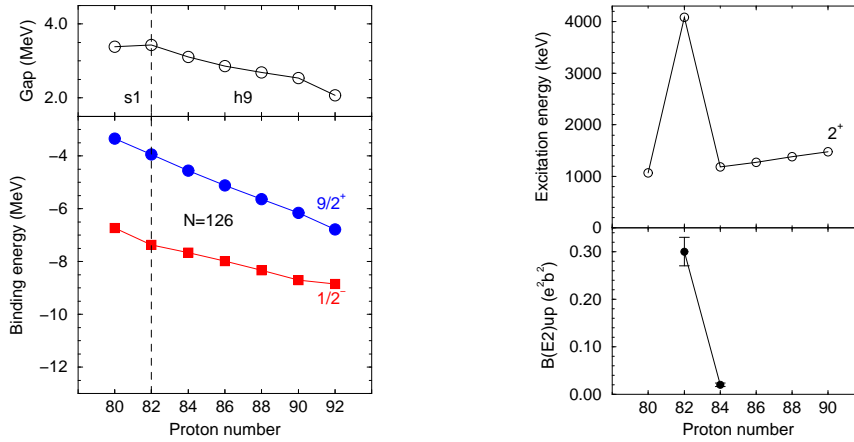


Figure 43: **Left:** Binding energies of the states $1/2^-$ ($9/2^+$) located below (above) the $N = 126$ magic number and difference of the binding energies of these two states surrounding the gap at $N = 126$ (see Sect. 11). **Right:** Experimental $E(2^+)$ and $B(E2; 0^+ \rightarrow 2^+)$ values in the $N = 126$ isotones.

The 2_1^+ energies and $B(E2; 0^+ \rightarrow 2^+)$ values measured so far in the $N = 126$ isotones are drawn in the right part of Fig. 43. Except the case of the doubly magic ^{208}Pb showing a very large value, all the other energies are close to 1.2 MeV. For $84 < Z < 90$, the valence protons being mainly in one particular orbit, $\pi h_{9/2}$, this can be understood in terms of seniority scheme. Besides the 2_1^+ state, the low-lying part of the level schemes of these isotones display the same structure with the 4^+ , 6^+ , and 8^+ states coming from the $(\pi h_{9/2})^2$ configuration. This interpretation has been confirmed by large-scale shell model calculations [265]. On the other hand, the $B(E2; 0^+ \rightarrow 2^+)$ value of ^{210}Po measured by the (d, d') inelastic scattering is very puzzling. The experimental result is more than a factor of 6 less than the SM predictions, while the calculations describe very well all the E2 strengths measured in the upper part of its $(\pi h_{9/2})^2$ structure.

In conclusion, the experimental knowledge of the $N = 126$ isotonic chain remain very scarce at the present time, particularly on the nuclei belonging to the r-path involved in the nucleosynthesis of heavy masses.

9 The super-heavy elements: What is the next proton shell closure?

It has long been known that in absence of shell effects, any super-heavy element would have vanishing barrier against fission and a spontaneous fission half-life of the order of 10^{-22} sec. An extrapolation of nuclear shell structure to super-heavy nuclei has been done forty years ago [266]. The possible existence of "islands of stability" is already mentioned in that publication. The hypothetic presence of magic numbers beyond the end of the periodic table was analyzed, it would give an extra binding energy of the corresponding nucleus leading to a barrier against fission around 9 MeV, which is enough to stabilize the otherwise highly fissile nucleus. Even at that time, it was suggested that shapes other than spherical might be stabilized by special shell structure. Several years later, the nuclear potential energy surfaces were systematically studied [267] using the liquid-drop energy and shell corrections. The latter were evaluated by the Strutinsky method which, being not restricted to the spherical shape, allows for the map of a whole range of deformation. For $102 < Z < 114$ and $N < 176$, all the nuclei appear to have deformed ground states as, even though the liquid drop would favour spherical shapes, shell corrections are enough to create a deformed minimum in the energy surface. On the other hand, the ground states of nuclei with $N > 176$ remain spherical whereas secondary minima are found at large deformation, which correspond to the fission isomers discovered in the 1960s. These secondary deformed minima are also due to shell effects¹⁸. During the last 25 years, self-consistent microscopic calculations have been largely developed, giving similar conclusions. A review of theoretical studies on the structure of super-heavy elements have been recently published [269], with a particular emphasis on the region of deformed nuclei. In this section, we only report on the candidates for *spherical* proton magic number next to $Z = 82$.

As shown in the previous sections, the amplitude of *spherical* shell effects decreases as the size of the system size is increased. Moreover the occurrence of a spherical proton shell closure is linked to proton-neutron interaction. It becomes therefore difficult to find well pronounced gaps for super-heavy elements. The proton shell closure beyond $Z = 82$ was surmised to be $Z = 114$ for many years, due to the large spin-orbit splitting calculated for the $5f$ shell. This prediction was common to various models in which the spin-orbit interaction was of similar strength, such as for the Woods-Saxon or some potentials derived from HF calculations [37].

More recently the shell structure of superheavy nuclei has been investigated within various parametrizations of relativistic and nonrelativistic nuclear mean-field models [270]. Spherical doubly-magic superheavy nuclei are found at ${}_{184}^{298}114$, ${}_{172}^{292}120$, or ${}_{184}^{310}126$ depending on the parametrization. The $Z = 114$ shell closure is predicted only by forces which overestimates the proton spin-orbit splitting in ${}^{208}\text{Pb}$, which makes the existence of a large shell gap at $Z = 114$ very questionable. The $Z = 120$ and $N = 172$ shell closures are predicted by the relativistic models and some Skyrme interactions [270]. These self-consistent microscopic calculations find a *central depression* in the nuclear density distribution which generates a wine-bottle shaped nucleonic potential. This peculiar shape brings different magic numbers from those obtained with flat-bottom potential wells. The central depression is a consequence of the different density distributions of the single-particle states : high- j orbits are located near the surface and low- j orbits near the center. As high- j proton orbits are pushed to large radii by the Coulomb interaction, the depression at the interior of the nucleus is enhanced.

¹⁸Such secondary deformed minima have been identified many years later in the whole chart of nuclides, giving rise to the superdeformed states [268]

When the nucleon numbers are increased beyond $Z = 120$ and $N = 172$, the occupation of low- j orbits removes this central depression. This creates new shell gaps, corresponding to a flat density distribution in the central part of the nucleus [271]. From a very simple extrapolation of nuclear shell structure to superheavy nuclei, $Z = 126$ would be the next spherical shell closure. Within the relativistic mean-field theory, spherical shell gaps appear at $Z = 126$ and $N = 184$.

The "cold fusion" reaction has been successfully used during the last two past decades to synthesize new elements with $Z = 107 - 112$ using $_{82}\text{Pb}$ and $_{83}\text{Bi}$ targets [272]. At GSI the heaviest element obtained so far ($Z = 112$, $N = 165$) has been produced by the $^{70}\text{Zn} + ^{208}\text{Pb}$ reaction with a cross section as low as 1 pb. More recently, one event has been assigned to the decay chain of the new element $^{278}113$ which has been synthesized in the cold fusion $^{70}\text{Zn} + ^{209}\text{Bi}$ at RIKEN [273]. As reaction cross section are expected to plummet as Z is increased, this method will probably not be suitable to reach the proton magic numbers $Z = 120$ and $Z = 126$.

The situation has been recently improved by using more neutron-rich actinides isotopes as targets and less massive nuclei as projectiles, the compound nuclei being produced in "hot fusion" reactions. After positive results obtained on the synthesis of the new isotopes, $^{283}112$ and $^{287}114$, the 116 and 118 elements have been produced for the first time [274]. Three α -decay chains have been attributed to the even-even $^{294}118_{176}$ isotope, which was produced with a cross section of 0.5 pb in the 3n-evaporation channel of the $^{48}\text{Ca} + ^{249}\text{Cf}$ fusion. On the face of it, these experimental results cannot confirm or reject the theoretical predictions for the next proton magic number. Similar sets of results are expected for neighboring nuclei to learn about nuclear shell closures.

As the variation of the spin-orbit splittings - and their isospin dependence both from the SO potential through the modification of the nucleon density and from the tensor terms of the $\pi\nu$ monopole interactions- is the leading factor for determining the location of the island of stability of the superheavy elements, a global understanding of the NN interaction along the chart of nuclides is required. New studies foreseen for lower- Z exotic nuclei would bring a complementary information into the present quest.

10 Conclusions and Outlooks

Every localized fermionic object, such as atomic cluster, molecule, atom or nucleus, displays shell structure. The non uniform energy distribution of the shells gives rise to shell gaps. In atomic nuclei it has thorough consequences, among which : (i) The stable magic nuclei -which exhibit large shell gaps between the last occupied and the first empty orbit- are the most abundant on earth, and the radioactive ones are expected to be the main 'survivors' in explosive stellar environments such as in X-ray bursts and supernovae, (ii) The closed-shell nuclei are the major building blocks which serve for a global description of all existing nuclei.

The concept of a magic number has remained a solid pillar for a long time, until the study of nuclei with extreme N/Z ratios has revealed their fragility. Guided by various spectroscopic information (e.g. binding energies of orbits on each side of the gap, trends of excitation energy, collective properties of states, spectroscopic factors,...) the present work intended to review the vulnerability of the major-shell closures, and the emergence of new ones. An exploratory 'journey' throughout the chart of nuclides has therefore been undertaken to address these evolutions, which were tentatively ascribed to specific properties of the NN force, particularly the tensor term which strongly acts in proton-neutron configurations, either between orbitals having the same orbital momenta $\Delta\ell = 0$ or $\Delta\ell = 1$. Nevertheless the single-particle states often easily couple to collective states since contrary to molecular systems, there is no clean cut between single-particle excitation,

vibrational and rotational states in the atomic nucleus. Therefore the present statements on the observed structural evolution in terms of fundamental properties of the nuclear force remain *semi-quantitative*, as a proper unfolding with collective motions has still to be achieved in most of the cases.

Two major kinds of shell gaps exist in atomic nuclei and their ability to resist to erosion depends on their origin, size and composition. The shell gaps 8, 20 and 40 are provided by the mean field description of the nuclei using a Harmonic Oscillator potential, which is a consequence of the saturation of the nuclear interaction. In heavier systems, these shell gaps are replaced by those created by the strong spin-orbit interaction, which originates from the spin-dependence of the nuclear interaction.

The HO shell gaps are formed between two orbits of opposite parity. Consequently excitation which preserve parity, such as quadrupole ones, should occur through a minimum of one pair of particle excitations, e.g. $(2p - 2h)$, across the gap. This specific property gives rise to a relatively enhanced rigidity with respect to collective excitations, unless the size of the gap is reduced or/and many particle excitations are permitted, as in semi-magic nuclei. It is remarkable that these two effects thrive in the three known cases of HO shells in a similar and sudden manner. Starting from the very rigid $^{14}_6\text{C}_8$, $^{34}_{14}\text{Si}_{20}$ and $^{68}_{28}\text{Ni}_{40}$ nuclei the removal of only two protons provokes a sudden deformation of the $^{12}_4\text{Be}_8$, $^{32}_{12}\text{Mg}_{20}$ and $^{66}_{26}\text{Fe}_{40}$ nuclei, respectively, in which the intruder deformed states have the lowest energy. This is illustrated in Fig. 44 by the large changes in the energy of the 2_1^+ state for $N = 8$, $N = 20$ and $N = 40$.

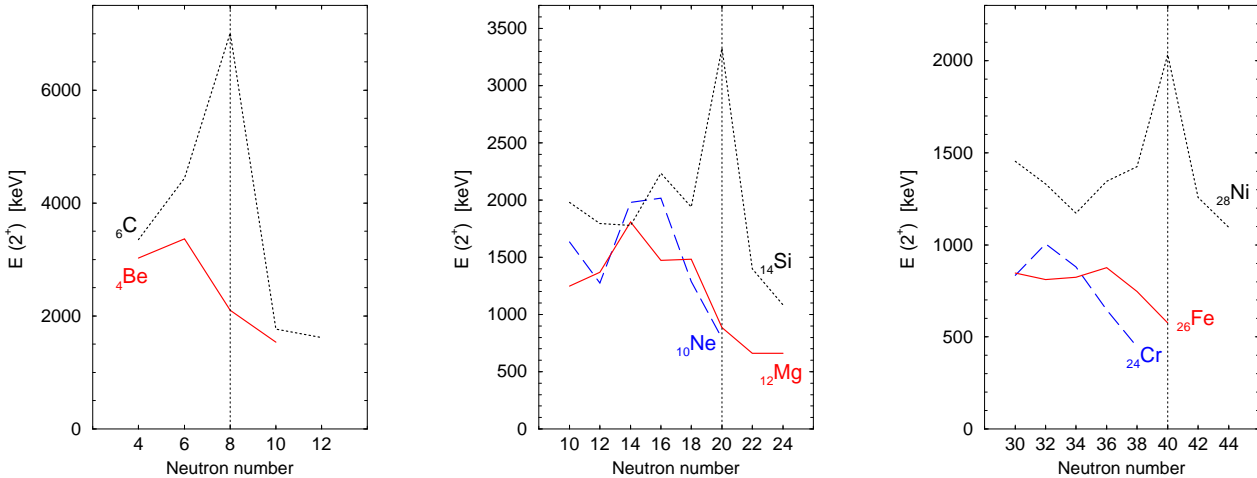


Figure 44: Experimental $E(2_1^+)$ values for several isotopic chains, as a function of the neutron numbers where the $N = 8$ (left), $N = 20$ (middle) and $N = 40$ (right) shell closures are crossed.

Noteworthy is the fact that this passage from a rigid configuration with a normal filling of the orbits to the so-called island of inversion is triggered by the same phenomenon : the sudden release of a strong *spin-flip* $\Delta\ell = 0$ proton-neutron force. For the three rigid nuclei mentioned above, the forces that came into play to produce large $N = 8$, $N = 20$ and $N = 40$ gaps are $\pi p_{3/2} - \nu p_{1/2}$, $\pi d_{5/2} - \nu d_{3/2}$ and $\pi f_{7/2} - \nu f_{5/2}$, respectively (see the first three rows of Fig. 45). As soon as protons are removed from the $p_{3/2}$, $d_{5/2}$ or $f_{7/2}$ orbits, the corresponding neutron orbits ($p_{1/2}$, $d_{3/2}$ or $f_{5/2}$) become less bound. Thus the neutron gaps $N = 8$, $N = 20$ or $N = 40$ are reduced significantly and become more vulnerable to excitations. In parallel new shell gaps $N = 6$,

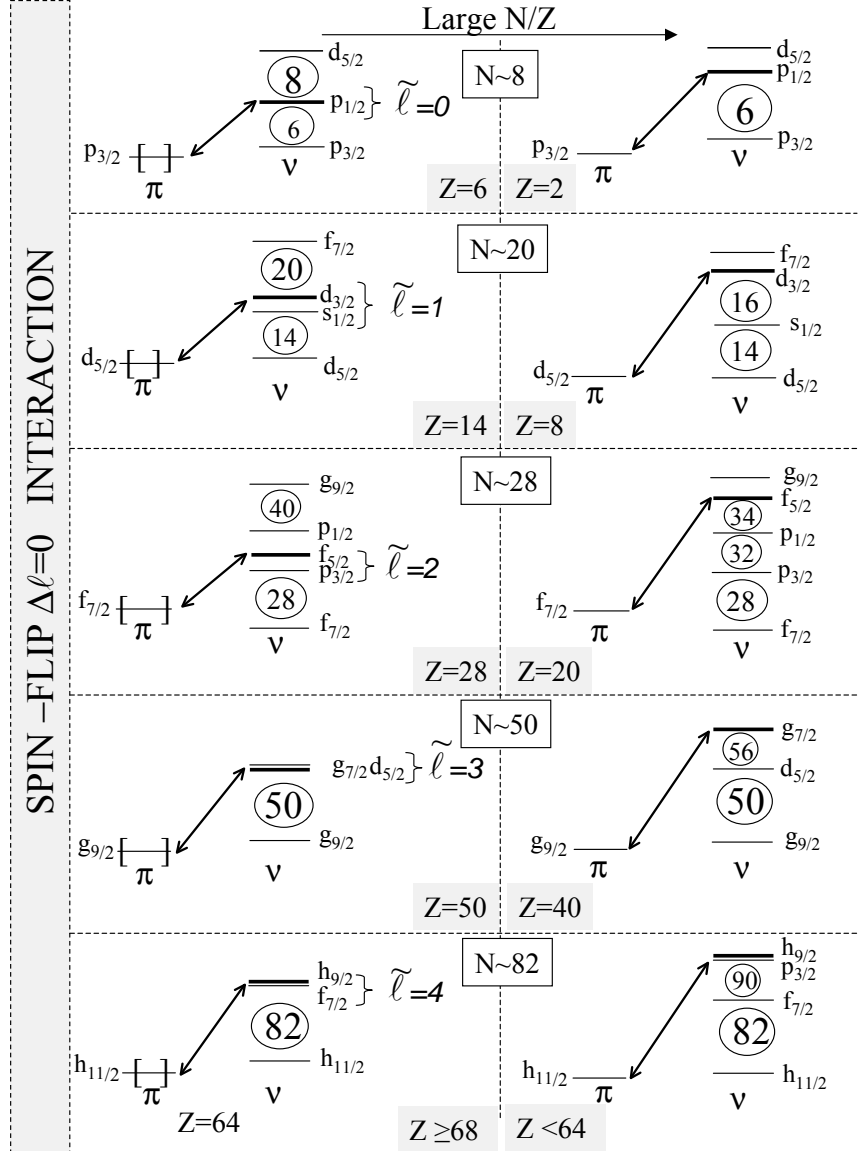


Figure 45: The qualitative effect of the spin-flip $\Delta\ell = 0$ proton-neutron interaction is shown for different regions of the chart of nuclides. By comparing the left and right hand sides of the Figure, the removal of protons induces a change in the spacing and possibly ordering of the neutron states. When this interaction is missing, the major Harmonic Oscillator shell gaps $N = 8, 20, 40$ are reduced to the benefit of new subshell gaps at $N = 6, 16, 32$. Additionally the degeneracy of the pseudo-spin doublets $\tilde{\ell} = 1, 2, 3, 4$ is lifted.

$N = 16$, or $N = 32, 34$ are created below, as shown in the right part of Fig. 45.

The SO-like magic numbers, such as 14, 28 and 50, have different properties. As shown in Fig. 46 for the K, Cu and Sb isotopic chains, these magic numbers are defined between the two SO partners (having aligned and anti-aligned spin and angular momenta), in between which another orbit with $\ell - 2$ is present. In these examples the spin-aligned orbits $d_{5/2}, f_{7/2}$ and $g_{9/2}$ are located at the bottom of the shell gaps $Z = 14$, $Z = 28$ and $Z = 50$, respectively. The couples of valence orbits above the shell gaps are $(s_{1/2}, d_{3/2})$, $(p_{3/2}, f_{5/2})$, and $(d_{5/2}, g_{7/2})$, respectively. The *spin-flip*

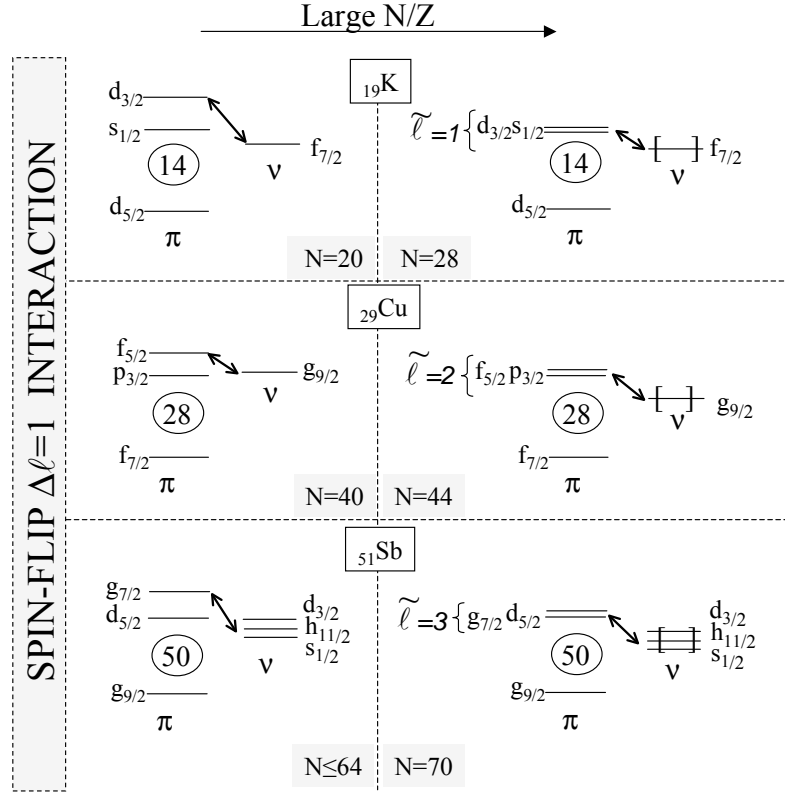


Figure 46: The spin-flip $\Delta\ell = 1$ proton-neutron interaction acts in a similar manner in different regions of the chart of nuclides, as shown in the K, Cu and Sb isotopic chains. By comparing the left and right hand sides of the Figure, the addition of neutrons induces a shrink in the spacing and possibly ordering of the proton states forming the doublets labelled with $\tilde{\ell} = 1, 2, 3$ values. When this interaction operates, the spin-orbit shell gaps $Z = 14, 28, 50$ are reduced.

$\Delta\ell=1$ proton-neutron force acts to reduce the SO splittings and shrink the space between the two valence states (see comparison of the proton orbits on the left- and right-hand sides of Fig. 46). This situation seems to be generic in the whole chart of nuclides. This reduction could trigger quadrupole collectivity -and the development of deformation- between the occupied and valence states. This jeopardizes the rigidity of the spherical shell gap, as in the case of the neutron-rich nucleus $^{42}_{14}\text{Si}_{28}$. The very low energy of its first excited state indicates the erosion of both the $Z = 14$ and $N = 28$ shell closures by the action of the mutual proton and neutron spin-flip $\Delta\ell = 1$ forces ($\pi d_{5/2}$ acts to reduce the neutron $f_{7/2} - f_{5/2}$ SO splitting and $\nu f_{7/2}$ to shrink the proton $d_{5/2} - d_{3/2}$ one). The next doubly-magic nucleus formed with two SO shell gaps at $Z = 28$ and $N = 50$, is $^{78}_{28}\text{Ni}_{50}$. It is being thought to behave as a spherical rigid nucleus. Whether it would develop a permanent quadrupole ground-state deformation or not, depends on both the size of the $Z = 28$ and $N = 50$ gaps and on the strength of the quadrupole correlations. As regards the evolution of the shell gaps, significant reductions are foreseen from the experimental results obtained so far while approaching ^{78}Ni . Complementary to what was discussed in the different sections of this review, it is instructive to look at the evolution of the 2^+ energies in the Si, Ca, and Ni isotopic chains during the filling of the high- j neutron shell involved ($f_{7/2}$ for Si and Ca,

and $g_{9/2}$ for the Ni isotopes). Starting at ^{34}Si , ^{40}Ca , and ^{56}Ni which exhibit large 2^+ energies, the three chains behave similarly up to the mid occupancy of the shell, i.e. at ^{38}Si , ^{44}Ca , and ^{62}Ni (see Fig. 47). Then the 2^+ energy of the Si isotopes does not follow the parabola curve as for the Ca isotopes, but strongly decreases. The actual trend of the 2^+ energy in the Ni isotopic

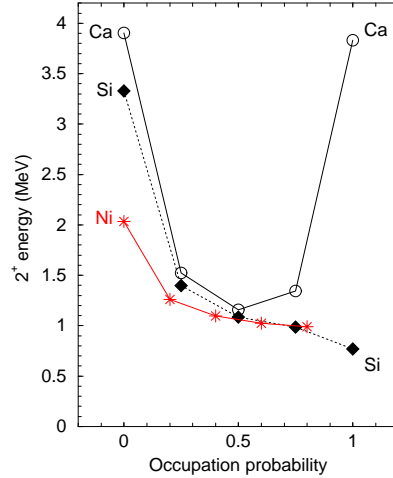


Figure 47: Evolution of the energy of the 2^+_1 states in the ^{14}Si , ^{20}Ca , and ^{28}Ni isotopic chains during the filling of the high- j neutron shell (see text). The occupation probability is calculated on the assumption of spherical shapes. The doubly-magic nuclei $^{34}\text{Si}_{20}$, $^{40}\text{Ca}_{20}$, and $^{56}\text{Ni}_{28}$ are present in the left-hand side of the Figure. On the right-hand side, it is the turn of the $^{42}\text{Si}_{28}$, $^{48}\text{Ca}_{28}$, and $^{78}\text{Ni}_{50}$ nuclei.

chain, immediately before reaching ^{78}Ni , looks very close to the one in the Si isotopes. This might indicate that ^{78}Ni would behave like ^{42}Si , rather than ^{48}Ca . This feature is very challenging to look at in the future. For heavier nuclei, the combination of the magic numbers of SO-origin gives rise to spherical rigid nuclei, such as $^{132}_{50}\text{Sn}_{82}$ and $^{208}_{82}\text{Pb}_{126}$.

As shown in the various examples presented in Figs. 45 and 46, the 'spin-flip $\Delta\ell = 0$ ' and 'spin-flip $\Delta\ell = 1$ ' $\pi\nu$ forces play decisive roles in the evolution of shell gaps, would they be of HO or SO origin. They also remarkably bring the quasi-degeneracy of two states separated by two units of orbital momentum (i.e. ℓ and $\ell + 2$). These states belong to the so-called 'pseudo-spin' doublet, having pseudo-orbital angular momentum $\tilde{\ell} = \ell + 1$ and pseudo-spin \tilde{s} , such as $j = \tilde{\ell} \pm \tilde{s}$. For instance, the proton doublet with $\tilde{\ell} = 1$, formed with the $\pi s_{1/2}$ ($\ell = 0$) and $\pi d_{3/2}$ ($\ell = 2$) states, become degenerate when the $\nu f_{7/2}$ orbit is full, e.g. in $^{47}\text{K}_{28}$. Same holds true for the other proton $\tilde{\ell} = 2, 3$ orbits which become degenerate while the neutron $g_{9/2}$, $h_{11/2}$ orbits are filled, respectively (see Fig. 46). Similarly the neutron $\tilde{\ell} = 2, 3, 4$ doublets are present while the proton $d_{5/2}$, $f_{7/2}$, $g_{9/2}$, $h_{11/2}$ orbits are filled, respectively, as shown in Fig. 45. This pseudo-spin symmetry has been shown by J. N. Ginocchio [275] to occur naturally in a relativistic mean-field description of single-particle states. Gathering the empirical results of Figs. 45 and 46 it is found that the breaking of this symmetry is linked to the spin-isospin dependence of the nuclear interaction (the spin-flip $\Delta\ell = 0, 1$ terms). Effective interactions which are not taking into account these effects will never reach a satisfactory level of predictive power.

The present review has addressed the evolution of shell closures for nuclei studied so far. Fascinating enough is to remind that the spin-dependence of the nuclear force governs the existence

of most of the magic nuclei. Despite many decades of research, the role of the various components of this force, and in particular the tensor one, is still veiled. With the future radioactive ion beam facilities worldwide and the increasing detector and spectrometer sensitivities, some of the scenarios suggested here on the evolution of shells and on the underlying nuclear forces at play will be confirmed or refuted. In parallel the way to link the 'bare' NN force to the in-medium forces, would they be in the valley of stability or very weakly bound, is being searched for. These experimental and theoretical progresses are to be led together. This is essential to build up a consistent description of all kind of nuclear systems.

11 Annex: Binding energy of the last nucleon in nuclei close to the semi-magic nuclei

The spherical nuclei having nucleon numbers close to magic numbers can be considered as systems of independent nucleons moving in a common potential well. The eigenvalues of the corresponding Hamiltonian give the single-nucleon spectra. From an experimental point of view, the binding energies of such nuclei can be used to determine the separation energies of nucleons, that are supposed to be close to the single-particle energies we are looking for. For that, we have to assume that the semi-magic core remains closed when adding or removing one nucleon, i.e. there are no rearrangement or collective excitation.

The energy ϵ_b of the orbit located below a proton gap is equal to the inverse of the proton separation energy $S_p(Z_{magic})$ of the semi-magic nucleus having Z_{magic} protons, i.e. $\epsilon_b = -S_p(Z_{magic})$, where $S_p(Z_{magic})$ is the difference between the binding energies, $BE(Z_{magic}, N) - BE(Z_{magic} - 1, N)$. Similarly, the energy ϵ_a of the orbit situated above the proton gap is equal to the inverse of the proton separation energy of the nucleus having $Z_{magic} + 1$ protons, i.e. $\epsilon_a = -S_p(Z_{magic} + 1)$. The distance between these two orbits is representative of the gap in energy between the last-occupied and the first-valence orbit, $E_{gap}(Z_{magic}, N) = S_p(Z_{magic}, N) - S_p(Z_{magic} + 1, N)$. As said before, the use of this relation has to be limited to spherical nuclei, for which the ϵ_a and ϵ_b values are close to the single-particle energy of the first valence and last occupied orbitals, respectively. Note that the mean field potential, which is an average of nucleon-nucleon interactions inside a nucleus, is slightly changing between the nuclei with Z_{magic} and $Z_{magic} + 1$ which are used here to define the size of the gap, $E_{gap}(Z_{magic}, N)$. Therefore, the intrinsic value of $E_{gap}(Z_{magic})$ is approximate. Rather, its evolution along an isotopic chain is meaningful to look at the modification of shell closures.

The same procedure applies to the evolution of gaps $E_{gap}(Z, N_{magic})$ formed by between occupied and valence neutron single-particle orbitals. In addition to these definitions and words of caution, several other considerations apply to the binding energy curves that are used extensively throughout the present work :

- Only the *measured* values reported in the AME2003 atomic mass evaluation [10] have been used, not the extrapolated ones. Added to these are the recent atomic mass measurements of ^{23}N and ^{24}O [70], ^{47}Ar [139], $^{70,72}\text{Ni}$ and ^{73}Cu [180], ^{83}Ge [216], and $^{131-133}\text{Sn}$ [243].
- The uncertainties on the neutron (proton) separation energies are shown in the figures, except when they are smaller than the size of the symbols.
- We restrict the plots to data corresponding to spherical nuclei, whose shapes are confirmed by the properties of their first excited states. In the case of deformed nuclei, the nucleon

separation energies, that is the energy required to remove the least bound particle from the nucleus, are the results of a complex situation, the two involved nuclei even having different deformations.

- The curves are labeled by the j^π values of the states of the odd-A nuclei and not by the quantum numbers (ℓ, j, π) of the expected single-particle orbits. This choice is governed by the fact that the spectroscopic factor of the first j^π state does not always exhaust the sum rule arising from the j^π orbit. Such cases are discussed in the sections following the results on the binding energies.
- Most of the figures only display the binding energies of the two states which surround the magic number that is considered. When two orbits are crossing each others, would it be above or below the shell gap, both are displayed in the figures.
- Many results involving doubly-magic nuclei display singularities in the curves. One has to notice that the so-called Wigner term which gives an additional binding to nuclei with neutrons and protons occupying the same shell-model orbitals, is the largest when $N = Z$. As a consequence, every separation energy calculated using a doubly-magic $N = Z$ nucleus displays a sudden variation at this number of nucleons, resulting in a very large value of the shell gap. Chasman [63] has recently proposed a method to calculate values of shell gap associated to the $N = Z$ nuclei by combining the binding energies of various nuclei surrounding the self-conjugated isotopes, in such a way they are free from the Wigner energy contribution. The obtained values are now very close to those predicted in mean-field approaches.
- The small effects possibly observed for the $N \neq Z$ doubly-magic nuclei (^{48}Ca , ^{132}Sn or ^{208}Pb) show evidence of the limits of this method. Even though all the nuclei chosen for the plots shown in this paper have a spherical shape attested by their excited states, various correlations can give more stability to the odd-A nuclei than to the semi-magic core, leading to a larger binding energy of its ground state. Therefore for nucleon number between two magic numbers, the value of the separation energy is not inevitably the energy of the orbit in interest. Nevertheless any sharp variation remains relevant for the analysis of the single-particle behavior.

Acknowledgments

This review owes much to discussions with many colleagues. Related to the theoretical parts, F. Nowacki, A. Poves, D. Lacroix, S. Typel, T. Otsuka and B.A. Brown are greatly acknowledged. M.-G.P. thanks M. Girod and S. Péru for providing her with the HFB-D1S code and for many helpful discussions. Concerning the experimental topics, discussions and comments from close colleagues as F. Azaiez, Z. Dombrádi, L. Gaudefroy, S. Grévy, K.-L. Kratz, A. Navin, and J.C. Thomas, to name a few, were very enlightening. O.S. also wishes to thank P. Chomaz, who trusted us to write this review article.

References

- [1] W. Elsasser, J. de Phys. et Rad. 5 (1934) 625

- [2] M. Goeppert-Mayer, *Phys. Rev.* 74 (1948) 235
- [3] M. Goeppert-Mayer, *Phys. Rev.* 75 (1949) 1969
- [4] O. Haxel, J.H.D. Jensen and H.E. Suess, *Phys. Rev.* 75 (1949) 1766
- [5] C. Thibault et al., *Phys. Rev.* C12 (1975) 644
- [6] G. Hubert et al., *Phys. Rev.* C18 (1978) 2342
- [7] C. Détraz et al., *Phys. Rev.* C19 (1979) 164
- [8] D. Guillemaud-Mueller et al., *Nucl. Phys.* A426 (1984) 37
- [9] ENSDF database, <http://www.nndc.bnl.gov/ensdf/>
- [10] G. Audi, A.H. Wapstra and C. Thibault, *Nucl. Phys.* A729 (2003) 337
- [11] S. Raman, C.W. Nestor, and P. Tikkanen, *At. Data Nucl. Data Tables* 78 (2001) 1
- [12] J. Dobaczewski, N. Michel, W. Nazarewicz, M. Ploszajczak and J. Rotureau, *Prog. in Part. and Nucl. Phys.* 59 (2007) 432 and references therein
- [13] D.J. Dean, INPC2007 Proceedings, to be published in *Nucl. Phys. A*, arXiv 0709-0441 [nucl-th]
- [14] R.B. Wiringa, V.G.J. Stoks, R. Schiavilla, *Phys. Rev.* C51 (1995) 38
- [15] R. Machleidt, *Phys. Rev.* C63 (2001) 024001
- [16] S.K. Bogner, T.T.S. Kuo, and A. Schwenk, *Phys. Rep.* 386 (2003) 1
- [17] S.C. Pieper and R.B. Wiringa, *Ann. Rev. Nucl. Part. Sci.* 51(2001) 53
- [18] R. Roth and P. Navrátil, *Phys. Rev. Lett.* 99 (2007) 092501
- [19] D.J. Dean, G. Hagen, M. Hjorth-Jensen, T. Papenbrock and A. Schwenk, arXiv 0709-0449 [nucl-th]
- [20] B.A. Brown, *Prog. in Part. and Nucl. Phys.* 47 (2001) 517
- [21] H. Grawe, *Lect. Notes in Phys.* 651 (2004) 33
- [22] E. Caurier, G. Martinez-Pinedo, F. Nowacki, A. Pòvès, A.P. Zuker, *Rev. Mod. Phys.* 77 (2005) 427
- [23] A. Schwenk and J.D. Holt, arXiv 0802-3741 [nucl-th]
- [24] A.P. Zuker, *Phys. Rev. Lett.* 90 (2003) 042502
- [25] M. Bender, P.-H. Heenen, and P.-G. Reinhard, *Rev. Mod. Phys.* 75 (2003) 121
- [26] J.R. Stone and P.-G. Reinhard, *Prog. Part Nucl. Phys.* 58 (2007) 587
- [27] D. Vretenar, A.V. Afanasjev, G.A. Lalazissis and P. Ring, *Phys. Rep.* 409 (2005) 101
- [28] J. Meng et al., *Prog. Part Nucl. Phys.* 57 (2006) 470
- [29] T. Otsuka, T. Matsuo, and D. Abe, *Phys. Rev. Lett.* 97 (2006) 162501
- [30] B.A. Brown, T. Duguet, T. Otsuka, D. Abe, and T. Suzuki, *Phys. Rev. C* 74 (2006) 061303(R)
- [31] G. Colò, H. Sagawa, S. Fracasso, and P.F. Bortignon, *Phys. Lett. B* 646 (2007) 227
- [32] T. Lesinski, M. Bender, K. Bennaceur, T. Duguet and J. Meyer, *Phys. Rev. C* 76 (2007) 014312
- [33] M. Zalewski, J. Dobaczewski, W. Satula and T.R. Werner, *Phys. Rev. C* 77 (2008) 024316
- [34] A. Bohr and B. Mottelson, *Nuclear Structure*, volume 1, Benjamin, New York (1969)
- [35] P. Ring and P. Schuck, *The Nuclear Many-Body Problem*, Springer-Verlag (1980)
- [36] K. L. G. Heyde, *The Nuclear Shell Model*, Springer-Verlag (1994)
- [37] S.G. Nilsson and I. Ragnarsson, *Shapes and Shells in Nuclear Structure*, Cambridge University Press, Cambridge, England, (1995) chapter 6
- [38] D. Vautherin and D.M. Brink, *Phys. Rev.* C5 (1972) 626
- [39] J. Dobaczewski, I. Hamamoto, W. Nazarewicz, and J.A. Sheikh, *Phys. Rev. Lett.* 72 (1994) 981
- [40] D.J. Dean, T. Engeland, M. Hjorth-Jensen, M.P. Kartamyshev, and E. Osnes, *Prog. Part. Nucl. Phys.* 53 (2004) 419
- [41] M. Moinester, J.P. Schiffer and W.P. Alford, *Phys. Rev.* 179 (1969) 984
- [42] M. Dufour and A. Zuker, *Phys. Rev. C* 54 (1996) 1641
- [43] R.F. Casten, *Nuclear Structure from a Simple Perspective*, ed. P.E. Hodgson, Oxford Univ. Press (1990)
- [44] W.W. Daehnick, *Phys. Rep.* 96 (1983) 317

- [45] Y. Uozumi et al., *Phys. Rev. C* 50 (1994) 263
- [46] Y. Uozumi et al., *Nucl. Phys. A* 576 (1994) 123
- [47] J.P. Schiffer, W.W. True, *Rev. Mod. Phys.* 48 (1976) 191
- [48] M.-G. Porquet et al., in preparation
- [49] B.A. Brown, W.A. Richter, R.E. Julies and B.H. Wildenthal, *Ann. Phys. (NY)* 182 (1988) 191
- [50] A. Umeya and K. Muto, *Phys. Rev. C* 69 (2004) 024306
- [51] A. Umeya and K. Muto, *Phys. Rev. C* 74 (2006) 034330 and private communication (July 2007)
- [52] J. Millener, private communication (August 2006)
- [53] T. Otsuka, T. Suzuki, R. Fujimoto, H. Grawe and Y. Akaishi, *Phys. Rev. Lett.* 95 (2005) 232502
- [54] T. Otsuka et al., *Phys. Rev. Lett.* 87 (2001) 082502
- [55] T. Otsuka and D. Abe, *Prog. in Part. and Nucl. Phys.* 59 (2007) 425
- [56] R.R. Scheerbaum, *Phys. Lett.* 63B (1976) 381 and references therein.
- [57] W. von Oertzen and H.-G. Bohlen, *C.R. Physique* 4 (2003) 465
- [58] M. Freer, *C.R. Physique* 4 (2003) 475
- [59] W. von Oertzen, M. Freer, and Y. Kanada-En'yo, *Phys. Rep.* 432 (2006) 43
- [60] I. Tanihata and R. Kanungo, *C.R. Physique* 4 (2003) 437
- [61] N. Orr and F.M. Marqués, *C.R. Physique* 4 (2003) 451
- [62] K. Riisager, *Lect. Notes Phys.* 700 (2006) 1
- [63] R.R. Chasman, *Phys. Rev. Lett.* 99 (2007) 082501 and references therein
- [64] I. Talmi and I. Unna, *Phys. Rev. Lett.* 4 (1960) 469
- [65] A. Gade et al., *Phys. Rev. C* 76 (2007) 024317
- [66] A.B. MacDonald et al., *Nucl. Phys.* A258 (1976) 152
- [67] H. Iwasaki et al., *Phys. Lett. B* 491 (2000) 8
- [68] D.J. Millener et al., *Phys. Rev. C* 28 (1983) 497
- [69] A. Navin et al., *Phys. Rev. Lett.* 85 (2000) 266
- [70] B. Jurado, *Phys. Lett. B.* 649 (2007) 43
- [71] H. Sakurai et al., *Phys. Lett. B* 448 (1999) 180
- [72] S. Michimasa et al., *Phys. Lett. B.* 638 (2006) 146
- [73] E. Sauvan et al., *Phys. Lett. B.* 491 (2000) 1
- [74] S. Sugimoto, H. Toki and K. Ikeda, *Phys. Rev. C* 76 (2007) 054310
- [75] A. Signoracci and B.A. Brown *Phys. Rev. C* 75 (2007) 024303
- [76] B.H. Wildenthal, *Prog. Part. Nucl. Phys.* 11 (1984) 5
- [77] B.A. Brown and W.A. Richter, *Phys. Rev. C* 74 (2006) 034315
- [78] M. Stanoiu PhD Thesis, Caen (2003) GANIL T03-01
- [79] P.G. Thirolf et al., *Phys. Lett. B.* 485 (2000) 16
- [80] E. Becheva et al., *Phys. Rev. Lett.* 96 (2006) 012501
- [81] B.A. Brown, private communication
- [82] M. Stanoiu et al., in preparation
- [83] P.M. Campbell et al., *Phys. Rev. Lett.* 97 (2006) 112501
- [84] D. Bazin et al., *Phys. Rev. C* 57 (1998) 2156
- [85] D. Bazin et al., *Phys. Rev. Lett.* 74 (1995) 3569
- [86] F.M. Marqués et al. *Phys. Lett. B* 381 (1996) 407
- [87] T. Nakamura et al., *Phys. Rev. Lett.* 83 (1999) 1112
- [88] X. Campi et al., *Nucl. Phys.* A251 (1975) 193
- [89] A. Poves and J. Retamosa, *Phys. Lett. B* 184 (1987) 311
- [90] W. Warburton, J. A. Becker and B. A. Brown, *Phys. Rev. C* 41 (1990) 1147

- [91] D. Guillemaud-Mueller et al., *Phys. Rev.* C41 (1990) 937
- [92] O. Tarasov et al., *Phys. Lett.* B409 (1987) 64
- [93] S. M. Lukyanov, *J. Phys.* G28 (2002) L41
- [94] M. Notami et al., *Phys. Lett.* B542 (2002) 49
- [95] M. Fauerbach et al., *Phys. Rev.* C53 (1996) 647
- [96] R.W. Ibbotson et al., *Phys. Rev. Lett.* 80 (1998) 2081
- [97] P. Baumann et al., *Phys. Lett.* B228 (1989) 458
- [98] T. Motobayashi et al., *Phys. Lett.* B346 (1995) 9
- [99] H. Iwasacki et al., *Phys. Lett.* B522 (2001) 9
- [100] B. V. Pritychenko et al., *Phys. Rev.* C63 (2000) 011305(R)
- [101] J.A. Church et al., *Phys. Rev.* C72 (2005) 054320
- [102] Y. Yanagisawa et al., *Phys. Lett.* B566 (2003) 84
- [103] E. Caurier et al., *Phys. Rev.* C58 (1998) 2033
- [104] K. Heyde et al., *J. Phys.* G17 (1991) 135
- [105] Y. Utsuno et al., *Phys. Rev.* C60 (1999) 054315
- [106] T. Otsuka et al., *Eur. Phys. J A* 15 (2002) 151
- [107] R. Neugart and G. Neyens, *Lect. Notes Phys.* 700 (2006) 135
- [108] M. Kowalska et al., *Phys. Rev.* C77 (2008) 034307
- [109] G. Klotz et al., *Phys. Rev.* C47 (1993) 2502
- [110] G. Neyens et al., *Phys. Rev. Lett.* 94 (2005) 022501
- [111] F. Maréchal et al., *Phys. Rev.* C72 (2005) 044314
- [112] D. Yordanov et al., *Phys. Rev. Lett.* 99 (2007) 212501
- [113] S. Piétry, Ph. D. Thesis, Caen (2003)
- [114] J. Terry et al., *Phys. Rev.* C77 (2008) 014316
- [115] S. Nummela et al., *Phys. Rev.* C64 (2001) 054313
- [116] A. Obertelli et al., *Phys. Lett.* B633 (2006) 33
- [117] J. Terry et al., *Phys. Lett.* B640 (2006) 86
- [118] Z. Elekes et al., *Phys. Rev. Lett.* 98 (2007) 102502
- [119] A. Schiller et al., *Phys. Rev. Lett.* 99 (2007) 112501
- [120] T. Otsuka et al., *Nucl. Phys.* A685 (2001) 100
- [121] A. Ozawa et al., *Phys. Rev. Lett.* 84 (2000) 5493
- [122] E. Sauvan et al., *Phys. Rev.* C69 (2004) 044603
- [123] D. Cortina-Gil, *Phys. Rev. Lett.* 93 (2004) 062501
- [124] M. Stanoiu et al., *Phys. Rev.* C69 (2004) 034312
- [125] E. Ideguchi et al., *Phys. Rev. Lett.* 87 (2001) 222501
- [126] S.D. Pain et al., *Phys. Rev. Lett.* 96 (2006) 032502
- [127] M. Hannawald et al., *Phys. Rev. Lett.* 82 (1999) 1391
- [128] O. Sorlin et al., *Eur. Phys. J. A* 16, (2003) 55
- [129] P. Doornenbal et al., *Phys. Lett.* B647 (2007) 237
- [130] A. Bürger et al., AIP Conf. Proc. 831 (2006) 418
- [131] A. Huck et al., *Phys. Rev.* C31 (1985) 2226
- [132] S.N. Liddick et al., *Phys. Rev.* C70 (2004) 064303
- [133] J.I. Prisciandaro et al., *Phys. Lett.* B 510 (2001) 17
- [134] D.-C. Dinca et al., *Phys. Rev.* C71 (2005) 041302
- [135] A. Bürger et al., *Phys. Lett.* B 622 (2005) 29
- [136] M. Honma, T. Otsuka, B.A. Brown, and T. Mizusaki, *Phys. Rev.* C65 (2002) 061301

- [137] M. Rejmund et al., *Phys. Rev. C* 76 (2007) 021304(R)
- [138] A. Gade et al., *Phys. Rev. C* 74 (2006) 034322
- [139] L. Gaudefroy et al., *Phys. Rev. Lett.* 97 (2006) 092501
- [140] B. Bastin et al., *Phys. Rev. Lett.* 99 (2007) 022503
- [141] P. Doll, G.J. Wagner, K.T.Knöpfle and G. Mairle, *Nucl. Phys.* A263 (1976) 210
- [142] S.M. Banks et al., *Nucl. Phys.* A437 (1985) 381
- [143] G.J. Kramer, H.P. Blok and L.Lapika, *Nucl. Phys.* A679 (2001) 267
- [144] *Nuclear Data Sheets* 76 (1995) 191
- [145] F. Perrot, PhD thesis, Strasbourg (2004), IReS05-009
- [146] J. Dechargé and D. Gogny, *Phys. Rev. C* 21 (1980) 1568; J.-F. Berger, M. Girod, and D. Gogny, *Comp. Phys. Commun.* 63 (1991) 365
- [147] J. Retamosa, E. Caurier, F. Nowacki and A. Poves, *Phys. Rev. C* 55 (1997) 1266
- [148] S. Nummela et al., *Phys. Rev. C* 63 (2001) 044316
- [149] L. Gaudefroy et al, *Phys. Rev. Lett.* 99 (2007) 099202
- [150] E. Caurier, J. Menéndez, F. Nowacki and A. Poves, *Phys. Rev. C* 75 (2007) 054317
- [151] G.A. Lalazissis, D. Vretenar, W. Pöschl, and P. Ring, *Phys. Lett. B* 418 (1998) 7
- [152] B. G. Todd-Rutel, J. Piekarewicz, and P.D. Cottle, *Phys. Rev. C* 69 (2004) 021301(R)
- [153] O. Sorlin et al., *Phys. Rev. C* 47 (1993) 2941
- [154] F. Sarazin et al., *Phys. Rev. Lett.* 84 (2000) 5062
- [155] T. Glasmacher et al., *Phys. Lett. B* 395 (1997) 163 and references therein
- [156] X. Liang et al., *Phys. Rev. C* 67 (2003) 024302
- [157] J.A. Winger et al., *Phys. Rev. C* 64 (2001) 064318
- [158] H. Scheit et al, *Phys. Rev. Lett.* 77 (1996) 3967
- [159] D. Sohler et al., *Phys. Rev. C* 66 (2002) 054302
- [160] S. Péru et al., *Eur. Phys. J. A* 49 (2000) 35
- [161] S. Grévy et al, *Eur. Phys. J. A* 25 (2005) s01-111
- [162] S. Grévy, private communication
- [163] K. Heyde and R.A. Meyer, *Phys. Rev. C* 37 (1988) 2170
- [164] P.D. Cottle and K.W. Kemper, *Phys. Rev. C* 58 (1998) 3761
- [165] O. Sorlin et al., *Eur. Phys. J. A* 22 (2004) 173
- [166] J. Fridmann et al., *Nature* 435 (2005) 922
- [167] J. Fridmann et al., *Phys. Rev. C* 74 (2006) 034313
- [168] R. Abegg et al., *Nucl. Phys.* A303 (1978) 121
- [169] Y. Uozumi et al., *Nucl. Phys.* A576 (1994) 123
- [170] K. E. Rehm et al., *Phys. Rev. Lett.* 80 (1998) 676
- [171] D.C. Kocher and W. Haeberli, *Nucl. Phys.* A196 (1972) 225
- [172] E. Caurier F. Nowacki and A. Poves *Nucl. Phys.* A742 (2004) 14
- [173] T.R. Werner et al., *Nucl. Phys.* A597 (1996) 327
- [174] P.-G. Reinhardt et al., *Phys. Rev. C* 60 (1999) 014316
- [175] G.A. Lalazissis et al., *Phys. Rev. C* 60 (1999) 014310
- [176] R. Rodriguez-Guzman et al., *Phys. Rev. C* 65 (2002) 024304
- [177] B. Blank et al., *Phys. Rev. Lett* 84 (2000) 1116 and C. Dossat et al., *Phys. Rev. C* 72 (2005) 054315
- [178] Ch. Engelmann et al., *Z. Phys. A* 352 (1995) 351
- [179] P. T. Hosner et al., *Phys. Rev. Lett* 94 (2005) 112501
- [180] S. Rahaman et al., *Eur. Phys. J. A* 34 (2007) 5
- [181] O. Kenn et al., *Phys. Rev. C* 63 (2001) 064306

- [182] T. Ishii et al., *Phys. Rev. Lett* 84 (2000)39
- [183] H. Grawe et al., Tours Symposium on Nuclear Physics IV, Tours 2000, *AIP Conf. Proc.* 561 (2001) 287
- [184] A.M. Oros-Peusquens and P.F. Mantica, *Nucl. Phys. A* 669 (2001) 81
- [185] O. Sorlin et al., *Phys. Rev. Lett.* 88 (2002) 092501
- [186] M. Sawicka et al., *Phys. Rev. C*68 (2003) 044304
- [187] K.H. Langanke et al., *Phys. Rev. C*67 (2003) 044314
- [188] P. T. Hosmer et al., *Phys. Rev. Lett.* 94 (2005) 112501
- [189] C. Mazzochi et al., *Phys. Lett.* B622 (2005) 45
- [190] O. Perru et al., *Phys. Rev. Lett.* 96 (2006) 232501
- [191] K. L. Yurkewicz et al., *Phys. Rev. C*70 (2004) 054319
- [192] I. Talmi, Proc. Int. School Enrico Fermi, Elementary Modes of Excitation in Nuclei, eds. A. Bohr and R.A. Broglia, North Holland (1977) 352
- [193] G. Kraus et al., *Phys. Rev. Lett.* 73 (1994) 1773.
- [194] Y. Yanagisawa et al., in proc. of the ENAM98 conference, eds B. M. Sherrill et al., p. 610.
- [195] T. Otsuka et al., *Phys. Rev. Lett.* 81 (1998) 1588.
- [196] A. Poves, *Proc. 6th Int. Spring Seminar on Nuclear Physics - "Highlights of modern nuclear structure"*, ed. A. Covello, World Scientific, Singapore, (1999) 129
- [197] M. Lewitowicz et al., *Nucl. Phys.* 654 (1999) 687c
- [198] H. Mach et al., *Nucl. Phys. A* 719 (2003) 213c
- [199] A.F. Lisetskiy et al., *Phys. Rev. C*70 (2004) 044314
- [200] A.F. Lisetskiy et al., *Eur. Phys. J. A* direct 25 (2005) 95
- [201] S. Franchoo et al ., *Phys Rev. C*64 (2001) 054308
- [202] N.A. Smirnova, A. De Maesschalck, A. Van Dyck and K. Heyde, *Phys Rev. C*69 (2004) 044306
- [203] X.G. Zhou et al ., *Phys. Rev. C*53 (1996) 982
- [204] B. Zeidman and J.A. Nolen, *Phys. Rev. C*18 (1978) 2122
- [205] F. Ajzenberg-Selove, R.E. Brown, E.R. Flynn and J.W. Sunier *Phys. Rev. C*24 (1981) 1762
- [206] S Franchoo et al ., *Phys. Rev. Lett.* 81 (1998) 3100
- [207] I. Stefanescu et al., *Phys. Rev. Lett.* 100 (2008) 112502
- [208] M. Hjorth-Jensen, T. T. S. Kuo, and E. Osnes, *Phys. Rep.* 261 (1995)125
- [209] F. Nowacki, PhD Thesis, Strasbourg (1996) CRN 96-7
- [210] J. Sinatkas, L.D. Skouras, D. Strottman and J.D. Vergados, *J. of Phys.* G18 (1992) 1377 and 1401
- [211] E. Padilla-Rodal et al., *Phys. Rev. Lett.* 94 (2005) 122501
- [212] J Van de Walle et al., *Phys. Rev. Lett.* 99 (2007) 142501
- [213] A. Prévost et al., *Eur Phys. J. A.* 22 (2004) 391
- [214] T. Rząca-Urban, W. Urban, J.L. Durell, A.G. Smith, and I. Ahmad, *Phys. Rev. C*76 (2007) 027302
- [215] A. Blazhev et al., *Phys. Rev. C* 69 (2004) 064304
- [216] J.S. Thomas et al., *Phys. Rev. C*71 (2005) 021302
- [217] O. Perru et al ., *Eur. Phys. J. A* 28 (2006) 307
- [218] D.W. Bardayan, *Eur. Phys. J. A* direct (2006) and J.S. Thomas et al., *Phys. Rev. C*76 (2007) 044302
- [219] M.-G. Porquet et al., to be published
- [220] M.-G. Porquet et al., *Eur. Phys. J. A* 28 (2006) 153
- [221] J.P. Omtvedt, B. Fogelberg and P. Hoff, *Z. Phys. A* 339 (1991) 349
- [222] O. Kavatsyuk et al., *Eur. Phys. J. A* 31 (2007) 319
- [223] D. Seweryniak et al., *Phys. Rev. Lett.* 99 (2007) 022504
- [224] M. Lipoglavsek et al ., *Phys. Rev. C*66 (2002) 011302(R)
- [225] C. Vaman et al., *Phys. Rev. Lett.* 99 (2007) 162501

- [226] A. Banu et al., *Phys. Rev. C* 72 (2005) 061305(R)
- [227] J. Cederkäll et al., *Phys. Rev. Lett.* 98 (2007) 172501
- [228] J.N. Orce et al., *Phys. Rev. C* 76 (2007) 021302(R)
- [229] D.C. Radford et al., *Nucl. Phys.* A752 (2005) 264c
- [230] J. Terasaki, J. Engel, W. Nazarewicz, and M. Stoitsov, *Phys. Rev. C* 66 (2002) 054313
- [231] M. Lipoglavsek et al., *Phys. Rev. C* 65 (2002) 051307(R)
- [232] M.-G. Porquet et al., *Eur Phys. J. A.* 25 (2005) 123
- [233] A. Korgul et al., *Phys. Rev. C* 64 (2001) 021302
- [234] J. Shergur et al., *Phys. Rev. C* 65 (2002) 034313
- [235] J. Shergur et al., *Phys. Rev. C* 72 (2005) 024305
- [236] A. Korgul et al., *Eur. Phys. J. A.* 24, s01 (2005) 39
- [237] L. Coraggio, A. Covello, A. Gargano, and N. Itaco, *Phys. Rev. C* 72 (2005)057302 and *Phys. Rev. C* 73 (2006) 069901 (E)
- [238] L. Coraggio, A. Covello, A. Gargano, and N. Itaco, *Phys. Rev. C* 73 (2006) 031302 (R)
- [239] M.-G. Porquet, S. Péru and M. Girod, *Eur. Phys. J. A.* 25 (2005) 319
- [240] J.P. Schiffer et al., *Phys. Rev. Lett.* 92 (2004) 162501
- [241] M. Conjeaud, S. Harar and Y. Cassagnou, *Nucl. Phys.* A117 (1968) 449
- [242] S. Galès, C.P. Massolo, S. Fortier, J.P. Schapira, P. Martin, and V. Comparat *Phys. Rev. C* 31 (1985) 94
- [243] M. Dworschak et al., *Phys. Rev. Lett.* 100 (2008) 072501
- [244] D.C. Radford et al., *Phys. Rev. Lett.* 88 (2002) 222501
- [245] G. Jakob et al., *Phys. Rev. C* 65 (2002) 024316
- [246] B. Fogelberg et al., *Phys. Rev. C* 70 (2004) 034312
- [247] I. Dillmann et al., *Phys. Rev. Lett.* 91 (2003) 162503
- [248] A. Jungclaus et al., *Phys. Rev. Lett.* 99 (2007) 132501
- [249] P. Hoff et al., *Phys. Rev. Lett.* 77 (1996) 1020
- [250] M. Piiparinen et al., *Z. Phys. A* 337 (1990) 387
- [251] B. Pfeiffer et al. *Nucl. Phys.* A 693 (2001) 282
- [252] K.-L. Kratz, K. Farouqi and B. Pfeiffer *Prog. Part. and Nucl. Phys.* 59 (2007) 147
- [253] T. Kautzsch et al., 2nd Intern.Workshop Nuclear Fission and Fission-Product Spectroscopy, Seyssins, France, AIP Conf. Proc. 447 (1998) 183
- [254] B. Chen et al., *Phys. Lett. B* 355 (1995) 37 and references therein
- [255] D. Lunney, J.M. Pearson and C. Thibault, *Rev. of Mod. Phys.* 75 (2003) 1021
- [256] T. Rauscher et al. *Phys. Rev. C* 57 (1998) 2031
- [257] F. Käppeler et al. *Astrophys. J.* 291 (1985) 319
- [258] E. Krausmann et al. *Phys. Rev. C* 53(1996)469
- [259] L. Gaudefroy et al. *Eur. Phys. J. A* 27, s01 (2006) 302
- [260] O. Sorlin, L. Gaudefroy, L.-K. Kratz and T. Rauscher, *C. R. Physique* 4 (2003) 541
- [261] K. Heyde, P. Van Isacker, M. Waroquier, J.L. Wood, and R.A. Meyer, *Phys. Rep.* 102 (1983) 291
- [262] A.N. Andreyev et al., *Nature* 405 (2000) 430
- [263] Yu. N. Novikov et al., *Nucl. Phys.* A697 (2002) 92
- [264] M. Bender et al., *Eur. Phys. J. A.* 14 (2002) 23
- [265] E. Caurier, M. Rejmund and H. Grawe, *Phys. Rev. C* 67 (2003) 054310
- [266] W.D. Myers and W.J. Swiatecki, *Nucl. Phys.* 81 (1966) 1
- [267] S.G. Nilsson et al., *Nucl. Phys.* A131 (1969) 1
- [268] B. Singh, R. Zywna and R.B. Firestone, *Nucl. Data Sheets* 97 (2002) 241
- [269] A. Sobiczewski and K. Pomorski, *Prog. Part. Nucl. Phys.* 58 (2007) 292

- [270] M. Bender, K. Rutz, P.-G. Reinhard, J.A. Maruhn, and W. Greiner *Phys. Rev. C* 60 (1999) 034304
- [271] A.V. Afanasjev and S. Frauendorf, *Phys. Rev. C* 71 (2005) 024308
- [272] S. Hofmann and G. Münzenberg, *Rev. Mod. Phys.* 72 (2000) 733
- [273] K. Morita et al., *J. Phys. Soc. Japan* 73 (2004) 2593
- [274] Yu. Ts. Oganessian et al., *Phys. Rev. C* 74 (2006) 044602 and references therein
- [275] J.N. Ginocchio, *Phys. Rev. Lett.* 78 (1997) 436 and *Phys. Rep.* 414 (2005) 165

